Water Scarcity Assessments in River Nile Delta Region Using Integrated GIS and Remote Sensing Technologies

A Dissertation

Presented to the Department of Ichthyology and Aquatic Environment, School of Agricultural Sciences, University of Thessaly

In Partial Fulfillment of the Requirements for the Degree of

Doctor of Philosophy

By

Mohamed Elhag, M.Sc

Department of Agriculture Ichthyology and Aquatic Environment, School of Agricultural Sciences, University of Thessaly

Volos, Greece 2013

Supervision Committee

Dr. Aris Psilovikos, Assistant Professor, University of Thessaly, Supervisor.

Dr. Maria Sakellariou Makrantonaki, Professor, University of Thessaly, Member.

Dr. Konstantinos Perakis, Professor, University of Thessaly, Member.

Examination Committee

Dr. Aris Psilovikos, Assistant Professor, University of Thessaly.

Dr. Maria Sakellariou Makrantonaki, Professor, University of Thessaly.

Dr. Konstantinos Perakis, Professor, University of Thessaly.

Dr. Christos Tzimopoulos, Emeritus Professor, Aristotle University of Thessaloniki.

Dr. George Zalidis, Professor, Aristotle University of Thessaloniki.

Dr. Ifigeneia Kagalou, Professor, University of Thraki.

Dr. Ioannis Argyrokastritis, Associate Professor, Agricultural University of Athens.

Acknowledgments

I am greatly indebted to **Dr. Aris Psilovikos** for accepting me as a PhD student at the Department of Agriculture Crop Production and Rural Environment, School of Agricultural Sciences, University of Thessaly. I thank Dr. Psilovikos for his valuable and critical comments that enhanced my capability to come up with a result oriented research.

I also want to thank **Prof. Dr. Maria Sakellariou Makrantonaki** for her supervision, contributions, and support during my studies and work at the Department of Agriculture Crop Production and Rural Environment, School of Agricultural Sciences, University of Thessaly.

Sincerely, I thank **Dr. Konstantinos Perakis** at the Department of Planning and Regional Development, School of Engineering, University of Thessaly.

I would like to thank all the **members of the examination committee** for the fruitful advices that they gave to me for all the issues of the PhD.

Deep appreciation and thanks is also dedicated to **MAICh personnel** for their friendship and continuous help.

During the field work in Egypt, many institutions and people have supported me. I extend my sincere thanks to them. I am much indebted to the National Authority for Remote Sensing and Space Sciences (**NARSS**) staff for providing me all kinds of support required during the field work.

I am grateful that the Greek State Foundation (**IKY**) gave me the opportunity to pursue the PhD study in Greece.

At last my heartfelt love and affection goes to my beloved wife **Amina Abdel Reheem** and my sons **Youssef** and **Yahiya** for their inspiration, support and understanding of their responsibility during this work. I am deeply indebted to them for the time I did not spend with them.

Table of Contents

List of Tables

List of Figures

List of Appendix Tables

List of Appendix Figures

List of abbreviation

Abbreviations	Name
µS/cm	Micro-Simens Per centimeter
AATSR	Advance Across Track Scanner Radiometer
ABL	Atmospheric Boundary Layer
AE	Available Energy
ANN	Artificial Neural Net
AR	Autoregressive
ARE	Arenosols
ARIMA	Autoregressive Integrated Moving Average
ASL	Atmospheric Surface Layer
ASTER	Advanced Spaceborne Thermal Emission and Reflection Radiometer
BAS	Bulk Atmospheric Similarity
BCM	Billion Cubic Meter
BR	Bowen Ratio
CCD	Charge Coupled Device
C_j	Criterion Score of Constraint $_J$
CL	Calcisols
CLD	Causal Loop Diagram
C_p	Specific Heat Capacity of the Air
C_t	Heat Transfer Coefficient of the Leaf
CWSI	Crop Water Stress Index
CWSI	Crop Water Shortage Index
DEM	Digital Elevation Model
DSI	Drought Severity Index
DSME	Dominant Soil Map of Egypt
DWIP	Drainage Water Irrigation Project
Ea	Actual Evapotranspiration
EAAE	Egyptian Association of Agricultural Economics
EB	Energy Balance
EC	Eddy Covariance
ECMWF	European Centre for Medium-Range Weather Forecasts
ECw	Electric Conductivity
e_s	Saturation Vapor Pressure
ET	Evapotranspiration
ETM+	Enhanced Thematic Mapper
ETMA	Evapotranspiration Mapping Algorithm
FAO	Food and Agriculture Organization
fAPAR	Fraction of Photosynthetically Active Radiation
FC	Fractional Vegetation Cover
f_c	Fractional Canopy Coverage
fCover	Gap Fraction for Nadir Direction
FL	Fluvisols

G	Soil Heat flux,
g	Acceleration Due to Gravity
GCP	Ground Control Point
GIS	Geographical Information System
GY	Gypsisols
H	Sensible Heat flux
IIP	Irrigation Improvement Plan
IR	Infrared
IWRI	International Water Resources Institute
K_{cr}	Crop Coefficient
LAI	Leaf Area Index
$LAI.C_{ab}$	Calculated Chlorophyll Content
LE	Latent Heat Flux from Evapotranspiration
LP	Leptosols
LULC	Land Use Land Cover
MA	Moving Average
MCDA	Multi Criteria Decision Analysis
MERIS	Moderate Resolution Imaging Spectrometer
METRIC	Mapping Evapotranspiration with Internalized Calibration
MNP	Most Probable Number
MODIS	Moderate Resolution Imaging Spectroradiometer
MOMO	Matrix Operator MethOd
MOS	Monin–Obukhov Similarity
MWRI	Ministry of Water Resources and Irrigation
NARSS	National Authority of Remote Sensing and Space Science
NBCs	Nile Basin Countries
NBI	Nile Basin Initiative
NDVI	Normalized Difference Vegetation Index
n_{ec}	Wind Speed Profile Extinction Coefficient
Nile-COM	Nile Basin Council of Ministers
NIR	Near-Infrared
NWRP	National Water Resource Plan for Egypt
PBL	Planetary Boundary Layer
PC	Principle Component
PCA	Principal Component Analysis
PCC	Post-Classification Comparison
PolDER	Polarization and Directionality of Earth Reflectance
P_r	Prandtl Number
R	Red Band Reflectance
r_{ah}	Aerodynamic Resistance for Heat Transfer
RG	Regosols
R_{lwd}	Downward Long Wave Radiation
RMSE	Root Mean Square Errors

Rn	Net Radiation
$R_{n,d}$	Daily Net Radiation
$R_{n,i}$	Instantaneous Net Radiation
RS	Remote Sensing
R_s	Incoming Short Wave Radiation
R_{swd}	Downward Solar Radiation
RTM	Radiative Transfer Models
SARIMA	Seasonal Autoregressive Integrated Moving Average
SAVI	Soil Adjusted Vegetation Index
SDSS	Spatial Decision Support System
SEBAL	Surface Energy Balance Algorithm for Land
SEBI	Surface Energy Balance Index
SEBS	Surface Energy Balance System
SMAC	Simplified Method for the Atmospheric Correction
SMACEX	Soil Moisture Atmosphere Coupling Experiment
S-SEBI	Multifaceted Surface Energy Balance Index
T	Temperature (K)
TCT	Tasselled Cap Transformation
TM	Thematic Mapper
T_o	Aerodynamic Temperature
TOA	Top of Atmosphere
TOC	Top of Canopy
T_s	Remotely Sensed Radiometric Surface Temperature
u (h)	Horizontal Wind Speed
UNCCA	United Nation's Common Country Assessment
UNDSD	United Nations Division for Sustainable Development
VEG	Vegetation
VIS	Visible
VIs	Vegetation Indices
VR	Vertisols
WHO	World Health Organization
WMRI	Water Management Research Institute
WSVI	Water Supply Vegetation
z_{0h}	Scalar Roughness Height for Heat Transfer
ε	Emissivity
ε_a	Actual Vapor Pressure
θ_v	Potential Virtual Temperature Near The Surface
λE	Turbulent Latent Heat Flux
Λ_r	Relative Evaporative Fraction
ρ_a	Air Density
ρ_ω	Density of Water
ψ	Stability Correction Functions

1. Introduction

One of the greatest challenges facing humanity is how to use scarce resources in an equitable and sustainable way. According to Seckler (1999) water scarcity is now the single greatest threat to human health, the environment and the global food supply. Besides the qualitative aspect of water, (e.g. polluted water affecting human health), the available quantity of water has a direct impact on a region's potential to produce food. Worldwide, agriculture is the main consumer of water. In Egypt more than 85% of the water withdrawal from the Nile is used for surface irrigated agriculture. Water availability therefore has a direct influence on national food security. Resources such as land and water, as well as the general political and economic situation play crucial roles. For countries that share the same river, such as the Nile catchment countries, competitive usage can accentuate the threat of running dry (Aboul Enien et al., 2000).

1.1. Background

The Nile River is shared by ten countries (Egypt, Sudan, Ethiopia, Eritrea, Tanzania, Uganda, Burundi, Rwanda, D.R. Congo, and Kenya). It is the home to more than 160 million people. The population is growing by 2-3% per year. The Nile Basin covers an area of 3.1 million km^2, of which 1% is urban, 2% are covered by forest, 3% by wetlands, 3% by open water, 4% by shrub, 5% by irrigated cropland, 10% by cropland, 30% by desert/semi-desert and 42% by grassland (NBI, 2001). Many countries; like Egypt, in the Nile Basin are highly dependent on the Nile's water, as they are situated in arid or semi-arid regions. More than 95% of Egypt's water comes from the Nile, this means that it depends on rainfall outside of its territory. There are four main development needs concerning water use in the Nile Basin countries:

- Water for irrigation and hydroelectric power production;

- Prevention of floods;
- Minimization of erosion and siltation of reservoirs; and
- Prevention of water pollution.

According to Mason, (2004), the national economic capacity to address these issues is limited. The Nile Basin Initiative (NBI) was formally launched in February 1999 by the Ministers of Water Affairs of the ten countries that share the Nile River: Burundi, Democratic Republic of Congo, Egypt, Ethiopia, Eritrea, Kenya, Rwanda, Sudan, Tanzania and Uganda. Together, these ministers make up the Nile Basin Council of Ministers (Nile-COM). The NBI provides a framework through which its member states can cooperatively develop the resources of the Nile Basin to fight poverty and promote socio-economic development in the region.

But through joint management and development of the Nile Basin's resources which the NBI is designed to make possible the Nile has the potential to catalyze sustainable economic growth for all ten countries with benefits far beyond those that can be derived from the river itself.

The Nile Basin Initiative (NBI), functions as a broad program of international importance. The Nile Basin region and related state and regional tensions are of great concern to the international community due to its volatility of and proximity to the Middle East. Further tensions and conflict in nearby regions have the potential to spread through regional uncertainty concerning issues of political, social, and economic stability. Additionally, the NBCs and the international community recognize the importance of developing regional relationships through environmental cooperation because of its potential to spread into other conflict-prone areas where regional collaboration is needed.

The need for international water agreements continues because of the increasing possibility for water-induced conflict from issues of water scarcity and degradation, which poses as a continual threat to local, state, regional, and international stability. Individual states, armed with sovereign rights to territorial resources, use water to serve political, economic, and social goals. Scholars agree that conflict has the greatest potential to emerge when the downstream (most-vulnerable) nation is militarily stronger than the upstream (water-controlling) nation and it feels its interests are threatened, as in the case of the Nile River (Gleick, 2001).

Internationally shared bodies of water create political, social, and economic tensions and disputes concerning the distribution and use of resource management. Furthermore, when a resource base extends across a political border, misunderstandings or a lack of agreements about allocations are more likely (Conca et al., 2006). The increased potential for conflict intensifies threats to state stability and national security. Therefore these threats includes: *"Any action or sequence of events that threatens to drastically and over a relatively brief period of time to degrade the quality of life for the inhabitants of a state, or threatens to narrow the range of policy choices available to a state or private, nongovernmental entities (persons, groups, corporations) within the state"* (Ullman, 1983).

The threat of water scarcity and subsequent tensions exemplify the relationship between environment and political interests. Change in water usage or development of water resources poses a challenge to the status quo, which, as Ullman (1983) argues, threatens to alter the quality of life of the nation and restricts policy options (Sprinborg, (1979).

State security involves the ability of states and societies to maintain their independent identities, as well as their physical and functional integrity (Lowi, 1999). These factors are compromised, however, through adjustments in water development, distribution, and use. In

terms of resource conflict resolution, Conca et al., (2006) states that progress exists in trying to identify policies for reducing the risks of disputes over water sources that will lead to conflict, as well as in a better understanding of mechanisms for promoting cooperation and collaboration over shared water resources. Authors also argued that considerable progress has been made both in understanding the nature of the connections between water resources and conflict and in evaluating regional cases where such connections may be particularly strong.

Despite progress, Conca et al., (2006) contend: There is a long way to go before nations or regions produce a common policy agenda or set of initiatives that truly incorporate environmental and resources issues into approaches to reduce the risk of regional and national conflicts. Nevertheless, construction has begun on a new framework that will permit scholars and policymakers to apply new tools, set new priorities, organize responses to a range of environmental threats to peace and security. Thus, advances in conflict resolution and environmental cooperation function as an emerging platform for national and regional collaboration.

Within these state and regional institutions, however, the broader discourse on water scarcity involves the political, social, and economic influences and consequences of environmental, and in this, instance water-induced conflict.

The objective of the NBI is to recognize the cooperative development that holds the greatest prospects for bringing benefits to the entire region, and aware of the challenges, the Nile riparian's took an historic step in establishing the Nile Basin Initiative. Formally launched in February 1999, the initiative provides an institutional mechanism, a shared vision, and a set of agreed policy guidelines to provide a basin wide framework for cooperative action. The policy guidelines define the following as the primary objectives of the NBI:

- To develop the Nile Basin water resources in a sustainable and equitable way to ensure
- To ensure efficient water management and the optimal use of the resources
- To ensure cooperation and joint action between the riparian countries
- To target poverty eradication and promote economic integration
- To ensure that the program results in a move from planning to action.

The Strategic Action Program represents the Nile catchment's strategic approach to achieving sustainable socioeconomic development in the basin through "equitable utilization of, and benefit from, the common Nile Basin water resources." The Strategic Action Program provides the means for translating this shared vision into concrete activities through a two-fold, complementary approach:

a) Lay the groundwork for cooperative action through a regional program to build confidence and capacity throughout the basin (the Shared Vision Program)
b) Pursue, simultaneously, cooperative development opportunities to realize physical investments and tangible results through sub-basin activities (Subsidiary action programs) in the Eastern Nile and the Nile Equatorial Lakes regions.

Egypt is now fully utilizing its share of the Nile river flow according to the Agreement of 1959 with Sudan (NBI, 2001) and is effectively reusing drainage water, treated waste water and shallow groundwater. Challenging new development projects are being implemented by the government such as the El-Salam and Toshka agriculture projects. These projects will have a large impact on the distribution and use of presently available water resources. Continued population and economic growth will exert further pressure on the existing water resources. Major water quality problems are still limited to a number of hot spots, but proper attention will have to be given to the effects of expected socioeconomic developments on

water quality. The threats of the available water resources being insufficient to meet the demands from all socio-economic sectors requires an adequate and integrated water resources management (NWRP, 2001; Chowdary et al., 2009).

Planning is central in water resources management, as it is needed to develop strategies to reduce water use and use it more efficiently (demand management), to optimize the supply (supply management) and to maintain or improve water quality (pollution control). Various planning studies were implemented in Egypt in the past, such as the NWRP (2001) and Water Security Projects. The present situation, with limited possibilities for extension of water supply and growing demands (Kijne, 2001), provides new challenges for to achieve the previously mentioned objective. The Egyptian government, with support of international planning experience and in cooperation with national scientific and consultant institutions has agreed to support the implementation of the National Water Resources Plan (NWRP, 2001), that targets the year 2017 as a reference for measuring the success of the plan objectives.

The overview of the Egyptian experience in implementing its National Water Resources Plan is to optimally meet food security as well as water scarcity challenges from a socio-economic and ~~from~~ environmental point of view. The following review is structured as follows: concepts of water security are introduced, followed by an overview of water availability and quality in term of conservation measures (Muthuwatta et al., 2010). Based on these environmental aspects, the socio-economic water demand and water supply balance to reach the sustainability are presented. The increased focus on water reuse and efficiency increase of the National policy is then highlighted. The review ends by envisaging the concepts of remote sensing and agricultural practices. One key conclusion is that Egypt's water security strategy is influenced by both national and international factors in term of water use and efficiency.

1.2. Problem statement

The main users of water resources are agriculture, industry, and households. Moreover, there is also another use that is taking into account the last years, the ecological one. This is expressed with constraints in the hydrologic regime in water bodies, like recharge and water level, so that in no case the use of water to be harmful for the ecosystem. A major consumer of all fresh water withdrawals is agriculture sector; especially this is the case if the agriculture is surface irrigation-based. Therefore, serious disturbances in provision of adequate water supplies for food production puts at risk the basic needs of human livelihood. The agriculture practices in term of food and livestock fodder production takes up to 80 % of all fresh water withdrawals per year (Abu Zeid, 1998). As the agriculture is the basis on which the development of other sectors of the economy relies, the water stress and water scarcity conditions put whole economy at risk.

First of all the water shortages will impose the major problems to the most vulnerable parts of the society restricting their ability of food production (Abu Zeid, 1998). Water withdrawal for irrigation purposes is expected to increase only by 4 % versus to the non-irrigation uses, which are predicted to increase by 62% due to population growth and rising per capita domestic water use. This will endanger the fresh water supply levels of countries heavily dependent on irrigation agriculture (Rosegrant, et al., 2002).

Consistent with Hamdy, et al., (2003): *"Experience leads us to the fact that to sustain the use fresh water resources for irrigation over the next 25 years will have to be augmented by an additional 15–20%, even under favorable assumptions regarding improvements in irrigation efficiency and agronomic potential to meet food requirements. This will amount to an additional 0.6–0.7% of water supply per year"*. Despite the fact that Egypt as country of a

very limited fresh water resources can't sustain such increase without more attentions and efforts paid to more effective water resource management.

1.3. Research objective

1.3.1. General objective

The objective of this study is to understand to what extent the water conservation measures have the potential to upgrade the demand-supply balance and at the same time meet the social, environmental and economic interests of society. The controversial character of water saving measures does not always allow for the matching up of all previously mentioned interests embraced in water saving. The present study tries to take a closer look at the irrigation water saving measures such as efficiency, water loss through evapotranspiration and reuse which are being or can be applied in Egypt. Consequently, the study aimed to identify possible environmental constraints for the implementation of such measures and find out if they can meet sustainability objectives under adequate policies adopted and implemented by decision makers.

1.3.2. Specific objective

a) Estimating the Daily Evapotranspiration over the Nile Delta region using remote sensing data
b) Nile Delta land cover land use change detection analysis using three temporal satellite images acquired in 1984, 2000 and 2005
c) Daily Evapotranspiration time series analysis over the Nile Delta region for five years from August 2005 till December 2009

d) Develop strategies how Geographical Information System (GIS) and Remote Sensing (RS) can be used to produce rice cultivation suitability map in command area in Nile Delta as an example of the efficiency of water resources management plans

1.3.3. Research questions

1) What are the current legislations and agriculture polices used in Egypt?
2) What are the current irrigations techniques used in Egypt?
3) What is the exact water balance in Nile Delta perimeter?
4) What are the major crops in within Nile Delta diameter?
5) What is the exact area used in the Nile Delta area for agriculture practices?
6) What is the real extent of water conservation plans used in Nile Delta?
7) How far these plans and legislations depend on GIS and RS in Egypt?

1.3.4. Hypothesis

Limited supplies of fresh water create an urgent need for rationalizing the water use, but the ways aiming at the optimal use of water differ and are complexed. The main hypothesis of water conservation pointed out as follow: “reducing the demand for water by fostering water conservation habits, stopping wasteful uses, decreasing peak consumption and charging for water at the appropriate rates. It also means taking advantage of technological developments and improved management techniques, coordinating water resources planning and management with land-use planning and economic and social planning and establishing new or updated standards and regulations. In short, water conservation means optimal water use. It should be stressed that except in drought or other exceptional conditions, a water conservation policy is not intended to enforce arbitrary cuts in water consumption levels at the expense of the quality of life of the population. Its main purpose is different: the efficient use of a limited resource, which is essential to life”.

Water conservation can be implemented through effective water resources management, which involves both supply and demand side management measures. Supply side conservation measures would include the efficiency improvements in water exploitation and infrastructure, its reuse, whereas the demand side conservation measures seek for demand regulations through public education and effective water use practices (Bau, 1994; Postel, 1997). The most difficult is to find the balanced approach, which would avert society from trade-offs between the economic, social or environmental interests and interests of the future generation (UNDSD, 2003). This is especially important in case of developing countries, like Egypt.

There is big challenge for such society to improve the social conditions of their population and ensure economic growth but not compromise the environmental interests. The sustainability concept requires a holistic approach including many aspects that drive society and longtime perspective in decision-making.

1.3.5. Assumption

Using satellite imagery in the form of remote sensing data integrated with GIS interpretation and analyses for the purpose of estimating more accurately the amount of evapotranspiration in order to categorize the problematic zones in the pilot area which will be extrapolated to the whole Nile Delta, seems to be effective tool for water resource management. Spatial Decision Support System would be a very powerful tool to sustain the use of fresh water resources in the Nile Delta.

1.4. Structure of the thesis

This thesis is divided in to six chapters, in addition to the current Chapter 1 “Introduction” with the content of each summarized below:

Chapter 2, Water Framework: This chapter reviews the concept of water scarcity in Egypt and reviews the evolutionary steps of evapotranspiration estimation using remote sensing assessment methods. In addition to the different review of the vegetation indices introduced to agricultural water saving schemes, water reuse and crop production and give some spatial information on crop water relationship.

Chapter 3, Materials: This chapter describes the study area as well as the remote sensing and GIS data which were used in this study. The different software applied is also mentioned.

Chapter 4, Methods: The methodological steps implemented to produce daily evapotranspiration maps and its time series analysis, land use and land cover maps and corresponding change maps, rice cultivation maps are explained. The planning of the field work and the subsequent collection of ground truth data are documented. The analyses of the remotely sensed data are presented. Finally a detailed description of the sustainable water resources management is given.

Chapter 5, Results and Discussion: This chapter is a representation of the important research achievements. The results were pertaining to the segmentation and classification of the satellite imagery; a display of land use and cover maps, and land use/cover change maps, as well as the use of tables and graphs to interpret the changes. The different results obtained from remotely sensed data and the ground truth data in term of the current agriculture practices are elaborated. Finally the integration of all these achievements into the water resource management is disadvantageous and the output for test areas evaluated suggestion of a management plan for the different test area.

Chapter 6, Conclusions and Outlook: This section summarizes the main topic of the research and draws the implications for the future research efforts.

Chapter 7, Recommendations: the use of the findings of the research in term of applicable integrated water resources management based on adequate decisions.

Finally, the summary of the thesis will be presented in three languages, English, Greek and Arabic.

2. Water framework in Egypt

2.1. Water scarcity

2.1.1. Subsidies

Despite the fact that availability of water resources is declining year by year and in some regions in Egypt are already experiencing water stress, combing with wasteful practices of irrigation are widely spread. As the practice shows the lack of proper incentives discourages the promotion of water saving technologies and changes in land management. Subsidies are responsible for "failure to value water at anything to its true worth" and underpricing assists in anchoring believes that water resources are plenty and abundant (Postel, 1997). Heavy subsidies for irrigation are not only a luxury the developed countries' farmers benefit from, but the practice of undercharging is widely spread in developing countries as well, especially in Egypt. The most challenging is the fact that the free of charge approach for irrigation service is used in countries, which have high risks of acute water shortages in the near future. (Postel, 1997; Myers and Kent, 1998).

The main reasons behind the irrigation subsidies lay in social and economic objectives the governments are aiming at:

1) Providing water for farmers regardless of their disparate income levels (Johansson, et al., 2002);
2) It has been used to promote growth in agriculture and other sectors of economy as well (Rogers, et al, 2002) and;
3) The subsidies in the irrigation sector have aimed at sustaining the agriculture economy, ensuring the self-sufficiency of farmers in Egypt.

In fact, almost free accessibility to the irrigation service boosted water demands and discouraged farmers from investing in efficient technologies and carrying out water saving practices (Postel, 1997; Rogers, et al, 2002).

Other negative effects from irrigation subsidies pointed out in different literatures are the low self sufficiency of the irrigation sector. The cost recovery is not enough for operation and maintenance of the system, let alone the repayment of investment costs. Lack of funds in irrigation sector is compensated from the public funds diverting money from other projects and programs. Especially negative could be outcomes of such actions in Egypt, as a country with budget deficits (Postel, 1997). Environmental consequences from the water overuse enhanced by irrigation subsidies lead to such problems as water logging, soil salinization and other forms of environmental degradation (Postel, 1997; Myers and Kent, 1998; Sur, et al, 2002). Therefore removal of subsidies is considered to be an effective mechanism for avoiding the water overuse and environmentally harmful practices connected with the over extraction of groundwater and depletion of aquifers (Rogers, et al., 2002).

The main argument against such measure is the equity consequences of subsidy removal because it is suggested that the poor will be underprivileged in secure access to the water needed for food production. On one hand, it might generate the water conservation but at the expenses of certain groups of citizens who might be disadvantaged in the basic needs. The water pricing mechanisms are not considered effective enough in redistributing the income. Authors of other studies point out the need for adoption of different pricing mechanism in order to *"account disparate income levels"* (Johansson, et al., 2002). Mohamed and Savenije (2000), recognizing the needs for efficiency improvements, emphasize also the fact that basic needs should not be sacrificed, since the main objective of efficiency increase is not restricted to the economic benefits only but it must ensure socio-economic net benefits to whole society.

Many authors emphasize the fact that poor already do spend a considerable part of their income on pumping the water from groundwater to compensate the unreliability of water supply in Egypt. In these studies authors consider this as a good measure for farmer's willingness to pay for the proper service (Myers and Kent, 1998; Rogers, et al., 2002; Ahmad, 2002).

There is another factor which makes the subsidy removal difficult task, as mentioned by Perry, (2001) "In most developing countries similar to Egypt, the agricultural sector is politically and socially sensitive, sometimes even dominant. Changes that will reduce farm incomes are viewed with great caution by politicians."

2.2. Conservation measures

Limited supplies of fresh water create an urgent need for rationalizing the water use, but the ways aiming at the optimal use of water differ and are complex. Before reviewing different water saving measures the concept of water conservation itself need to be reviewed. Defined by Tate, (1994) water conservation is any socially beneficial reduction in water use or water loss. The main objectives of water conservation pointed out by Bau, (1994) are as follow: "

1) Reducing the demand for water by fostering water conservation habits,
2) Stopping wasteful uses,
3) Decreasing peak consumption and
4) Charging for water at the appropriate rates.

It also means taking advantage of technological developments and improved management techniques, coordinating water resource planning and management with land-use planning and economic and social planning; and establishing new or updated standards and regulations. In short, water conservation means optimal water use (Aboul Enien et al., 2000).

It should be stressed that except in drought or other exceptional conditions, a water conservation policy is not intended to enforce arbitrary cuts in water consumption levels at the expense of the quality of life of the population. Its main purpose is different, under the efficient use of a limited resource, which is essential to life. Water conservation can be implemented through effective water resources management, which involves both supply and demand side management measures. Supply side conservation measures would include the efficiency improvements in water extraction, transfer and conveyance, its reuse, whereas the demand side conservation measures seek for demand regulations through public education and effective water use practices (Bau, 1994; Postel, 1997). The other measures, which would enhance demand side conservation, are economic instruments such as taxes, quotas and water pricing.

Water pricing has many constraints. First of all it is the cultural perception, believes sanctioned by the Egyptian's religion and tradition, which perceive water not as commodity but one of the basic human needs. Thus the perception of water as a non-commodity resource persists to the increasing or introduction of charge for irrigation services (Abu Zeid, 1998; Perry, 2001; Rogers et al., 2002). Water pricing is considered important strategy for water conservation purposes as it will be allocated for most valuable uses and avoided the waste of resources. The objectives of water pricing simply can be shown with the following causal relationship:

Pricing ⟶ **Efficient allocation** ⟶ **Meet increasing water demand**

The main objective of the water pricing policy is maximizing efficient allocation of water resources, promote conservation but at the same time it should not compromise the social objectives such as affordability of water resources (Rogers et al., 2002). According to Rogers et al. (2002), the full price of water consists of operation and maintenance cost together with

capital charges, adding economic and environmental externalities. However, nowhere is paid more than operation and maintenance cost. Different methods have been used for pricing, which can be placed in four major categories according to Johansson et al. (2002):

1) Volumetric pricing,
2) Non-volumetric pricing (based on land size or crop cultivated on land),
3) Quotas and;
4) Water markets.

The current review is focusing on the first two pricing mechanisms leaving out the quota and market considerations.

Water pricing policy as an effective measure for water conservation provokes some doubts, as the practice does not confirm emergence of water saving habits among farmers if the prices fixed per Feddan (4200 m^2). In this situation the cost for maintenance and operation might be recovered but the main target of water saving is not achieved, as farmer does not have incentive for optimizing the water use. Only high prices would result in substantial water saving levels but last will compromise the social welfare of user groups. Suggested best pricing mechanism is volumetric pricing, according to delivered water quantities (Perry, 2001; Ahmad, 2002; Yang et al., 2003; Psilovikos et al., 2004).

An attempt tries to analyze the possible environmental and social constraints of irrigation water conservation measures stemming from the subsidy removal and introduction of cost recovery charge for the irrigation service in Egypt had been implemented, then the main core mechanism which should lead to the water saving is presented in Figure 2.1. A step at a time study is needed to examine each link and see how the causal relationships are limited and what these limiting factors, in case of Egypt, are. Even though the main goal of the conservation measures is the water saving, it does not imply that other factors involved in

water saving will be affected as positively as the water supply system. Therefore each of the variables must undergo the sustainability test to prove the overall positive effect for whole society which embodies not only need for economic development but environmental and social security as well.

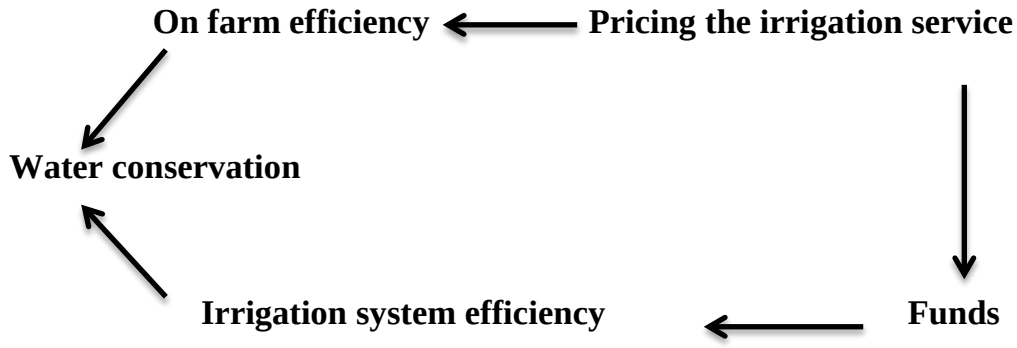

Figure 2.1: The causal relationship between pricing and water conservation (Pricing of irrigation service should encourage the investments in efficiency increase on farm, which would lead to rationale water use.

At the same time the cost recovery would add capital to the funds and ensure the investments for improving the operation and maintenance. The last would increase the irrigation system efficiency in whole. This would result in achieving the main objective of water conservation measures).

2.3. Sustainability

To evaluate the effectiveness of conservation measures, the present study takes an attempt to use sustainability criteria for evaluation of the current state of irrigation water availability in Egypt and situation, which might occur while implementing the water saving policy.

Simple explanation of sustainability concept would refer to importance of living within the carrying capacity: “Capacity of ecosystem in the size of population or community that can be supported indefinitely upon the available resources and services of that ecosystem... A

community that is degrading or destroying the ecosystem on which it depends is using up its community capital and is living unsustainably" (Encyclopedia of sustainable development).

Human Being can be supported only if availability of crucial resources are ensured and protected from deterioration, but at the same time social welfare must be improved for billions of people who would enjoy better life generated by sound economic growth and fair distribution of the wealth. Sustainability of society is up to achieving multiple goals and not only one of them. Sustained welfare of human kind can be maintained and further developed only if sound conjunction of three main basic aspects of human society is in place: a) economic development, b) social welfare and c) environmental quality (UNDSD, 2003).

The most difficult is to find the balanced approach, which would avoid society from trade-offs between the economic, social or environmental interests and interests of the future generation (UNDSD, 2003). This is especially important in case of developing countries particularly in Egypt.

There is big challenge for societies to improve the social conditions of their population and ensure economic growth but not compromise the environmental interests. The sustainability concept requires a holistic approach including many aspects that drive society and longtime perspective in decision-making.

2.4. Definition of efficiency

The efficiency improvements of the irrigation system are important water saving measures as they results in reduction of water losses at each level of the irrigation system. Figure 2.2 gives a simple scheme of irrigation can be visualized in the following way:

1) Water withdrawn from the river Nile is kept in the reservoir,
2) The water from storage flows into the main canals,

3) The irrigation canals enrich their water flow with extracted water from aquifer and groundwater, drainage water and discharge from industrial and domestic users,
4) From the main canal water is delivered to the farms passing the secondary canals and water distribution system which itself consists of tertiary canals and mesqa (Mesqa - name for irrigation canals) (Holmen, 1991; Tiwari and Dinar 2002) and,
5) After transmission water is applied on the field.

Plants for crop production consume the part of it, another fraction ends up in the drainage network and the third is just lost to seepage. Thus taking into consideration the structure of water distribution scheme, efficiency can be discussed at different levels.

The part of water carried by irrigation schemes is lost to seepage and percolation as a result of poor technical conditions of distribution system and topography. Some water evaporates during conveyance. So the water use efficiency can be splitted into conveyance, distribution and application efficiency. If the conveyance efficiency points to the ratio "between water storage facilities and delivery systems at farm level" (Martinez, 1994) the application efficiency refers to the water use at the farm level (Tiwari and Dinar, 2002).

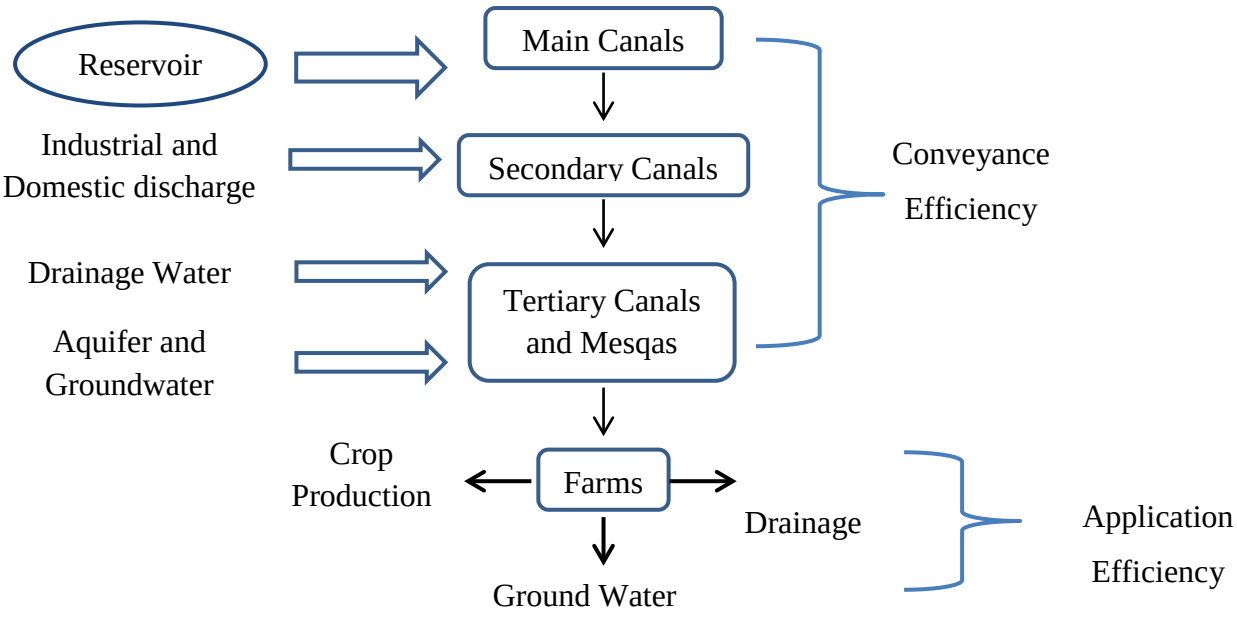

Figure 2.2: Irrigation water distribution scheme (based on Tiwari and Dinar, 2002).

The worldwide overall surface irrigation efficiency is estimated at 37-50 % (Carruthers, et al., 1997; Tiwari and Dinar, 2002). Conveyance efficiency is around 60 % (Martinez, 1994), application efficiency while using the traditional methods of irrigation accounts 40 %, whereas advanced systems show high performance with 60 to 70 % efficiency (Martinez, 1994; Myers and Kent, 1997). In Egypt average leakage during conveyance from outlets to the fields is 11 % and those between outlets and main canals 25 % (Tiwari and Dinar, 2002). These figures left a side about 10 billion cubic meters (BCM) lost in canals (El Filaly et al., 2004). The figures indicate poor performance of distribution systems in Egypt. This brings us to the suggestion that improvements in efficiency rates leave a significant scope for water conservation. However, the data obtained during the field trip shows a variation.

Irrigation efficiency figures in Egypt seem surprisingly high taking into account the fact that the most common method used in farms is the flood irrigation. According to the information obtained from Water Management Research Institute (WMRI) average efficiency rate of irrigation system is around 75 %, which makes it highest in the world. Much the same applies to the conveyance and application efficiency. So the Conveyance efficiency on the old lands is 70 % and on new lands it reaches 80 %. Application efficiency rates are higher - 80 and 90 % on the old and new lands respectively. Keller (1992) argues the same, he points out the facts that in Egypt efficiency rates are considerably high – 89 %. The high efficiency levels mentioned above create much confusion taking into account the worldwide irrigation efficiency rates. The significant divergence between the world average and country figures can be explained by the different methods applied for calculation of efficiency rates. The estimations used in case of low irrigation efficiency rates refer to the ratio of the amount of water applied at the root zone (used by plant) and water delivered (Tiwari and Dinar, 2002).

The estimates in case of higher efficiency rates apply the methodology, which is considering the natural water-recycling factor in equations. To understand such approach, a definition of

what so-called “IWRI paradigm” is required. The point the International Water Resources Institute (IWRI paradigm) is making is that water lost to seepage and percolation during conveyance and application cannot be considered as loss. Moreover, as Perry points out (Perry, 1999), losses and efficiency are “misused and …misleading for understanding water resource systems”.

The main idea of the approach is as follows:

1) water diverted from the reservoir and other sources partly evaporates,
2) Some fraction of water is taken up by plants and used for evapotranspiration. The water, which is lost to seepage from canals and fields, percolates to the deep aquifers and groundwater,
3) The water is recaptured and ground water and aquifers are recharged,
4) The lost water is reused as additional source of supply later on, obtaining it from wells or aquifers and,
5) The drained water, which is collected in drains, is returned into the irrigation system as well.

So the water can be returned to the system again and go through the same cycle until almost all of the water is consumed (Keller, 1992; Perry, 1999). Therefore the efficiency rates still go upwards in spite of the great losses during the conveyance and field application.

The calculations of efficiency suggested by IWRI, which include the natural recycling factor, lead to very controversial conclusions. In fact it diminishes the importance of efficiency improvement measures. So the study of Keller, (1992) concludes that due to high irrigation efficiency rates in Egypt, potential for improving the general overall basin wide system performance from physical water use efficiency standpoint is limited. The benefits of

investing in on-farm efficiency in such systems are substantially reduced by system wide effects, perhaps even to zero (Seckler, 1992).

The logic of the paradigm is convincing unless we do not pay any attention to the deterioration of water quality that accompanies each cycle of reuse. Going through the continuous recycling phase water picks up considerable amounts of salt from the soil, saline sinks, fertilizers, pesticides (Keller, 1992; Fernandez-Jauregui, 1994; DWIP, 1997; Tiwari and Dinar, 2002). The reused water quality becomes so deteriorated that it is questionable whether water can be used for irrigation or not (Martinez, 1994). The issue of water quality and reuse will be disused in this chapter later on. Moreover, the fact that estimates offered by the "IWRI Paradigm" unplaced such important factor as an environmental efficiency.

In a study done by Tiwari and Dinar (2002) environmental efficiency is defined as an "available water resources (that) must be managed in a way so as not reduce opportunity for potential use by future generations for various ecological reasons". High irrigation efficiency rates in Egypt, as suggested by some authors, might be subjected to a great cut down if considering the environmental efficiency (Figure 2.3). Negative changes in water quality require higher amounts of water applications on fields to leach out salts and avoid salinization of soil. Thus water use can increase due to low environmental efficiency rates and bring the gains from natural recycling to zero. The negative environmental effects will be discussed later on again.

Figure 2.3 illustrates another form of recycling, such as drainage water reuse, has the same effects on environmental efficiency. Drainage water used for irrigation must be drained quickly and applied in larger quantities in order to avoid salt accumulation and soil contamination from pesticides and polluted sewage water. The short retention time of drainage water requires frequent irrigation operations (DWIP, 1997; Water management in

Fayoum, 2002) and therefore increase in water use diminishes the high efficiency scored from natural recycling.

More sufficient seems saving the water through the increased technical efficiency of irrigation system so the high quality fresh irrigation water from river is not lost. It can be used down streams instead of naturally recycled saline water that would contribute to an increase of salt concentration in the soil. It turns out that even though the recycling compensates water losses, costs of same fraction of Water Mountain, as obtaining naturally recaptured water from the wells and aquifers is quite costly. Unfortunately it is impossible to carry out further studies in limited time and take a look at the possibilities for synergy of these two approaches.

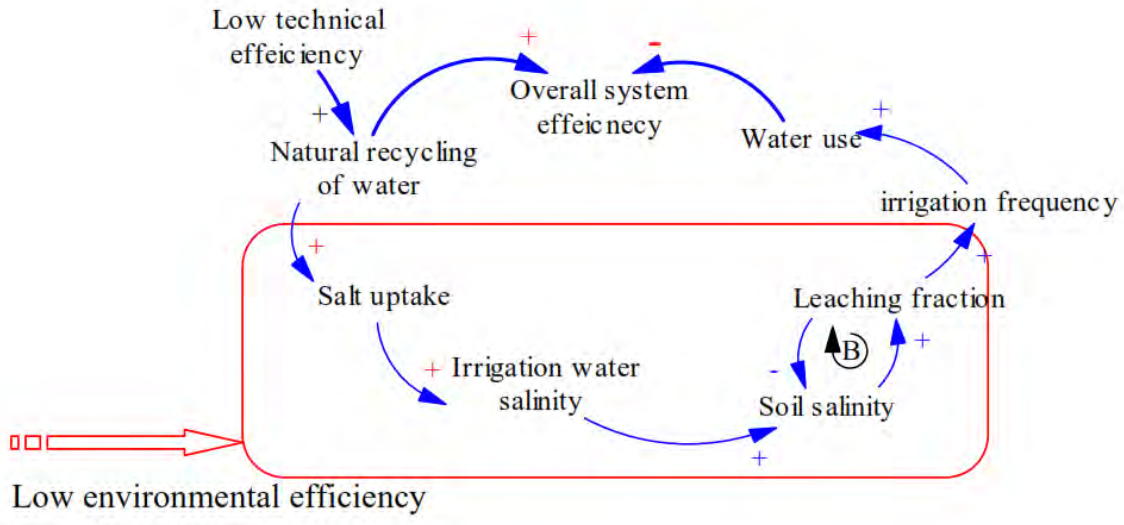

Figure 2.3: Causal Loop Diagram (CLD) for irrigation efficiency.

Technical and environmental efficiency must be considered together in order to draw picture closer to reality and consider all side effects. In spite of the mentioned in interviews and in some publications, high efficiency levels of irrigation in Egypt, importance of the efficiency improvements is widely recognized and the Irrigation Improvement Plan (IIP) has been under way. Though improvement of irrigation systems one billion cubic meter was expected to be saved for year 2000 (Abu Zeid, 1991). MWRI, (2002) report points to the necessity of the

irrigation improvements virtuously managing to avoid any discussion regarding the current efficiency estimates. The document does not contain any data referring to the efficiency in irrigation sector. Thus, the suggested constrain for efficiency increase, such as limited possibilities for improvements due to the present maximum efficiency levels in Egypt, has some objections. However, there are other limitations for efficiency increase such as land fragmentation, low public funds and environmental constraints as it schemed in Figure 2.4.

2.5. Water reuse

The efficiency increase implies not only improvements in technical performance of the system but irrigation water reuse as well. The drainage water reuse is given great importance in Egypt which is reflected in plans to increase the recycling levels by almost two folds (from present 4.5 BCM to 8.4 BCM) in 2017 (UNCCA, 2001). About 6300 $km^2$are currently irrigated with drainage water (MWRI, 2002) and reuse rate is about 2.5 fold of the current reuse of the drainage water (El Filali et al., 2004). However, ~~as~~ the final report of Drainage Research Institute concludes that the, "*increased salinity level will limit full utilization of this amount of the proposed recycled water*" (DWIP, 1997).

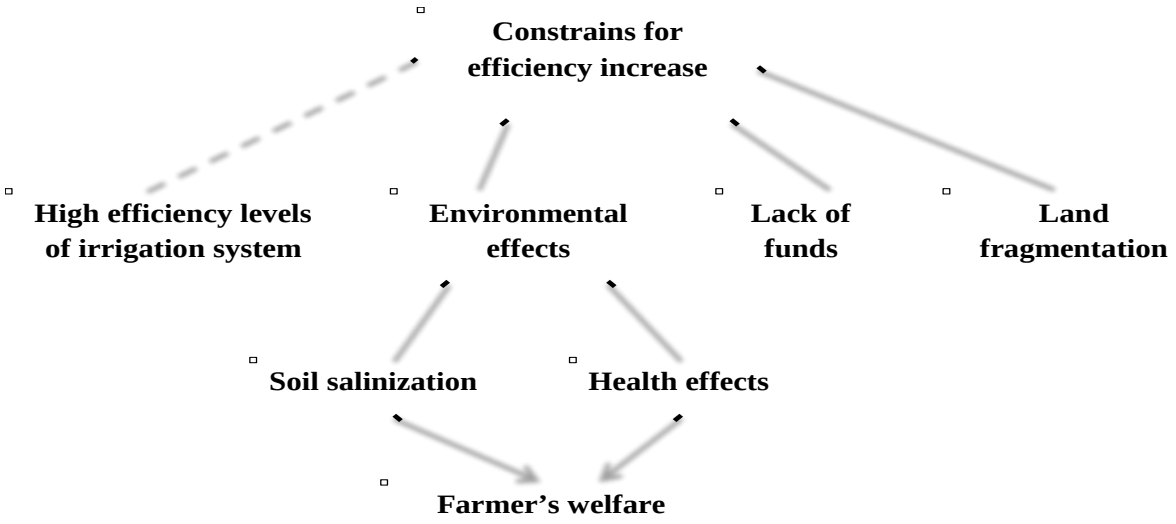

Figure 2.4: Diagram presenting the constraints for efficiency increase (The dash line indicates weak causal relationship; Abdel Elmontalbe, 2006)

The main reason behind this is adverse effects on soil and farmer's welfare. The reuses of water have an adverse impact on different aspects including:

Environmental impacts: There are negative environmental effects, which might emerge with efficiency increase due to drainage water reuse. These negative effects include the extensive accumulation of salt in the soil and the degradation of groundwater quality. The review intends to introduce briefly the environmental aspects of soil salinity before the discussion of region-specific constraints.

Soil salinization is the process that "results from the accumulation of free salts to such an extent that leads to the degradation of soils and vegetation" (Hillel, 2000). The problem of soil salinization in arid conditions emerges with irrigation and agricultural practices. Soils naturally containing sizeable amounts of salt are enriched with salt from other sources such as the irrigation water and fertilizers (Hillel, 2000; Umali, 1993; Adamo and Crews-Meyer, 2006). There are other factors that influence the salinity of soil as for example seawater intrusion, but the main focus will be only on salinity elements that can be linked to irrigation.

The irrigation water with its content of salt added to the soil can cause the increase in soil salinity levels if there is no sufficient leaching (Figure 2.4). At the root zone of plant salt concentration raises imposing unfavorable conditions to grow. As the osmotic pressure surrounding the root zone is high, extraction of water becomes more troublesome for plant and requires more metabolic energy. To prevent plants from damage, the soil must be sufficiently leached. Moreover, in saline soils; soil flocculation can occur as a result of increased salt concentration. The clay particles conglomerate together and forming flocks hinders plants' root to access the oxygen (Hillel, 2000). The negative relation between saline soils and plant survival is reflected in declined crop yields. As the DWIP (1997) reports there is a strong negative correlation between the Electrical Conductivity (EC) as it used as an

indicator of soil salinity and is measured in μS/cm micro-Simens per centimeter of soil and crop yield of rice and maize, moderate negative correlation for cotton and low negative correlation for wheat.

In Egypt the irrigation water shows large uptake of salt. For example the salinity of irrigation water at the Aswan dam accounts 400 μS/cm while already in Cairo it raises up to 550 μS/cm (Keller, 1992; Abdel Elmontalbe, 2006). The increment of water salinity partly is determined by salt contributions from domestic and industrial discharges but it is considerably low in comparison to the salt leached from drainage or groundwater. Reuse of water again and again mountains the concentration of salts in water. So in Fayoum fresh water salinity averages 500-700 μS/cm (DWIP, 1997), while in drainage catchments the salinity of water varies between 1560-3.12 μS/cm. In the Delta, near the coast, the concentrations of drainage water increases significantly to the values up to 7800-9360 μS/cm (high salinity partly is determined by presence of saline groundwater in the north (MWRI, 2005). Comparisons are described in Table 2.1.

Table 2.1: Classification of water quality according to the total salt concentrations

Water	Electrical Conductivity in μS/cm	Category
Fresh water	< 600	Drinking, irrigation
Slightly brackish	600-1500	Irrigation
Brackish	1500-3000	Irrigation with caution
Moderately saline	3000-8000	Primary drainage
Saline	8000-15000	Secondary drainage, saline groundwater
Highly saline	14000-45000	Very saline groundwater
Sea Water	>45000	Sea water

There is a clear tendency of declining yield as quality of irrigation water is deteriorated. Table 2.2 presents the average crop yields in the Delta for different types of irrigation water. The effects on crop production levels are sizable. The rice yields are subjected to 40 % decline in comparison to the production rates from the land irrigated with fresh water. For wheat this figure is 29 % and for cotton is 23 %.

Irrigation with marginal quality water requires strict adjustment of irrigation practices to the soil and crop in order to avoid negative impacts on crop yields (Diaz et al., 1983) The production losses and increase in inputs can bring to zero the benefits from water reuse on the large scale as the use of drainage water for irrigation requires more frequent applications and weeding, therefore more labor force is needed and production costs increase (DWIP, 1997). The effects on crop productivity are very important as the Egyptian farmer's practice subsistence farming and produced crop is mainly sufficient only for meeting the family needs (Figure 2.5).

Table 2.2: Average crop yields in the Delta for different types of irrigation water

Crop	Yield irrigated with Fresh Water (EC_{iw}– 720 μS/cm, EC_e – 2270 μS/cm)	Yield irrigated with Mixed Water (EC_{iw} – 1470 μS/cm, EC_e– 3010 μS/cm)	Yield Irrigated with Drainage Water (EC_{iw} – 2610 μS/cm, EC_e– 3930 μS/cm)
Cotton	840	760	650
Wheat	2750	2420	2000
Maize	2030	1920	1750
Rice	3500	3000	2100
Clover	6340	5840	4140

Source: DWIP, 1997

ECiw-Electrical conductivity of irrigation water, ECe-Electrical conductivity of soil

Social impacts: The drainage water reuse has negative impact on farmers' income. As shown in Figure 2.5, low quality drainage water causes the salinization of land, therefore decrease in

yields and increase of inputs lower down the net returns. This reduces farmer's ability to invest; therefore farm inputs are declining negatively affecting the crop production rates. As DWIP report (1997) states the average net return per square kilometer for crop mixes on lands irrigated with drainage water is 80 % of the net returns from the fields irrigated with fresh water.

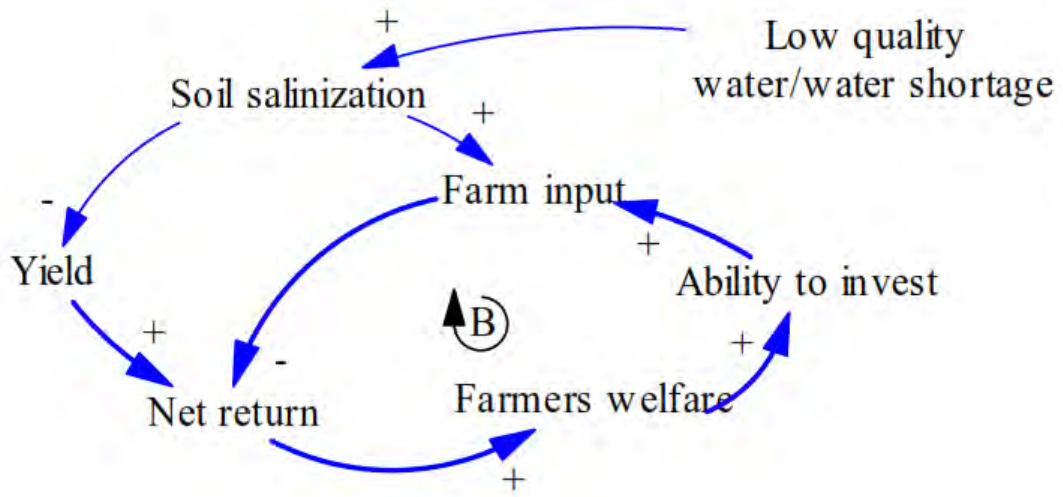

Figure 2.5: Causal Loop Diagram for the impacts of low quality water reuse and water shortage conditions on welfare. (Under farm input is considered any kind of input needed for farm production purposes; based on Tiwari and Dinar, 2002).

The drainage water reuse has some positive effect on reduction of fertilizer requirements for crops (as it contains the fertilizers residues from previous use) but in this case the careful and precise ~~land~~ management of land is needed to avoid salinity.

In the concluding remarks of the final report of DWIP, (1997) is stated " farmers using the drainage water will be more at risk that those using mixed water and therefore with require more technical assistance and other support mechanism". It goes further by suggesting the establishment of compensation fund financed by fresh water users (DWIP, 1997). So the small farmers, which constitute the majority of farmers in Egypt, are vulnerable to the impacts from irrigation water quality. In regard to soil salinity much the same applies to the

under-irrigation and water shortage conditions. The applications of lower water quantity results in poor leaching of salts and further salinization of soil with all its negative outcomes for farmer.

Health impacts: Another factor, which makes reuse cautious, is the concentrations of pathogens in drainage water. As the bacteriological and parasitological examinations of fresh, mixed irrigation water and drainage water show the concentration of fecal coliform bacteria and parasitic eggs usually exceed standards set by World Health Organization (WHO) for unrestricted use of irrigation water. According to the DWIP, (1997) study only 15 % of drainage irrigation water comply WHO guidelines for unrestricted use with regard to fecal coliform bacteria and parasite eggs concentration in water, where the figures for fresh water are not better either; only 22 % of fresh water meets the WHO requirements (DWIP, 1997). WHO standard is 100 Most Probable Number (MPN)/100 ml (MWRI, 2005).

Other concerns, in respect of water reuse but from non-irrigation sources, are evoked by waste water reuse with its high concentrations of nutrients, heavy metals, toxic materials that can enter food chains. Wastewater contain also salt and thus pose the danger of soil salinization as well (Umali, 1993).

The constraints for technical efficiency improvement are the same as the increase of soil salinity problems. As the on farm irrigation efficiency increases, the applied water on field decreases which makes leaching non-sufficient enough and can lead to the soil salinization (Perry, 1999; Hillel, 2000; Bazza and Ahmad, 2003). This point is used for justification of over-irrigation and low farm efficiency. However, the precise application of water to the crops and careful management of land could probably ease a problem

2.6. Geographical information system and agriculture practice

Geographical information systems (GIS) are systems for the storage, analysis and presentation of spatial data (Bregt, 1997). A combination of GIS and simulation models is highly relevant for agriculture practices. Currently only static one – or two – dimensional simulation models can be fully supported by commercial GIS systems (Buick, 1997). GIS based modeling of an agro-ecosystem is expected to give a new approach in order to provide agricultural managers with a powerful tool to simultaneously assess the effect of farm practices on crop production in addition to soil and water resources (Priya et al., 1998). At present, most of the crop models provide location-specific information. Therefore, development of spatially or raster based biophysical crop model will help greatly in understanding many intricacies of modeling large areas (Gage et al., 2000).

GIS is used in many applications as a tool for spatial analysis (Nehme and Simões, 1999). Consequently, they are used to support spatial aspects of knowledge based systems for land evaluation. This information system helps support the decision making procedure and can be a powerful tool for land use planning and environmental management. The collection and management of data from site-specific crop and soil management systems will soon overwhelm the standard farm record system (Reetz and Westervelt, 2004). GIS provides a systematic approach to managing the large amounts of data accumulated, along with the tools necessary for analysis and interpretation.

In theory, spatial modeling moves the derived relationships in space or time to determine the "optimal" actions, such as the blend of phosphorous, potassium and nitrogen to be applied at each location in the field (Berry, 1999; Mantzafleri et al., 2009). In current practice, these translations are based on existing science and experience without a direct link to data analysis of on-farm data. For example, a prescription map for fertilization is constructed by noting the

existing nutrient levels (condition), then assigning a blend of additional nutrients (action) tailored to each location forming an if-(condition)-then-(action) set of rules (Berry, 2005). The issues surrounding spatial modeling are similar to data analysis and involve the validity of using traditional "goal seeking" techniques, such as linear programming or genetic modeling, to calculate maps of the optimal actions.

In a GIS, one can use regression to derive a production function relating map variables such as the links among a map of corn yield and maps of soil nutrients like analyzing thousands of sample plots (Berry, 1998). However, technical concerns, such as variable independence and autocorrelation, have yet to be thoroughly investigated. Statistical measures assessing results of the analysis, such as a spatially responsive correlation coefficient, await discovery and acceptance by the statistical community, let alone the farm community.

The modeling capabilities of GIS can be combined with remotely sensed landscape imagery to evaluate the effects of management practices and to assist resource managers and public decision makers in making informed decisions (Ortigosa et al., 2000).

Digital maps are constructed using a map model whereby values are represented as a set of blocks, the centers of which are located on a grid (Whelan et al., 2001). Any form of spatial prediction is based on the premise that observations made in close proximity to each other are more likely to be similar than observations separated by larger distances. This is the concept of spatial dependence (Walter et al., 2001). The process of spatial prediction requires that a model of the spatial variability (spatial dependence) in a data set be constructed or assumed so that estimates at the unsampled locations (prediction points) may be made on the basis of their location in space relative to actual observation points (Vaughan and suarez, 1998). The prediction technique of choice for map production in precision agriculture will depend on the expected use of the map.

There are many incentives for applying a crop model on a regional scale, that is, over an area larger than that for which it has been developed (Faivre et al., 2004). This is referred to as "spatializing" a crop model. These large areas can have very heterogeneous soil, climate and management practices.

Consequently, spatializing a crop model can raise serious problems. One set arises from the fact that the basic concepts, hypotheses and validity domains of crop models, are derived on the plot scale and may not apply on a larger scale. Another set arises from the lack of adequate and sufficient data to run the model on a regional scale.

Spatial Analysis extends the basic set of discrete map features of points, lines and polygons to surfaces that represent continuous geographic space as a set of contiguous grid cells (Berry, 2005). The consistency of this grid-based structuring provides a wealth of new analytical tools for characterizing “contextual spatial relationships”, such as effective distance, optimal paths, visual connectivity and micro-terrain analysis. In addition, it provides a mathematical/statistical framework by numerically representing geographic space. Traditional Statistics is inherently non-spatial as it seeks to represent a data set by its typical response regardless of spatial patterns. The mean, standard deviation and other statistics are computed to describe the central tendency of the data in abstract numerical space without regard to the relative positioning of the data in real-world geographic space (Berry et al., 2005).

Spatial statistics, on the other hand, extends traditional statistics on two fronts. Firstly, it seeks to map the variation in a data set to show where unusual responses occur, instead of focusing on a single typical response (Gang et al., 1999). Secondly, it can uncover “numerical spatial relationships” within and among mapped data layers, such as generating a

prediction map identifying where likely customers are within a city based on existing sales and demographic information (Sadler et al., 2002).

Crop water requirement in term of crop yield is influenced by soil-related, anthropogenic, topographic, biologic, and meteorological factors that are highly spatially variable (Corwin, 2005). Because of the complex spatial interaction of these factors, GIS and other advanced information technologies (e.g., spatial statistics, remote sensing, and crop-water response models) are essential tools in water saving measures in irrigation agriculture.

2.7. Remote sensing and agriculture practice

Remote sensing has gained a lot of interest as a potential management tool for natural resource and agricultural practices (Morgan and Ess, 1997). Several applications have been developed to use remotely sensed data to infer both plant and soil characteristics (Barnes et al., 1996). Images from satellites and aerial photographs may allow the decision maker experts to quickly view crops of entire farm and decide which areas need further management (Manakos et al., 2000). The information developed from remote sensing data must be accurate. It must be shown that measured reflectance can be correlated with crop properties of field conditions that will affect crop yield.

Three approaches of development appear to be emerging in the application of remote sensing and site-specific agriculture in Egypt (Shalaby and Tateishi, 2007).

1- In the first approach, multi-spectral images are used for anomaly detection; however, anomaly detection does not provide quantitative recommendations that can be directly applied to precision farming.
2- A second approach involves correlating variation in spectral response to specific variables such as soil properties or nitrogen deficiency. In the case of nitrogen

deficiency for example, once site-specific relationships have been developed, multi-spectral images can then be translated directly to maps of fertilizer application rates (Barnes et al., 2001). Nitrogen nutrition is known to influence leaf chlorophyll concentration and greenness and through the use of remote sensing it is possible to estimate the nutritional status of a crop to assist in establishing more accurate side-dress nitrogen rates. The quantity of fertilizer nitrogen required by a crop is determined by an integration of soil and climatic factors and their effects on crop growth and nitrogen losses (Jennifer and Varco, 2004 and Bronson et al., 2005). Due to the highly transient nature of soil available nitrogen, there is no simple or routine soil test that can be used to predict availability and fertilizer needs and crop models have been shown to be inaccurate in predicting nitrogen nutrition requirements of cotton across soils (Varco et al., 2000). Nitrogen itself does not reflect or absorb, but significantly large amounts of nitrogen combine with the chlorophyll proteins in the leaves of plant. Therefore, the nitrogen content can be derived indirectly via chlorophyll content, which has characteristic absorption features in the visible wavelength region (400-700 nm) A strong relationship exists between leaf chlorophyll and nitrogen content in several plant species – maize and wheat for example (Oppelt and Mauser, 2003).

3- The third approach is converting multi-spectral data to quantitative units with physical meaning (such as Leaf Area Index or surface temperature) and integrating this information into physically based growth models (Smith et al., 2005). Based on later approach, a major part of the framework of the research study will follow and additional literature will be stated.

A sequence of remotely sensed images over time can provide information about crop growth and spatial variation within fields (Sonka et al., 1997). Detailed, spatially distributed multi-

temporal information in visual form is not readily obtainable from conventional crop management systems or from site-specific crop management methods (Byrne et al., 1980). Remote sensing images show spatial and spectral variation resulting from soil and crop characteristics. In general, remote sensing offers a fully pictorial representation of an area that improves the orientation of a farmer and his perception to traditional point measurements, since the experts are able to identify heterogeneities in their spatial context (Jürgens, 2000).

Remotely sensed images provide a visual method for observing the effects of managed inputs such as fertilizer and cultural practices such as tillage (Casady and Palm, 2002). They are also useful in understanding the impact of environmental factors such as drainage problems or pest infestations. In contrast to yield maps, which affect only future decisions, remotely sensed images may be collected several times throughout the growing season and allow timely management decisions to correct problems or deficiencies in the current crop. For this reason, remote sensing technology adds an important dimension to site-specific management of crops (Yuan et al., 1998; 2005).

The reflectance value for each pixel is dictated by contributions of all the surfaces within the pixel's coverage and the characteristics of the sensor, namely the spectral bands (Dalsted et al., 2003; Zhou et al., 2008). For example, a pixel could contain both bare soil and a growing crop within it. If this pixel encompasses 40 % bare soil with a relative reflectance value of 20 % and 60 % vegetative cover with a relative reflectance value of 60 %, then the average reflectance value for the pixel should be about 44 % (0.4x20 + 0.6x60). Pixels containing two or more elements are classified as mixed pixels. A critical component in selecting remote sensing products is matching the pixel resolution to the amount of acceptable mixing. It is important to realize that most pixels, regardless of resolution, are affected by spectral mixing. Pixel mixing can diminish the ability to accurately map boundaries of abnormalities.

2.7.1. Estimation of evapotranspiration

Evapotranspiration (ET) has been long been recognized as the most important process that plays an essential role in determining exchanges of energy and mass between the hydrosphere, atmosphere and biosphere (Sellers et al., 1996; Olioso et al., 1999). In agriculture, it is a major consumptive use of irrigation water and precipitation on agricultural land. Any attempt to improve water use efficiency must be based on reliable estimates of ET, which includes water evaporation from land and water surfaces and transpiration by vegetation. ET varies regionally and seasonally according to weather and wind conditions (Hanson, 1991). Understanding these variations in ET is essential for managers responsible for planning and management of water resources especially in arid and semi-arid regions of the world where crop water demand generally exceeds precipitation and requires irrigation from surface and/or groundwater resources to meet the deficit.

At a field scale, ET can be measured over a homogenous surface using conventional techniques such as Bowen Ratio (BR), Eddy Covariance (EC) and lysimeter systems. However, these systems do not provide spatial trends (or distribution) at the regional scale especially in regions with adventive climatic conditions. Remote sensing based ET models are better suited for estimating crop water use at a regional scale (Allen et al., 2007). Numerous remote sensing-based ET algorithms that vary in complexity are available for estimating magnitude and trends in regional ET. The following section discusses remote sensing based regional ET prediction algorithms and their limitations, data needs and availability, knowledge gaps, and future opportunities and challenges with respect to agriculture.

2.7.2. Remote sensing based ET algorithms

Remote sensing has long been recognized as the most feasible means to provide spatially distributed regional ET information on land surfaces (Park et al., 1968; Jackson 1984; Choudhury et al., 1987). The use of remote sensing to estimate ET is presently being developed along two approaches: (a) land surface energy balance (EB) method that uses remotely sensed surface reflectance in the visible (VIS) and near-infrared (NIR) portions of the electromagnetic spectrum and surface temperature (radiometric) from an infrared (IR) thermal band, and (b) Reflectance based crop coefficient (generally denominated K) and reference ET approach where the crop coefficient (Kcr) is related to vegetation indices derived from canopy reflectance values (Ormsby et al., 1987). The first approach is based on the rationale that ET is a change of the state of water using available energy in the environment for vaporization (Su et al., 2005). Remote sensing based EB models convert satellite sensed radiances into land surface characteristics such as albedo, leaf area index, vegetation indices, surface emissivity and surface temperature to estimate ET as a ‘‘residual’’ of the land surface energy balance equation:

$$LE = R_n - G - H \qquad \text{Eq. 2.1}$$

Where, *Rn* is the net radiation resulting from the budget of short and long wave incoming and emitted radiation respectively, *LE* is the latent heat flux from evapotranspiration, *G* is the soil heat flux, and *H* is the sensible heat flux (all in W m^{-2} units). *LE* is converted to ET (mm h^{-1} or mm day^{-1}) by dividing it by the latent heat of vaporization (λv; ~ 2.45 MJ kg^{-1}) and an appropriate time constant. R_n and *G* may be estimated locally using meteorological measurements (Allen et al., 1998) and regionally by incorporating spatially distributed reflected and emitted radiation (Jackson et al. 1985; Lagouarde et al., 2002) as:

$$R_n = (1 - \alpha) R_s + \varepsilon_a \sigma T_a^4 - \varepsilon_s \sigma T_a^4 \qquad \text{Eq. 2.2}$$

Where α is surface albedo, R_s is incoming short wave radiation (W m^{-2}) measured with pyranometers or calculated using the angstrom formula based on the solar constant, location and time of the year (Allen et al., 1998) or by using the solar constant, the cosine of the solar incidence angle, the inverse squared relative earth–sun distance, and atmospheric transmissivity based on the area of interest (image) ground elevation respect to mean sea level (Allen et al. 2007), σ is the Stefan–Boltzmann constant (5.67 E^{-08} W m^{-2} K^{-4}), ε is emissivity and T temperature (K) with subscripts ''*a*'' and ''*s*'' for air and surface, respectively. T_s is the remotely sensed radiometric surface temperature which is obtained after correcting the sensor brightness temperature imagery for atmospheric effects and for surface emissivity considering, for example, procedures by Hipps (1989), Brunsell and Gillies (2002) and Chen et al., (2005). The surface emissivity correction is performed assuming typical bare soil and fully vegetated surface emissivities of 0.93 and 0.98, respectively, and the fractional vegetation cover from the scaled normalized difference vegetation index (NDVI). Alternatively, surface albedo for vegetated areas is generally estimated using the Brest and Goward (1987) model. This model is based on the red (R) and NIR band reflectance:

$$\alpha = 0.512\,\mathrm{R} + 0.418\,\mathrm{NIR} \qquad \text{Eq. 2.3}$$

The emissivity of air can be obtained from the Brutsaert (1975) equation:

$$\alpha = 0.0172\,(\frac{e_a}{T_a})^{1/7} \qquad \text{Eq. 2.4}$$

Where e_a is actual vapor pressure measured in (kP_a). *G* is commonly estimated as a fraction of R_n depending on leaf area index (LAI) or NDVI. Chavez et al. (2005) found that a combination of a linear and a logarithmic model could estimate *G* for soils planted to corn and soybean crops in central Iowa (r^2 = 0.73):

$$G = R_n\ (0.3324 - 0.024\ \text{LAI})(0.8155 - 0.3032\ \text{LN}\ (\text{LAI}))$$ Eq. 2.5

Where, *H* is then estimated using the aerodynamic surface–air temperature gradient (or combination of gradients) and aerodynamic resistance (Kalma and Jupp, 1990), where generally radiometric temperature (T_s) has been used as a surrogate for aerodynamic temperature (T_o). In the second approach, R and NIR reflectance measurements are used to compute a vegetation index such as NDVI (Rouse et al., 1974) or the soil adjusted vegetation index "SAVI" (Huete, 1988; Huete et al., 2008), and the vegetation index is then used in place of calendar days or heat units to drive or scale the crop coefficient. The reference *ET* is then computed using local meteorological measurements of incoming solar radiation, air temperature, relative humidity or dew temperature, and wind speed.

Some early applications of remote sensing based EB models include Brown and Rosenberg (1973), Brown (1974), Stone and Horton (1974), Idso et al. (1975), Heilman et al., (1976), Verma et al., (1976), Kanemasu et al., (1977), and Jackson et al., (1977). Most of these studies used airborne scanners as first demonstrated by Bartholic et al., (1972). Price (1982), Seguin and Itier (1983), and Taconet et al., (1986) were among some of the first to use thermal data obtained from satellites to estimate ET. They proposed to use surface temperature derived from remotely sensed data to estimate regional ET in the form:

$$LE = R_n - G - \frac{\rho_a\, C_p\, (T_s - T_a)}{r_{ah}}$$ Eq. 2.6

Where ρ_a is air density (kg m^{-3}), C_p is specific heat capacity of the air (J $kg^{-1}K^{-1}$), and r_{ah} is aerodynamic resistance for heat transfer (s m^{-1}). T_s and T_a are expressed in K. For example, Brown and Rosenberg (1973) and Brown (1974) used the surface radiometric temperature and air temperature difference, ($T_s - T_a$), and the aerodynamic resistance (r_{ah}) to estimate *H* where the canopy or surface temperature was obtained from remotely sensed radiometric

temperature using thermal scanners having a bandwidth mostly in the range of 10–12 μm. Later, Rosenberg et al. (1983) incorporated the term surface aerodynamic temperature (T_o) in the *H* parameter, instead of surface radiometric temperature, considering that the temperature gradient (for *H*) was a gradient between air temperature within the canopy (at a height equal to the zero plane displacement plus the roughness length for heat transfer) and air temperature above the canopy (at a height where wind speed was measured or height for r_{ah}). They indicated that for partially vegetated areas and for water stressed biomass, radiometric and aerodynamic temperatures of the surface were not equal.

Hatfield et al. (1983) evaluated the surface temperature with the energy balance approach at seven locations throughout the United States equipped with weighing lysimeters and ground-based instrumentation. In their study, daily *G* was assumed negligible. Crops were sorghum, clover, tomato and wheat at full cover, and tomato at 80% cover. They concluded that remotely sensed T_s may be used in the EB model to estimate regional ET. Estimated *LE* values, using atmosphere stability corrected aerodynamic resistances, were very closely matched to those measured by the lysimeters. Reginato et al., (1985) refined estimates of R_n using reflected shortwave and emitted long wave measurements as outlined by Jackson et al. (1985). They also used ground-based instrumentation to estimate ET of wheat and achieved good agreement with lysimeters and neutron scattering. Later, Jackson et al., (1987) applied this procedure using an airborne radiometer and compared with Bowen Ratio (BR) measurements for cotton, clover, and wheat with homogenous crop surfaces (full canopy with no contribution from soil background). Comparison of the remote sensing based *LE* estimates for 5 days with BR values resulted in a greatest difference of 12% while errors in daily *ET* estimates were less than 8% for 3 days and 25% on the other two. Moran et al. (1989) and Moran et al., (1996), then applied this procedure using R/NIR (simple ratio) and thermal data

from the Landsat Thematic Mapper (TM) satellite and reported agreement within 12% with the BR and airborne data from Jackson et al., (1987).

Accurate estimates of H are very difficult to achieve, mainly when T_s is used instead of T_o and when atmospheric effects and surface emissivity are not considered properly. In such cases, H prediction errors have been reported to be around 100 W m^{-2} (Cha´vez and Neale, 2003; Matsushima, 2000). Consequently, more recent EB models differ mainly in the manner that H is estimated. These models included the two-source model (TSM; Norman et al., 1995; Kustas and Norman, 1996; Chehbouni et al., 2001), where the energy balance of soil and vegetation are modeled separately and then combined to estimate total LE, surface energy balance algorithm for land (SEBAL; Bastiaanssen et al., 1998; Wu et al., 2010) that uses hot and cold pixels to develop an empirical temperature difference equation, and surface energy balance index (SEBI; Menenti and Choudhury, 1993) based on the contrast between wet and dry areas.

Modern models include multifaceted surface energy balance index (S-SEBI; Roerink et al., 2000); surface energy balance system (SEBS; Su, 2002); the excess resistance (kB^{-1}), (Kustas and Daughtry 1990; Su, 2002); the aerodynamic temperature parameterization models proposed by Crago et al., (2004) and Cha´vez et al., (2005); Beta (β) approach (Chehbouni et al., 1996); and recently ET mapping algorithm (ETMA; Loheide and Gorelick, 2005) and Mapping Evapotranspiration with Internalized Calibration (METRIC TM; Allen et al., 2002, 2005, 2007). The sections below discuss the main SEBS model in detail.

SEBI, SEBS and S-SEBS: SEBI, proposed by Choudhury and Monteith, (1988) and Menenti and Choudhury (1993), is based on the Crop Water Stress Index (CWSI; Jackson et al., 1981; Moran et al., 1994) concept in which surface meteorological scaling of CWSI is replaced with planetary boundary layer (PBL) scaling. It uses the contrast between wet and dry areas

appearing within a remotely sensed scene to derive ET from the relative evaporative fraction (Λ_r). It determines Λ_r by relating surface temperature observations to theoretical upper and lower bounds on the difference between surface and air temperature (Menenti et al., 2003). Evaporative fraction (Λ), as utilized by Bastiaanssen et al,. (1998), is defined as the ratio of latent heat flux to the available energy ($AE = R_n - G$) and is assumed to remain nearly constant during the day.

Surface Energy Balance System (Su, 2002) was developed using the SEBI concept. It uses a dynamic model for thermal roughness (Su, 2001, Su et al., 2001), Bulk Atmospheric Similarity (BAS) (Brutsaert 1999) and Monin–Obukhov Similarity (MOS) theories for regional ET estimation, and Atmospheric Surface Layer (ASL) scaling for estimating ET at local scale. SEBS requires wet and dry boundary conditions to estimate H. Under dry conditions, the calculation of H_{dry} is set to the available energy AE as evaporation becomes zero due to the limitation of water availability and H_{wet} is calculated using the Penman–Monteith parameterization (Monteith 1965, 1981) as:

$$H_{wet} = AE - \frac{\left(\frac{\rho_\alpha C_p}{r_{ah}}\right)\left(e_s - \frac{e}{7}\right)}{1+\frac{\Delta}{\gamma}} \qquad \text{Eq. 2.7}$$

Where e is the actual vapor pressure (kP_a), e_s is the saturation vapor pressure (kP_a), c is the psychrometric constant ($kP_a\ {}^oC^{-1}$), γ is the rate of change of saturation vapor pressure with temperature ($kP_a\ {}^oC^{-1}$) and r_{ah} is the bulk surface external or aerodynamic resistance ($s\ m^{-1}$) estimated under the assumption that the bulk internal resistance is zero. Finally, relative evaporative fraction (Λ_r), evaporative fraction (Λ) and LE for each pixel in the remote sensing image is calculated as:

$$\Lambda_r = 1 - \frac{H - H_{wet}}{H_{dry} - H_{wet}} \qquad \text{Eq. 2.8}$$

$$\Lambda = \frac{\Lambda_r\,(R_n - G - H_{wet})}{R_n - G} \qquad \text{Eq. 2.9}$$

$$LE = \Lambda\,(R_n - G) \qquad \text{Eq. 2.10}$$

The evaporative fraction ($\Lambda = LE/(R_n - G)$) is used in the estimation of *LE* because it is assumed to remain constant throughout the day and can be obtained for short periods and be used for *LE* extrapolation to daily values. Brutsaert and Sugita, (1992) presented the assumption that the partitioning of available energy (*AE*) into *H* and *LE* is constant (self-preservation of the available energy partitioning) or that the evaporative fraction remains almost constant during the daytime. Zhang and Lemeur, (1995) added that the evaporative fraction indicates how much of the available energy is used for ET and that the assumption that the instantaneous Λ is representative of the daily energy partitioning, is an acceptable approximation for clear-sky conditions. Crago, (2000) concluded that the Λ has the tendency to be nearly constant during daytime, permitting the estimation of daytime evaporation from one or two estimates of the evaporative fraction during the middle of the day at the satellite overpass time.

Su et al., (2005) evaluated SEBS with two independent, high-quality datasets that were collected at a field scale during the Soil Moisture Atmosphere Coupling Experiment (SMACEX) in the Walnut Creek agricultural watershed near Ames, IA, USA. Meteorological and EC measurements from ten locations within the watershed were used to estimate and compare fluxes during a period of rapid vegetation growth and varied hydrometeorology. Results indicated that ET estimates from the SEBS were close to 85–90% of the measured ET values from EC systems for both corn and soybean surfaces. In the same study, regional fluxes were calculated using Landsat enhanced thematic mapper plus (ETM+) data for a clear day during the field experiment. Results at the regional scale showed that ET prediction accuracies were strongly related to crop type with improved ET estimates for corn surfaces

compared to those of soybean. Differences between the observed and predicted ET values were approximately 5%. Further, McCabe and Wood (2006) used thermal data from Landsat ETM+ (60 m), advanced spaceborne thermal emission and reflection radiometer (ASTER; 90 m), Advance Across Track Scanner Radiometer and Moderate Resolution Imaging Spectrometer (AATSR and MERIS; 1,000 m) sensors to independently estimate ET using SEBS. The main limitation with the SEBS is that it requires aerodynamic roughness height. Currently, several methods are available to estimate this variable using wind profile, vegetation index, and crop height (measured in m) or by assigning nominal values based on the land use to conduct results more accurately.

S-SEBI (Roerink et al. 2000) is a simplified method derived from SEBS to estimate surface fluxes from remote sensing data. Consequently, this model is based on Λ and the contrast between the areas with extreme wet and dry temperature, T_{wet} and T_{dry}, respectively. The instantaneous *LE* is calculated as:

$$LE_i = \Lambda_i \, (R_n - G) \qquad \text{Eq. 2.11}$$

Where the subscript ''*i*'' means instantaneous. Λ_i is expressed as:

$$\Lambda_i = \frac{T_{dry} - T_s}{T_{dry} - T_{wet}} \qquad \text{Eq. 2.12}$$

Λ_i is assumed constant through the day. Daily *LE* (LE_d) is calculated as:

$$LE_d = \frac{LE_i \, R_{n,d}}{(R_n - G)_i} \qquad \text{Eq. 2.13}$$

Where $R_{n,d}$ is daily net radiation (W m^{-2}), can be estimated from a known relationship at solar noon as:

$$C_{d,i} = \frac{R_{n,d}}{R_{n,i}} \qquad \text{Eq. 2.14}$$

Where $R_{n,i}$ is the instantaneous net radiation, and $C_{d,i}$ is approximately 0.30 (±0.03) for summer months. Finally, ET can be estimated as:

$$ET_d = \frac{\Lambda_i \, C_{d,i} \, R_{n,i}}{\gamma^{\nu}} \qquad \text{Eq. 2.15}$$

The disadvantage of this method may be that it requires extreme T_s values, which cannot always be found on every image. However, the major advantages are that it is a simpler method that does not need additional meteorological data and it does not require roughness length as in the case of SEBS. Go´mez et al., (2005) used the Λ concept based on S-SEBI for estimating ET_i and to extrapolate it to ET_d. The method was applied using airborne sensor: PolDER (Polarization and Directionality of Earth Reflectance) and a thermal camera. Validation with a BR system showed *LE* estimation error of 26% and 1 mm day^{-1} for ET_d over corn, clover, wheat and sunflower crops.

2.8. Land use land cover in Nile Delta

Most of the Egyptian agricultural land is located in Nile Delta region. Therefore urban encroachment and land degradation are the main driving forces of land cover changes in Nile Delta region. Egyptian government is demanding to control the urban encroachment and the loss of agricultural land in Nile Delta throughout applying an effective horizontal urban expansion and reclaim more land along the desert areas and near the fringes of the Nile delta (Shalaby, and Gad, 2010). The government aims also to redirect the loss of agricultural land driving forces away from the old and highly productive agricultural land of the Nile Delta (Springborg, 1979).

Applications of change detection and monitoring of LULC vary and are useful in many fields related to: a) land degradation and desertification (Adamo and Crews-Meyer, 2006; Gao and

Liu, 2010), b) urban sprawl (Shalaby and Tateishi, 2007) and c) urban landscape pattern change (Batisani & Yarnal, 2009; Dewan and Yamaguchi, 2009).

The most common practice of Remote sensing data analyses are anomaly detection, quantification, and mapping of LULC patterns and changes due to the fact of its availability and its high degree of accuracy (Chen, et al., 2005; Lu, et al., 2004; Geymen and Baz, 2008; Abd El-Kawy et al., 2011). Several techniques for accomplishing change detection have been formulated, applied and evaluated. The common principle method for the detection of LULC change is to compare two or more successive imageries covering the same area at different dates of acquisition. Change detection generally employs one of two basic methods: a) pixel-to-pixel comparison and b) post-classification comparison (PCC) (Lu et al., 2004).
The PCC method is the most accurate change detection technique that detects land cover changes by comparing independently the classification maps from different dates (Singh, 1989; Yuan, et al., 1998). Temporal data are independently classified, therefore direct comparability do not require any further adjustment (Coppin, et al., 2004; Rivera, 2005; Singh, 1989; Warner and Campagna, 2009; Zhou, et al., 2008). The PCC method has the additional advantage of indicating the nature of changes thematically (Mas, 1999; Yuan, et al., 2005).

The necessity for evaluating the magnitude and pattern of different land cover types is a must for projecting the future of water resources and land development especially when the major land cover in the study area is water dependent (agricultural land). Remote sensing data in form of satellite images, in conjunction with geographic information systems (GIS), has been widely applied and been recognized as a powerful and effective tool in detecting of land cover changes (Chen et al., 2005; Jensen, 1996; Lu et al., 2004; Geymen and Baz, 2008; Wang and Xu, 2010).

2.9. Forecasting of daily evapotranspiration

One definition of a time series is that of a successive record of specific parameters observation on predetermined time intervals. Time series are analyzed in order to understand the underlying structure and function that produce the observations. Understanding the theoretical explanation of a time series analysis, allows a mathematical model to be developed to explain the data trend in such a way that monitoring, simulation, prediction, assessment and management can occur (Box and Jenkins, 1976; Brockwell and Davis, 2001; Box et al., 2008; Sentas and Psilovikos, 2010).

It is assumed that a time series data set has at least one systematic pattern. The most common patterns are trends and seasonality. Trends are generally linear or quadratic. To find out trends, and/or moving averages regression analysis is often used. Specifically for trends, they can be detected using the Spearman's non parametric criterion, the Kendall criteria and criteria for trace sudden trend (Psilovikos et al., 2009). Seasonality is a trend that repeats itself systematically over time (Box and Jenkins, 1976; Vandaele, 1983). A second assumption is that the data exhibits enough of a random process so that it is hard to identify the systematic patterns within the data. Time series analysis techniques often employ some type of filter to the data in order to dampen the error. Other potential patterns have to do with lingering effects of earlier observations or earlier random errors (Gouveia and Fletcher, 2000; Kocak et al., 2000; Kyriakidis and Journal, 2001).

Time series analysis became very complex and unstable if the consequent time series observation is dependent upon a previous observation (Box and Jenkins 176; Box et al., 2008), and often it is influenced by more than one previous observation. Random error is also influential from one observation to another. These influences are called autocorrelation dependent relationships between successive observations of the same variable and have the

same unstable influence on the time series analysis (Box et al., 2008; Chen et al., 2009). The estimation of Daily evapotranspiration using SEBS model doesn't violate the independency rule. The estimation of daily evapotranspiration of time "*x+1*" is not dependent on the estimation of daily evapotranspiration of time "*x*" and thus time series analysis is still preformed steadily (Diaz et al., 1983; Kumar and Panu, 1997; Kumar, 1998; Roberts, 2003). Thus, the challenge of time series analysis is to extract the autocorrelation elements of the data, either to understand the trend itself or to model the underlying mechanisms more adequately (Hanke and Reitsch, 1995; Smith, 1998; Sentas and Psilovikos, 2010).

Remote sensing is identified as an important tool supporting the management of natural resources and agricultural practices for wider spatial coverage. Thus, daily evapotranspiration models derived from remote sensing techniques were better suit the estimation of crop water use at a regional agriculture scale (Allen et al., 2007; Chowdary et al., 2009; Muthuwatta et al., 2010).

2.10. Vegetation indices

Vegetation indices (VIs) have been widely used to monitor terrestrial landscapes by satellite sensors and have been highly successful in assessing vegetation condition, foliage, cover, phenology (Pettorelli et al., 2005; Kerr, and Ostrovsky, 2003; Huete et al., 2008). VI's are robust satellite data products computed the same way across all pixels in time and space, regardless of surface conditions. As ratios, they can be easily cross-calibrated across sensor systems, ensuring continuity of data sets for long-term monitoring of the land surface and climate-related processes (Edward et al., 2008).

Studies have been carried out by Pettorelli et al., (2005); Kerr, and Ostrovsky, (2003); Huete et al., (2008) demonstrated that VIs have been employed exclusively in estimation of vegetation parameters such as Fractional Vegetation Cover (FC), Leaf Area Index (LAI),

Water Supply Vegetation Index (WSVI), Crop Water Shortage Index (CWSI), and Drought Severity Index (DSI).

Other studies have reported strong linear (Ormsby et al., 1987) or non-linear (Li et al., 2005) relationships between VIs and FC in a variety of landscape types. However, Li et al., (2005) pointed out a potential practical problem in using VIs to estimate FC over mixed scenes. At 100% cover, different plant species may have different VIs due to differences in chlorophyll content and canopy architecture.

Criteria selection of suitability map is arbitrary where the decision will base on them. For this reason Malczewski (1999) proposed Spatial Decision Support System (SDSS) as semi-structured problems solution. SDSS was constructed with Decision Support module available in IDRISI, which is a widespread, friendly and affordable GIS software tool. Multi Criteria Decision Analysis (MCDA) was among the many possible methods and techniques of SDSS (Dragan et al., 2003). The evaluation of land in term of rice cultivation was based on the methods described in Food and Agriculture Organization (FAO; 1976; 1978; 1983; 1984; 1985; 2005) guideline for land evaluation and rice cultivation preferences concerning the study area. The essence of land evaluation for rice cultivation is to compare or match the requirement of each potential land cover with the characteristics of each kind of land. A land unit is obtained by overlaying of the selected theme layers, which has unique information of land qualities for which the suitability is based on (Dragan et al., 2003).

3. Materials

In this chapter materials and available data were used for the water resource management in the Nile Delta are presented to meet the objectives of the current study

3.1. Description of the study area

3.1.1. Location

The Nile delta was selected for this study because it is representative of farming scenarios in the whole ~~of~~ Egypt (different agricultural systems, different soil types, different systems of fertilizer application, irrigation and drainage systems) consequently the research in this study area can be applied to farms in other regions of Egypt. Also, the problems affecting agriculture in this area are a miniature of that of the entire territory (salinity, alkalinity and water logging).

The huge triangle of the Nile Delta extends to the north of Cairo between Lake Mareotis in the west and the Suez Canal in the east, forming a wide arc along the Mediterranean coast bordered by lagoons and sand spits. Formed over millions of years by the deposits of mud brought down by the regular annual inundation and sediment transport and deposition of Nile, it marks the end of the river's long journey, when, emerging from its narrow bed at the edge of the desert plateau, it breaks up into separate arms which pursue their meandering courses towards the sea (Figure 3.1).

This study was carried out in the one of the main agricultural regions of Egypt represented by several Governorates located centrally at 30.07°N, 30.57°E. The Governorates are: Alexandria, Buhayra, Cairo, Daqahliya, Damietta, Gharbiya, Ismailia, Kafr El-Sheikh, Minufiya, Port Said, Qalyubiya, Sharqiya and Suez) and covers around 25,000 km^2 in total representing 2.5 % of the total area of Egypt (Figure 3.2).

The Governorates contribute to the industrial activities by many major industries: dairy products, oil and soap, fodders, milling rice, cotton ginning and spinning, and beets sugar. There are several fish farms in several governorates as well. In an effort to enhance investment, the Prime Minister issued a decree that provides for the establishment of the first industrial zone in Balteem, covering almost 0.48 km^2 and a second industrial zone along the international coastal road in Metobbas over 4.9 km^2.

The governorates host natural protectorates pursuant to the Prime Minister's decree No.1444/1998 stipulating that el Burullus Lake is a natural protectorate which is located on the north east of Rosetta Branch and is bordered in the north by the international coastal road extending from Rafah till Saloum.

Figure 3.1: Administrative boundaries of Egypt.

Figure 3.2: Nile Delta administrative governorates

The study area is highly heterogeneous comprising three main zones i.e., coastal plain, alluvial plain and an interference zone lying in between. This area is considered as an unstable ecosystem due to the active degradation processes resulting from climate, relief, soil properties and inadequate farming system. According to Gao and Liu, (2010), the most active factors of land degradation are; wind, water erosion, water logging, salinization and compaction. On the other hand, land reclamation processes are very active in this study area due to human activities. The land use and land cover systems are agriculture, bare soil, sand area, salt flat, swamps, fish farms, water bodies and urban areas. Figures 3.3-3.9 below shows some different land use and cover forms in the study area.

Figure 3.3: Rice cultivation.

Figure 3.4: Cotton cultivation

Figure 3.5: Maize cultivation.

Figure 3.6: Fish farms.

Figure 3.7: Costal vegetation.

Figure 3.8: Sand dune formation

Figure 3.9: Salt flat formation

3.1.2. Climate

The climatic conditions are characteristic of the eastern Mediterranean, with hot summers and mild winters as indicated on the meteorological data on Figure 3.10. The total average annual precipitation here is about 62mm. The maximum temperature is about 34.3 ^{o}C (in July), the minimum is about 6.6 ^{o}C (in January), and the mean annual temperature is 20.2 ^{o}C. Evapotranspiration is relatively high during the summer. The maximum evapotranspiration is 6.3 mm d^{-1} in June and the minimum 1.6 mm d^{-1} in December. The relative humidity is rather low during summer and high during winter: on average 50% in May and 73% in January. Wind speeds range from 2.1 m/sec in August to 3.7 m/sec in April. Annual average relative humidity is estimated at about 62.59 %. The average sun radiation is ranged from 12MJ m^{-2} in January to 28.9 MJ m^{-2} in June. A summary of the different climatic parameters for the study area is indicated on Table 3.1.

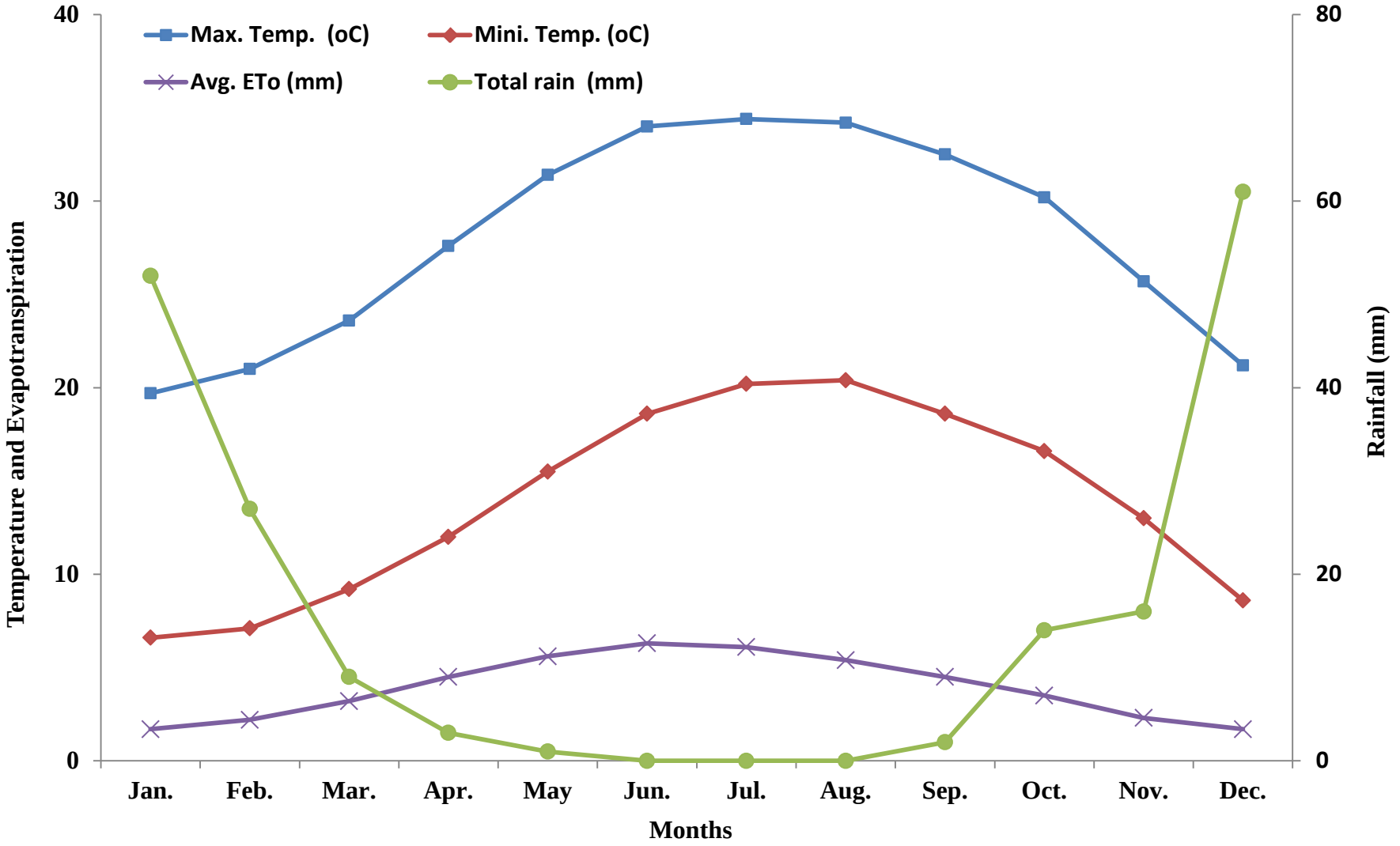

Figure 3.10: Climatologic condition of the study area.

Table 3.1: Climatologic data of the study area (monthly averages in 2008) from the Climatic Centre of Agriculture, Ministry of Agriculture, Giza, Egypt.

Month.	Avg. Temp.	Max. Temp.	Mini. Temp.	Relative humidity	Wind speed	Avg. Sun shine	Avg. radi.	Total rain	Avg. ETo
	(^{o}C)	(^{o}C)	(^{o}C)	(%)	(Knot)	(Hrs)	(MJ/m^2)	(mm)	(mm)
Jan.	13.2	19.7	6.6	71.0	3.0	6.9	12.1	6.7	1.7
Feb.	14.1	21.0	7.1	66.0	3.0	7.4	14.9	5.6	2.2
Mar.	16.4	23.6	9.2	62.0	3.0	8.6	19.3	3.8	3.2
Apr.	19.8	27.6	12.0	55.0	3.7	9.8	23.2	2.0	4.5
May	23.5	31.4	15.5	50.0	3.6	11.0	26.2	2.6	5.6
Jun.	26.3	34.0	18.6	52.0	3.3	12.6	28.9	0.0	6.3
Jul.	27.3	34.4	20.2	59.0	2.7	12.3	28.1	0.0	6.1
Aug.	27.3	34.2	20.4	64.0	2.1	11.4	25.9	0.0	5.4
Sep.	25.6	32.5	18.6	65.0	2.2	10.7	22.8	0.0	4.5
Oct.	23.4	30.2	16.6	65.0	2.7	9.3	17.9	1.8	3.5
Nov.	19.4	25.7	13.0	69.0	2.3	7.7	13.4	4.3	2.3
Dec.	14.9	21.2	8.6	73.0	2.7	6.9	11.4	6.1	1.7

Avg.	(Average)	Max.	(Maximum)
Min.	(Minimum)	Rad.	(Radiation)
ETo	(Evapotranspiration)	Temp.	(Temperature)

3.1.3. Geomorphology

The area displays distinctly different geomorphologic units (Abdel Elmontalbe, 2006):

Fluvio-marine deposits: These flats belong to the alluvial clays of the Nile Delta. They are low lying and therefore poorly drained. The natural drainage is even worse as one move towards the lakes of El-Manzala due to a slight fall in elevation. This has resulted in the

occurrence of vast areas of clay swamps around the shores of the lake. They have a heavy clay texture and are generally very saline.

Young deltaic plains: These deposits consist essentially of dark greyish brown Nile suspended matter due to the presence of micaceous mineral, biotite and hydrated magnetite. These plains are occupied by very fine sand, silt and clay, which were essentially derived from the upstream portions of the Nile.

Old deltaic plains: These constitute the old river terraces of fluvial origin, having a high elevation of up to 30 m above the present Nile level. It consists of almost flat or undulating gravelly loamy and partly fine sandy to silty materials rich in lime.

Sub-deltaic deposits: These deposits are located in small scattered areas. They occur as hillocks generally known as turtle backs. They are found as outcrops of sandy deposits underlying the more recent clay cap.

Aeolian (Windblown) deposits: These "recent" deposits are of local origin. The predominantly coarse wind-blown sand without fine clay and silt usually forms a hummocky area, or sand dunes relief. It also occurs on nearly flat plains. Some of the dunes are still shifting. The wind accumulations on the clay flats consist of fluffy clay, or mixed fluffy sand and clay mate

3.1.4. Geology

The east Nile Delta is occupied by sedimentary rocks belonging to the Quaternary and late Tertiary geological periods. At least seven tributaries flowed across the Nile Delta and discharged in the Mediterranean at varous times during the Middle to Late Holocene (Said, 1981). During the past millennium flow in most Nile distributaries diminished and only two distributaries are still active at the present (Damiatta and Rosetta). The formation of the Nile

Delta was a result of sediment transportation came along the Nile River from its source till the sediment deposition at the Mediterranean forming the Nile Delta. Succession from top to bottom is shown on the Table 3.2.

Table 3.2: Geological formation in the study area

Age	Formation
Holocene	Beach sands
	Young deltaic silts
	Young fluviomarine gypsiferous clay
	Young aeolian sands
	Old Aeolian sands
	Wadi fillings
Pleistocene	Rivers sands
	Old fluviomarine calcareous sand and clay
	Old deltaic sands and gravels
Pliocene	Pyritic clays and gypseous marls
Miocene	Alternating sandstone and marly limestone
Oligocene	Alternating sand and gravels, basalt silts are found

*Source: Abdel Elmontalbe, (2006)

3.1.5. Soils

Egypt has an area of about one million square kilometers. The total agricultural land in Egypt amounts to nearly around 3.5 % of the total area.

Around 10000 km^2 in the irrigated areas suffer from salinization problems, water logging and sodicity. The majority of salt-affected soils are located in the northern-central part of the Nile Delta and on its eastern and western sides. Increased attention is being given to the improvement of salt-affected soils, since they are potentially productive and require less investment, effort, and time for restoring their productivity, than the reclamation of new land. Based on the World Reference Base for Soil Resources, the main Egyptian soil groups are: Arenosols (AR), Calcisols (CL) associated with Gypsisols (GY), Fluvisols (FL), Leptosols

(LP), Regosols (RG), Solonchaks (SC) and Vertisols (VR) as it shown in Figure 3.11 and Table 3.3.

The soil of the Nile Valley and Delta originates from Holocene alluvial deposits, which consisted mainly of dark greyish brown sediments suspended in the Nile, the dark color being attributed mainly to the presence of micacous minerals (biotite) and hydrated magnetite. These deposits accumulated to a considerable thickness because for thousands of years the Nile annually overflowed its banks and deposited its loads. The thickness of the deposits varies according to localities because the river from time to time changed its path, with the result that materials which had been deposited were subsequently scoured away and replaced by fine sand from the river itself (Ball, 1952).

Recent studies carried out by Hanna, (2000) in Egypt sorted out studies started in the mid of last century to simplify the detection of the soils through different decades during 1950 till recent time. Soils in the old-irrigated areas in the Nile valley and delta are described as young alluvium. The depth varies between 5 and 50 meters depending on location relevant to the main course of the river. Textures of the deep, homogenous profiles are generally, light in the south and in fields close to the river and change gradually to heavy northwards and away from the course. Salinities is generally low in the south but increases northwards towards the lakes and the Mediterranean sea, which alkalinity is a characteristic dominating feature.

The northern part of the study area represents large areas of heavy clay soils with low permeability and consequently also a low agricultural production potential. These soils are always threatened by a shallow saline groundwater. In the irrigated area, saline groundwater is a permanent source of soil salinization that causes poor productivity. The groundwater contribution in soil salinization is characterized to a large extent by its fluctuation and solute movement through the soil profile, whether in saturated or unsaturated state. This behavior is

a function of the interaction between climatic and soil environmental conditions. Table 3.4 describes the relevant soil characteristics of the study are.

Table 3.3: Major soil groups and land cover in Egypt

Soil groups/land cover	Percentage of total
Arenosols (AR)	25.80
Calcisols (CL), associated with Gypsisols (GY)	0.37
Calcisols (CL)	9.12
Fluvisols (FL)	0.80
Leptosols (LP)	24.87
Water Bodies	15.44
Regosols (RG)	8.68
Solonchaks (SC)	0.48
Vertisols (VR)	4.85
Soils outside the area surveyed	9.59

*Source: FAO, (1998).

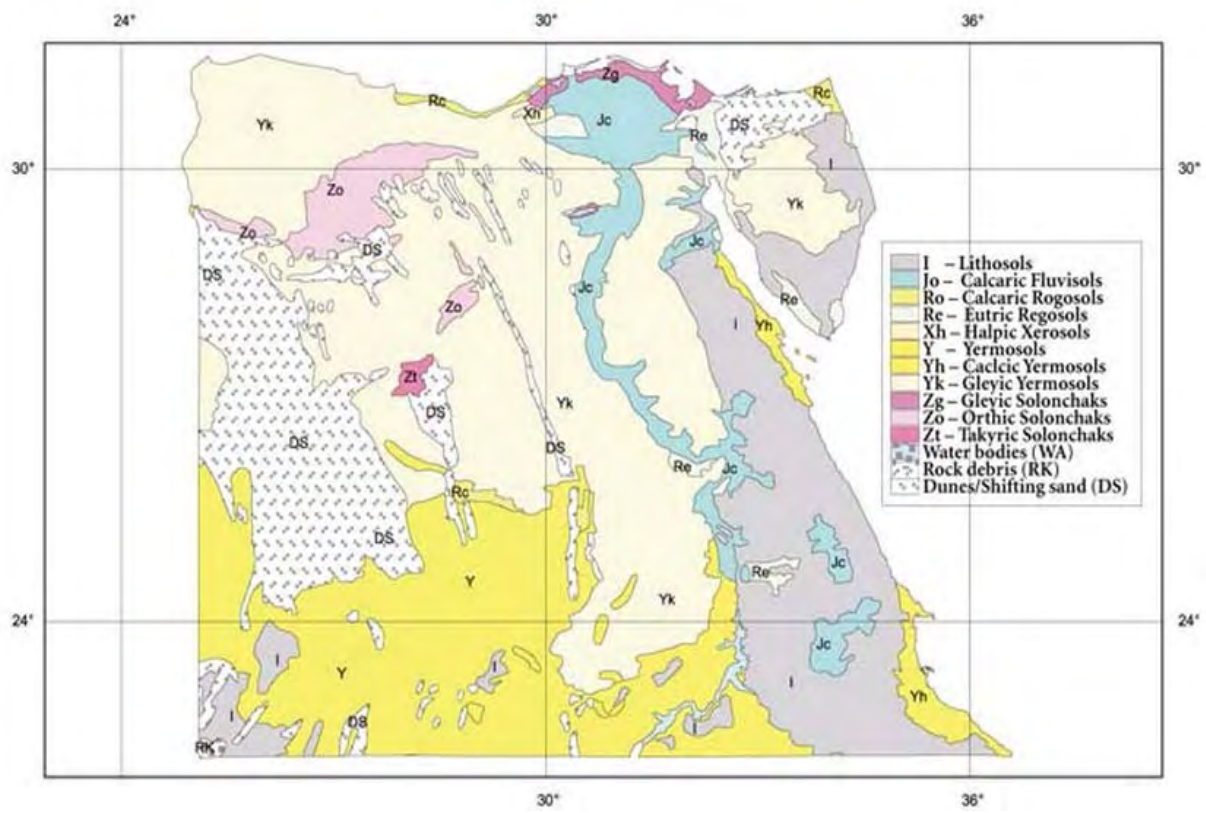

Figure 3.11: Dominant soil map of Egypt (DSME-FAO, 1998).

Table 3.4: Relevant soil characteristics (soil retention capacity)

Soil description	Medium
Maximum rain infiltration rate (mm/day)	40.0
Maximum rooting depth (m)	2.0
Initial soil moisture depletion (% of total available depletion moisture)	50
Initial available soil moisture (mm/m depth)	55.0
Total available soil moisture (mm/m depth)	110.0

*Source: FAO, (1998).

The north eastern Nile Delta could be divided into four soil units' that is, alluvial plain soils, fluvio-marine soils, soils of old deltaic plain and aeolian soils. The description of each is designated below:

Soils of alluvial plains: These are formed from the Nile sediments with its special pattern of sedimentation. These soils follow a certain trend of variation in their technical composition, that is, the soil texture is relatively coarse in areas near the river and becomes finer in the flood plain. Also, ground water depth varies from 70 cm to about 200 cm depending on the distance from the Manzala Lake and the efficiency of the drainage systems.

Soils of fluviomarine plains: The northern part of the area is occupied by fluviomarine marshes and swamps around the El-Manzala Lake. These soils are characterized by a heavy texture, a high water table and are partly cracked and saline. The salt efflorescence covers the surface of most soils and the salt increases with depth. Their surface color ranges between dark grayish brown and very dark grayish brown.

Soils of old deltaic plains: The soils of the old river terraces have a sandy texture with an apparent dominancy of coarse sand fraction or sand clay loam in the upper surface layers.

The lower surface layers are characterized by non-saline to slightly saline, non-alkali with low concentrations of calcium carbonate and gypsum.

Soil of aeolian plains: These soils are deep, lying more than 100 cm below the surface of gently undulating slopes of approximately 3 %. They are of coarse sand, which are soft or slightly hard cemented due to the presence of soft powdery lime and/or gypsum. These soils are also characterized by a light yellowish brown color. The sand is blown out and redeposited in elongated dunes.

3.1.6. Crop growth and rotation

The study area essentially has two major growing seasons in which crops are cultivated under irrigation: summer (May to October) and winter (November to April). Spring and autumn are quite short. When annual crops are grown in the same place year after year, there is a risk that soil characteristics and disease will become a problem, and that plant health and vigor will decline. A better system is to rotate crops around the growing area. The crop rotation benefits both soil and plants. Crop rotation is thus an easy way to control diseases and insects at no extra cost. Crop rotation is a common practice on the study area because of its potential for soil saving. Rotation also reduces fertilizer needs because clover and other leguminous species replace some of the nitrogen which grain crops remove (Abdel Elmontalbe, 2006).

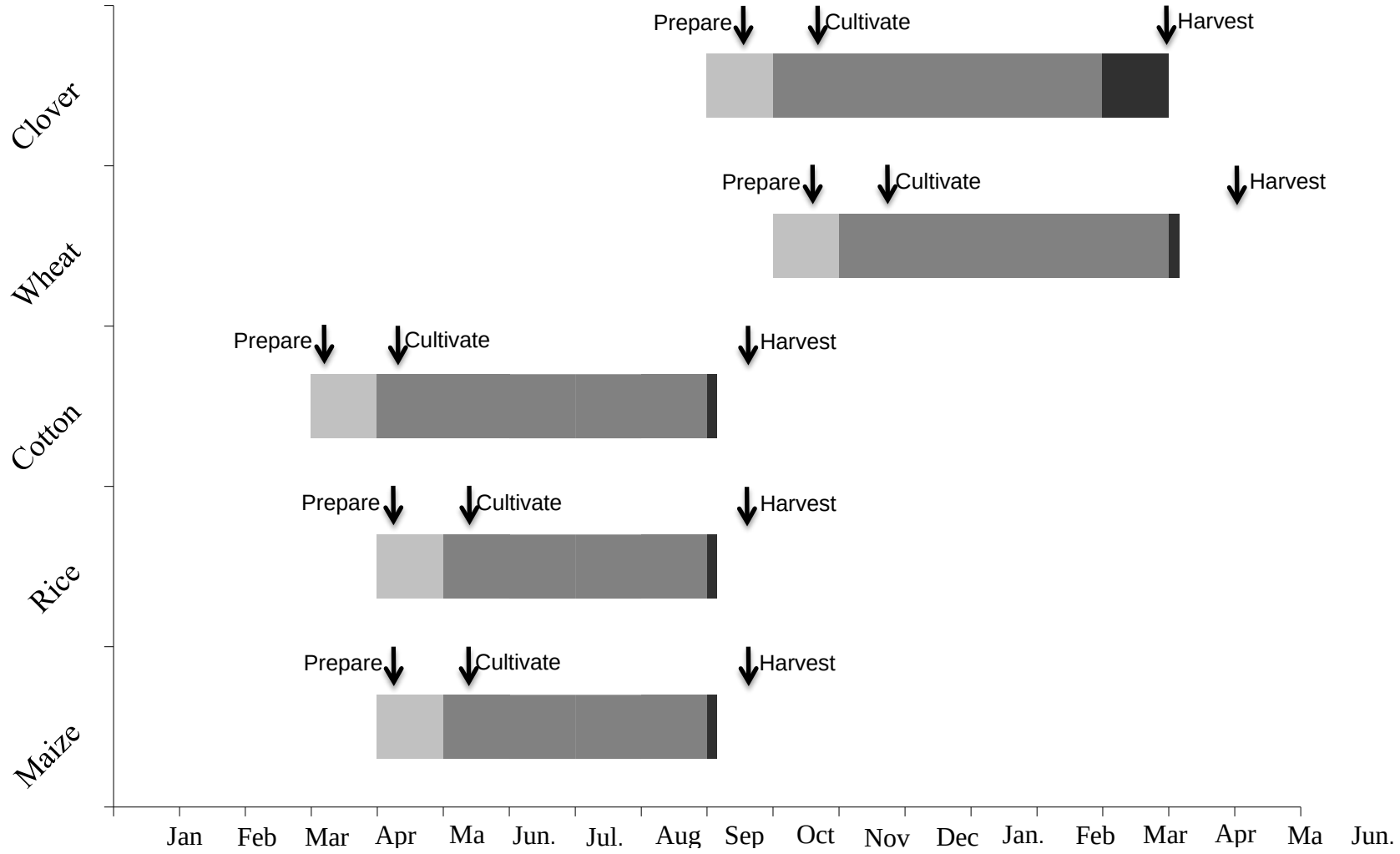

Figure 3.12: Crop rotation in Nile Delta region.

3.2. Water resources

3.2.1. Irrigation system

Irrigation systems in Egypt fall into three categories: surface, sprinkler, and drip. The main irrigation system in the study area is surface irrigation. Surface irrigation systems rely on surface grade and channels to help distribute the irrigation water. Surface irrigation consists of basin irrigation and furrow irrigation. The entire field can be flooded (basin irrigation) and the water is then fed into small channels (furrows irrigation). Basin irrigation was used after levelling the land and surrounded it by low bunds. The bunds prevent the water from flowing to the adjacent fields. Basin irrigation is commonly used for rice grown on flat lands and crops that are not affected by standing in water for long periods but furrows irrigation is constructed with a ridger, which the farmer uses with a tractor to make the ridge. Furrows are small channels which carry water down the land slope between the crop rows. Water infiltrates into the soil as it moves along the slope. The crop is usually grown on the ridges between the furrows. This method is suitable for all row crops and for crops that cannot stand in water for long periods, for example cotton and maize.

The reuse of low-quality water such as drainage water has become a viable option to meet part of the agricultural sector's water demand in Egypt. The main water source for irrigation where the fresh irrigation water is scarce e.g. in the northern part of the study area, is drainage water. The reuse of drainage water is from the main drains (official reuse) in the test area through the reuse mixing station, which has been under increasing pressure because of water quality deterioration. Due to the increasing deterioration of water quality, new opportunities for reuse of drainage water are being explored. Between the centralized official reuse and the localized unofficial reuse (where farmers pump drainage water from the collector drains directly onto fields), there is the option of capturing drainage water from

branch drains and pump it into the branch canals at their own intersections, of course under the treatment constraints.

Irrigation scheduling is aimed principally at applying the right amount of water at the right time to achieve maximum crop production. Decisions for scheduling are based on knowledge of the climate, the availability of soil water, the needs of the plant and the capacity of the irrigation system. The complexity of the crop elements, soil and inter water relationships make it difficult for the farmer to develop his own irrigation scheduling plan. Consequently, the Ministry of Water Resources and Agriculture is responsible for designing this plan for farmers. This rotation schedule varies from 10 to 15 days.

The cultivated lands in the study area are irrigated from two sources: either directly from the Nile (fresh water) or indirectly through drainage water (re-used water). The irrigation system is a combined gravity – open channel – and water pumping – closed conduit – system. The main canal system (first level) takes its water from head regulators, located upstream of the Nile dams. Water is distributed along branches (second level) where the flow is continuous. At the third level, distributaries which are 0.5 m below the level of the field receive water according to a rotation schedule. The water is then pumped from these distributaries to irrigate the fields. Figure 3.13 shows the irrigation system in the study area.

This system of using drainage water to irrigate agricultural fields is common in the northern parts of this study area where there is a shortage of fresh water from the Nile. All of the irrigated areas are drained. Normally, the subsurface drain does not cover all of the study area. The pump stations are devoted to pumping of drainage effluent. Drainage water in the northern part of the study area is sometimes pumped back into irrigation canals for re-use and drainage water in the other parts is pumped into the northern lake or the Mediterranean Sea (FAO, 1995).

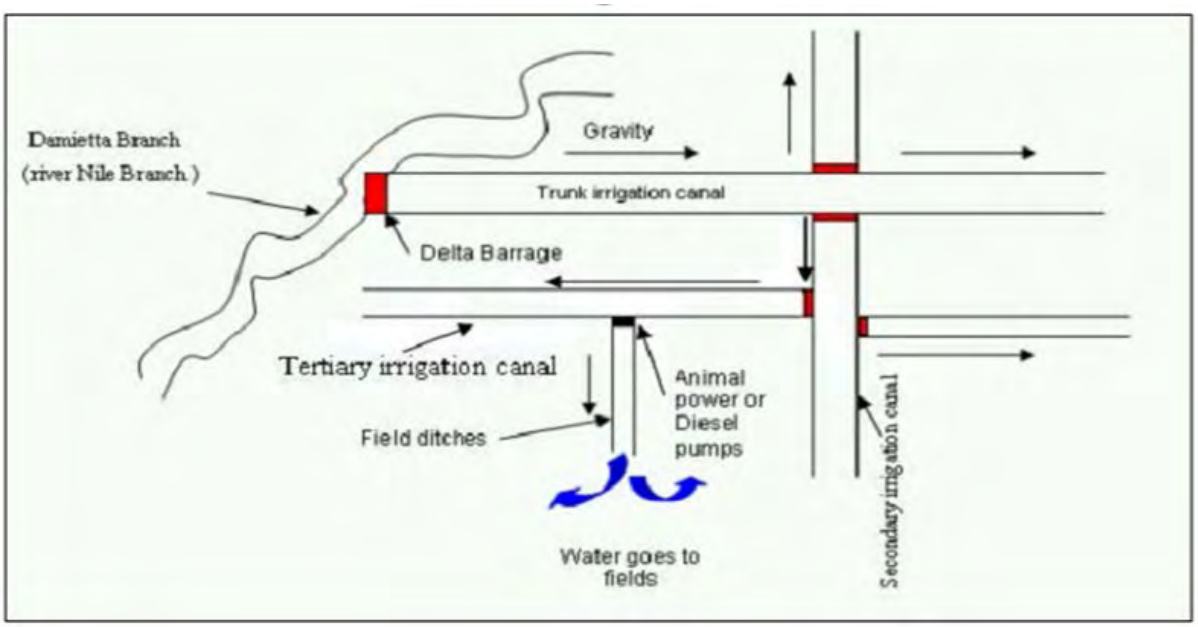

*Source: MWRI, (2002).

Figure 3.13: Surface irrigation system flow in a command area in Sakha.

3.2.2. Drainage system

Drainage has long since been an important component of land management on the alkali soil. On flat soils, intensive drainage is necessary to facilitate seedbed preparation and planting in order to minimize plant stress and subsequent yield reduction resulting from poor soil aeration associated with water logging.

The agricultural drainage is used to provide for a root zone environment that facilitates plant growth and optimizes crop production. In arid and semi-arid regions, drainage is linked with irrigation to make it possible to dispose of excess irrigation water and allow for the leaching of soils and the control of high level groundwater.

Drainage is accomplished by two methods: a) open-ditch systems designed to provide primarily surface drainage (surface runoff) or b) underground systems comprised of drainage tile designed to lower the water table by subsurface flow. Surface runoff develops when the

rate of irrigation water exceeds the soil's capacity to absorb water, thereby resulting in surface ponding.

A subsurface drain has a perforated conduit, such as tile, pipe or tubing, installed below the ground surface to intercept, collect, and/or convey drainage water. Subsurface drains were designed to remove excess water from the soil to improve the soil environment for vegetative growth by regulating the water table and ground water flow. A subsurface system provides drainage when the water table rises above the drain depth and water flows towards and into the drain. The drainage processes whereby water infiltrates into the soil and moves within the soil profile are referred to as subsurface drainage, shallow ground water flow, or sometimes interflow.

The subsurface drainage system implemented in the study area is a composite of the gridiron type, consisting of laterals and a main collector drain. The area served by one collector drain varies from 0.2 to 1km^2 depending on the topography, field size and layout of main irrigation and drainage systems (El Filaly et al., 2004). Figure 3.14 shows the subsurface drain used in the study area.

Open drains are similar to subsurface drains and differ only in that they are dug into the surface of the earth. Open drains have the advantage that they can receive overland flow directly, but the disadvantages often outweigh the advantages. The main disadvantages are a loss of land, interference with the irrigation system, the splitting-up of the land into small parcels, which hampers farming operations, and a maintenance burden. Open drains consist of lateral drains, collector drains and outfall drains. Shallow surface drains (hoe drains) are often utilized to effectively convey ponded surface water to ditches. The design system of surface and subsurface drains depends on the government plan for development of the drainage systems.

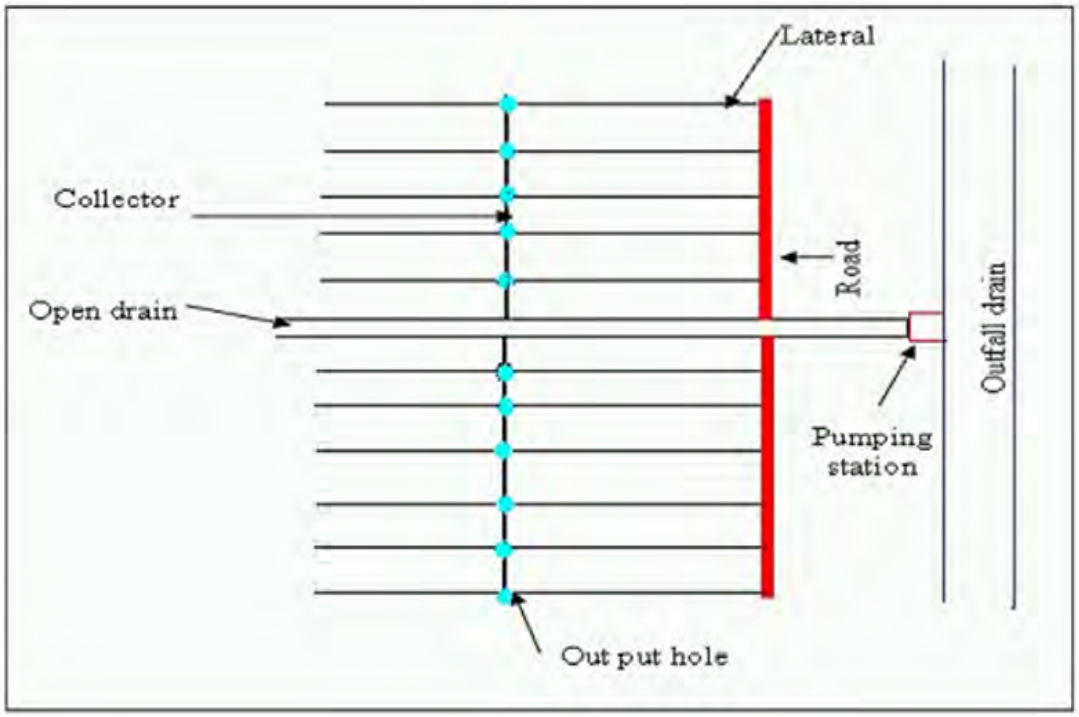

*Source: MWRI, (2002).

Figure 3.14: Subsurface drain systems in command area in Sakha.

3.3. Ago-climatic zones

Soils in the Nile River and Delta are silt-clay mixtures of good quality, deposited during thousands of years of Nile flooding. The total cropped area is estimated at approximately 58.000 km^2 with a cropping intensity of 180 % (Abdel Elmontalbe, 2006). Most of the newly reclaimed desert areas use modern irrigation practices such as drip and sprinkler systems.

An estimated 3.5 million farmers cultivate holdings of about 0.01 km^2. Production is intensive and yields are relatively high compared with world standards in countries with similar agroclimatic conditions (Figure 3.15). This is due to the reason that recycled water is assumed as water for irrigation in the water balance.

Based on soil characteristics and water resources, four agro-ecological zones are demonstrated in Figure 3.16. These agro-ecological zones can be identified as follows:

1- ***Old land***: This land is located in the Nile Valley and Delta Regions. It covers a total area of 22.500 km^2 (almost 4.5 million feddan) and is characterized by alluvial soils (clay to loamy). The Nile is the main source of water for irrigation.

2- ***New land***: This land is located mainly on both the east and west sides of the Delta and scattered over various areas in the country. It covers 2500 km^2 (almost 0.6 million feddan). Reclamation of this land was started in the early 1950s and is continuing. Nile water is the main source of irrigation water but in some desert areas underground water is the only source of irrigation water. Sprinkler and drip irrigation regimes are practiced.

3- ***Oases***: Oases are characterized by alluvial, sandy and calcareous soils. They cover a total area of 400 km^2. Underground water is the main source for irrigation and formed mainly by limestone spring water, or canats.

4- ***Rainfed areas***: These include approximately 1700 km^2 of land located in the north coastal areas, where rainfall fluctuates between 100 and 200 mm annually.

Traditional soil fertility management can lead to the minimizing of nutrients from the soil due to an insufficient application of nutrients, to nutrient imbalances and to environmental contamination through the over-application of fertilizers.

The agricultural land in Egypt is determined by climate and water availability. The country is divided into three main agro-ecological zones: Delta (Lower Egypt), Middle Egypt and Upper Egypt. These are further subdivided into nine zones. From north to south these are: 1. Coastal zone, 2. Central Delta zone, 3. East and West zone, 4. Giza zone, 5. Menia zone, 6. Asuitt and Sohag zone, 7. North Qena zone, 8. South Qena zone and 9. Aswan zone.

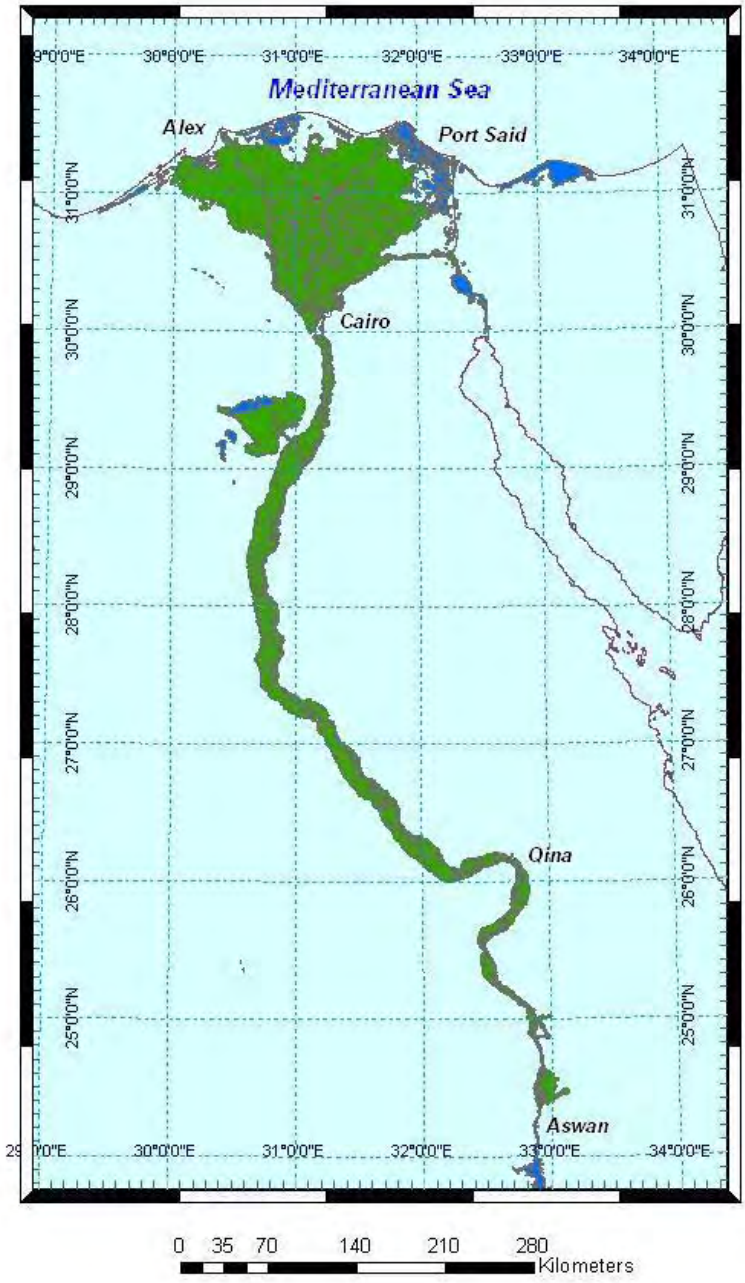

Figure 3.15: Overall view of the old cultivated land.

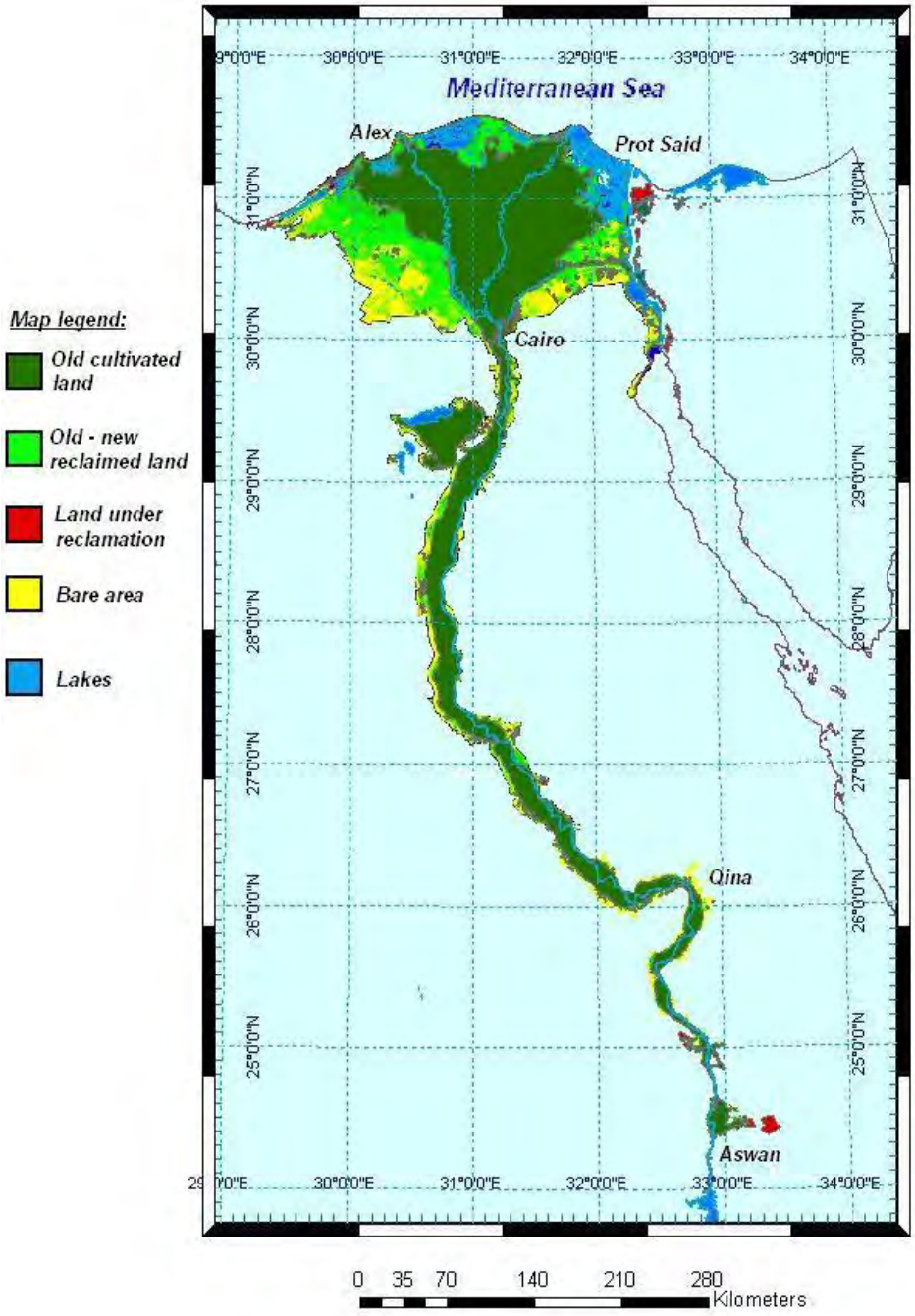

Figure 3.16: Overall view of different land – cultivated pattern.

3.4. Remote sensing data

Five different types of Earth Observation data were used for this study:

1) A total of three different data sets of Landsat (TM and ETM+) belong to three different date of acquisitions were downloaded from Global Land Cover Facility website" http://glcfapp.glcf.umd.edu:8080/esdi/index.jsp". Each data set comprises of 4 Landsat scenes fallen into two successive paths to cover the whole Nile Delta region. The first data set is Landsat-5 TM acquired in 1984 and the other two data sets are Landsat-7 ETM+ acquired in 2000 and 2005 consequently. TM and ETM+ images are of 30 m Spatial Resolution.
2) A total number of seven strips of Egypt-Sat_1 were acquired between June 2008 and July 2009. The Egypt-Sat_1 multi-spectral had a spatial resolution of 7.8 m with four spectral bands: blue, green, red and near infrared. The strips were provided by the National Authority of Remote Sensing and Space Science (NARSS).
3) A total number of five of Advanced Spaceborne Thermal Emission and Reflection Radiometer (ASTER) data were acquired in August 2003 till April 2004. The images were provided by the National Authority of Remote Sensing and Space Science (NARSS).
4) A total number of 53 images of Advanced Along Track Scanning Radiometer (AATSR) data were acquired on monthly basis starting from August 2005 till December 2009. The data sets were downloaded from ESA official FTP site http://ats-merci-uk.eo.esa.int:8080/merci.
5) A total number of 53 images of Medium Resolution Imaging Spectrometer Instrument (MERIS) data were acquired on monthly basis starting from August 2005 till December 2009. The data sets were downloaded from ESA official FTP site http://ats-merci-uk.eo.esa.int:8080/merci.

The general characteristics of the Landsat (TM and ETM+), Egypt-Sat_1, ASTER, AATSR and MERIS data are summarized in Appendix Tables 1-6 respectively.

3.5. Maps

Digital copies of the following maps were obtained from the Egyptian National Survey Authority, in the following scales:

Topographic maps	1:10,000
Geologic map	1:100,000
Hydrologic map	1:100,000

3.6. Software

The digital analyses (interpretation) of the satellite data and related models were performed using the following software and the used manual:

- ERDAS Imagine 9.2: Image pre-processing, unsupervised classification and DEM establishment (http://www.gis.usu.edu/manuals/labbook/erdas/manuals/FieldGuide.pdf).
- ENVI 4.7: Image interpolation and supervised classification and post classification (http://aviris.gl.fcen.uba.ar/Curso_SR/biblio_sr/ENVI_userguid.pdf).
- Beam 4.8: Basic ENVISAT Toolbox for (A)ATSR and MERIS for different energy fluxes mapping and to conduct SEBS model (http://www.brockmann-consult.de/beam/doc/help/index.html).

- CROPWAT 4.3: Calculate water crops requirement for the major cultivated crops in the Nile Delta area (http://tarwi.lamolina.edu.pe/~jgoicochea/Manuales/CROPWAT4W.pdf).
- CLIMWAT 2: Feed CROPWAT programme with required meteorological data (http://www.juergen-grieser.de/downloads/CLIMWAT_2.pdf).
- Arc-View 3.2a and ARCGIS 9.3: Digitizing the topographic maps, design the data base, layout of maps and spatial modeling (http://www.gep.uchile.cl/Publicaciones/Libro-_Tutorial_de_ArcGis_9.3.pdf).
- IDRISI: Applying Weighted Linear Combination for Multi Criteria Analysis (http://gisgeek.pdx.edu/G424-GIS/KilimanjaroTutorial.pdf).
- JMP 8: Applying ARIMA model to conduct Time Series Analysis (http://www.jmp.com/support/downloads/pdf/jmp8/jmp_user_guide.pdf).
- Excel and feature selection and statistical analyses (http://excel-manual-pdf.fyxm.net/).

4. Methods

The methodology implemented in this study is illustrated in Figure 4.1

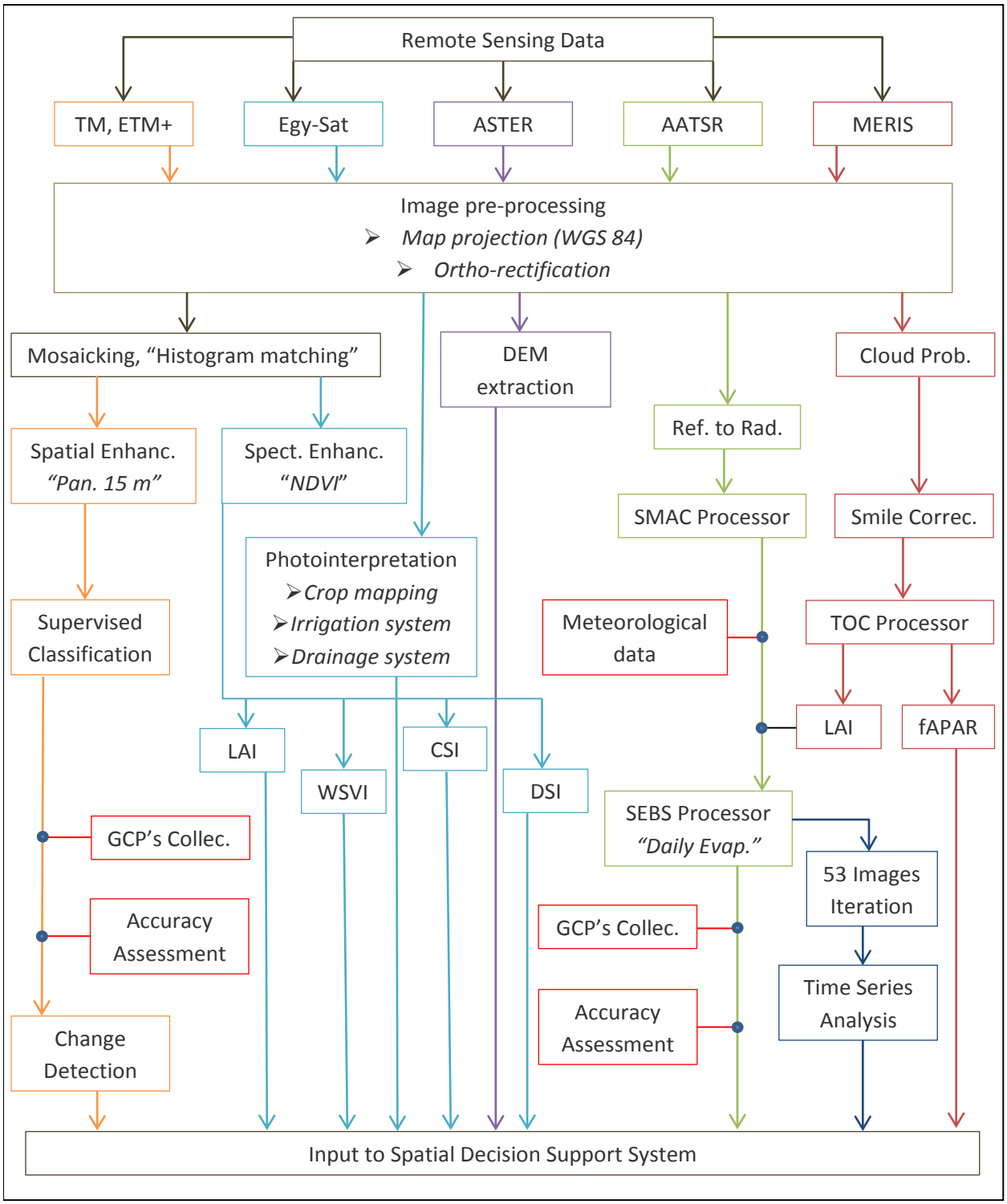

Figure 4.1: Methodological framework.

4.1. Estimating the daily evapotranspiration using remote sensing data

4.1.1. AASTR and MERIS data processing

4.1.1.1. Cloud detection

Algorithm specification

The cloud probability algorithm has been developed and implemented by Free University Berlin and Brockmann Consult. It is also used in the Global MERIS (Delwart et al., 2007) Land Albedo map project. The cloud probability algorithm is using 9 spectral bands of MERIS, the ratio of band 11 and 10, which is an indication of the absorption due to oxygen, the European Centre for Medium-Range Weather Forecasts (ECMWF) surface pressure and the exact wavelength of band 11 as input. As an output, it yields a probability value (0 to 1) indicating if a pixel can be regarded as a cloud or not. Such a probability permits a more flexible way to work with identified clouds compared to a binary cloud mask.

The algorithm uses two different artificial neural networks. The first one is used over the open ocean and the second one over land. The distinction between ocean and land is done using the altitude information. If the altitude is lower than 50 meters (the most common threshold used in scientific community) the ocean net is used.

The following Figure (4.2) shows the general structure of the cloud detection algorithm. During development of the algorithm, using the radiative transfer model MOMO (Matrix Operator MethOd), simulated cloud and non-cloud top of atmosphere radiance have been produced and an Artificial Neural Net (ANN) has been trained. This neural net is now used in the Cloud Probability Processor, where it is fed with the reflectances and the pressure as shown in the Figure 4.2. A post-processing is applied after the network (nn2prop) which scales the output of the neural network into a probability value.

Algorithm basics

Clouds are easily to detect when a manual classification of satellite images is done, their automatic detection is difficult. Clouds have four special radiative properties that enable their detection: 1) clouds are white, 2) clouds are bright, 3) clouds are higher than the surface and 4) clouds are cold. However clouds, as the most variable atmospheric constituent, seldom show all four properties at the same time.

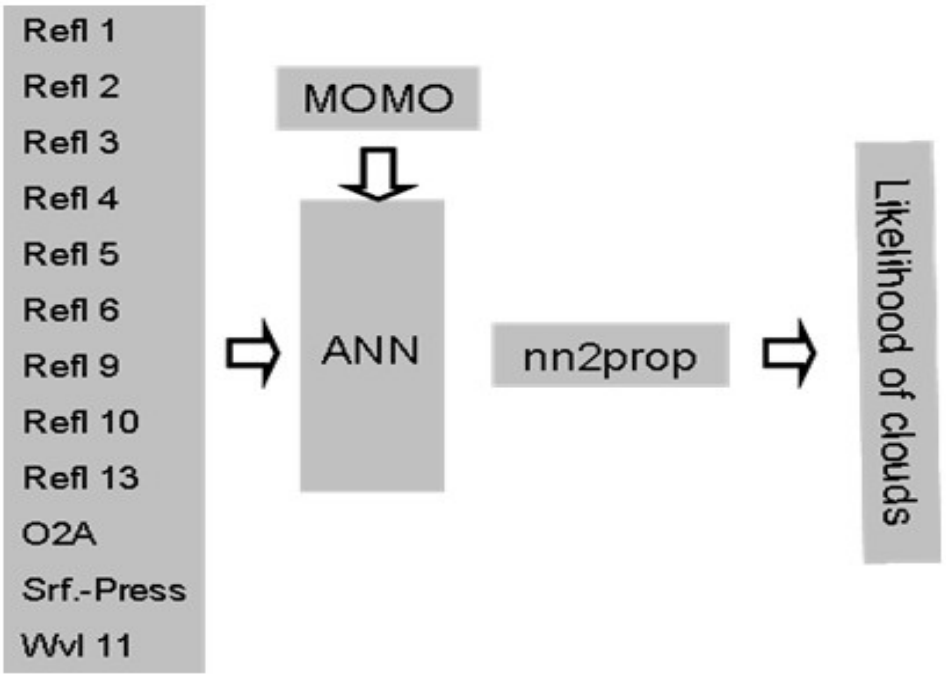

Figure 4.2: Cloud detection algorithm.

Thin clouds show a portion of the underlying surface spectral properties, and low clouds are sometimes quite warm. Additionally some surface types, like snow and ice have spectral properties that are very similar to some of the cloud properties.

Therefore simple thresholding algorithms often fail and existing cloud detection schemes use a number of different cascaded threshold based tests to account for the complexity (Ackermann et al., 2000; King et al., 1992; Saunders and Kriebel 1988). MERIS measures

radiances in 15 channels between 400nm and 1000nm. Thus the very valuable thermal information and information about the liquid and ice water absorption at 1.6μm and 3μm are not available. The cloud detection for MERIS must therefore rely on bands 1), 2) and 3). In addition a slight absorption of snow at 900nm could be used to discriminate snow from low clouds (Delwart et al., 2007).

In general, cloud detection algorithms can be separated into two classes: a) clear sky conservative and b) cloud conservative. Clear sky conservative algorithms are constructed such that the probability of a first order error in clear sky detection is very low. In other words, if a pixel is detected as clear, the probability of cloudiness should be very low. This often has the side effect that many cloud free pixels are detected as cloudy. The opposite is true for cloud conservative algorithms. Here the probability of a first order error in cloud detection is low, with the side effect that many cloudy pixels are missed.

Pure “clear sky” conservative algorithms mark pixels as cloud free or as probably cloudy, whereas “pure cloud” conservative algorithms detect cloudy or probably cloud free pixel. However, in practice most cloud detection algorithms try to minimize the probability of the first and second order errors in cloud and cloud free detection, only with the tendency to cloud or to clear sky conservative respectively. What kind of cloud detection algorithm should be used is mainly a question of the successive algorithm. Algorithms relying on cloudy pixels need a cloud conservative detection and vice versa; climatological applications often require balanced detection to be bias free.

4.1.1.2. Smile correction

MERIS is measuring the reflected sun light using Charge Coupled Device (CCD) technique. A CCD is measuring in one of its dimensions one image line, and in the other dimension the spectrally dispersed radiance for each pixel along the image line. I.e., the spectral

measurements of each pixel along an image line are made by its own set of sensors of the CCD. This causes small variations of the spectral wavelength of each pixel along the image. This is called the "smile effect". The MERIS instrument is composed of 5 cameras, each equipped with its own CCD sensor. The variation of the wavelength per pixel is in order of 1nm from one camera to another, while they are in the order of 0.1nm within one camera.

Even though this variation is small compared to the spectral bandwidth of a band, which is typically 10nm, and can hardly be seen in an image, it can cause disturbances in processing algorithms which require very precise measurements, for example the retrieval of chlorophyll in the ocean. These disturbances can result in visual artifact ("camera borders") or reduced accuracy of the Level 2 products. Therefore, the MERIS Level 2 processor corrects the smile effect. The Level 1b product is not smile corrected, because this product shall provide what the instrument is measuring, and that is in fact the radiance at the given wavelength of each pixel.

The Smile Correction is an exact implementation of the Level 2 smile correction, in order to generate smile corrected Level 1b products. While the Level 1b product provides the radiance measurement for individual wavelengths within one spectral band, the smile corrected product has normalized the wavelengths within one spectral band to one reference wavelength (Appendix Table 7).

Algorithm specification

The smile correction consists of two terms: a) the irradiance correction and b) the reflectance correction.

The irradiance correction corrects the variation of the solar irradiance, which is different between the wavelength of the pixel and the reference wavelength:

$$L_{corr,irr}\,(\lambda_0) = L_{meas,pixel}\,(\lambda_0) \times \frac{F_{0,ref}\,(\lambda_0)}{F_{0,pixel}\,(\lambda_0)} \quad \text{Eq. 4.1}$$

The reflectance correction is interpolating along the slope of the reflectances between adjacent wavelengths "λ" from the pixel-wavelengths to the reference wavelength:

$$L_{corr,ref}\,(\lambda_0) = \left[L_{meas,pixel}\,(\lambda_2) \times \frac{F_{0,ref}\,(\lambda_0)}{F_{0,ref}\,(\lambda_1)} - L_{meas,pixel}\,(\lambda_1) \times \frac{F_{0,ref}\,(\lambda_0)}{F_{0,ref}\,(\lambda_1)}\right] \times \frac{(\lambda_{ref} - \lambda_1)}{(\lambda_2 - \lambda_1)} \quad \text{Eq. 4.2}$$

The smile corrected radiance is the sum of the two terms:

$$L_{corr}\,(\lambda_0) = L_{corr,irr}\,(\lambda_0) + L_{corr,ref}\,(\lambda_0) \quad \text{Eq. 4.3}$$

While the irradiance correction can be applied to all 15 bands, it is not possible to define for each band two adjacent bands, which are suitable universally to give a good estimation of the spectral slope within the band. In order to overcome this problem at least partially, different adjacent bands have been selected for land and water pixels. However, for the bands in absorption lines, i.e. bands 11 and 15, it is totally impossible to find suitable adjacent bands. Also, over land the shape of the spectrum varies very much for bands greater band 3, i.e. it is not possible to select adjacent bands for those bands. In these cases, the reflectance correction is not applied. Appendix Table 7 specifies the bands, which are reflectance corrected, and which bands are being used as adjacent bands.

The activation switch defines if the reflectance correction is applied or not. The lower and upper band indices specify the adjacent bands which are used in the reflectance correction. The reference wavelength is the wavelength to which all pixels of a band are normalized, and the $F_{0,ref}$ column lists the solar irradiance (not day-corrected) which is used for the irradiance

correction. This solar irradiance is irradiances which are integrated over the spectral widths of the band.

4.1.1.3. SMAC

Simplified Method for the Atmospheric Correction (SMAC) is a semi-empirical approximation of the radiative transfer in the atmosphere (Rahman and Dedieu, 1994). The signal at the satellite is written as the sum of the following components, which are then expressed in simple analytical terms:

- Two way gaseous transmission
- Atmospheric spherical albedo
- Total atmospheric transmission
- Rayleigh scattering
- Aerosol scattering

The spherical albedo, *S*, is expressed as a function of the aerosol optical depth at 550nm:

$$S = 1 - 1/(a_0 + a_1 \times \delta_{550}) \quad \text{Eq. 4.4}$$

Where, a_0 and a_1 are parameters which need to be determined for a given spectral band and aerosol model. These parameters can be retrieved by a best-fit against a full radiative transfer model. The well establishes 6*S* code was used for this purpose.

With this technique the radiative transfer in the atmosphere can be computed much faster than with a full model. A comparison has shown that the gain in computation time is several hundred times in comparison with the full model. However, numerous coefficients have to be determined in advance from best-fits with a full numerical model. Also, changes in the spectral band characteristics require new coefficients. The accuracy of the SMAC

approximation in comparison with 5*S* is generally better than 3% difference between the TOA reflectances.

The practical application of such a simplified model is to invert the radiative transfer equation, and to calculate the surface reflectance from satellite measurements. Because of its "speed", this method is best suited for application to large data volumes (Gillies et al., 1997; Geymen and Baz, 2008).

The SMAC requires as input, in addition to the measured top of atmosphere radiances, the surface pressure, the ozone content and the water vapor content, and, most important, the aerosols. SMAC has also implemented these in a very useful way. Aerosol, for example, requires the selection of an aerosol model and the aerosol optical depth at 550nm. The processor implementation gives the choice to select the MERIS meteorological data for pressure, ozone and humidity. The algorithm is described by Rahman and Dedieu (1994).

4.1.1.4. Vegetation processor

The proposed algorithm called here MERIS TOA/TOC-VEG (Gower et al., 1999) is based on the training of neural networks over a data base simulated using radiative transfer models. It requires top of atmosphere/ top of canopy MERIS reflectances and associated geometry as inputs and allows the derivation of four vegetation biophysical variables:

fAPAR: it corresponds to the fraction of photosynthetically active radiation absorbed by the canopy and depends both on the canopy structure and illumination conditions. In order to be consistent with most of the potential users who are dealing with daily integrated fAPAR value as well as with other fAPAR products that are considering the instantaneous fAPAR value at the time of the satellite overpass under clear sky conditions (e.g. MODIS), we decided to use the fAPAR at 10:00 solar time under clear sky conditions. Note also that the

fAPAR refers only to the green parts (leaf chlorophyll content higher that 15µg.cm-2) of the canopy.

fCover: it corresponds to the gap fraction for nadir direction. It is a canopy intrinsic variable that does not depend on variables such as the geometry of illumination as compared to fAPAR. For this reason, it is a very good candidate for the replacement of classical vegetation indices for the monitoring of green vegetation. Note that similarly to LAI and fAPAR, only the green elements (leaf chlorophyll content is higher than 15µg.cm-$^{2)}$ will be considered.

LAI: it is defined as half the developed area of green (leaf chlorophyll content is higher than 15 µg.cm^{-2}) vegetation elements per unit of horizontal soil Note that LAI of vegetation as estimated from remote sensing will include all the green contributors, i.e. including understory when existing under forest canopies.

LAI.C_{ab}: the chlorophyll content can be calculated both at the leaf level and at the canopy level by multiplication of the leaf level chlorophyll content by the leaf area index. As the medium resolution scale of MERIS is generally associated with heterogeneous pixels, the product LAI.C_{ab} more sound than the leaf level chlorophyll content: what would be the chlorophyll content of a pixel with half of very sparse canopy with very high leaf chlorophyll content and half of very dense canopy with very low leaf chlorophyll content? Therefore, the estimation of LAI.C_{ab} has been preferred to that of the leaf chlorophyll content.

TOA/TOC-veg processor algorithm specification: The proposed algorithm called here TOA_VEG (Gower et al., 1999) is based on the training of neural networks over a data base simulated using Radiative Transfer Models (RTM, Gower et al., 1999, Figure 4. 3). The SAIL, PROSPECT and SMAC are coupled and used to simulate the reflectance in the 13 MERIS bands considered (412 nm, 442 nm, 490 nm, 510 nm, 560 nm, 620 nm, 665 nm,

681.25 nm, 708.75 nm, 753.75 nm, 778.75 nm, 865 nm, 885 nm). The oxygen and water absorption bands have not been used because they would convey significant uncertainties associated, while providing only marginal information on the surface. The background optical properties are simulated using a collection of soil, water and snow typical reflectance spectra. A brightness factor is used to provide additional flexibility of the background reflectance. Finally, to account for the medium resolution of MERIS observations, mixed pixels are simulated with variable fractions of pure background and pure vegetation.

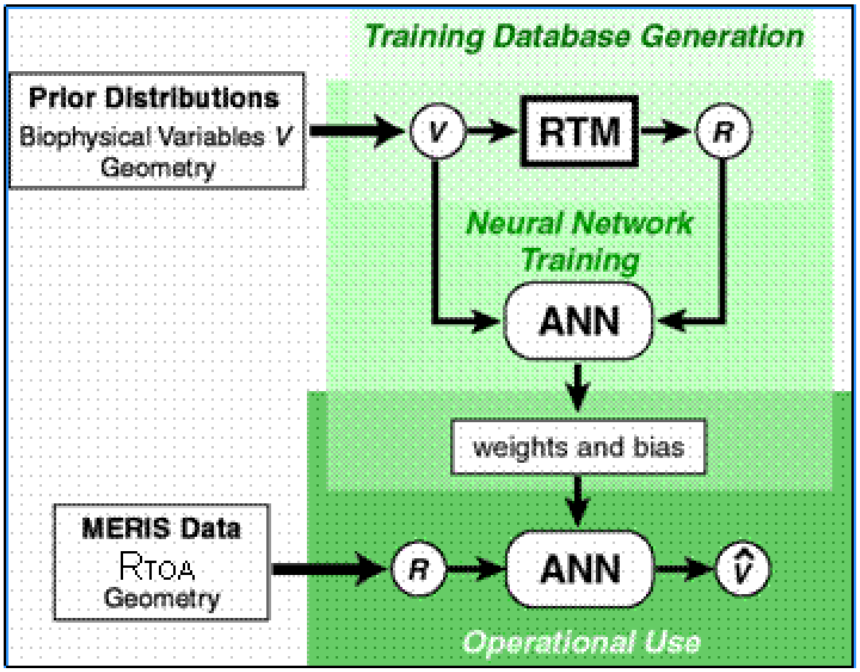

Figure 4.3: Overview of the TOA-VEG algorithm.

The simulation of the top of atmosphere reflectance in the 13 MERIS bands requires 15 input variables. They were drawn randomly according to an experimental plan aiming at getting a more evenly populated space of canopy realization. To provide more robust performances of the network, the distributions of each input variable was close to the actual distributions and, when possible. Realistic co-distributions were also used. This was achieved by considering a representative distribution of targets over the earth surface that constrains the observation

geometry, as well as possible vegetation amount. A total number of 73,728 cases were simulated. Half of this data set was used for training, one quarter to evaluate hyper-specialization, and the last quarter to quantify the theoretical performances.

Back-propagation neural networks were trained for each variable considered (Gower et al., 1999). The architecture was optimized, resulting in 2 hidden layers of tangent-sigmoid neurones corresponding (Gower et al., 1999) to a total around 300 coefficients to adjust, and providing a good ratio (50-100) with the size of the training data base.

The theoretical performances were evaluated over the test simulated data set (Figure 4. 4). It allowed providing estimates of uncertainties. They are close to 0.06 (absolute value) for fAPAR and fCover, and close to 25% (relative value) for LAI and LAI.C_{ab} that shows some loss of sensitivity for the larger values of LAI and LAI.C_{ab} due to saturation effects.

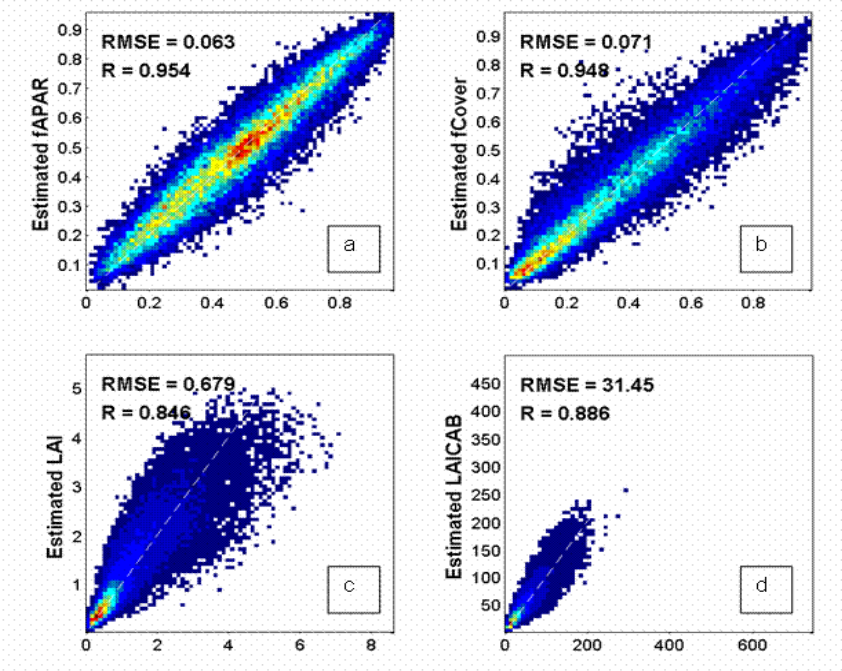

Figure 4.4: Density plots of a) fAPAR, b) fCover, c) LAI, d) LAI.C_{ab}, ANN estimates vs. the true values from the test database. The corresponding values of the Root Mean Square Errors (RMSE) and determination coefficients (R) are provided.

Algorithm validation

Various validation exercises have been performed by Katul and Parlange, (1992) on both full and reduced resolution images. In particular, the algorithm has been validated over ground measurements of images from the following satellite instruments; VALERI, MODLAND, BigFoot and CCRS data) and inter-compared over 26 sites during the whole year 2003 with other satellite instruments like: MODIS, CYCLOPES, ECOCLIMAP. The main results are the following:

- The temporal consistency between the MERIS TOA/TOC-VEG, MODIS, CYCLOPES and ECOCLIMAP products is very good and the vegetation cycle is well detected.
- The MERIS products show a relatively good agreement with the MODIS products for LAI below 2.0. Above LAI of 2.0, MODIS LAI is systematically higher than that of MERIS
- A better agreement is observed between CYCLOPES and MERIS products for all the cover types as compared to CYCLOPES and MODIS.
- Concerning the consistency between products, TOA/TOC-VEG shows a relatively strong relationship between LAI and fAPAR.
- Figure 4.5 shows the results that were obtained on the comparison with LAI ground measurements, providing a root mean square error of 0.85.
- The quality of the results is not guaranteed when solar zenith angle is larger than 60° due to the limitations in representatively of the canopy radiative transfer model used for training the neural network.

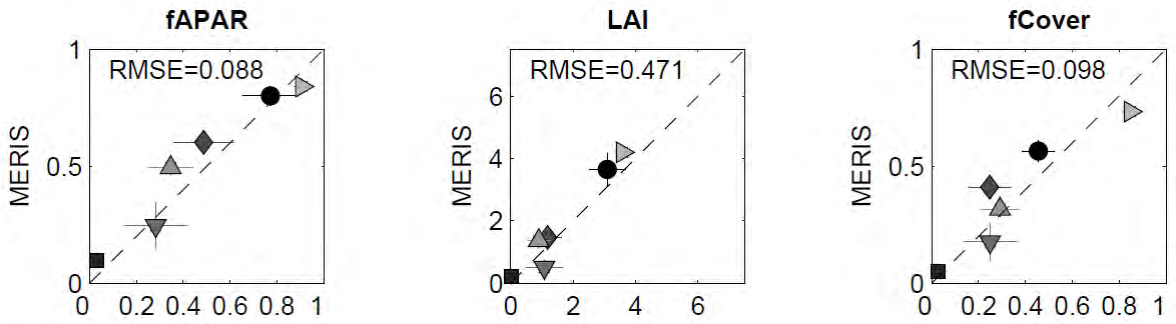

Figure 4.5: Validation on TOA/TOC-VEG LAI product over VALERI ground measurements. ●(Chile), ■ (Bolivia), ♦ (Morocco), ▼(Spain), ▲(Romania) and ►(Canada).

Normalized Difference Vegetation Index – NDVI algorithms

The NDVI exploit the strength and the vitality of the vegetation on the earth's surface. The spectral signature of wholesome vegetation shows abrupt rise of the reflection level at 0,7 µm, whereas land without vegetation, according to the type of surface, has a continuous linear course. So much more active the chlorophyll of the plants, so much bigger is the boost of the reflection level at the near infrared (0.78 - 1 µm). Beside the determination between of the vegetation and other objects it allows to detect the vitality of the vegetation.

The NDVI results from the following equation:

$$NDVI = \left(IR_{factor} \times NIR - R_{factor} \times R\right)/\left(IR_{factor} \times NIR + R_{factor} \times R\right) \quad \text{Eq. 4.5}$$

Where, *IR* is the infrared band, *R* is the red band and *NIR* is near infrared band

In the area of red the incoming solar radiation won´t be extensively absorbed by the pigments of the mesophyll inside the folios, primarily by the chlorophyll. In the area of the near infrared, in contrast, the bigger part of the incoming radiation was reflected. The NDVI

composes a measurement for the photosynthetic activity and is strongly in correlation with density and vitality of the vegetation. The normalizing reduces topographicaly and atmospheric effects and enables the simultaneous examination of a wide area.

Applied to the MERIS Level 1b TOA radiances, using the following bands and factors:

- As the near IR band: radiance_10 (753.75 nm)
- As the IR factor: 2.0
- As the red band: radiance_6 (620.00 nm)
- As the red factor: 1.0

Leads to the following equation:

$$NDVI = \left(IR_{factor} \times Radiance_{10} - R_{factor} \times Radiance_6\right)/\left(IR_{factor} \times Radiance_{10} + R_{factor} \times Radiance_6\right) \quad \text{Eq. 4.6}$$

~~A~~lso the processor computes an additional flags band called “NDVI_flags” with the following bit coding with the following description:

- Bit 0 The computed value for NDVI is NAN or is Infinite
- Bit 1 The computed value for NDVI is less than 0 (zero)
- Bit 2 The computed value for NDVI is greater than 1 (one)

4.1.2. SEBS Definition

The Surface Energy Balance System algorithms are used to estimate the evaporative fraction and daily evaporation from satellite earth observation data, in combination with meteorological information at a proper scale.

SEBS consists of: a) a set of tools for the determination of the land surface physical parameters, such as albedo, emissivity, temperature, vegetation coverage etc., from spectral reflectance and radiance measurements, b) a model for the determination of the roughness length for heat transfer and c) a new formulation for the determination of the evaporative fraction on the basis of energy balance at limiting cases.

Surface Energy Balance Terms

The surface energy balance is commonly written as:

$$R_n = G_0 + H + \lambda E \quad \text{Eq. 4.7}$$

Where, R_n is the net radiation (W M^{-2}), G_0 is the soil heat flux (W M^{-2}), H is the turbulent sensible heat flux (W M^{-2}), and λE is the turbulent latent heat flux (λ is the latent heat of vaporization measured in W M^{-2} and E is the actual evapotranspiration measured in mm/day).

The equation to calculate the net radiation is given by:

$$R_n = (1 - \alpha) \times R_{swd} + \varepsilon \times R_{lwd} - \varepsilon \times \sigma \times T_0^4 \quad \text{Eq. 4.8}$$

Where α is the albedo, R_{swd} is the downward solar radiation (J), R_{lwd} is the downward long wave radiation (J), ε is the emissivity of the surface, σ is the Stefan-Bolzmann constant, and T_0 is the surface temperature (K).

The equation to calculate soil heat flux is parameterized as:

$$G_0 = R_n \times [\Gamma_c + (1 - f_c) \times (\Gamma_s - \Gamma_c)] \quad \text{Eq. 4.9}$$

In which it is assumed that the ratio of soil heat flux to net radiation Γ_c = 0.05 for full vegetation canopy (Monteith, 1973) and Γ_s = 0.315 for bare soil (Kustas and Daughtry, 1990). An interpolation is then performed between these limiting cases using the fractional

canopy coverage, f_c. In order to derive the sensible and latent heat flux, the similarity theory will be used. In this study, distinction will occur between the Atmospheric Boundary Layer (ABL) or Planetary Boundary Layer (PBL) and the Atmospheric Surface Layer (ASL). ABL refers to the part of atmosphere that is directly influenced by the presence of the Earth's surface and responds to the surface forcing with a timescale of an hour or less, while ASL refers to usually the bottom 10% of ABL (where turbulent fluxes and stress vary by less than 10% of their magnitude, Stull, 1988) but above the roughness sublayer. The latter (or the interfacial layer) is the near surface thin layer of a few centimeters where molecular transport dominates over turbulent transport. The thickness of the roughness sublayer is thought to be around 35 times the surface roughness height, or three times that of the vegetation height (Katul and Parlange, 1992). In ASL, the similarity relationships for the profiles of the mean wind speed, u, and the mean temperature, $\theta_0 - \theta_a$, are usually written in integral form as:

$$u = \frac{u_*}{K}\left[\ln\left(\frac{Z-d_0}{Z_{0m}}\right) - \Psi_m\left(\frac{Z-d_0}{L}\right) + \Psi_m\left(\frac{Z_{0m}}{L}\right)\right] \quad \text{Eq. 4.10}$$

$$\theta_0 - \theta_a = \frac{H}{k u_* \rho C_p}\left[\ln\left(\frac{Z-d_0}{Z_{0h}}\right) - \Psi_h\left(\frac{Z-d_0}{L}\right) + \Psi_h\left(\frac{Z_{0h}}{L}\right)\right] \quad \text{Eq. 4.11}$$

Where, Z is the height above the surface (m), $u_* = (t_0/\rho)1/2$ is the friction velocity, t_0 is the surface shear stress, ρ is the density of air (kg/m^3), k = 0.4 is von Karman's constant, d_0 is the zero plane displacement height (m), Z_0m is the roughness height for momentum transfer (m), θ_0 is the potential temperature at the surface (K), θ_a is the potential air temperature at height Z, Z_{0h} is the scalar roughness height for heat transfer, ψ_m and ψ_h are the stability correction functions for momentum and sensible heat transfer respectively, L is the Obukhov length defined as:

$$L = \frac{\rho C_p\, u_*^3\, \theta_v}{k_g\, H} \quad \text{Eq. 4.12}$$

Where, g is the acceleration due to gravity (m/s^2) and θ_v is the potential virtual temperature near the surface. For field measurements performed at a height of a few meters above ground, clearly since the surface fluxes are related to surface variables and variables in the atmospheric surface layer, all calculations use the Monin-Obukhov Similarity (MOS) functions given by Brutsaert (1999). By replacing the MOS stability functions with the Bulk Atmospheric Boundary Layer (ABL) Similarity (BAS) functions proposed by Brutsaert (1999), the system of Eqns. (4.7-4.12) relates surface fluxes to surface variables and the mixed layer atmospheric variables. The criterion proposed by Brutsaert (1999) is used to determine if MOS or BAS scaling is appropriate for a given situation. The above functions are valid for unstable conditions only. For stable conditions the expressions proposed by Beljaars and Holtslag (1991) and evaluated by van den Hurk and Holtslag (1995) are used for atmospheric surface layer scaling and the functions proposed by Brutsaert (1982) for atmospheric boundary layer scaling.

The friction velocity, the sensible heat flux and the Obukhov stability length are obtained by solving the system of non-linear Eqns. (4.7-4.12) using the method of Broyden (Press et al., 1997). Derivation of the sensible heat flux using Eqns. (4.7-4.12) requires only the wind speed and temperature at the reference height as well as the surface temperature and is independent of other surface energy balance terms.

4.1.2.1. An extended model for determination of the roughness length for heat transfer

In the former mention derivations, the aerodynamic and thermal dynamic roughness parameters need to be known. When near surface wind speed and vegetation parameters (height and leaf area index) are available, the within-canopy turbulence model proposed by Massman (1997) can be used to estimate aerodynamic parameters, d0, the displacement height, and, z0m, the roughness height for momentum. This model has been shown by Su et

al. (2001) to produce reliable estimates of the aerodynamic parameters. If only the height of the vegetation is available, the relationships proposed by Brutsaert (1982) can be used. If a detailed land use classification is available, the tabulated values of Wieringa (1986; 1993) can be used. However, since the aerodynamic parameters depend also on wind speed and wind direction as well as the surface characteristics (Bosveld, 1999), the latter two approaches should be used only when the first method cannot be used due to lack of data. When all of the above information is not available or not convenient to use, the aerodynamic parameters can be related to vegetation indices derived from satellite data. However, in this case care must be taken because the vegetation indices saturate at higher vegetation densities and the relationships are dependent on vegetation type.

The scalar roughness height for heat transfer, z_{0h}, which changes with surface characteristics, atmospheric flow and thermal dynamic state of the surface, can be derived from the roughness model for heat transfer proposed by Su et al., (1999) and Su et al., (2001). However, their model requires a functional form to describe the vertical structure of the vegetation canopy to calculate the within-canopy wind speed profile extinction coefficient, n_{ec}. For local studies, this information is easily obtained, but for large scale applications, it is generally impossible to obtain detailed information on the vertical structure of the canopy. In this study, n_{ec}, is formulated as a function of the cumulative leaf drag area at the canopy top:

$$n_{ec} = \frac{C_d \times LAI}{2u_*^2/u(h)^2} \qquad \text{Eq. 4.13}$$

Where C_d is the drag coefficient of the foliage elements assumed to take the value of 0.2, LAI is the one-sided leaf area index defined for the total area, u (h) is the horizontal wind speed at the canopy top. The scalar roughness height for heat transfer, Z_{0h}, can be derived from:

$$Z_{0h} = Z_{0m}/exp(kB^{-1}) \qquad \text{Eq. 4.14}$$

Where B^{-1} is the inverse Stanton number, a dimensionless heat transfer coefficient. To estimate the kB^{-1} value, an extended model of Su et al., (2001) is proposed as follows:

$$kB^{-1} = \frac{kC_d}{4C_1 \frac{u_*}{u(h)}\left(1 - e^{-n_{ec}/2}\right)} f_c^2 + 2f_c f_s \frac{k \times (u_*/u(h)) \times (Z_{0h}/h)}{C_1^*} + kB_s^{-1} f_s^2 \quad \text{Eq. 4.15}$$

Where f_c is the fractional canopy coverage and f_s is its complement. C_t is the heat transfer coefficient of the leaf. For most canopies and environmental conditions, C_t is bounded as $0.005N \leq C_t \leq 0.075N$ (N is number of sides of a leaf to participate in heat exchange), the heat transfer coefficient of the soil is given by

$$C_t^* = P_r - \frac{2}{3} Re^* - \frac{1}{2} \quad \text{Eq. 4.16}$$

Where P_r is the Prandtl number and,

$$R_e^* = \frac{hsu^*}{v} \quad \text{Eq. 4.17}$$

Where, the roughness Reynolds number (R_e^*) with hsu* the roughness height of the soil (m).

The kinematic viscosity of the air measured in Ns/m^2 is v, where v is estimated by:

$$v = 1327x10^{-5} \frac{P_o}{P} x \frac{T}{T_o} x\ 1.81 \quad \text{Eq. 4.19}$$

with P and T the ambient pressure and temperature (Massman, 1999) and P_0 = 101.3 kP$_a$ and T_0 = 273.15 K. Physically and geometrically, the first term of Eq. (4.20) follows the full canopy only model of Choudhury and Monteith (1988), the third term is that of Brutsaert (1982) for a bare soil surface, while the second term describes the interaction between vegetation and a bare soil surface. A quadratic weighting based on the fractional canopy coverage is used to accommodate any situation between the full vegetation and bare soil conditions. For bare soil surface kB $^{-1}$ is calculated according to Brutsaert (1982):

$$kB^{-1} = 2.46(Re_*)^{1/4} - \ln[7.4]$$ Eq. 4.20

A new formulation for determination of evaporative fraction on the basis of energy balance at limiting cases 'Application of SEBS model'. The application of the SEBS algorithm requires parameters derived from three different data sets: 1) AATSR data, 2) MERIS data and 3) Meteorological data. These data sets are described in the following subheadings.

4.1.2.2. AATSR

The AATSR sensor has a spatial resolution of 1 km at nadir. AATSR has three channels at thermal infrared wavelengths, from which surface temperatures are derived over both sea and land surfaces. In addition, AATSR has four visible and near-infrared wavelength channels, which are commonly used to identify cloudy areas and to measure solar radiation that is scattered and reflected from the Earth's surface and atmosphere (Huot et al., 2001). The principal objective of the sensor is to provide data with high levels of accuracy and revisiting frequency required for monitoring and carrying out research regarding the Earth's climate. The image used was acquired on the 10th of August 2007.

4.1.2.3. MERIS

The MERIS sensor has a spatial resolution of 1 km at nadir designed to acquire data over the earth whenever illumination conditions are suitable (Huot et al., 2001). The primary objective of MERIS is to derive estimates of the concentration of chlorophyll-a and suspended sediments in the water. MERIS is very useful to monitor the evolution of terrestrial environments (Kerr and Ostrovsky, 2003), such as the fraction of the solar radiation effectively used by plants in the process of photosynthesis. The image used was acquired on the 9th of August 2007.

4.1.2.4. Meteorological data

Six different weather stations located in the study area were used to obtain the average meteorological input data for the purpose of this study. The meteorological data used are: a) mean temperature, measured using a psychrometer, b) wind speed, measured using the CSAT3 instrument by Campbell, c) humidity, measured using hygrometers, d) surface pressure, measured using the PTB101b instrument and e) solar radiation, measured using the CNR1 instrument by Kipp and Zonen. The data were collected during August 2007. Figure 4.6

Figure 4.6: Location map of the study area and selected weather stations.

4.1.3. Application of SEBS model

The model consists of: a) a set of tools for the determination of the physical and biological parameters of the surface, such as albedo, emissivity, temperature, and vegetation coverage, b) a model for the determination of the roughness length for heat transfer, and c) a formulation for the determination of the evaporative fraction on the basis of energy balance at limiting meteorological conditions (Su et al., 2001; Su, 2001; Su, 2002).

Following the previous equations, SEBS basic used equations are:

$$R_n = G_0 + H + \lambda E \quad \text{Eq. 4.21}$$

Where

R_n net radiation measured in watt per square meter,

G_0 soil heat flux measured in watt per square meter,

H turbulent sensible heat flux measured in watt per square meter,

λE turbulent latent heat flux measured in watt per square meter,

λ latent heat of vaporization measured in watt per square meter, and

E actual evaporation measured in millimeters per day.

Estimation of evaporative fraction requires both dry and wet limiting conditions. At dry limiting condition the latent heat becomes zero due to the limitation of soil moisture, while the sensible heat flux is at its maximum value (Su et al., 2003). Equation (4.21) is reformed:

$$\lambda E_{dry} = R_n - G_0 - H_{dry} \equiv 0, \text{ or}$$

$$H_{dry} = R_n - G_0 \quad \text{Eq. 4.22}$$

Under the wet limiting condition, the evaporation takes place at its maximum rate, λE_{wet} due to the fact that evaporation is only limited by the available energy under the given surface and atmospheric conditions. The sensible heat flux takes its minimum, H_{wet}:

$$\lambda E_{wet} = R_n - G_0 \, , or \quad \text{Eq. 4.23}$$

$$H_{wet} = R_n - G_0 - \lambda E_{wet} \quad \text{Eq. 4.24}$$

Then evaporative fraction can be formulated as:

$$\Lambda_r = \frac{\lambda E}{\lambda E_{wet}} = 1 - \frac{\lambda E_{wet} - \lambda E}{\lambda E_{wet}} \quad \text{Eq. 4.25}$$

By substituting Eqs. (4.21) – (4.23) in Eq. (4.24), the evaporative fraction equation is transformed to:

$$\Lambda_r = 1 - \frac{H - H_{wet}}{H_{dry} - H_{wet}} \quad \text{Eq. 4.26}$$

Where

H is the actual sensible heat flux and determined by the bulk atmospheric similarity approach. Actual sensible heat flux is limited by the H_{dry} and H_{wet} limiting conditions. H_{dry} is obtained from Eq. (4.24) and H_{wet} is derived by a combination equation (Menenti, 1984) holding the assumption of a completely wet condition (Su et al., 2003). Therefore the daily evapotranspiration E_{daily} is expressed as:

$$E_{daily} = \Lambda_0^{24} \times 8.68 \times 10^7 \times \frac{R_n - G_0}{\lambda_{\rho\omega}} \quad \text{Eq. 4.27}$$

Where

Λ_0^{24} Daily evaporative fraction,

ρ_ω density of water measured in kilograms per cubic meter.

Units used in Eqs. 4.22 – 4.25 are in watt per square meter (W m^{-2}) while, the daily evapotranspiration is in millimeters per day (mm d^{-1}), the density of water is in kilograms per cubic meter (kg m^{-3}) and the evaporative fraction is dimensionless. Further details are given by Su, (2002).

The SEBS model was applied to obtain daily evapotranspiration and evaporative fraction with the following data sets:

a) The AATSR image is the source data to generate daily evapotranspiration and the evaporation fraction. The image was firstly preprocessed for geometric correction and then simple atmospheric correction was applied. In addition to that, surface kinetic temperature and surface emissivity were calibrated by the approach of normalizing the emissivities by their average value (Frey et al., 2007) with an accuracy rate of about 1.45 K and emissivities about ± 0.0145 for surface kinetic temperature and surface emissivities respectively.

b) The MERIS image was preprocessed for geometric correction, and then was spectrally corrected to eliminate the "smile effect" (Delwart et al., 2007), which accounts for a small variation of the spectral wavelength of each pixel along the image. The Leaf Area Index (LAI) map was generated by applying the MERIS TOA/TOC-VEG algorithm, which is based on the training of neural networks over a database simulated using radiative transfer models (Gower et al., 1999). It requires top-of-atmosphere and top-of-canopy MERIS reflectance readings and associated canopy structure as inputs, and it allows the derivation of different vegetation biophysical variables including LAI.

c) Meteorological data are used to determine Planetary Boundary Layers (Su et al., 2003).

4.1.4. Accuracy assessment

92 points of actual daily evapotranspiration values were collected during August 2008 (Figure 4.7). The points were uniformly distributed over the entire Nile Delta region. The lysimeter method for daily evapotranspiration estimation was conducted according to Liu and Wang (1999) and the calibrated accuracy was ± 0.025. The calibration was done by placing double infiltrometers above the lysimeter and comparing amounts applied to the saturated profile with amounts collected by the lysimeter (Taylor, 1981). The collection of the actual evapotranspiration data was done within an area of 1 km^2 surrounding the selected point due to accessibility limitations and to stay within the one-pixel size of the AATSR sensor.

The term lysimeter means differential measuring instrument and may be taken, in general, to apply to all instruments which measure weight changes, especially weight reduction due to evapotranspiration in a particular volume of soil with or without accompanying vegetation.

There are two main types of lysimeter in use: the drainage and the weighing types. In the first case, potential evaporation is obtained as the difference between added and drained water quantity. In the second case, changes in the total weight of the soil sample are measured, whereby the real evapotranspiration during as short a time as ten minutes can be estimated. There are two types i.e. the mechanical and the hydraulic weighing lysimeter. In the mechanical weighing lysimeter the soil sample is placed directly on the balance. The sensitivity will be high, if friction can be reduced using an advanced support construction. In the hydraulic weighing lysimeter the soil sample is placed in a tank floating on a fluid. Changes in level reflect weight changes in the sample. Extremely small weight changes can be detected using this method. A collection of lysimeters of varying design has been published by World Meteorological Organization (WMO) 1961 [Technical note no 831]. Lysimeters demand large soil volumes in order that heat and water transport within the soil sample be comparable to conditions in undisturbed soil. When the soil supports vegetation, root growth must be able to proceed without obstruction. These conditions result in very extensive and expensive installation work, particularly in the case of lysimeters using hydraulic weighing. During the years 1971-74 Torbjorn Johnson, at the University of Umeá, constructed a lysimeter according to a modified principle: the dynamic lysimeter. Since 1974 the prototype, including the measuring and recording systems, has been developed and adapted to field use. Hydraulic weighing lysimeter is the used lysimeter type used to collect the giurnd truth data for accuracy assessment, the lysimeter belong to the National Authority for Remote Sensing and Space Sciences (NARSS) located in Cairo, Egypt.

The input data were masked in the ARCGIS environment (ESRI, 2008) in such a way that only the agricultural area in the Nile Delta region was being assessed. The actual evapotranspiration points were intersected with the estimated raster image. A linear

regression model was established to test the correlation between the estimated and the actual measured values.

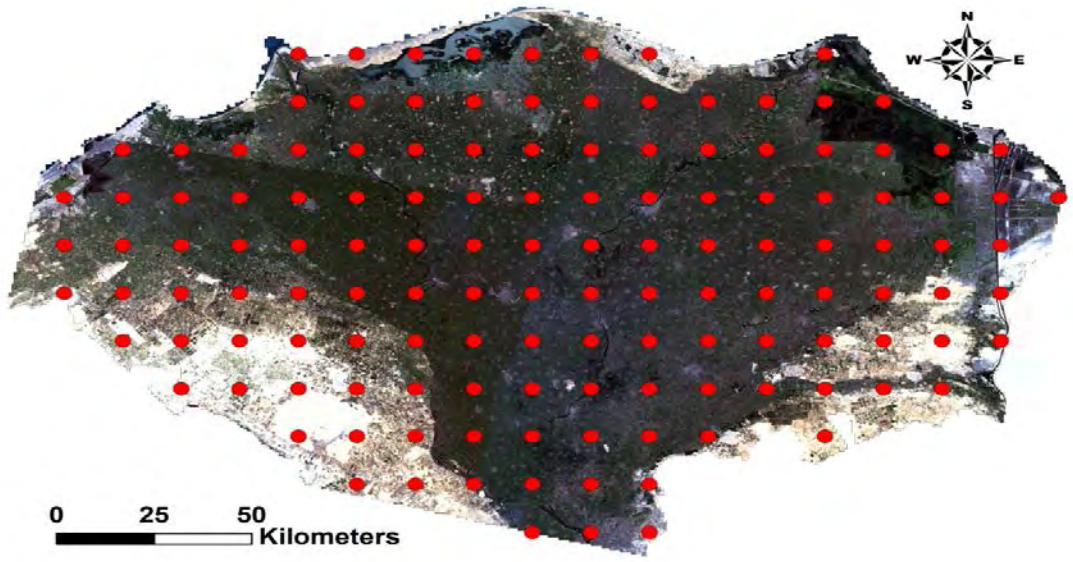

Figure 4.7: Location of the 92 points of actual evapotranspiration data collection.

4.1.5. SEBS Structure

Figure 4.8 demonstrates the basic steps of SEBS model in term of input and output. The main inputs of SEBS model are meteorological data combined with certain remote sensing imagery. On the other hand, the output data are mainly thermal maps where each of which is used for different data measures.

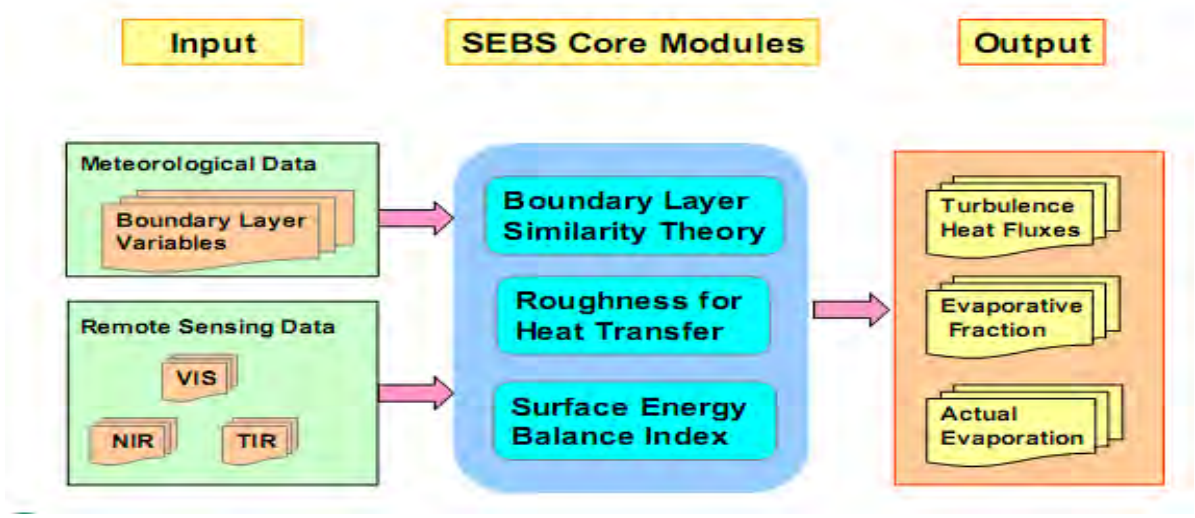

Figure 4.8: Basic steps of SEBS model.

4.2. Land use land cover change detection analysis

4.2.1. Image pre-processing

Distortions and degradations occur in remote sensing images during their acquisition. This is principally due to: variations in atmospheric conditions, variation in altitude, velocity of the sensor platform, platform perturbations, variation in scan speed and in the swath of the sensors field of view, earth curvature and relief displacement. Consequently, it was necessary to correct some of these errors before proceeding with the extraction of thematic information from the satellite images. Apart from correcting the effects of distortion, pre-processing techniques also increase the visual distinction between features. Generally, remote sensing image pre-processing includes the following geometric correction, atmospheric correction, noise removal and image enhancement. Atmospheric correction and noise removal were not implemented in this study because data relating to different atmospheric parameters were not available during image acquisition.

4.2.2. Rectification

Raw, remotely sensed image data gathered by a satellite or aircraft are representations of the irregular surface of the Earth. Even images of seemingly flat areas are distorted by both the curvature of the Earth and the sensor being used.

A map projection system is any system designed to represent the surface of a sphere or spheroid (such as the Earth) on a plane. There are a number of different map projection methods. Since flattening a sphere to a plane causes distortions to the surface, each map projection system compromises accuracy between certain properties, such as conservation of distance, angle, or area. For example, in equal area map projections, a circle of a specified diameter drawn at any location on the map represents the same total area. This is useful for

comparing land use area, density, and many other applications. However, to maintain equal area, the shapes, angles, and scale in parts of the map may be distorted (Jensen, 1996).

There are a number of map coordinate systems for determining location on an image. These coordinate systems conform to a grid, and are expressed as X,Y (column, row) pairs of numbers. Each map projection system is associated with a map coordinate system. Rectification is the process of transforming the data from one grid system into another grid system using a geometric transformation. While polynomial transformation and triangle-based methods are described in this chapter, discussion about various rectification techniques can be found in Yang (1997). Since the pixels of the new grid may not align with the pixels of the original grid, the pixels must be resampled. Resampling is the process of extrapolating data values for the pixels on the new grid from the values of the source pixels.

Georeferencing refers to the process of assigning map coordinates to image data. The image data may already be projected onto the desired plane, but not yet referenced to the proper coordinate system. Rectification, by definition, involves georeferencing, since all map projection systems are associated with map coordinates. Image-to-image registration involves georeferencing only if the reference image is already georeferenced. Georeferencing, by itself, involves changing only the map coordinate information in the image file. The grid of the image does not change.

Geocoded data are images that have been rectified to a particular map projection and pixel size, and usually have had radiometric corrections applied. It is possible to purchase image data that is already geocoded. Geocoded data should be rectified only if they must conform to a different projection system or be registered to other rectified data

4.2.3. Orthorectification

Orthorectification is a form of rectification that corrects for terrain displacement and can be used if there is a DEM of the study area. It is based on collinearity equations, which can be derived by using 3D GCPs. In relatively flat areas, orthorectification is not necessary, but in mountainous areas (or on aerial photographs of buildings), where a high degree of accuracy is required, orthorectification is recommended.

4.2.4. Image enhancement

The application of image enhancement techniques was to improve the interpretation of the image by increasing the apparent distinction between the land use and land cover classes in the scene.

4.2.4.1. Spatial enhancement

Spatial enhancement modifies pixel values based on the values of surrounding pixels. Spatial enhancement deals largely with spatial frequency, which is the difference between the highest and lowest values of a contiguous set of pixels. Jensen (Jensen, 1986) defines spatial frequency as “the number of changes in brightness value per unit distance for any particular part of an image.”

Landsat TM sensors have seven bands with a spatial resolution of 28.5 m. ETM+ panchromatic has one broad band with very good spatial resolution 15 m. Combining these two images to yield a seven-band data set with 15 m resolution provides the best characteristics of both sensors.

A number of models have been suggested to achieve this image merge (Chávez et al, 1991), among others, uses the forward-reverse principal components transforms with the ETM+ image, replacing PC-1.

It is assumed that the intensity component (PC-1 or I) is spectrally equivalent to the ETM+ panchromatic image, and that all the spectral information is contained in the other PCs or in H and S. Since ETM+ data do cover the full spectral range that TM data do, this assumption does strictly hold. It is unacceptable to resample the thermal band (TM 6) based on the visible (ETM+ panchromatic) image.

The Resolution Merge function used for resampling low spatial resolution data to a higher spatial resolution while retaining spectral information and is: principal components merge and cubic convolution as resampling method.

Principal Components Merge: Because a major goal of this merge is to retain the spectral information of the six TM bands 1 -5, 7), this algorithm is mathematically rigorous. It is assumed that: PC-1 contains only overall scene luminance; all interband variation is contained in the other 5 PCs, and scene luminance in the SWIR bands is identical to visible scene luminance. With the above assumptions, the forward transform into PCs is made. PC-1 is removed and its numerical range (min to max) is determined. The high spatial resolution image is then remapped so that its histogram shape is kept constant, but it is in the same numerical range as PC-1. It is then substituted for PC-1 and the reverse transform is applied. This remapping is done so that the mathematics of the reverse transform does not distort the thematic information (Welch and Ehlers, 1987; Jacob et al., 2002).

Convolution Filtering: Convolution filtering is the process of averaging small sets of pixels across an image. Convolution filtering is used to change the spatial frequency characteristics of an image (Jensen, 1996). A convolution kernel is a matrix of numbers that is used to average the value of each pixel with the values of surrounding pixels in a particular way. The numbers in the matrix serve to weight this average toward particular pixels. These numbers are often called coefficients, because they are used as such in the mathematical equations.

4.2.4.2. Spectral enhancement

The application of image enhancement techniques was to improve the interpretation of the image by increasing the apparent distinction between the land use and land cover classes in the scene. The following image enhancement techniques were used in the transformation of the satellite data: principal component analysis, Tasselled Cap Transformation and NDVI.

1- **Principal Component Analysis (PCA):** PCA was calculated for all the satellite images. Principal component analysis is an important data transformation technique used in remote sensing work with multi-spectral data. The principal components transformation is a reduction technique that leads to describing multidimensional data in which the variables are non-correlated with the first component containing most variance and the succeeding component, which normally contain decreasing proportion of data scattering.

2- **Tasseled cap transformation (TCT):** the TCT is used to enhance separation between soils and vegetation through the determination of three indices namely; soil brightness, greenness and soil moisture. TCT is an orthogonal transformation where the first index is a weighted sum of all bands in the direction of principle variation in soil reflectance that includes more soil reflectance or brightness information. The second index is the greenness axis that describes the contrast between the near infrared and the visible bands. The third component contrasts mid infrared reflectance with visible and near infrared reflectance and is important in confirming the separation of areas into vegetated and bare soil units. Tasselled cap was done only for TM and ETM+ data because it uses a complicated mathematical combination of as many as six bands to define vegetation.

4.2.5. Image classification process

Classification is the process of sorting pixels into a finite number of individual classes, or categories of data, based on their data file values. If a pixel satisfies a certain set of criteria, then the pixel is assigned to the class that corresponds to those criteria. For the first part of the classification process, the computer system must be trained to recognize patterns in the data. Training is the process of defining the criteria by which these patterns are recognized. The result of training is a set of signatures, which are criteria for a set of proposed classes.

4.2.5.1. Supervised classification

Image analyst "supervises" the selection of spectral classes that represent patterns or land cover features that the analyst can recognize, supervised classification accuracy is mainly based on the training sites "signatures".

A total number of 1200 training sites were selected in each data set. The 1200 training sites were divided based on class's separability and proportionally to the total area of each class per data set according to the following table:

Table 4.1: Total number of the training and validation points per class

Class name	Total number of the training points	Total number of the validation points	Training points percentage per class
Agriculture land	552	414	46 %
Urban	180	135	15 %
Desert	96	72	8 %
Fish farm	228	171	19 %
Surface water	144	108	12 %

Signatures, the result of training are a set of signatures that defines a training sample or cluster. Each signature corresponds to a class, and is used with a decision rule (explained

below) to assign the pixels in the image file to a class. Signatures in ENVI can be parametric or nonparametric.

- A parametric signature is based on statistical parameters (e.g., mean and covariance matrix) of the pixels that are in the training sample or cluster. Supervised and unsupervised training can generate parametric signatures. A set of parametric signatures can be used to train a statistically-based classifier (e.g., maximum likelihood) to define the classes.
- A nonparametric signature is not based on statistics, but on discrete objects (polygons or rectangles) in a feature space image. These feature space objects are used to define the boundaries for the classes. A nonparametric classifier uses a set of nonparametric signatures to assign pixels to a class based on their location either inside or outside the area in the feature space image. Supervised training is used to generate nonparametric signatures (Kloer, 1994).

The four scenes in each data set were first geometrically corrected (ENVI, 2009) to a reference image of known geographic coordinate system (UTM N 36, WGS_84 datum). Second, a relative radiometric correction method using image regression was implemented to minimize or eliminate the effects of dissimilar dates of acquisition (Jensen et al., 1995; Jensen, 1996). Third, the four scenes of each data set were mosaicked using linear contrast stretching and histogram equalization (ENVI, 2009) to create a single image covering the whole study area from each data set. Finally, supervised signature extractions with five different classification algorithms were applied to select the optimum classification algorithm. The different classification algorithms according to Richards, (1999) are:

1) **Mahalanobis Distance:** a direction-sensitive distance classifier that uses statistics for each class. It is similar to the maximum likelihood classification but assumes all class

covariances are equal and therefore is a faster method. All pixels are classified to the closest ROI class unless you specify a distance threshold, in which case some pixels may be unclassified if they do not meet the threshold.

2) **Minimum Distance:** The minimum distance technique uses the mean vectors of each endmember and calculates the Euclidean distance from each unknown pixel to the mean vector for each class. All pixels are classified to the nearest class unless a standard deviation or distance threshold is specified, in which case some pixels may be unclassified if they do not meet the selected criteria
3) **Maximum Likelihood:** Maximum likelihood classification assumes that the statistics for each class in each band are normally distributed and calculates the probability that a given pixel belongs to a specific class. Unless you select a probability threshold, all pixels are classified. Each pixel is assigned to the class that has the highest probability (that is, the maximum likelihood). If the highest probability is smaller than a threshold you specify, the pixel remains unclassified.
4) **Artificial Neural Networks:** Use Neural Networks to apply a layered feed-forward neural network classification technique. The Neural Net technique uses standard backpropagation for supervised learning. You can select the number of hidden layers to use and you can choose between a logistic or hyperbolic activation function. Learning occurs by adjusting the weights in the node to minimize the difference between the output node activation and the output. The error is backpropagated through the network and weight adjustment is made using a recursive method. You can use Neural Net classification to perform non-linear classification and,
5) **Parallelepiped:** Parallelepiped classification uses a simple decision rule to classify multispectral data. The decision boundaries form an *n*-dimensional parallelepiped classification in the image data space. The dimensions of the parallelepiped

classification are defined based upon a standard deviation threshold from the mean of each selected class. If a pixel value lies above the low threshold and below the high threshold for all *n* bands being classified, it is assigned to that class. If the pixel value falls in multiple classes, ENVI assigns the pixel to the last class matched. Areas that do not fall within any of the parallelepiped classes are designated as unclassified.

Five classes were assigned to describe the LULC in each data set, the LULC classes are: Urban, Agricultural Land, Surface Water, Desert and Fish Farms.

4.2.5.2. Classification accuracy assessment

A total number of 900 points of ground truth data were collected during July and august 2009, the points demonstrating the major land use/land cover in the Nile Delta desired as following: Urban, Agricultural Land, Surface Water, Desert and Fish Farms. The points were evenly distributed over the entire Nile Delta region. The points were converted into 300 m^2 polygons under ArcGIS environment (ESRI, 2008) for accessibility reasons.

Overall, producers and users accuracy were derived from the Error Matrix. The Kappa analysis is discrete multivariate technique used in accuracy assessment to statically determine whether one error matrix is significantly different to another (Cohen, 1960). The result of performing Kappa analysis is K_{hat} statistics (actually *K*, an estimate of Kappa), which is another measure of agreement of accuracy. This measure of agreement is based on the difference between the actual agreements in the error matrix (Congalton and Read, 1983). An accuracy assessment was then carried out following (Congalton, 1991) to estimate K_{hat} for different the employed classification algorithms:

$$K_{hat} = \frac{N\sum_{i=1}^{r} x_{ii} - \sum_{i=1}^{r}(x_{ij} \times x_{ji})}{N^2 - \sum_{i=1}^{r}(x_{ij} \times x_{ji})} \quad \text{Eq. 4.28}$$

4.2.6. Post classification comparison

Post Classification tools used to classify rule images, to calculate class statistics and to apply majority or minority analysis to the three different classification images (ENVI, 2009). The Post-Classification comparison change detection (Mas, 1999; Coppin et al., 2004) was done after classifying the rectified images separately from three time periods (1984, 2002 and 2009). Each date of imagery was satisfactorily classified using ENVI. The classified images were then, compared and analyzed in order to conduct and the change detection (Lu et al., 2004; Rivera, 2005; Huang et al., 2008). The fallow soil class in each data set was merged with agriculture class of the correspondent data set. This is due to the fact that fallow area exists for a short period approximately two to four weeks and coincidentally this period corresponded with the acquisition of the satellite image. Generally, the fallow areas are again cultivated with crops after this period. Figure 4. 9 shows the steps of post-classification in the study area.

4.3. Daily evapotranspiration time series analysis

A time series is a set y1, y2, ... ,yN of observations taken over a series of equally-spaced time periods. The analysis begins with a plot of the points in the time series. In addition, autocorrelations and partial autocorrelations of the series are displayed on graphs. These indicate how and to what degree each point in the series is correlated with earlier values in the series (Gouveia and Fletcher, 2000; Brockwell and Davis, 2001).

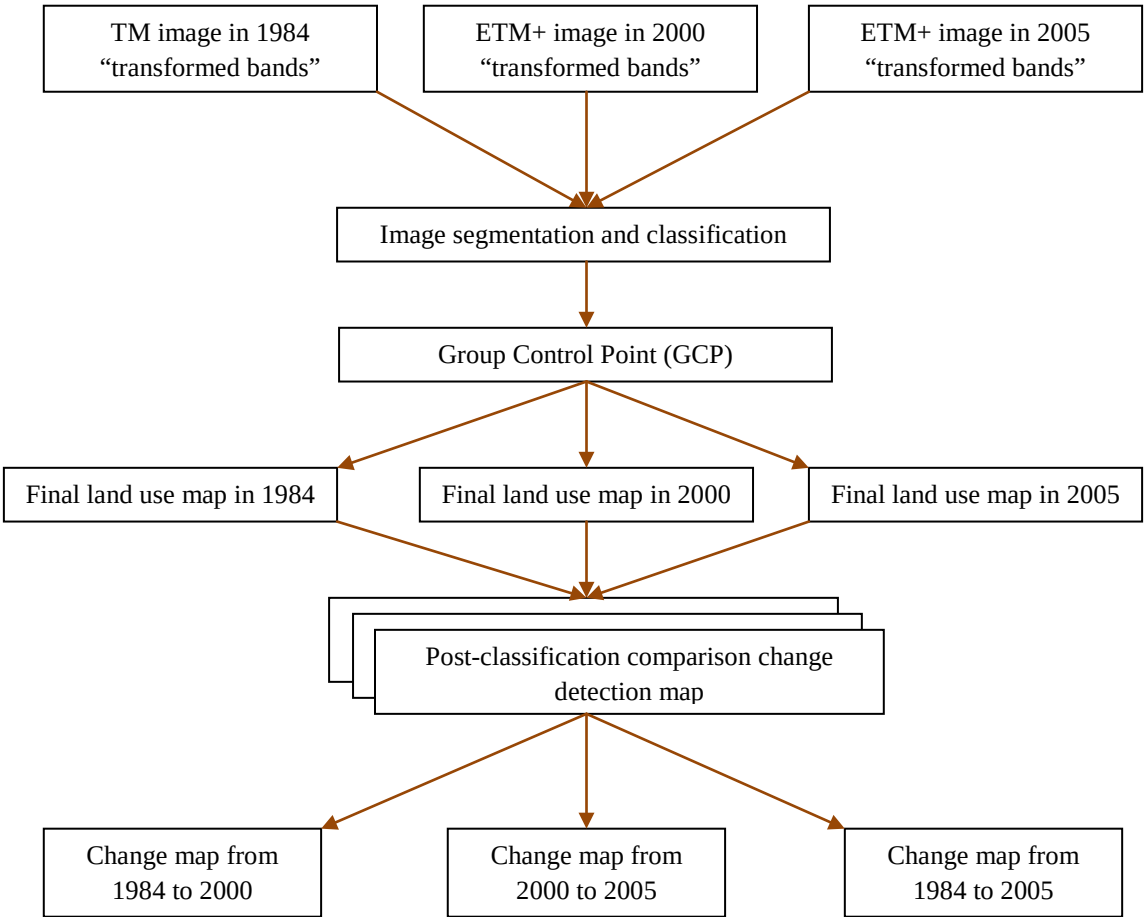

Figure 4.9: Change detection flow chart.

4.3.1. Autocorrelation

This function describes the correlation between all the pairs of points in the time series with a given separation in time or lag (Kocak et al., 2000). The autocorrelation for the k_{th} lag is

$$r_k = \frac{C_k}{C_0} \qquad \text{Eq. 4.29}$$

Where

$$C_k = \frac{1}{N} \sum_{r-k+1}^{N} (y_r - \bar{y})(y_r - k^{-\bar{y}}) \qquad \text{Eq. 4.30}$$

Where

$\bar{y}$ is the mean of the *N* nonmissing points in the time series.

By definition, the first autocorrelation (lag 0) always has length 1. The curves show twice the large-lag standard error (± 2 standard errors), computed as

$$SE_k = \sqrt{\frac{1}{N}\left(1 + 2\sum_{i=1}^{k-1} r_i^2\right)} \quad \text{Eq. 4.31}$$

In addition, the Ljung-Box Q and p-values are shown for each lag.The Q-statistic is used to test whether a group of autocorrelations is significantly different from zero or to test that the residuals from a model can be distinguished from noise.

4.3.2. Partial autocorrelation

The Partial Autocorrelation command alternately hides or displays the graph of the sample partial autocorrelations. The plot on the right in "Autocorrelation and Partial Correlation Plots" the partial autocorrelation function shows the Series data. It represents ± 2 standard errors for approximate 95% confidence limits, where the standard error is computed for all k as the following:

$$SE_k = \frac{1}{\sqrt{N}} \quad \text{Eq. 4.32}$$

4.3.3. Autoregressive integrated moving average model

ARIMA (p,d,q): ARIMA models are, in theory, the most general class of models for forecasting a time series which can be stationarized by transformations such as differencing and logging (Roberts, 2003). In fact ARIMA models ~~is~~ consists~~s~~ of adding lags of the differenced series and/or lags of the forecast errors to the prediction equation, as needed to remove any last traces of autocorrelation from the forecast errors.

Lags of the differenced series appearing in the forecasting equation are called "auto-regressive" terms, lags of the forecast errors are called "moving average" terms, and a time series which needs to be differenced to be made stationary is said to be an "integrated" version of a stationary series. Random-error and random-trend models, autoregressive models, and exponential smoothing models (i.e., exponential weighted moving averages) are all special cases of ARIMA models (Sall and Lehman 1996; Roberts, 2003).

A Seasonal ARIMA model is classified as an "ARIMA (p,d,q)" model, where:

- p is the number of autoregressive terms,
- d is the number of seasonal differences, and
- q is the number of lagged forecast errors in the prediction equation.

Appropriate ARIMA model for a time series depend on identifying the order(s) of differencing needing to stationarize the series and remove the gross features of seasonality, perhaps in conjunction with a variance-stabilizing transformation such as logging or deflating. At constant difference between the points in series and its predictions this merely fitted a random walk or random trend model. Random walk model predicts the first difference of the series to be constant, the seasonal random walk model predicts the seasonal difference to be constant, and the seasonal random trend model predicts the first difference of the seasonal difference to be constant usually zero. However, the best random walk or random trend model may still have autocorrelated errors, suggesting that additional factors of some kind are needed in the prediction equation. The following subcategories of ARIMA model are described following Box and Jenkins (1994).

ARIMA (0,1,0) = random walk: In models encountered two strategies for eliminating autocorrelation in forecast errors. One approach, which we first used in regression analysis, was the addition of lags of the stationarized series. For example, suppose we initially fit the

random-walk-with-growth model to the time series Y. The prediction equation for this model can be written as:

$$\hat{Y}(t) - Y(t-1) = \mu \quad \text{Eq. 4.33}$$

Where, the constant term (here denoted by "mu") is the average difference in Y. This can be considered as a degenerate regression model in which DIFF(Y) is the dependent variable and there are no independent variables other than the constant term. Since it includes (only) a seasonal difference and a constant term, it is classified as an "ARIMA (0,1,0) model with constant." Of course, the random walk without growth would be just an ARIMA (0,1,0) model without constant

ARIMA (1,1,0) = differenced first-order autoregressive model: If the errors of the random walk model are autocorrelated, perhaps the problem can be fixed by adding one lag of the dependent variable to the prediction equation--i.e., by regressing DIFF(Y) on itself lagged by one period. This would yield the following prediction equation:

$$\hat{Y}(t) - Y(t-1) = \mu + \emptyset\big(Y\,(t-1) - Y(t-2)\big) \quad \text{Eq. 4.34}$$

This can be rearranged to:

$$\hat{Y}(t) = \mu + Y(t-1) + \emptyset\big(Y\,(t-1) - Y(t-2)\big) \quad \text{Eq. 4.35}$$

This is a first-order autoregressive, or "AR (1)", model with one order of seasonal differencing and a constant term--i.e., an "ARIMA (1,1,0) model with constant." Here, the constant term is denoted by "μ" and the autoregressive coefficient is denoted by "φ", in keeping with the terminology for ARIMA models popularized by Box and Jenkins (Vandaele, 1983). (In the output of the Forecasting procedure in Statgraphics, this coefficient is simply denoted as the AR (1) coefficient.)

ARIMA (0,1,1) without constant = simple exponential smoothing: Another strategy for correcting autocorrelated errors in a random walk model is suggested by the simple exponential smoothing model. For some nonstationary time series (e.g., one that exhibits noisy fluctuations around a slowly-varying mean), the random walk model does not perform as well as a moving average of past values. In other words, rather than taking the most recent observation as the forecast of the next observation, it is better to use an average of the last few observations in order to filter out the noise and more accurately estimate the local mean. The simple exponential smoothing model uses an exponentially weighted moving average of past values to achieve this effect. The prediction equation for the simple exponential smoothing model can be written in a number of mathematically equivalent ways, one of which is:

$$\hat{Y}(t) = Y(t-1) - \theta\, e\,(t-1) \qquad \text{Eq. 4.36}$$

Where, *e*(t-1) denotes the error at period t-1. This resembles the prediction equation for the ARIMA (1,1,0) model, except that instead of a multiple of the lagged difference it includes a multiple of the lagged forecast error. The coefficient of the lagged forecast error is "θ" and it is conventionally written with a negative sign for reasons of mathematical symmetry. " θ " in this equation corresponds to the quantity "1-a" in the exponential smoothing formulas.

When a lagged forecast error is included in the prediction equation as shown above, it is referred to as a "moving average" (MA) term. The simple exponential smoothing model is therefore a first-order moving average ("MA (1)") model with one order of seasonal differencing and no constant term --i.e., an "ARIMA (0,1,1) model without constant." This means that in Statgraphics (or any other statistical software that supports ARIMA models) can actually fit a simple exponential smoothing by specifying it as an ARIMA (0,1,1) model

without constant, and the estimated MA (1) coefficient corresponds to "1- a " in the SES formula.

ARIMA (0,1,1) with constant = simple exponential smoothing with growth: By implementing the SES model as an ARIMA model, gains the model some flexibility. First of all, the estimated MA (1) coefficient is allowed to be negative: this corresponds to a smoothing factor larger than 1 in an SES model, which is usually not allowed by the SES model-fitting procedure. Second, the option of including a constant term in the ARIMA model in order to estimate an average non-zero trend is holding. The ARIMA (0,1,1) model with constant has the prediction equation:

$$\hat{Y}(t) = \mu + Y(t-1) - \theta\, e\,(t-1) \qquad \text{Eq. 4.37}$$

The one-period-ahead forecasts from this model are qualitatively similar to those of the SES model, except that the trajectory of the long-term forecasts is typically a sloping line (whose slope is equal to mu) rather than a horizontal line.

ARIMA (0,2,1) or (0,2,2) without constant = linear exponential smoothing: Linear exponential smoothing models are ARIMA models which use two seasonal differences in conjunction with MA terms. The second difference of a series Y is not simply the difference between Y and itself lagged by two periods, but rather it is the first difference of the first difference--i.e., the change-in-the-change of Y at period t. Thus, the second difference of Y at period t is equal to (Y(t)-Y(t-1)) - (Y(t-1)-Y(t-2)) = Y(t) - 2Y(t-1) + Y(t-2). A second difference of a discrete function is analogous to a second derivative of a continuous function: it measures the "acceleration" or "curvature" in the function at a given point in time.

The ARIMA (0,2,2) model without constant predicts that the second difference of the series equals a linear function of the last two forecast errors:

$$\hat{Y}(t) - 2Y(t-1) + Y(t-2) = -\theta_1\, e(t-1) - \theta_2\, e(t-2) \quad \text{Eq. 4.38}$$

Which can be rearranged as:

$$\hat{Y}(t) = 2Y(t-1) - Y(t-2) - \theta_1\, e(t-1) - \theta_2\, e(t-2) \quad \text{Eq. 4.39}$$

where θ_1 and $t\theta_2$ are the MA (1) and MA (2) coefficients. This is essentially the same as Brown's linear exponential smoothing model, with the MA (1) coefficient corresponding to the quantity $(1\text{-}a)^2$ in the LES model. The forecasting equation for the LES model is:

$$\hat{Y}(t) = 2Y(t-1) - Y(t-2) - 2(1-a)\, e\,(t-1) + (1-a)^2\, e(t-2) \quad \text{Eq. 4.40}$$

Upon comparing terms, the MA (1) coefficient corresponds to the quantity $(1\text{-}a)^2$ and the MA (2) coefficient corresponds to the quantity $-(1\text{-}a)^2$. If "a" is larger than 0.7, the corresponding MA (2) term would be less than 0.09, which might not be significantly different from zero, in which case an ARIMA (0,2,1) model probably would be identified.

A "mixed" model ARIMA (1,1,1): The features of autoregressive and moving average models can be "mixed" in the same model. For example, an ARIMA (1,1,1) model with constant would have the prediction equation:

$$\hat{Y}(t) = \mu + Y(t-1) + \emptyset\big(Y\,(t-1) - Y(t-2)\big) - \theta\, e(t-1) \quad \text{Eq. 4.41}$$

Normally, though, several attempts to stick to "unmixed" models with either only-AR or only-MA terms, because including both kinds of terms in the same model sometimes leads to overfitting of the data and non-uniqueness of the coefficients.

4.3.4. Accuracy assessment

36 entry of actual daily evapotranspiration values were collected from six weather stations distributed in the study area demonstrated in Figure 4.6). Daily evapotranspiration values

were calculated using Penman–Monteith method (FAO, 1995). The method calculates the net evapotranspiration value (mm) and requires as input daily mean temperature, wind speed, relative humidity and solar radiation conducted directly from the weather stations. A linear regression model was established to test the correlation between the actual evapotranspiration value and the estimated evapotranspiration value in corresponding to the same or the closer date of the actual measurement.

4.4. Development of GIS and RS strategies for water resources management plans

4.4.1. ASTER data DEM extraction

The ASTER Earth Observation Satellite is unique in that it offers nearly simultaneous capture of stereo images, minimizing temporal changes and sensor modeling errors. Band 3 of the VNIR sensor includes two channels, a Nadir looking scene and a Backward looking scene. This provides stereo coverage from which a Digital Elevation Model (DEM) can be automatically extracted

A DEM, Digital Elevation Model, is a raster file that depicts elevation in dark and light pixels; dark pixels denoting low areas of elevation, and light pixels denoting high areas of elevation. Points in a DEM are arranged in a regular grid. An output DEM is saved with the *.img extension and is accompanied by a *.wcs file.

4.4.2. Vegetation indices

Spectral Enhancement is the changing of the values of each pixel in the original image by transforming the values of each pixel along a multiband basis. Spectral Enhancement allows different features that have specific reflective characteristics in different bands of the electromagnetic spectrum to be compressed if data is similar. It also allows modifying of the

pixels of an image independent of the values of surrounding pixels. Spectral enhancement creates new bands of data that are more interpretable to the eye. NDVI derivatives are useful to recognize other vegetation indices including; Leaf Area Index (LAI) and Water Supply Vegetation Index (WSVI). Meanwhile, soil water relation in term of evapotranspiration is useful to calculate other vegetation indices including; Crop Water Shortage Index (CWSI) and Drought Severity Index (DSI).

Leaf Area Index (LAI): LAI represents the amount of leaf material in an ecosystem and is geometrically defined as the total one-sided area of photosynthetic tissue per unit ground surface area. Ground-based measurements have no standards as several methods, like harvesting methods, hemispherical photography or light transmission through canopies, can be used. The conversion of effective values, as available from measurements using optical devices, to allometric values requires additional information about the structure and architecture of the canopy, e.g. gap size distributions, at the appropriate spatial resolutions.

Monitoring the distribution and changes of Leaf Area Index (LAI) is important for assessing growth and vigor of vegetation on the planet. It is fundamentally important as a parameter in land-surface processes and parameterizations in climate models. This variable represents the amount of leaf material in ecosystems and controls the links between biosphere and atmosphere through various processes such as photosynthesis, respiration, transpiration and rain interception. The following equation is used to determine LAI from NDVI for agricultural land (Asrar et al., 1992):

$$LAI = NDVI \times 1.71 + 0.4 \qquad \text{Eq. 4. 42}$$

Water Supply Vegetation Index (WSVI): when crops are suffered from drought, their leaf apertures is partly closed in order to reduce the loss of water. It makes the increase of temperature of leaf surface. The more severe the drought is, the higher the temperature of leaf

surface is. At the same time, the growth of crops is affected by drought, resulting in the decrease of leaf area index (LAI). Besides, leaf will also be under high air temperature. All of these may result in reduction of NDVI. Water supply vegetation index (WSVI) is defined as follows:

$$WSVI = NDVI/T_s \quad \text{Eq. 4. 43}$$

Where, T_s is the brightness temperature channel or related remote sensing imagery. The smaller this index is, the more severe the drought is.

Crop Water Shortage Index (CWSI): the estimation of crop water shortage index is performed as follows:

$$CWSI = 1 - E_a/E_p \quad \text{Eq. 4.44}$$

Where, E_a is actual evapotranspiration, while E_p evapotranspiration capacity. The smaller the value of E_a, the higher the value of CWSI, indicating less water supply ability, namely land is arid. Because evapotranspiration has close relation with soil moisture content, namely water supply ability, so CWSI also has close relation with soil moisture content. Both CWSI and soil moisture content indicate the degree of soil drought.

Drought Severity Index (DSI): Drought is usually defined as a significant, temporary reduction in water availability below the expected amount for a specified period and for a defined climatic zone. Drought episodes may be described by means of different characteristics, namely drought duration and intensity, considered as the two dimensions of this agro-climatic phenomenon. Among the several methods proposed for describing drought, the run method appears as suitable to provide an objective characterization of drought events. A simple drought index, obtained from either by Relative Plant Available Soil Water Content (R) or heat flux (H):

$$DSI = 1 - R = (H - H_{wet})/(H_{dry} - H_{wet})$$ Eq. 4. 45

The equation is able to describe different dimensions of drought phenomena (duration, intensity and severity), and to recognize normal conditions, both in statistical and ecological terms, is meaningful.

4.5. Decision making

Decision making is the process that leads to a choice between a set of alternatives. Geographical decision-making means analyzing and interpreting geographical information that is related to the alternatives in question. Decision making is often used in land suitability analysis, or site selection, as well as location allocation modeling. All decision making has a degree of uncertainty, ranging from a predictable (deterministic) situation to an uncertain situation (Malczewski, 1999). The latter one can be subdivided into stochastic decisions (which can be modeled by probability theory and statistics) and fuzzy decisions (which can model by fuzzy set theory and others). Consequently, particularly in uncertain situations, decision making involves the risk of making a "wrong" decision, because the information acquired is insufficient or the approach used is inappropriate, when uncertainty is part of the process, this uncertainty may in some cases be quantified and as such add another decision criteria to the evaluation process (Elhag, 2010).

4.5.1. Basic steps of multi criteria analysis

The following Figure 4.10 shows the basic steps of multi-criteria decision analysis as implemented in any SDSS process (Saaty, 1977; Saaty, 1980). The decision process starts with problem structuring during which the problem to be solved is explored and available information is collected. The possible options – responses in terms of the Driving Forces-Pressures-State-Impacts-Responses (DPSIR) framework – are defined and criteria aiming at evaluation of their performance are identified. In the next step the options' performance in

terms of the criteria scores is modelled. As a result a matrix – called analysis matrix – is constructed. The analysis matrix contains the raw options' performance with different criteria scales (Saaty, 1977; Yager 1988).

Before any aggregation may start, the options' performance with regards to different criteria have to be made comparable. During the normalization procedures, or at least by applying a value function, the scores are transformed to values on a uniform scale. Since a simple standardization allows only the transformation of a given value range to a standardized one [0,1], the value function includes human judgments in the mathematical transformation. A value function translates the performance of an option into a value score, which represents the degree to which a decision objective is matched. Since the main aim of a multi-criteria decision analysis is to reduce option of each performance into a single value to facilitate the ranking process, the heart piece of any MCA decision rule is an aggregation procedure. The large quantity of known decision rules differ in the way the multiple options performances are aggregated into a single value. There is no single method that is universally suitable for any kind of decision problem, the decision maker has to choose the method which best corresponds with his purpose (Saaty, 1977).

In a situation where there is several decision makers involved in the decision process, the individual choices are to be compared and an option is to be chosen, which represents the group compromise decision.

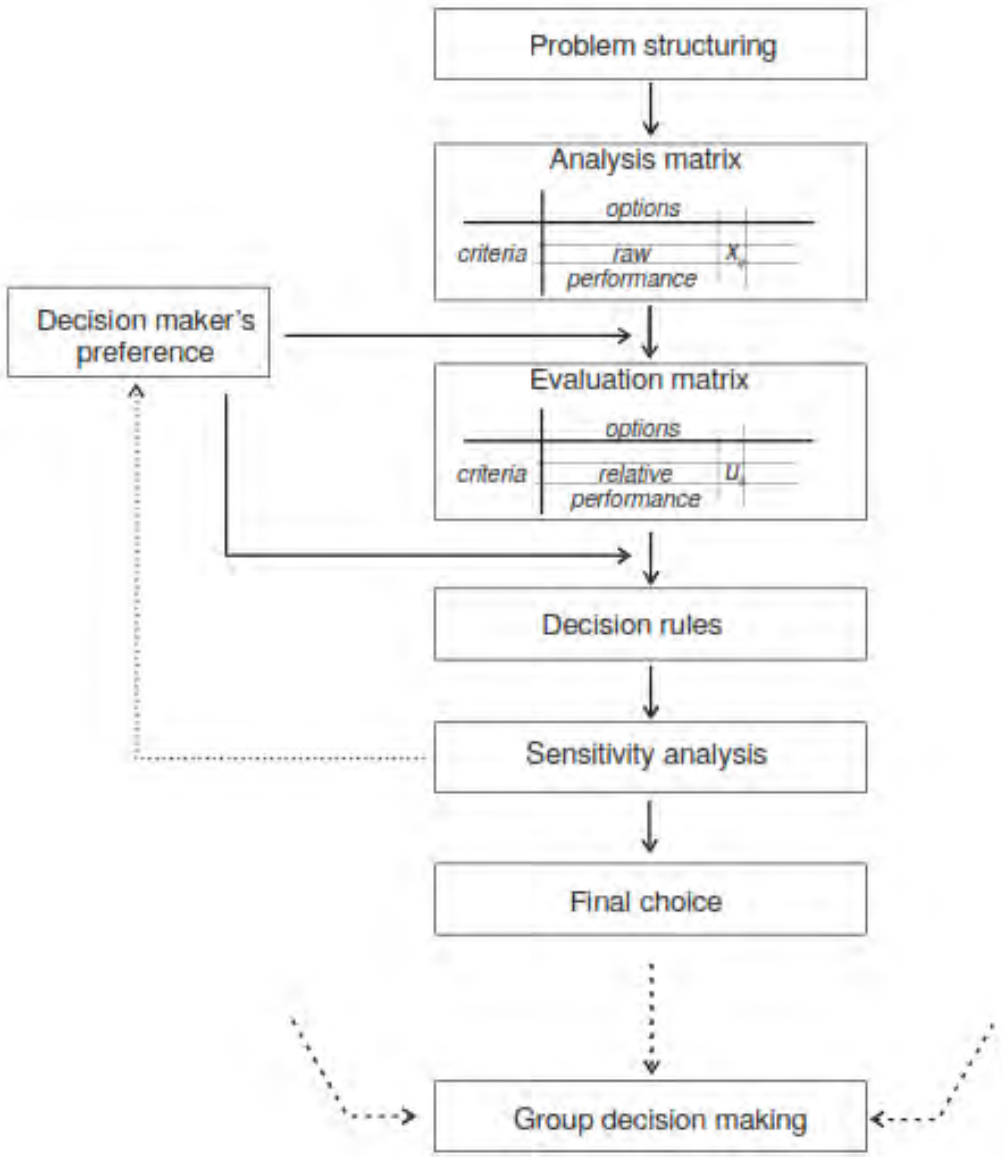

Figure 4. 10: The basic steps of the MCA that is implemented in the SDSS

4.5.2. Generating the analysis matrix

The analysis matrix (M x N: M options and N criteria) is to be built from the environmental indicators identified in the conceptual phase. The cells of the matrix relate to the option-criterion pairs and contain the outcomes or consequences for a set of options and a set of evaluation criteria.

In spatial decision-making, the options are a collection of points, lines, and areal objects with associated attributes. The decision outcomes, as in Figure 4.11 b-c, may have spatial extensions. For example, in the case of two-dimension a spatial extended decision outcomes

(Figure 4.11 c), a cell of the decision matrix corresponds to a map, which contains the spatially distributed consequences of an option with regards to a criterion. Different to the case of non-dimensional (value- or point-like outcomes, Figure 4.11 a) consequences, an additional aggregation must be done.

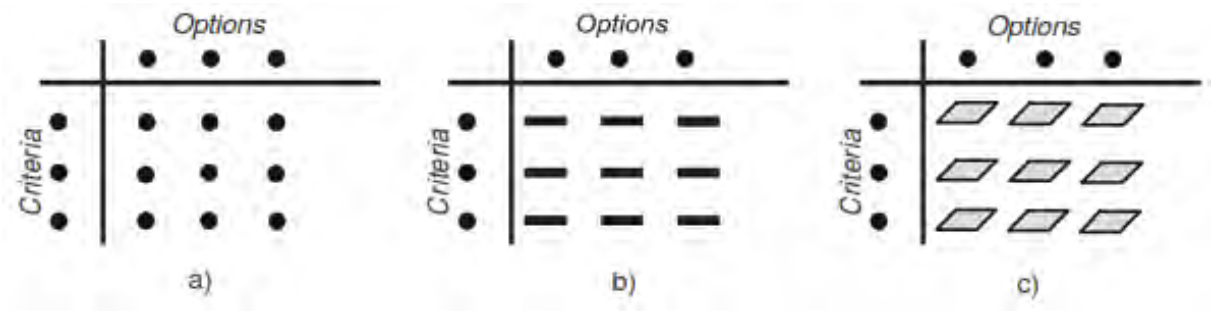

Figure 4. 11: Different dimensions of decision outcomes: spatial dimension 0 (a); 1 (b) and 2 (c).

Multiple criteria typically have varying importance. To illustrate this, each criterion can be assigned a specific weight that reflects it importance relative to other criteria under consideration. The weight value is not only dependent on the importance of any criterion; it is also dependent on the possible range of the criterion values. A criterion with variability will contribute more to the outcome of the alternative and should consequently be regarded as more important than criteria with no or little changes in their range. Weights are usually normalized to sum up to 1, so that in a set of weights (w 1, w 2, till w n) =1.

Weight Linear Combination formula is described as following:

$$Suitability = \sum w_i x_i \times \prod c_j \qquad \text{Eq. 4. 46}$$

Where W_i = weight of factor I, X_i = criterion score of factor and C_j = criterion score of constraint $_j$

To proceed with the analysis, criteria need to be identified; a criterion map is a layer in GIS database representing evaluation criteria. There are two different types of criteria, factor and constraint criterion. In the present study, seven factors and two constraints were used:

I - A factor is a criterion that enhancement or detract from the suitability of a specific alternative. The current study includes five factors; the following table describes the different layers and their classification according to deterministic transformation in Table 4.2.

II – A constraint serves to limit alternative under consideration. There are two different constraints considered in the current study, DEM and land cover classes. Slope less than 30% was considered to be suitable for rice cultivation and only agricultural land class was considered to be suitable for the same purpose.

The score range of each factor used in the establishment of weighted linear combination is described in Figure 4.12 (fuzzy sigmoidal function) and Figure 4.13 (fuzzy trapezoidal function). Distance from river suitability equations are fuzzy sigmoidal functions (Figure 4.10) according to Yager, (1988):

$$f(x,a,b,c) = \frac{1}{1+e^{-a(x-c)}} \quad \text{Eq. (4.47)}$$

Vegetation Indices suitability equations are fuzzy trapezoidal functions (Figure 4.11) according to Yager, (1988):

$$f(x,a,b,c,d) = \max\left(\min\left(\frac{x-a}{b-a}, 1, \frac{d-x}{d-c}\right), 0\right) \quad \text{Eq. (4.48)}$$

Table 4.2: List of the used factors and its transformation.

Layer	Factor	Function	Score Range
Canals	distance	fuzzy sigmoidal	cost
Drains	distance	fuzzy sigmoidal	cost
ET	Value	fuzzy trapezoidal	benefit/cost
CWSI	Value	fuzzy trapezoidal	benefit/cost
WVSI	Value	fuzzy trapezoidal	benefit/cost
DSI	Value	fuzzy trapezoidal	benefit/cost
LAI	Value	fuzzy trapezoidal	benefit/cost

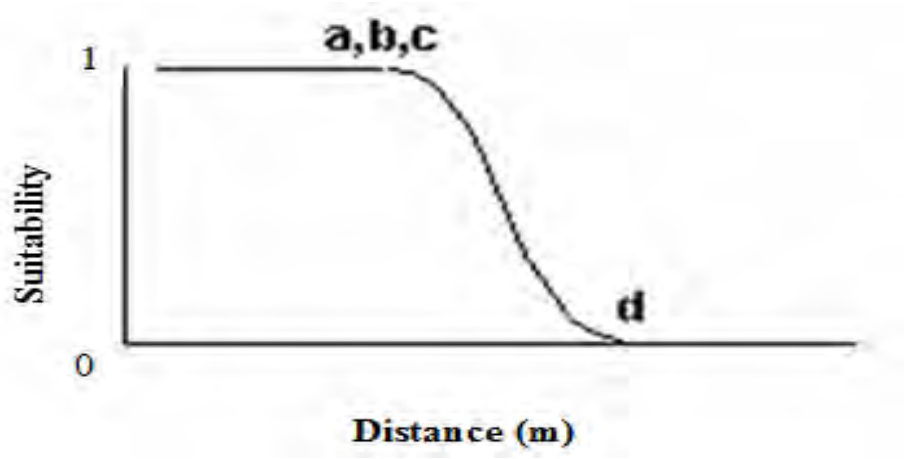

Figure 4.12: Sigmoidal function (Yager, 1988).

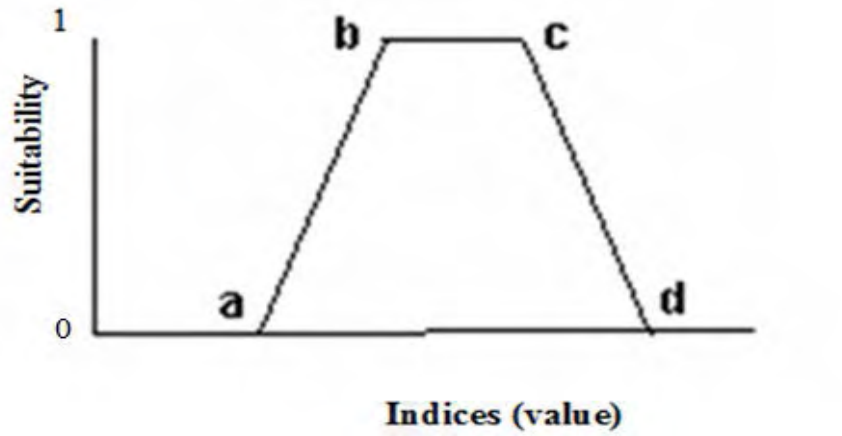

Figure 4.13: Trapezoidal function (Yager, 1988).

Where x, is the desired parameter, and a, b, c and d are the recommended factors specific threshold defined following FAO (1976; 1978; 1983; 1984; 1985; 2005) guidelines for rice cultivation and based on natural groupings inherent in the input data factors (Elhag, 2010).

Pairwise comparison method was developed by Saaty (1980, quoted by Malczewski 1999) in the context of his decision rule called Analytic Hierarchy Process. The method involves pairwise comparisons to create a ratio matrix. Through the normalization of the pairwise comparison matrix the weights are determined. The method uses an underling scale with values, from 1 to 9 to describe the relative preferences for two criteria. The result of the pairwise comparisons is a reciprocal matrix (Eastman, 2003). In mathematics, a multiplicative inverse or reciprocal matrix for a number *x*, denoted by $1/x$ or x^{-1}, is a number which when multiplied by x yields the multiplicative identity.

The significant point is that the estimated rank of $\boldsymbol{A}$ (if $\boldsymbol{A}$ is consistent) is 1 and the estimated *eigenvalue* is equal to number of compared criteria (n). In inconsistent cases the estimated maximum eigenvalue is greater than n while the others are close to zero. The *eigenvector* of matrix $\boldsymbol{A}$ is an estimate of the relative weights of the criteria being compared. In ideal cases the comparison matrix ($\boldsymbol{A}$) is fully consistent, the rank ($\boldsymbol{A}$) = 1 and $\lambda = \boldsymbol{n}$ ($\boldsymbol{n}$ = number of criteria). In this case, the following equation is valid:

$$A\ x\ X = n\ x\ X \qquad \text{Eq. 4.47}$$

Where $\boldsymbol{X}$ is the *eigenvector* of $\boldsymbol{A}$

5. Results and Decisions

5.1 Estimation of daily evapotranspiration

Application of the SEBS model over the target area has resulted in 21 different output maps related to energy fluxes. The results about the actual daily evapotranspiration are presented below due to their relative importance to the study objectives and the rest of the intermediate results were added to Appendix Figures 1-19.

The spatial distribution of daily evapotranspiration values varies over the Nile Delta region. The maximum daily evapotranspiration values are located at the East and West side of the Delta, while in the middle region of the Delta, daily evapotranspiration values range from low to medium, as illustrated in Figure 5.1.

Evaporative fraction values, as demonstrated in Figure 5.2, highly coincide with the pattern of the daily evapotranspiration values, suggesting variable dependency and positive correlation between the two variables.

According to the regression equation explained in Figure 5.3 ($Y= 0.9871$ x and $R^2= 0.8412$), the application of the SEBS model over the Nile Delta region is highly correlated with the measurements of the ground truth data (using Lysimeter). The idea behind finding the best fit line is based on the assumption that the data are actually scattered along a straight line called the least squares regression line, represented by the aforementioned equation.

The normal distribution of the daily evapotranspiration values are shown in Figure 5.4. Values less than 1.5 mm day^{-1} and more than 6 mm day^{-1} fall within a very small range of frequencies. The highest daily evapotranspiration values are recorded around 2.5 mm $d^{-1,}$ representing the majority of the Nile Delta agricultural area located centrally, so that it may be recognized as “old land cultivation”. The new reclaimed agricultural land in the Nile Delta indicates a wider range of daily evapotranspiration values ranging from 4 mm d^{-1} to 6 mm d^{-1}.

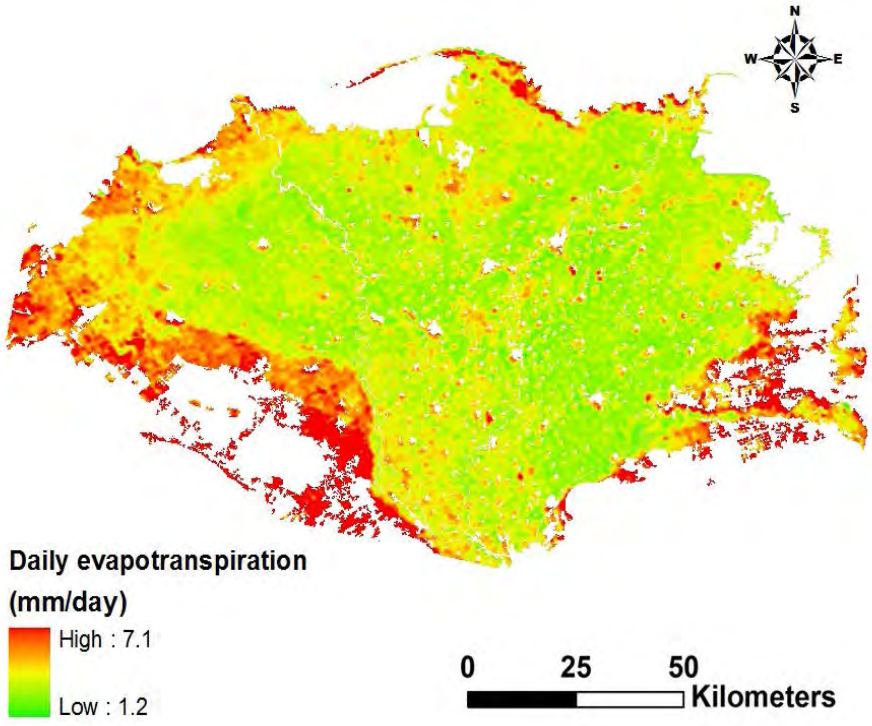

Figure 5.1: Daily evapotranspiration map over Nile Delta region estimated in August 2008.

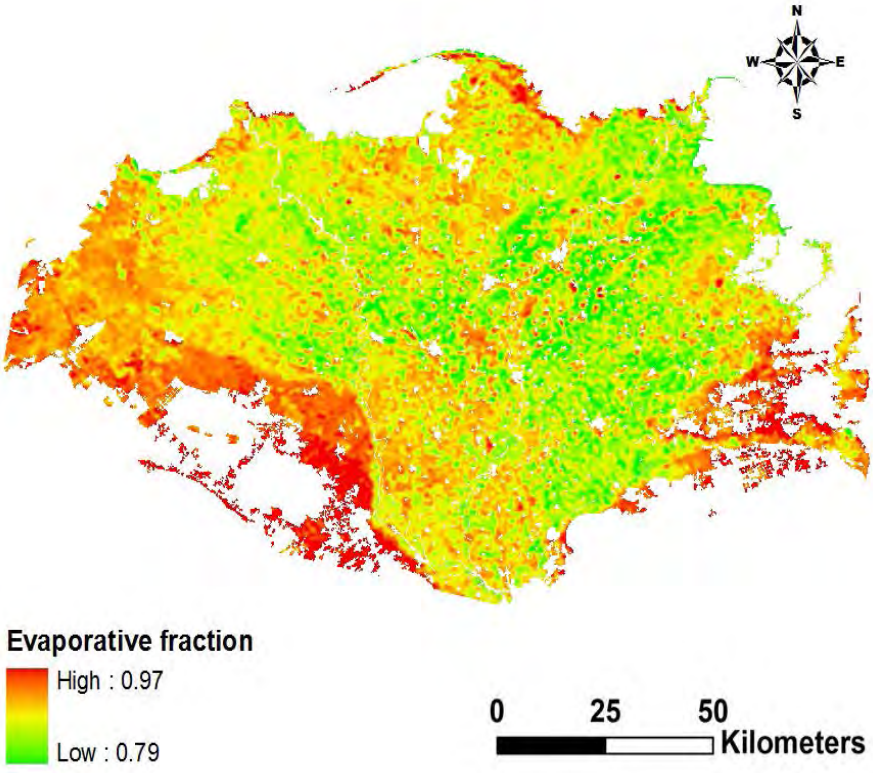

Figure 5.2: Evaporative fraction map over Nile Delta region estimated in August 2008.

The mean of the daily evapotranspiration values is 4.35 mm d^{-1} and the standard deviation is 1.91 mm d^{-1}. Economically, the irrigation costs of old land cultivation are considerably less than the irrigation costs of the "new land cultivation" taking into consideration the distances of the water streams voyaged to reach the new land (EAAE, 2000) .

The application of the SEBS model over the new reclaimed agricultural land, represented by the peripheral of the Nile Delta region, has resulted in higher daily evapotranspiration values than anticipated. This could be explained due to the fact that the main part of the energy was going into the sensible heat flux, while in the agricultural area the latent heat flux was dominating (Frey et al., 2010). In other words, the model tends to simulate the potential daily evapotranspiration rather than the actual daily evapotranspiration, which is identified as one of the model limitations (Li et al., 2009).

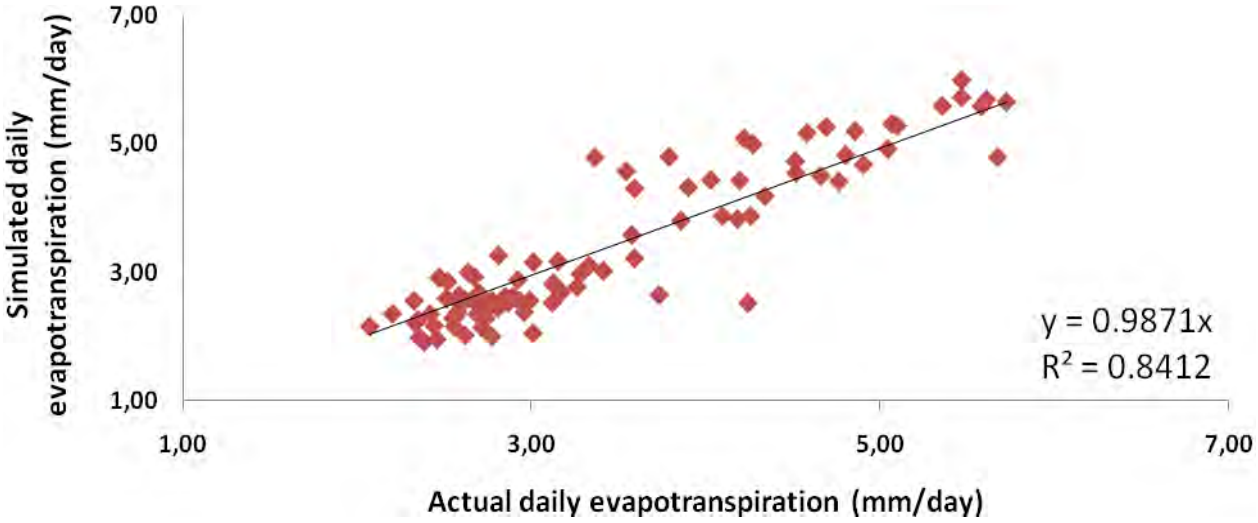

Figure 5.3: Relationship between actual daily evapotranspiration and simulated daily evapotranspiration over Nile Delta region.

Valuable information could be extracted from remote sensing data only when the limitation conditions are taken into account. Limiting conditions for the application of the SEBS model

may rely mainly on surface roughness (Su, 2002), the Planetary Boundary Layer (Su et al., 2003), and the type of land use (Li et al., 2005; Li et al., 2009).

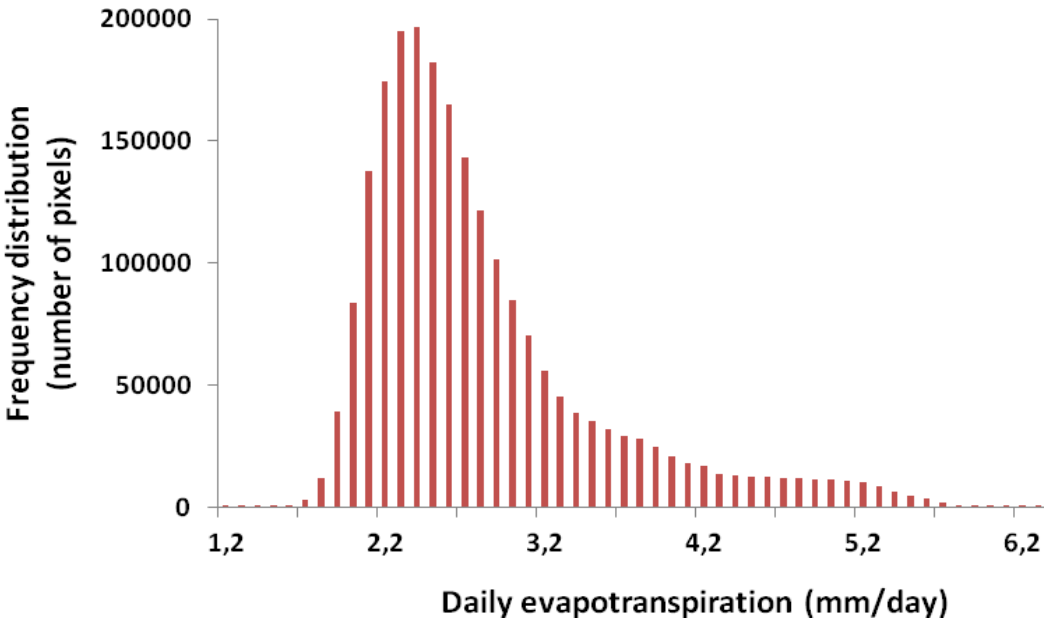

Figure 5.4: Frequency distribution of simulated daily evapotranspiration values over the Nile Delta region.

The frequency distribution of daily evapotranspiration values over the study area (Fig. 5.5) is quite similar to the frequency distribution of temperature values (Fig. 5.6). The strong values similarity indicates a strong dependency of the simulated daily evapotranspiration values on the corresponded temperatures (Appendix figures 18 and 19). Two peaks of frequency distribution values were reported from Figure 5.5 at 1.7 mm and 5.5 mm corresponded to the temperature distribution values (Fig. 5.6) of 300 K and 322 K respectively.

Due to the fact that the Nile Delta region has relatively plain surface relief the application of the SEBS model is more consistent over the agricultural lands (Hayes et al., 1999; Su et al., 2005). Under such conditions, the SEBS model relies basically on meteorological data conducted from various weather stations located in the Nile Delta region, and on the

corresponding cloud conditions at the time of image acquisition. According to Jin et al. (2005), the aforementioned parameters are in agreement with the results of this study.

The high correlation coefficient indicates the reliability of using the linear equation in order to obtain the daily evapotranspiration from satellite imageries. This equation is of significant practical use, where information about water balance is needed to determine the irrigation requirements of various crops in various locations around the country or under similar conditions (Boegh et al., 2002). So, the values of the actual daily evapotranspiration are needed from real data in situ measurements, because they can be used as independent variables in the linear equation.

The availability of the AATSR and MERIS imagery via simple web downloads without charges facilitates the application of the SEBS model. In addition, the temporal resolution of AATSR and MERIS imagery is very high (three days). This advantage supports decision makers to take into account the different phenology phases of the cultivated crops and fine-tune their water management plans in real time (Bouman and Tuong, 2001).

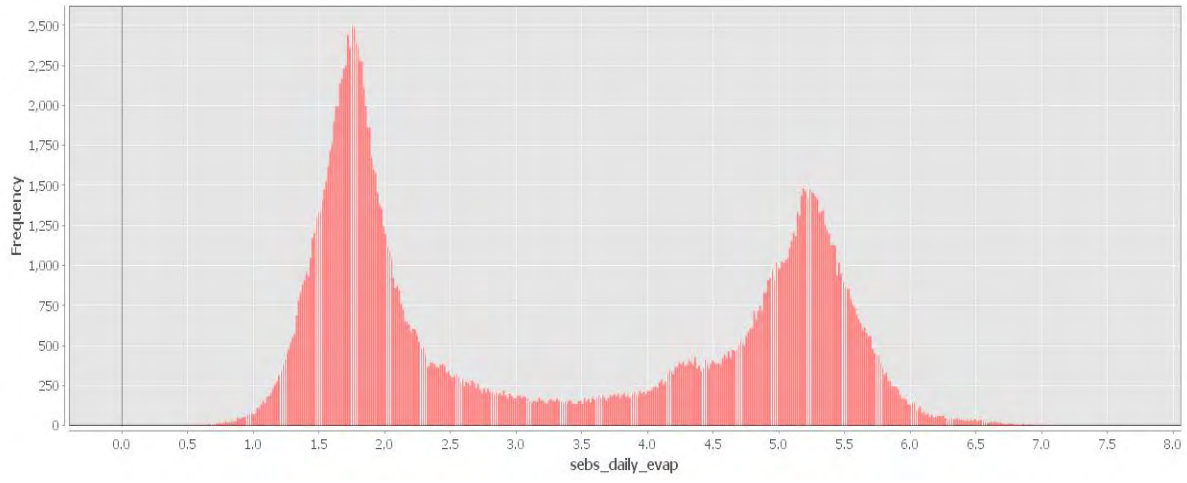

Figure 5.5: Frequency distribution of daily evapotranspiration values over Nile Delta region.

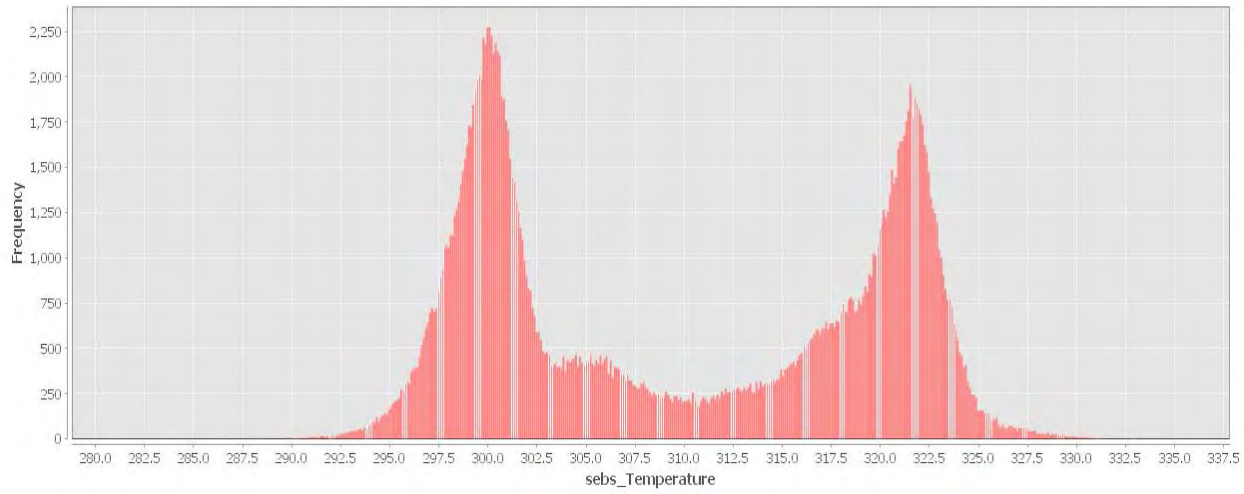

Figure 5.6: Frequency distribution of temperature values over Nile Delta region.

5.2. Change detection

Supervised classification using different classification algorithms were performed. Both statistical and graphical analyses of feature selection were conducted. All visible and infrared bands (except for the thermal infrared band) were included in the analysis. Table 5.1 shows the summary classification results in term of accuracy and Kappa statistics of each classification algorithm. Detailed classification tables were added to Appendix table 8-22.

Table 5.1: Overall accuracies and Kappa statistics of each classification algorithm

Year of acquisition	**1984**		**2000**		**2005**	
Classification algorithm	**Overall**	**Kappa**	**Overall**	**Kappa**	**Overall**	**Kappa**
Mahalanobis Distance	77.6%	0.71	77.8%	0.71	90.2%	0.87
Minimum Distance	78.0%	0.72	68.8%	0.59	84.5%	0.80
Maximum Likelihood	80.5%	0.75	93.5%	0.91	97.8%	0.97
Artificial Neural Net	37.5%	0.18	21.8%	0.05	26.7%	0.04
Parallelepiped	65.0%	0.57	71.7%	0.62	78.5%	0.73

Maximum Likelihood showed better classification results than the rest of classification algorithms. The result of the classification algorithm, both of overall accuracies and kappa

statistics were increased gradually from TM 1984 toward ETM+ 2005, in parallel the ML classifier also increased toward the classification map of ETM+ 2005. This could be explained due to the fact that the date acquisition of the third data set (ETM+ 2005) is relatively closer to the date of the training and validation points collection and also prove the adequacy of the ML classifier over the rest classifier in complex areas (Hsu et al., 2007; Batisani and Yarnal, 2009).

Figures 5.7 – 5.12 shows each data set in true color image and the respective classification map using ML as a supervised classification algorithm:

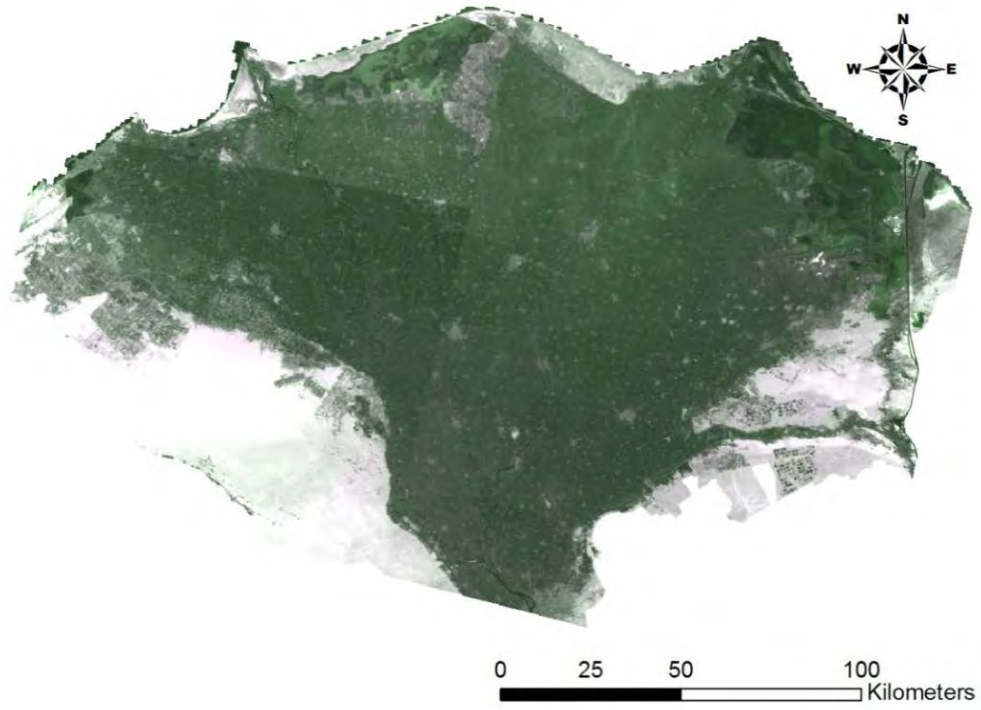

Figure 5.7: Landsat TM 1984 true color image.

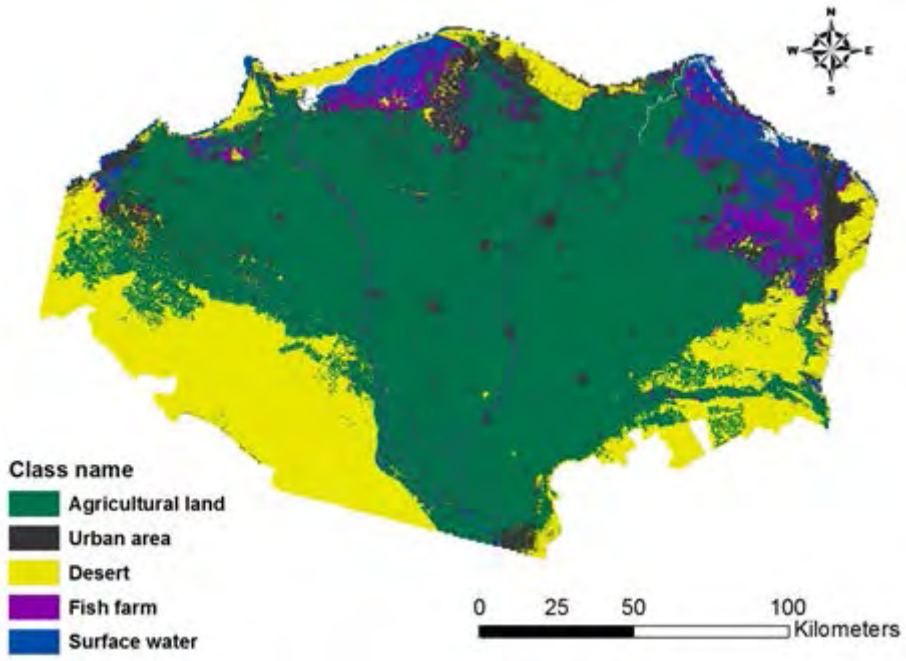

Figure 5.8: Landsat TM 1984 Maximum Likelihood classification map.

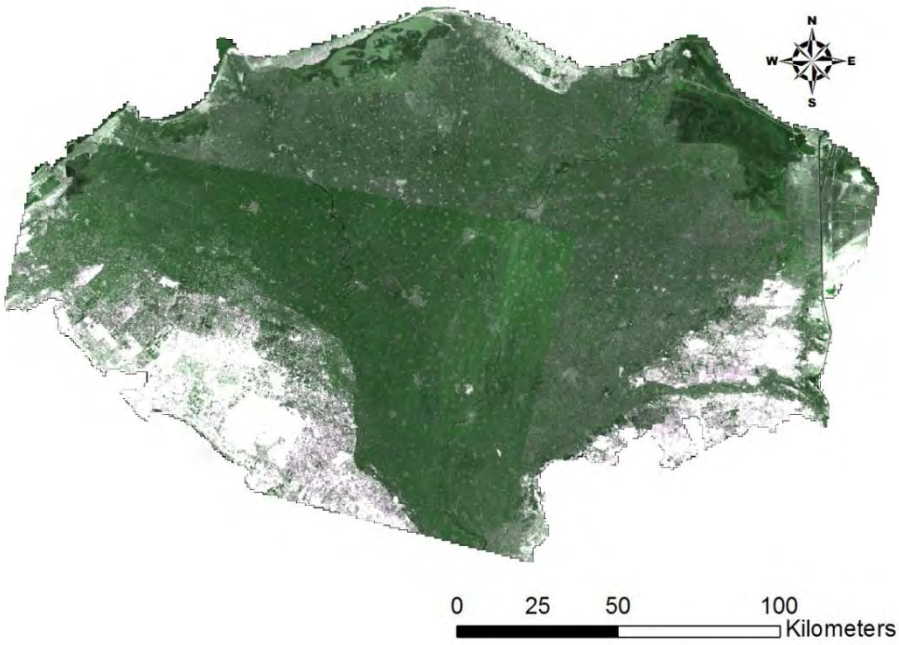

Figure 5.9: Landsat ETM+ 2000 true color image.

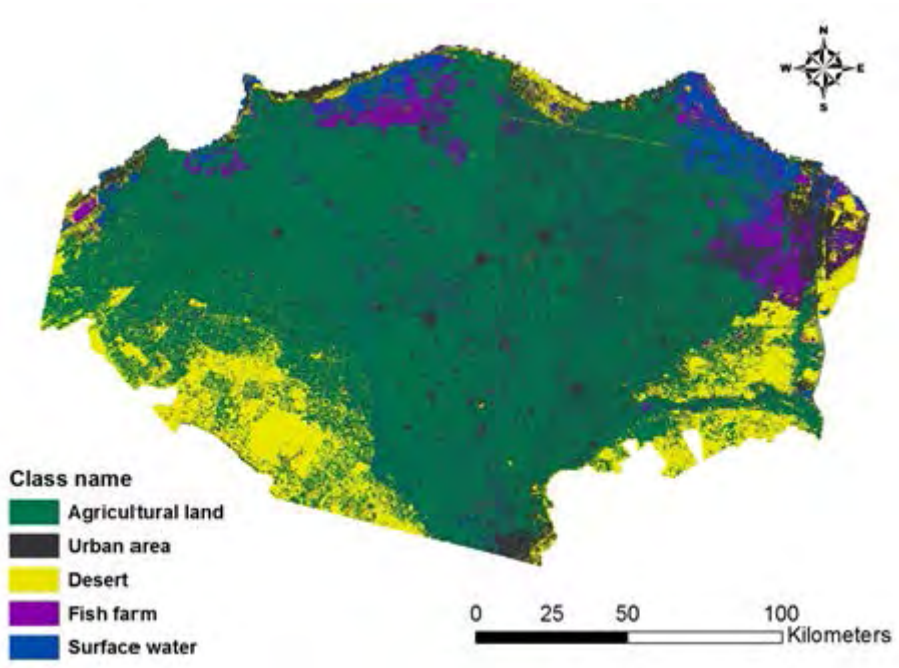

Figure 5.10: Landsat ETM+ 2000 Maximum Likelihood classification map.

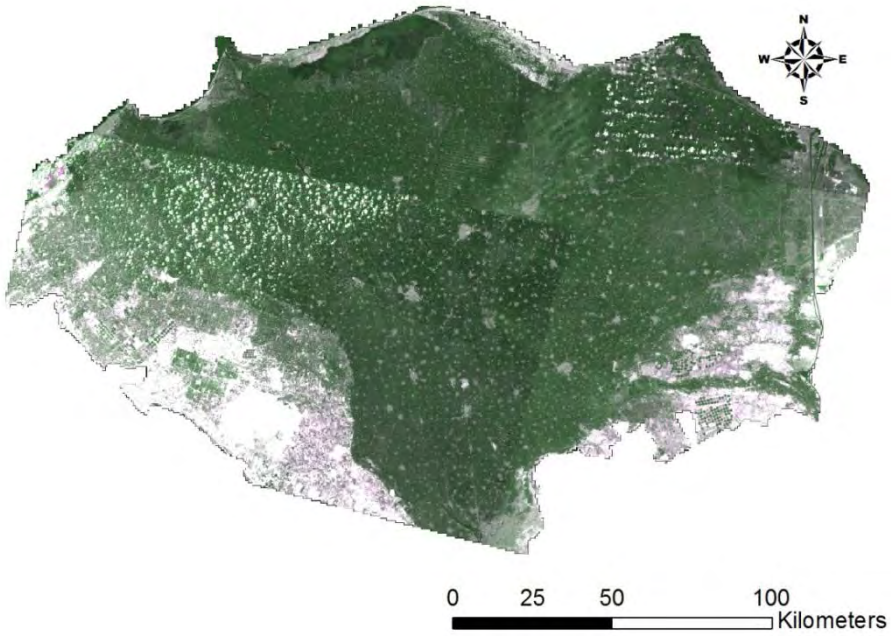

Figure 5.11: Landsat ETM+ 2005 true color image.

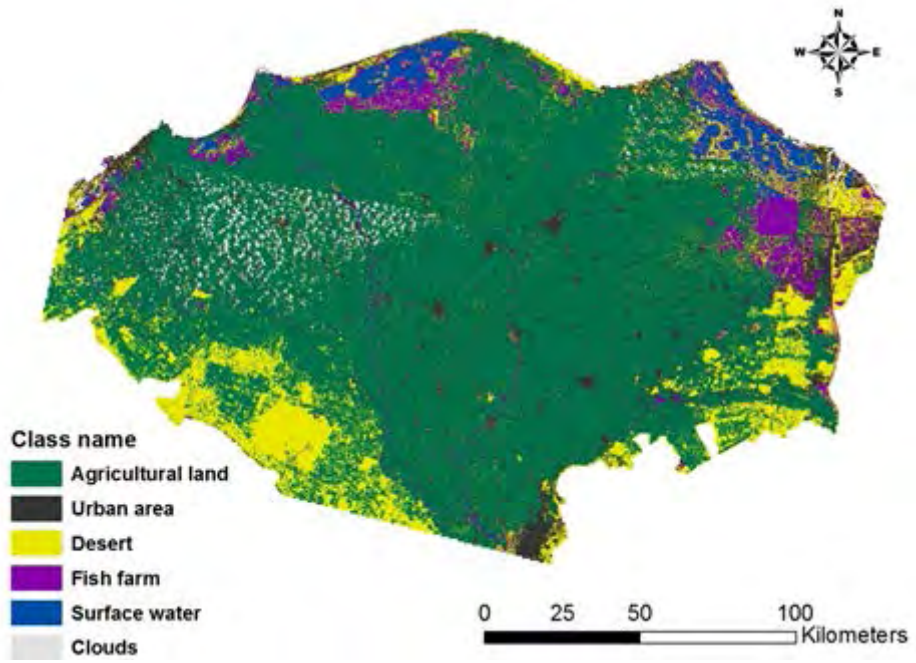

Figure 5.12: Landsat ETM+ 2005 Maximum Likelihood classification map.

The over estimation of the urban area in classification maps of the year 2000 and the year 2005 is due to the fact that approximately 85% of the irrigation network system (main and secondary canals) in the study area is constructed from concrete materials, which are the same materials used for building construction. This is why the cleanup analysis is mandatory to improve the classification accuracy (Singh, 1989; Wang et al., 2010; Abd El-Kawy et al., 2011).

Figures 5.13 – 5.15 shows the contribution of each LULC classes of the three different data sets to the total cover of the study area. Data set acquired in 1984 considered as reference point to the current changes in LULC of the Nile Delta region. Figure 5.13 demonstrates the ratio between the desert and the agriculture land, where the desert computed to be almost a half of the total area of the agricultural land. In the year 2000, the noticeable expansion of both agricultural land and urban area were directed against the total area of the desert land cover. Steady state in the total area of fish farms accompanied with slight decrease in the total area of the surface water was noticed (Figure 5.14). The final changes in the year 2005

demonstrate further loss in the total area of the desert land cover in accordance with agricultural land decreases, a slight increase in fish farms total area, the total area of the surface water remains the same (Figure 5.15).

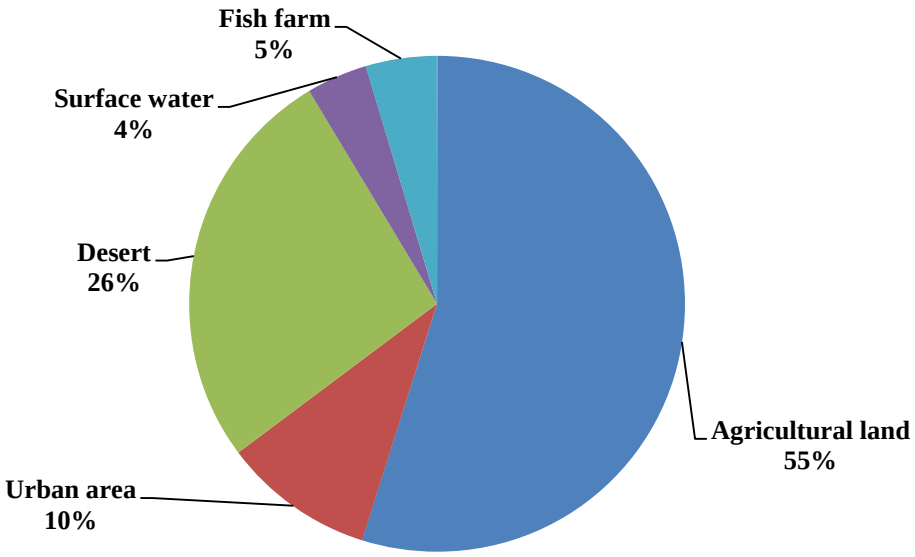

Figure 5.13: LULC classes' percentage in 1984.

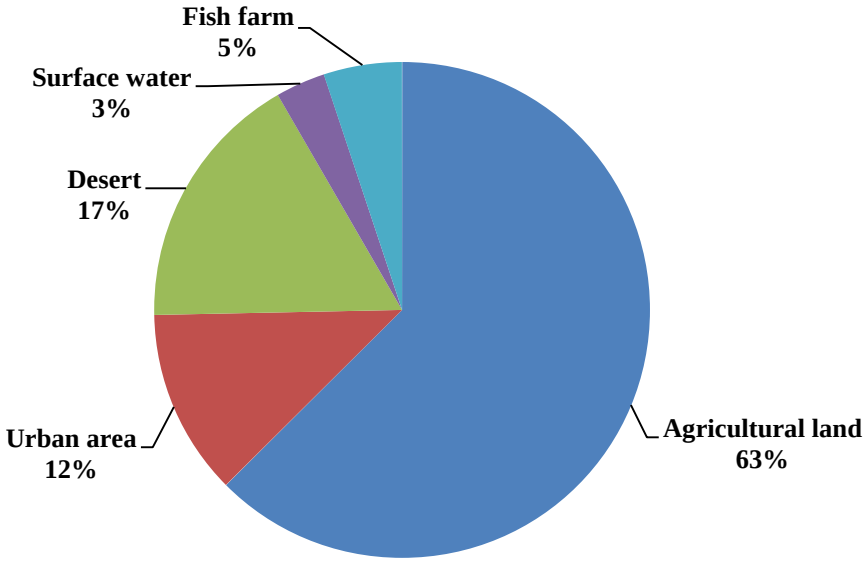

Figure 5. 14: LULC classes' percentage in 2000.

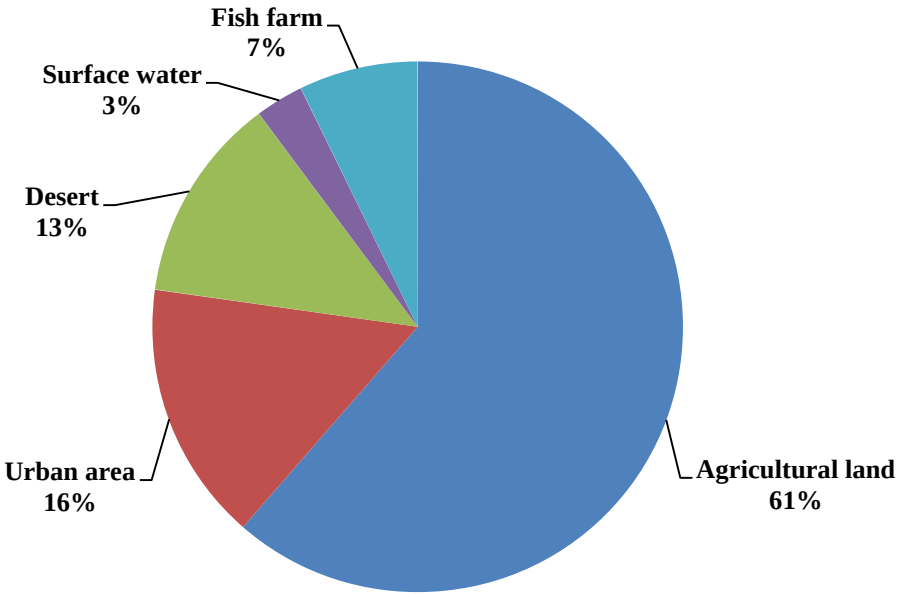

Figure 5. 15: LULC classes' percentage in 2005.

Post Classification Comparison is demonstrated in Figures 5.16 – 5.21 and explains the thematic changes occurred in different LULC classes that exist in the study area. Changes in LULC in term of percentages between the year 2000 and 1984 are demonstrated in Figure5.16. A strong loss in desert total area was induced by the expansion of both agricultural land and urban area. According to Figure 5.17, the expansion of the agricultural land was toward the desert, while the expansion of urban areas was toward the agricultural land. The slight increase in the total area of the fish farms took place toward the agricultural land also. LULC changes that occurred between the year 2005 and 2000 (Figure 5.18), revealed by additional loss in the total area of the desert in addition to decrease in agricultural land total area came along with increase of urban areas (Figure 5.19). Final stage of change detection demonstrated in Figure 5.20, the total area of the agricultural land was roughly increased by only 6.5 % over two decades which is rather similar to the increase of the urban area (5.9%), the expansion of urban areas and fish farms were noticed to be against the desert and the agricultural land. A slight decrease close to 1 % in lakes total area was observed (Figure 5.21).

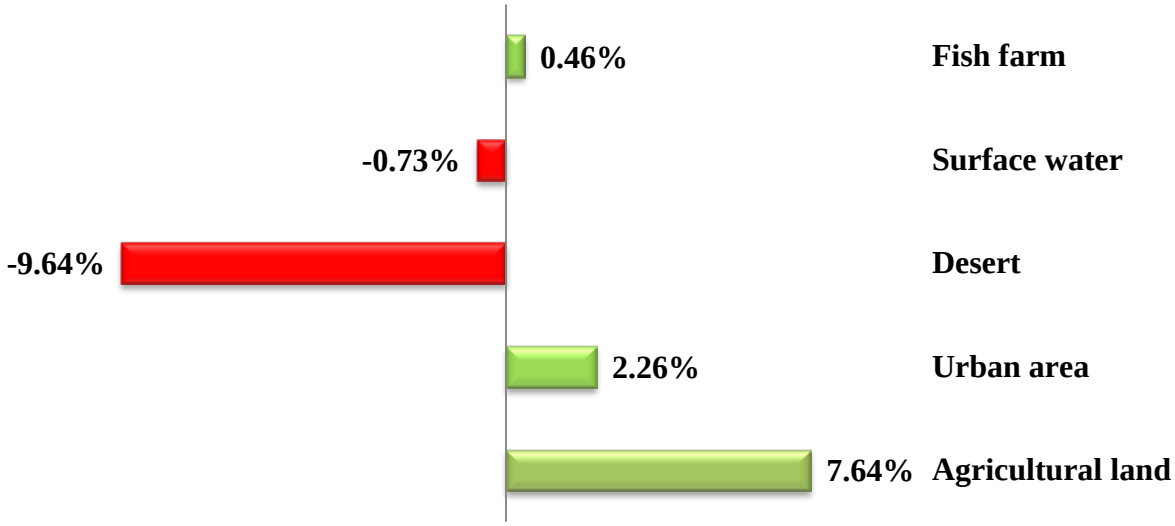

Figure 5.16: Post classification changes from the year 1984 till the year 2000.

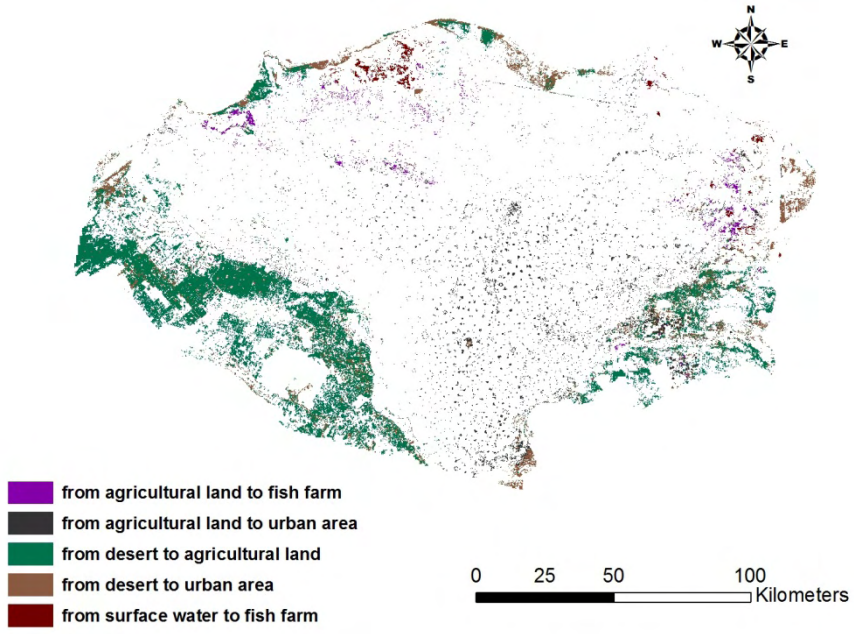

Figure 5.17: LULC thematic changes from the year 1984 till the year 2000.

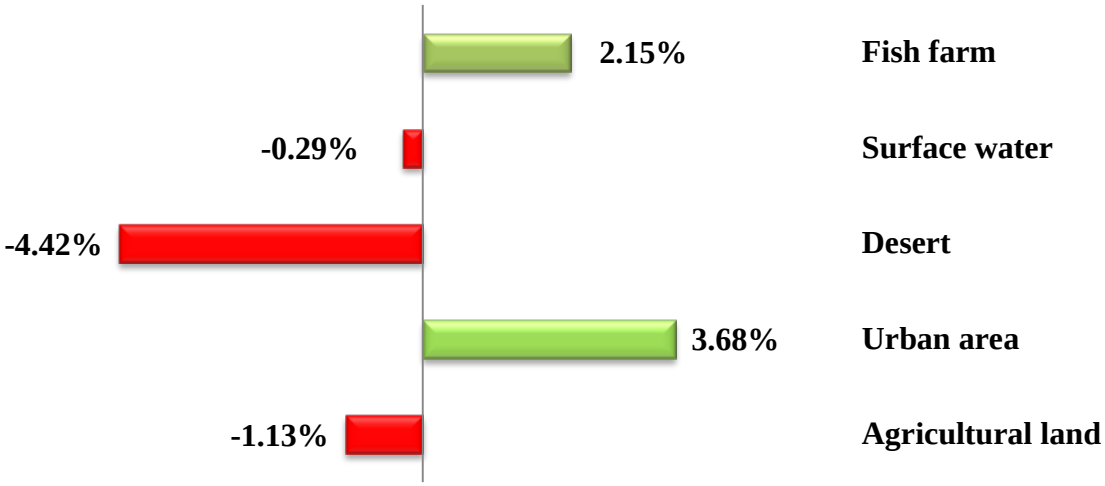

Figure 5.18: Post classification changes from the year 2000 till the year 2005.

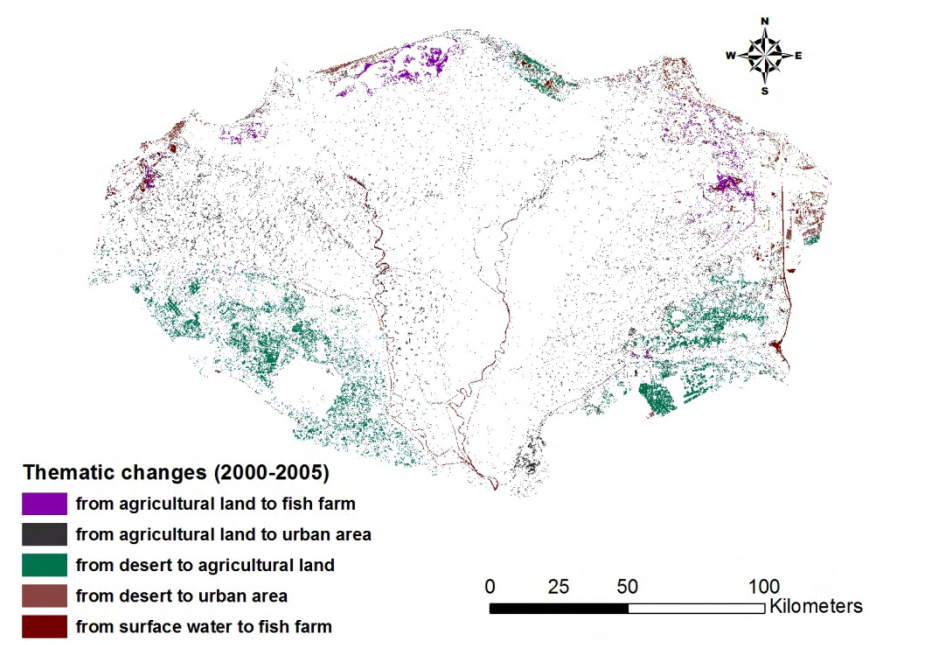

Figure 5. 19: LULC thematic changes from the year 2000 till the year 2005.

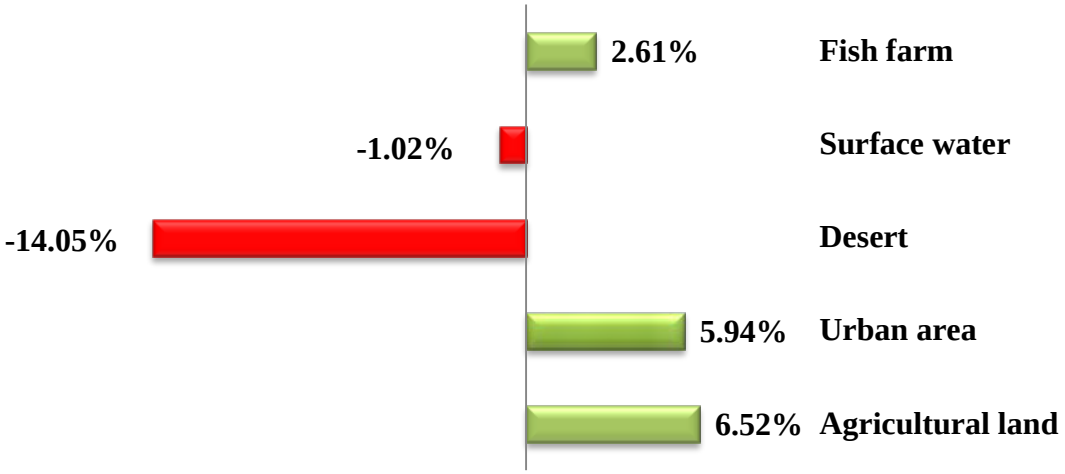

Figure 5.20: Post classification changes from the year 1984 till the year 2005.

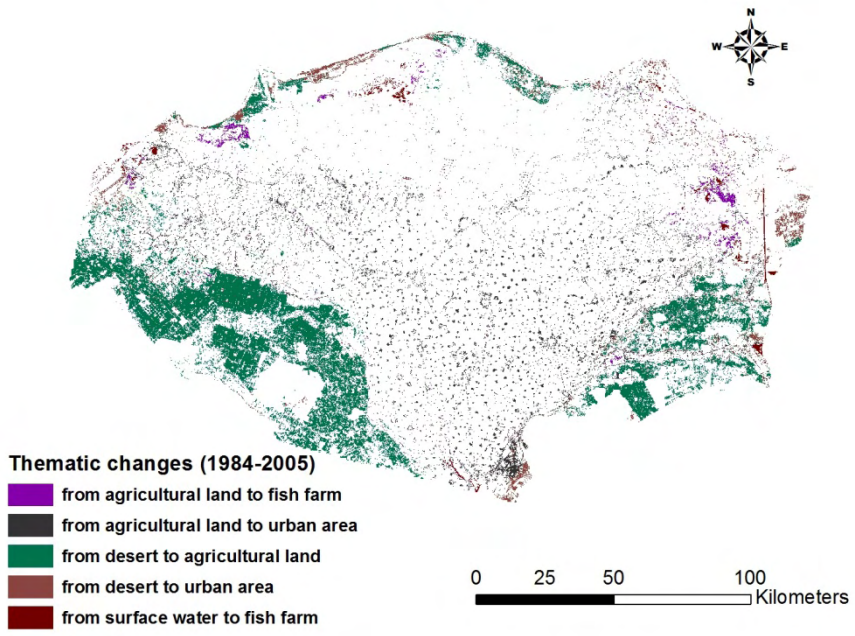

Figure 5.21: LULC thematic changes from the year 1984 till the year 2005.

The expansion took place toward the Eastern and Western side of the Delta region, reclaiming the desert into agricultural lands. This fact is related with high costly irrigation networks supplying water from River Nile to new agricultural lands in the desert and also

higher water consumption for agricultural use due to increased evapotranspiration in the desert (Elhag et al., 2011), comparing with the old lands in the inner Nile Delta region. The result is finally lack of rational water resources management in Nile Delta. Quantitatively, the total water requirements for old land (4.5 million feddan) is about 47.4 BCM with 80 % irrigation efficiency while the total water requirements for the new land (only about 0.6 million feddan) is about 6.9 BCM with irrigation efficiency of 90 % which means that the new land regardless the irrigation efficiency and the new irrigational techniques used in the new land requires about 14.5% of the total water budget based on the following table:

Table 5. 2: Crop water requirements in Nile Delta in the year 2005

	Summer crops		**Winter crops**		**Total consumption**	**Supply**	**Efficiency**	**Demand**
	Rice	Other crops	Cotton	Other crops				
Old land 4.5 MF (22500 km^2)	8000	2600	5800	2600	19000	47.4 BCM	80 %	85.5 BCM
New land 0.6 MF (2500 km^2)	8800	3400	6200	3400	22000	6.9 BCM	90 %	13.2 BCM
						98.7 BCM		54.3 BCM

* Source: MPWWR, 1998. Consumption calculated as m^2 per feddan per year

At the same time, urban encroachment took place over the exiting fertile agricultural lands of the Nile Delta. Similar results were described by El Banna and Frihy, (2009), Afify et al., (2011) and Shalaby and Gad, (2010). The loss of the desert area was also reported in Hereher (2010) after his mapping of the spatial changes in sand dune locations in the Western Desert of Egypt between 1987 and 2000. The construction of the high dam in Aswan had its negative effects on the sedimentation process of the wetlands and the lakes existing in the

Nile Delta region (Randazzo et al. 1998), due to the trapping of the suspended material coming from the upward catchment of River Nile. The loss of the wetlands and the lakes are also confirmed by Dewidar, (2004) and Ahmed et al., (2009). The drying of the wetlands and the lakes for agricultural and industrial purposes represents a new natural resource hazard added to other environmental hazards that may threaten the Nile Delta during the coming years (Dewidar, 2002; Frihy et al., 1998).

5.3. Times series analysis

Regardless of which technique is used, the first step in any time series analysis is to plot the observed values against time. A number of qualitative aspects were noticeable as it inspected the graph. Figure 5.22, shows that the series is non-stationary and there are seasonal fluctuations and no evidence of a linear trend and periodic variation from the mean standard deviation appears to be similarly distributed across time (Kocak et al., 2000; Brockwell and Davis, 2001).

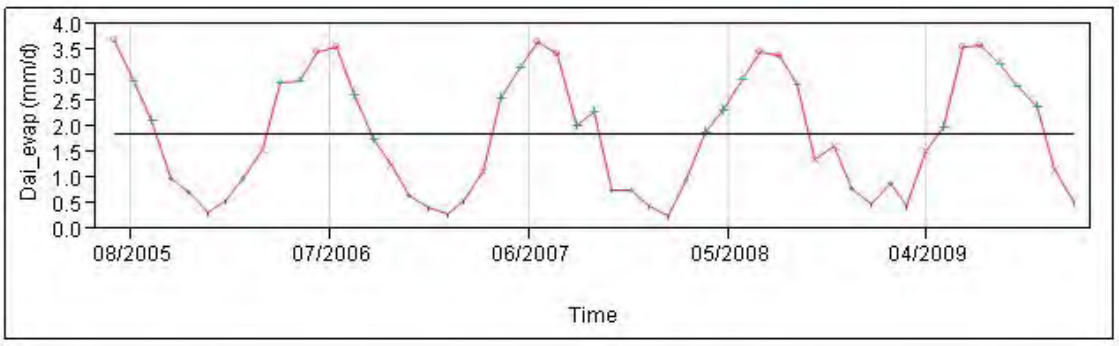

Figure 5.22: Daily evapotranspiration occurs periodically along with time starts from August 2005 till December 2009.

The simplest linear equation would be y = b + a, where b is the random error, of the data set. The linear equation for the data set is obtained to be with a slope value of -0.00007 to prove that there is no significant linear trend (Box and Jenkins, 1970). The data set needs further process to eliminate the quadratic trend embedded in the time series data set.

In order to explore the designated seasonality in the data set, Auto-Correlation Function (ACF) and Partial Auto-Correlation Function (PACF) were carried out and demonstrated in Figures 5.23 and 5.24. The graph of the residuals against a specified time interval is called a lagged autocorrelation function or a correlogram (Figure 5.23). The null hypothesis for the ACF is that the time series observations are not correlated one to another, and any pattern in the data is due to random error only. According to Figure 5.24, the PACF has a significant spike at lag 2 and at the non-seasonal level and a significant spike at lag 1 at the seasonal level, second ordered variogram in Figure 5.24 was counducted using JMP from SAS.

Plotting the time series observations against time, as well as the ACF and PACF have been graphed, and then patterns could be matched to enhance ARIMA models. The easy way to analyze a time series data set is simply to add numerous variations of ARIMA (Box et al., 1994). There are also systematic steps and several iterations that need to be followed to suggest the best values for the AR, I, and MA terms as it described in Table 5.3. In Table 5.3, different ARIMA parameters were used and a) Akaike's Information Criterion (AIC), b) Schwartz's Bayesian Criterion (SBC) and c) -2LogLikelihood were used to determine the most adequate ARIMA parameters to be ARIMA (2,1,2).

The use of the spectral density graph was to verify that the biggest seasonal pattern occurs at 12-month intervals. In Figure 5.25, notice the large peak at period 12 (Box et al., 1994). Figure 5.25 is the PACF of the precipitation data. In general, the PACF is the magnitude of correlation between a variable and its lag that is not explained by correlations at all lower-order lags.

Lag	ACF	Plot ACF	Ljung-Box Q	p-Value
0	1.0000	-.8 -.6 -.4 -.2 0 .2 .4 .6 .8	.	.
1	0.7640		32.7166	<.0001*
2	0.4114		42.3885	<.0001*
3	-0.0409		42.4858	<.0001*
4	-0.4590		55.0166	<.0001*
5	-0.7304		87.4133	<.0001*
6	-0.8176		128.877	<.0001*
7	-0.6632		156.746	<.0001*
8	-0.3737		165.791	<.0001*
9	0.0194		165.816	<.0001*
10	0.3724		175.218	<.0001*
11	0.6504		204.578	<.0001*
12	0.7106		240.483	<.0001*
13	0.6025		266.935	<.0001*
14	0.3403		275.590	<.0001*
15	-0.0126		275.602	<.0001*
16	-0.3379		284.599	<.0001*
17	-0.5536		309.415	<.0001*
18	-0.6075		340.154	<.0001*
19	-0.5205		363.382	<.0001*
20	-0.2807		370.342	<.0001*
21	0.0168		370.368	<.0001*
22	0.2895		378.250	<.0001*
23	0.4660		399.354	<.0001*
24	0.5105		425.552	<.0001*
25	0.4051		442.634	<.0001*
26	0.2147		447.612	<.0001*
27	-0.0238		447.675	<.0001*
28	-0.2418		454.495	<.0001*
29	-0.3814		472.162	<.0001*
30	-0.3984		492.275	<.0001*
31	-0.3163		505.529	<.0001*
32	-0.1587		509.027	<.0001*
33	0.0115		509.046	<.0001*
34	0.1647		513.210	<.0001*
35	0.2753		525.487	<.0001*
36	0.2824		539.160	<.0001*
37	0.2300		548.798	<.0001*
38	0.1166		551.441	<.0001*
39	-0.0011		551.441	<.0001*
40	-0.1194		554.637	<.0001*
41	-0.1794		562.459	<.0001*
42	-0.1869		571.711	<.0001*
43	-0.1642		579.572	<.0001*
44	-0.0619		580.814	<.0001*
45	0.0209		580.974	<.0001*
46	0.0961		584.818	<.0001*
47	0.1043		590.106	<.0001*
48	0.0832		594.141	<.0001*
49	0.0474		595.779	<.0001*
50	-0.0011		595.781	<.0001*

Figure 5.23: Visual inspection shows significant deviations from zero correlation at lag 1, 7, and 13 and very closes at lag 6 and 12. Interpretation suggests that there are two seasonal (wet season and dry season) patterns spaced about 6 months apart. Number of autocorrelation lags equals to 50.

Lag	Partial
0	1.0000
1	0.7640
2	-0.4137
3	-0.4899
4	-0.3672
5	-0.2394
6	-0.2736
7	-0.0829
8	-0.2109
9	-0.0690
10	-0.1318
11	0.1008
12	-0.1505
13	0.0145
14	-0.0295
15	-0.0419
16	-0.0492
17	0.1028
18	0.0071
19	-0.0216
20	0.0548
21	0.0861
22	-0.0397
23	0.0065
24	-0.0205
25	-0.1092
26	0.0439
27	-0.0002
28	-0.0509
29	-0.0425
30	0.1092
31	-0.0579
32	-0.0096
33	-0.1078
34	-0.0630
35	-0.0427
36	-0.0614
37	-0.0883
38	-0.0742
39	-0.0030
40	-0.0741
41	-0.0241
42	0.0004
43	-0.1162
44	0.1316
45	0.0361
46	0.0194
47	-0.0977
48	-0.0345
49	0.0101
50	-0.0094

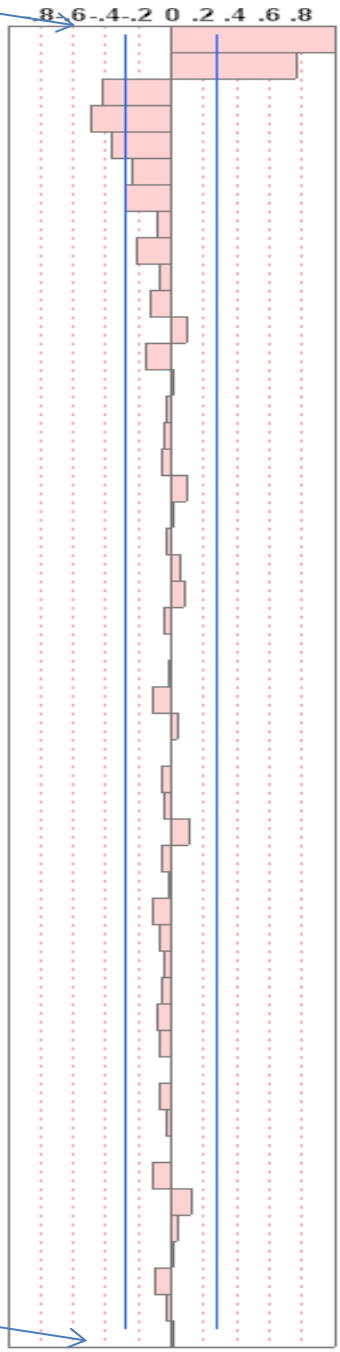

Lag	Variogram
1	1.0000
2	2.4937
3	4.4095
4	6.1808
5	7.3307
6	7.7003
7	7.0459
8	5.8195
9	4.1543
10	2.6587
11	1.4810
12	1.2259
13	1.6841
14	2.7948
15	4.2900
16	5.6680
17	6.5817
18	6.8102
19	6.4415
20	5.4256
21	4.1652
22	3.0099
23	2.2621
24	2.0737
25	2.5204
26	3.3268
27	4.3371
28	5.2610
29	5.8521
30	5.9241
31	5.5764
32	4.9089
33	4.1876
34	3.5385
35	3.0700
36	3.0402
37	3.2620
38	3.7424
39	4.2412
40	4.7422
41	4.9966
42	5.0280
43	4.9322
44	4.4988
45	4.1478
46	3.8294
47	3.7945
48	3.8840
49	4.0356
50	4.2413

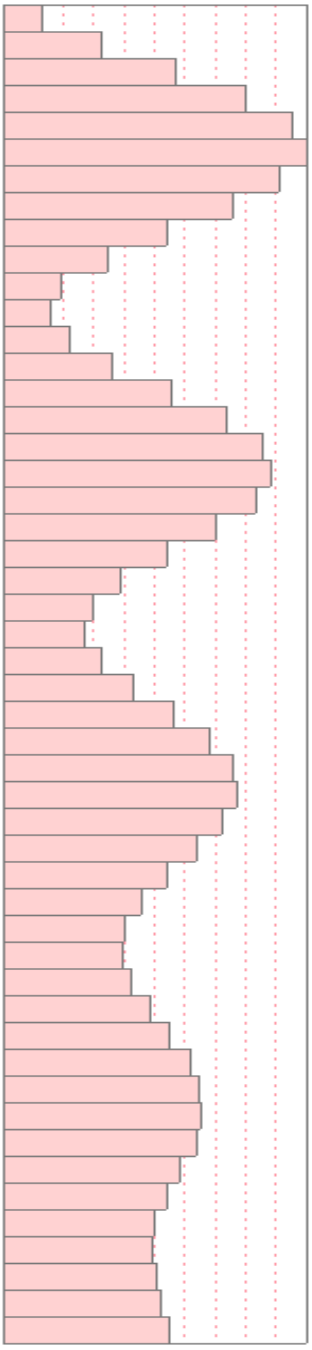

Figure 5.24: Lagged partial autocorrelation function. Significant deviation from zero is evident to suggest the same 6 months seasonal pattern. Time series exhibits seasonality of 4 to 5 cycles of observations in order to fit a seasonal model to the data.

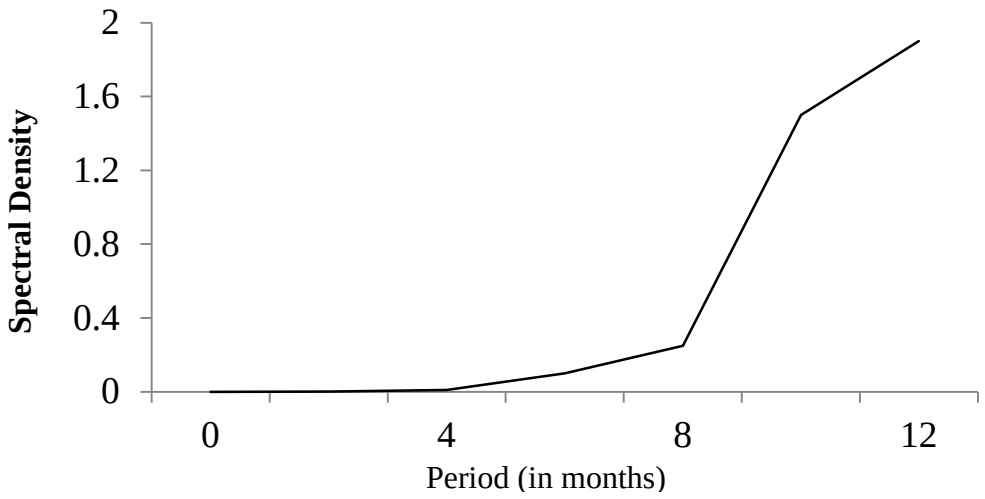

Figure 5.25: A strong signal appears at about period 12, corresponding to a yearly succession.

The model was able to forecast the daily evapotranspiration values over the Nile delta region for a period of three years as it shown in Figure 5.26. The blue line in the middle of the figure differentiate between the estimated daily evapotranspiration values on the left side of the line and the predicted evapotranspiration values represented by the fluctuated red line on the right side of the blue line. The range of the predicted values based on confidence intervals is represented by the two parallel blue lines drawn along with the red line. The ranger of the predicted daily evapotranspiration values increases with time which means that the prediction accuracy as well as the confidence intervals is decreasing with time probably due to the elimination of the quadratic trend was not successful. The prediction accuracy in August 2010 was only 62.5% and it kept decreasing dramatically during till August 2011 to accuracy prediction value of 38%. This could be explained by the disability of the model to predict daily evapotranspiration over a longer period (Box et al., 1994). Model parameter of 2,1,2 was the best to represent ARIMA model. The Application of ARIMA model using (2,1,2) as model parameter was summarized in Table 5.4, while ARIMA (2,1,2) estimates were summarized in Table 5.5.

Table 5.3: ARIMA model comparison parameter

Model	DF	Variance	AIC	SBC	R^2	-2LogLH	AIC Rank	SBC Rank	MAPE	MAE
AR (1)	51	0.4979579	116.47380	120.41438	0.600	112.4738	13	11	51.721235	0.594459
ARI (1, 1)	50	0.4624479	109.58528	113.48777	0.645	105.58528	4	3	40.655500	0.537350
ARIMA (1, 1, 1)	49	0.4579551	110.07144	115.92517	0.655	104.07144	5	4	39.456955	0.530691
ARIMA (1, 1, 2)	48	0.3792638	101.88204	109.68701	0.718	93.882039	2	2	34.146984	0.481918
ARIMA (1, 2, 1)	48	0.5019427	112.78817	118.58365	0.625	106.78817	8	9	44.775196	0.567253
ARIMA (1, 2, 2)	47	0.4788892	111.53778	119.26508	0.649	103.53778	6	10	40.185621	0.547796
ARIMA (2, 1, 1)	48	0.4359319	108.60303	116.40801	0.678	100.60303	3	5	38.946680	0.514890
ARIMA (2, 1, 2)	**47**	**0.1720585**	**70.379117**	**80.135336**	**0.851**	**60.379117**	**1**	**1**	**30.228141**	**0.346694**
ARIMA (2, 2, 1)	47	0.5094094	114.48055	122.20785	0.627	106.48055	11	12	45.121313	0.566662
ARIMA (2, 2, 2)	46	0.4829206	112.95723	122.61636	0.653	102.95723	10	13	39.910505	0.545151
ARMA (1, 1)	50	0.4457555	111.75023	117.66111	0.643	105.75023	7	7	47.022462	0.529181
I (1)	51	0.5317368	115.71632	117.66757	0.585	113.71632	12	8	45.163631	0.590832
IMA (1, 1)	50	0.4937248	112.88847	116.79096	0.622	108.88847	9	6	42.474597	0.556527
MA (1)	51	0.6481194	130.31642	134.25700	0.499	126.31642	14	14	67.255138	0.668426

Table 5.4: ARIMA model (2,1,2) summary

DF	**47**
Sum of Squared Errors	8.086751
Variance Estimate	0.172059
Standard Deviation	0.414799
Akaike's 'A' Information Criterion	70.379117
Schwarz's Bayesian Criterion	80.135336
RSquare	0.851342
RSquare Adj	0.838691
MAPE	30.228141
MAE	0.346694
-2LogLikelihood	60.379117
Stable	Yes
Invertible	Yes

Table 5.5: ARIMA model (2,1,2) parameter estimates

Term	Lag	Estimate	Std Error	t Ratio	Prob>|t|	Constant Estimate
AR1	1	1.69822	0.032980	51.49	<.0001	-0.0011262
MA1	2	-0.96401	0.029906	-32.23	<.0001	
MA2	1	1.93549	0.077458	24.99	<.0001	
Intercept	2	-0.99999	0.073358	-13.63	<.0001	

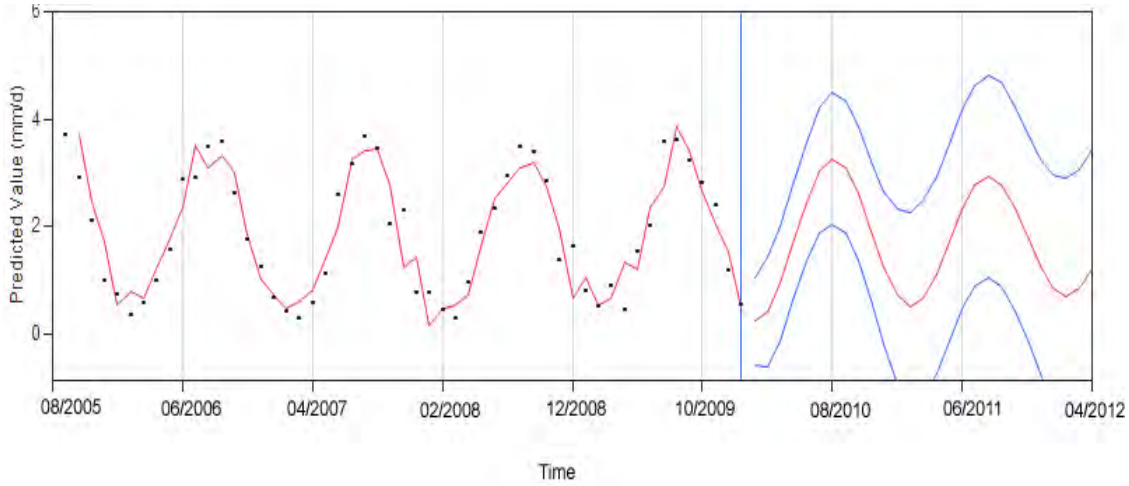

Figure 5.26: ARIMA model forecasting.

To improve the model performance, Seasonal ARIMA (SARIMA) was obtained and according to AIC and SBC values. Table 5.6 describes SARIMA model comparison parameter, comparison was made basically upon R^2 values and both of AIC and SBC ranks. Contradictorily, higher R^2 values of SARIMA models comparison reported to be less reliable and only lower R^2 values are preferred due to the seasonality behavior of the data set which is not stationarized series (Pfaff, 2008) in comparison to Table 5.3. Therefore, an R^2 of 20% is more acceptable (Pfaff, 2008). According to Smith (1998), lower R^2 vales preferability is explained by the occurrence of exogenous regressor in non-stationary dataset. In fact, an R^2 of 20% or even as little as 15% may be statistically significant in some applications especially in prediction in case of calculating R^2 as a percentage of the variance in the errors of the best time series model. This can be explained by adding exogenous regressors, since the coefficients of the additional regressors were significantly different from zero (Smith, 1998). Lower R^2 values are coherently agreed with both of AIC and SBC ranks to confirm the abnormal behavior of R^2 values under the resonance of seasonality condition. Table 5.7, describes SARIMA summary, to point out the values of the most adequate parameters used to obtain stable and reversible SARIMA model [(1,1,2)6], while Table 5.8, describes SARIMA [(1,1,2)6] parameters estimate (Chen et al., 2009).

Table 5.6: S-ARIMA model comparison parameter

Model	DF	Variance	AIC	SBC	R^2	-2LogLH	AIC Rank	SBC Rank	MAPE	MAE
S-AR (1)6	46	0.2647734	91.698345	103.40581	0.78	79.698345	9	9	33.697287	0.423723
S-ARI (1, 1)6	40	0.1773605	86.997248	97.969096	0.22	74.997248	7	7	39.033656	0.655489
S-ARIMA (1, 1, 1)6	39	0.1234228	83.526854	96.327344	0.79	69.526854	6	5	35.914405	0.59566
S-ARIMA (1, 1, 2)6	**38**	**0.0765481**	**75.062767**	**89.691899**	**0.20**	**59.062767**	**1**	**1**	**35.751255**	**0.607441**
S-ARIMA (1, 2, 1)6	33	0.208164	108.89546	120.71762	0.99	94.895465	11	11	138.54617	1.154698
S-ARIMA (1, 2, 2)6	32	0.1086119	110.54382	124.05486	0.99	94.543823	12	12	132.39024	1.122699
S-ARIMA (2, 1, 1)6	38	0.1210794	82.923641	97.552772	0.46	66.923641	5	6	36.689161	0.618606
S-ARIMA (2, 1, 2)6	37	0.0847592	76.163991	92.621763	0.35	58.163991	2	2	34.93849	0.592251
S-ARIMA (2, 2, 1)6	32	0.4393754	121.49083	135.00186	0.99	105.49083	14	14	151.31337	1.217954
S-ARIMA (2, 2, 2)6	31	0.277755	111.41754	126.61745	0.29	93.417535	13	13	62.248103	0.69638
S-ARMA (1, 1)6	40	0.1853084	81.77319	92.745038	0.74	69.77319	4	4	36.014799	0.429879
S-I (1)6	46	0.2737131	91.200125	102.90759	0.78	79.200125	8	8	27.854831	0.401941
S-IMA (1, 1)6	45	0.1960247	79.059621	92.718327	0.83	65.059621	3	3	30.328704	0.349779
S-MA (1)6	41	0.4356415	107.60783	116.75104	0.59	97.607831	10	10	50.052944	0.587561

Table 5.7: S-ARIMA (2, 1, 2) (1, 1, 2)6 model summary

DF	**38**
Sum of Squared Errors	2.9088265
Variance Estimate	0. 0847592
Standard Deviation	0.2766732
Akaike's 'A' Information Criterion	75.062767
Schwarz's Bayesian Criterion	89.6918986
RSquare	-0.1323976
RSquare Adj	-0.3409971
MAPE	35.7512554
MAE	0.6074412
-2LogLikelihood	59.0627674
Stable	Yes
Invertible	Yes

Table 5.8: S-ARIMA Parameter Estimates

Term	**Lag**	**Estimate**	**Std Error**	**t Ratio**	**Prob>|t|**	**Constant Estimate**
AR1,1	1	1	-1.12822	0.004749	-237.6	0.01669
AR1,2	1	2	-0.26576	0.00081	-328	
AR2,6	2	6	-1	5.44E-07	-2.0E+06	
MA1,1	1	1	-0.0031	0.00017	-18.21	
MA1,2	1	2	0.9969	0.101449	9.83	
MA2,6	2	6	0.000237	2.72E-05	8.71	
MA2,1,2	2	12	0.99975	0.000154	6487	
Intercept	1	0	0.003486	0.001743	2	

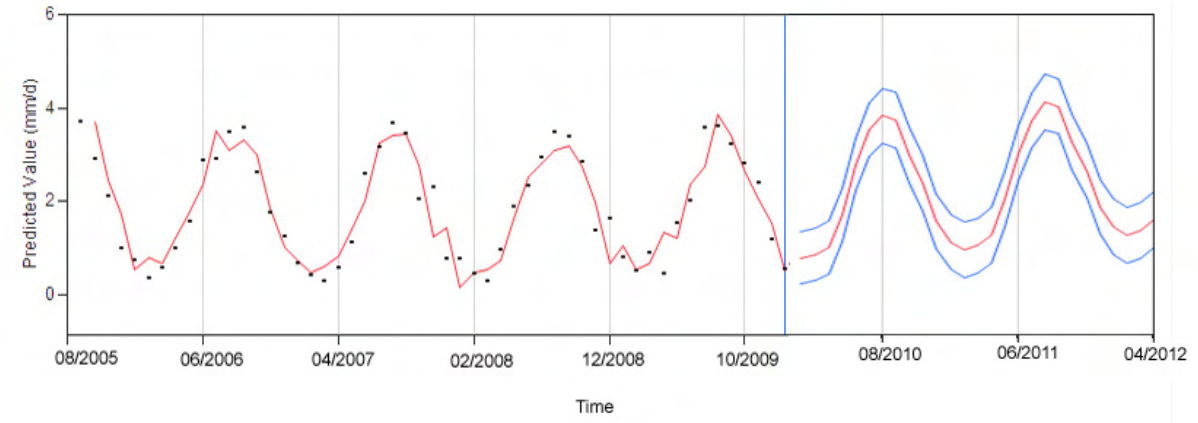

Figure 5.27: Seasonal ARIMA model forecasting.

In Figure 5.23, there are 2 residual values, at lag 7 and lag 13 that laid more than 2 standard errors within 95% confidence limits from the zero mean to comply with ACF rules. According to ACF rules regarding the plotted residuals of a value greater than 2 standard errors away from the zero mean are significantly autocorrelated (Box et al., 2008, Psilovikos et al., 2011). This was interpreted as a 6-month seasonal pattern of those cycles between summer, and winter. So, even though the linear equation reveals no trend, graphing the ACF reveals seasonality (Box et al., 1994; Sentas and Psilovikos, 2010). Seasonal ARIMA [(2,1,2)(1,1,2)6] was able to predict the values of the daily evapotranspiration more accurately over time (Figure 5.27), the range of the prediction values represented by the two blue lines surrounding the inner red line is relative fitted due to the high confidence intervals.

The prediction accuracy in August 2010 is 87 % while the prediction accuracy in August 2011 is about 85%, as an indicator of improvement compared with the respective ones computed with the ARIMA model only (Matzafleri et al., 2009). Predicted daily evapotranspiration values following Seasonal ARIMA model appeared to follow the upturn and the downturn of the conducted series reasonably well (Kyriakidis and Journal, 2001; Abebe and Forech 2008; Choudhury et al., 2008).

The daily evapotranspiration data set has the seasonal and trend patterns with increasingly variation variances which is mean that the data set satisfied the non-stationary condition of Seasonal ARIMA model (Psilovikos et al., 2011; Suhartono, 2011).

Thematic map of evapotranspiration according to Penman – Monteith method in august 2008 (Figure 5.28) was produced to investigate the adequate correlation between estimated SEBS daily evapotranspiration and both of daily evapotranspiration values conducted from dynamic lysimeter and Penman Monteith mothod respectively.

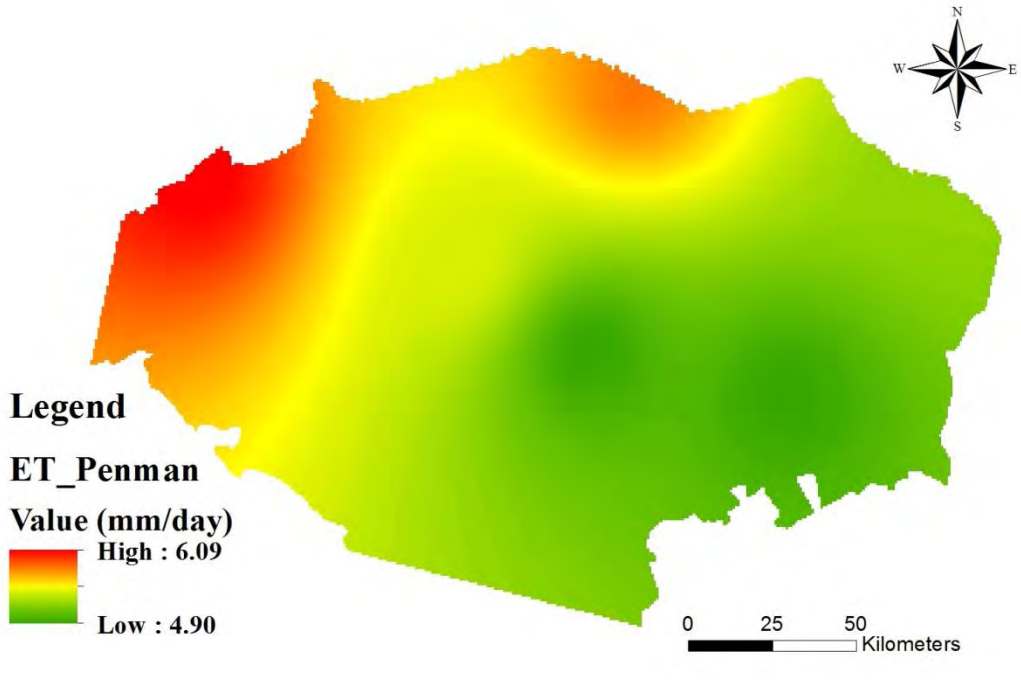

Figure 5. 28: Daily evapotranspitation values using Penman-Monteith (August 2008)

The correlation between the predicted daily evapotranspiration values using SEBS model and the actual daily evapotranspiration values conducted from Penman–Monteith method demonstrate a highly positive correlation represented by linear equation where Y= 1.1095x + 0.484 with R^2 = 0.9295 as is it illustrated in Figure 5.29.The correlation established between 36 archived FAO daily evapotranspiration data collected consistently from the year 2005 till the year 2011 for August recoreds and the corresponding exact (or the closest) date of MERIS data acquisition (simulated from SEBS daily evapotranspiration method).

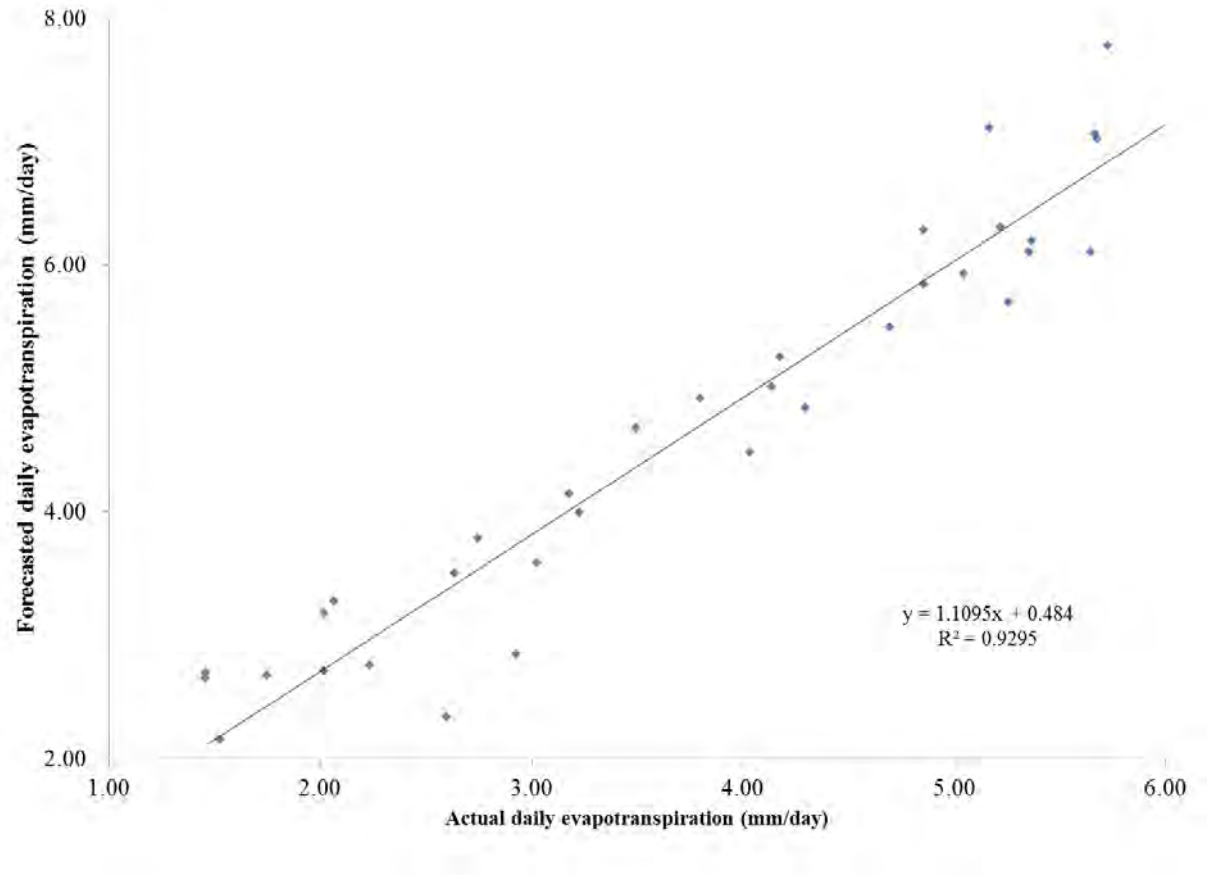

Figure 5. 29: Correlation between actual and forecasted daily evapotranspiration

Two previous studies were carried out (Strzepek et al., 1996; Yates and Strzepek, 1998) to correlate the daily evapotranspiration and climatic factors. These studies concluded a positive linear regression between the daily evapotranspiration and temperature and solar radiation.

The forecasting model of SARIMA, indicates an increase of the daily evapotranspiration rate up to 1.3 mm/d in summer time of the year 2012, which is based probably on the increase of temperature and solar radiation according to Richard, (2003) and Helman, (2011), regarding the climate change scenarios over Nile Delta region. Due to water limitation in the study area, such increase poses more risk to the water resources management in Egypt the total water requirements for irrigational use in the Nile Delta is about 54.3 BCM and to cope with the climate change with 1.3 mm/day higher evapotranspiration rate then the total water requirements will be 77.83 BCM which is not available (MPWWR, 1998; NWRP, 2005).

5.4. Rice cultivation suitability map

The study provides an approach to find out valuable parametric values in identifying rice cultivation suitability map based on SDSS approach where the total area of the highly suitable locations would be calculated (Kumar, 1998).

Table 5.9, describes the correlations of the used factors performed in a matrix known as "reciprocal matrix". The eigenvector weight of the seven used factors and its importance were estimated through the reciprocal matrix. The results of the matrix pointed out that the distance to canals is very important and had the biggest eigenvector weight followed by the distance to the drainage network (Afify et al., 2011). Moreover, the correlation between the Leaf Area Index and Evapotranspiration is the strongest among the rest of the used factors according to the reciprocal matrix key demonstrated below. Such a correlation need to be considered in water conservation plans regarding to rice cultivation (Pettorelli et al., 2005). Only ratios less than 0.1 are accepted for a proper Spatial Decision Support System, the importance and the weights of the used factor need to be reconsider in case of consistency ratios higher than 0.1 (Dragan et al., 2003; Elhag, 2010).

Evapotranspiration showed moderately importance with the rest of the Vegetation Indices (Crop Water Shortage Index, Water Vegetation Supply Index and Drought Severity Index) and need to be integrated together for satisfactory results (Edward et al., 2008). Each of eigenvector weights was multiply to its corresponded layer then the layers were overlaid all together to be introduced to a final suitability map (Dragan et al., 2003).

Rice cultivation suitability values ranging from zero to one were demonstrated in Figs. 5.30-5.36 according to the corresponding factor. The spatial distribution of rice cultivation suitable areas varies in whole Kafr El Sheikh Governorate (Afify et al., 2011).

Table 5.9: Reciprocal matrix of seven factors and their importance

	Canals	Drains	ET	CWSI	WVSI	DSI	LAI
Canals	1						
Drains	1/3	1					
ET	1/9	1/9	1				
CWSI	1/3	1/3	3	1			
WVSI	1/3	1/3	3	1/3	1		
DSI	1/3	1/7	3	1	1	1	
LAI	1/9	1/9	5	1/3	1/3	1/3	1

Where, the reciprocal matrix keys are given below:

$\left.\begin{matrix} \frac{1}{9}\ extremely \\ \frac{1}{7}\ very\ strongly \\ \frac{1}{5}\ strongly \\ \frac{1}{3}\ moderately \end{matrix}\right]$ Less Important

1 Equal

$\left.\begin{matrix} 3\ moderately \\ 5\ strongly \\ 7\ very\ strongly \\ 9\ extremely \end{matrix}\right]$ Very Important

The eigenvector of weights is:

1-Canals: 0.3545; 2-Drains: 0.2920

3-ET: 0.0263; 4-CWSI: 0.1144

5-WVSI: 0.0828; 6-DSI: 0.0855

7-LAI: 0.0446

Consistency ratio = 0.08

Suitable area for rice cultivation based on **Leaf Area Index** factor distributed on both east and west side of the governorate (Fig. 5.30) in contrary with the spatial distribution of **Water Supply Vegetation Index** (Fig 5.31). **Crop Water Shortage Index** suitable area distribution (Fig. 5.32) showed no definite pattern and distributed all over the governorate, **Drought Severity Index** (Fig. 5.33) expressed the same pattern of CWSI. Daily evapotranspiration suitable area (Fig. 5.34) demonstrated marginal spatial distribution pattern surrounding the lake and keep most of the governorate area with less rice cultivation suitable values. Vegetation indices were developed to monitor and conjecture agronomic variables (Diker and Ünlü, 1999). Crop monitoring can be guided irrigators and farmers especially when water saving crops is used. Therefore, vegetation cover can be necessary data for agriculture science in general and rice cultivation in specific (Edward et al., 2008, Afify et al., 2011).

Water supply and quality are important issues which are impacting water reuse, the reuse of the irrigational water without proper treatment declines water availability and intimidate food security in Egypt (Afify et al., 2011; Elhag et al., 2011). Irrigational water treatment is one of the major water reuse limitations in Egypt as the irrigational water is mostly reuse with no treatment (El Filaly et al., 2004). Highly suitable areas based on canals and drainages factors confined closely to the both networks, and leave the rest of governorate less suitable areas (Figs 5.35 and 5.36). Suitable area based on the implemented constrains (DEM derivative; slope and land cover classes) were mostly highly suitable for most of the governorate area.

Overall suitability map (Fig. 5.37) defined fewer areas for rice cultivation in Kafr El Sheikh Governorate mostly were located around the lake and according to Figure 5.38 the total of

area available to each suitability class is as follows: highly suitable (S1) 1157 km^2, moderately suitable (S2) 488 km^2, marginally suitable (S3) 490 km^2 and not suitable (N) 126 km^2 which represent 51%, 22%, 22% and 5% of land area respectively.

According to Figure 5.36, both of marginally suitable and not suitable areas (27%) of the total current water consumption must be saved (3.1 BCM). A wise decision need to be taken towards the moderately suitable areas to be used for rice cultivation or not, such decision my save additional 2.5 BCM every year. The decision should be based on the fact that some areas of the governorate must be used for rice cultivation to maintain the pressure on the ground water table to avoid water logging (Afify et al., 2011), generally the pressure need to be kept around the west side of the lake.

The Spatial Decision Support System mission is to develop and disseminate information about site-specific management methods that are profitable and practical for agricultural producers and those who supply inputs or process products (Kumar and Panu, 1997; Kumar, 1998; (Dewan and Yamaguchi, 2009).

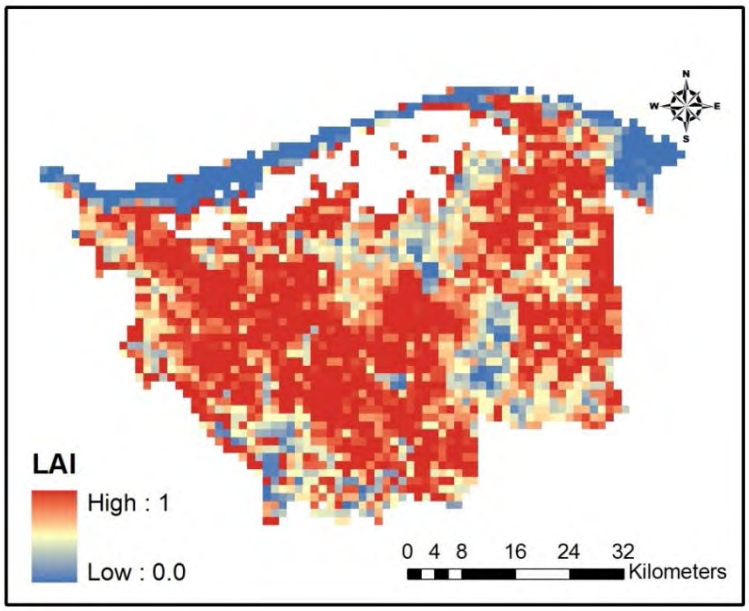

Figure 5.30: Leaf Area Index suitability map for Kafr El Sheikh Governorate.

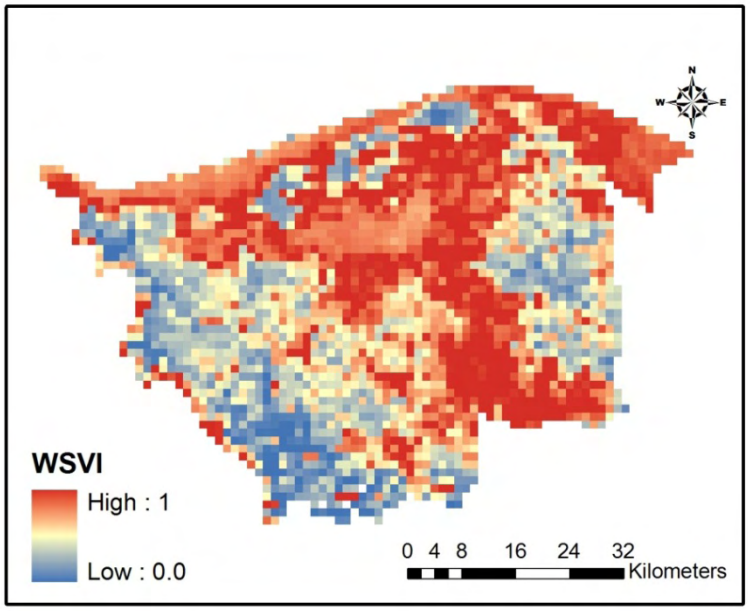

Figure 5.31: Water Supply Vegetation Index suitability map for Kafr El Sheikh Governorate.

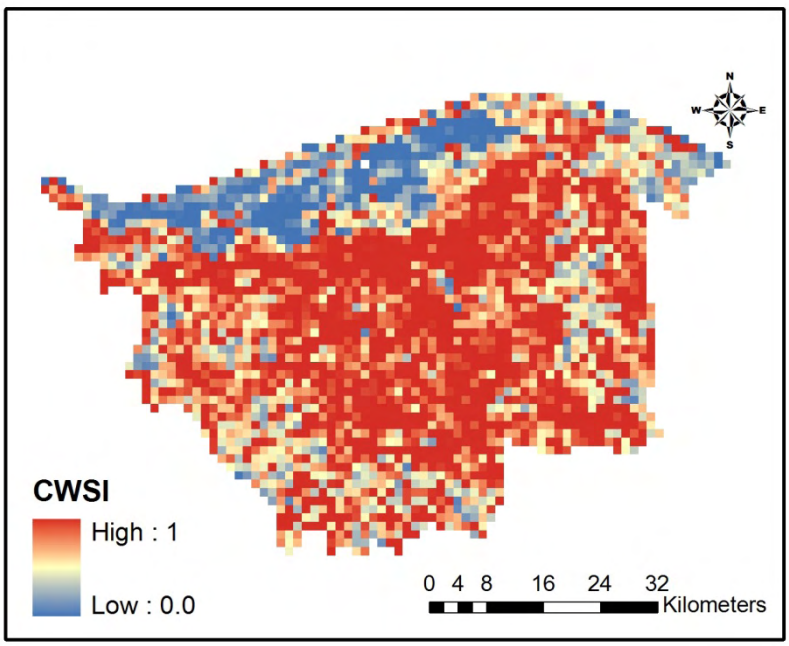

Figure 5.32: Crop Water Shortage Index suitability map for Kafr El Sheikh Governorate.

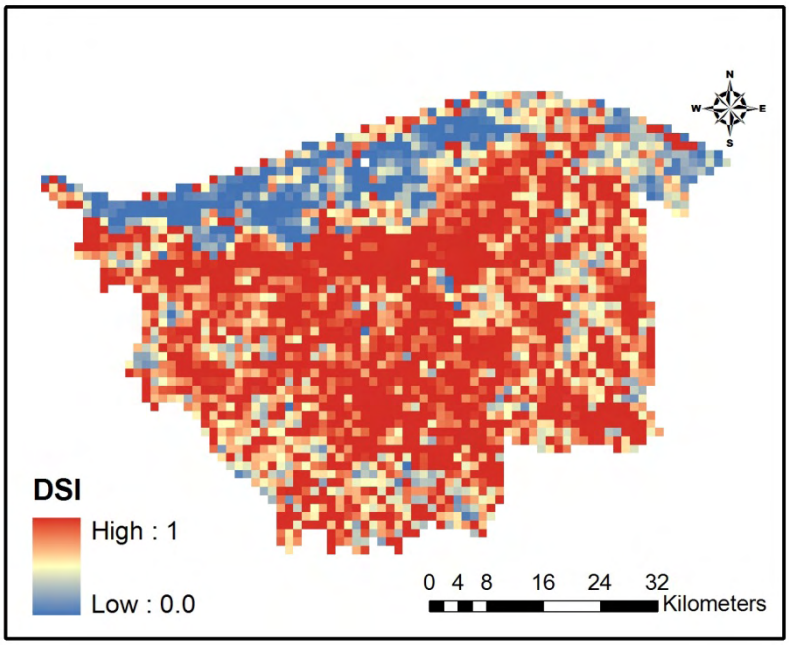

Figure 5.33: Drought Severity Index suitability map for Kafr El Sheikh Governorate.

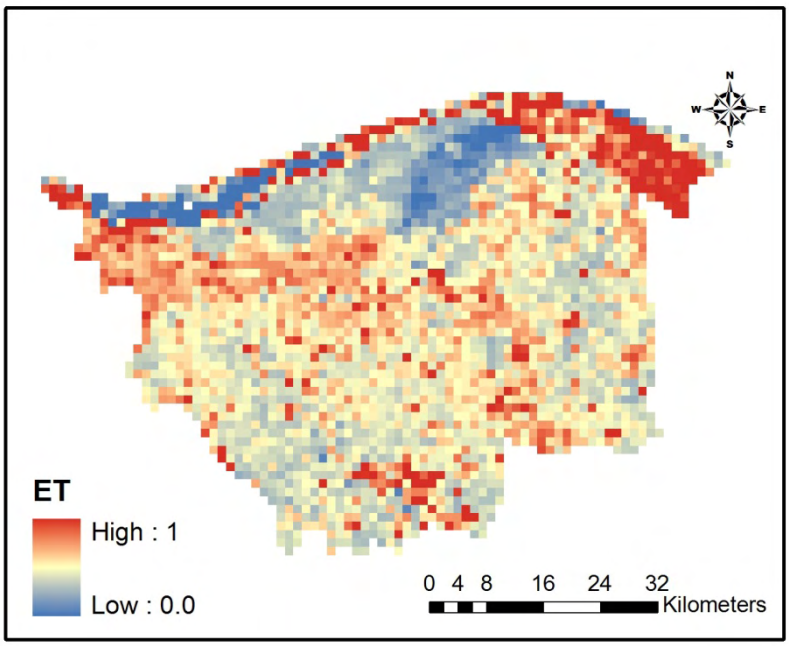

Figure 5.34: Evapotranspiration suitability map for Kafr El Sheikh Governorate.

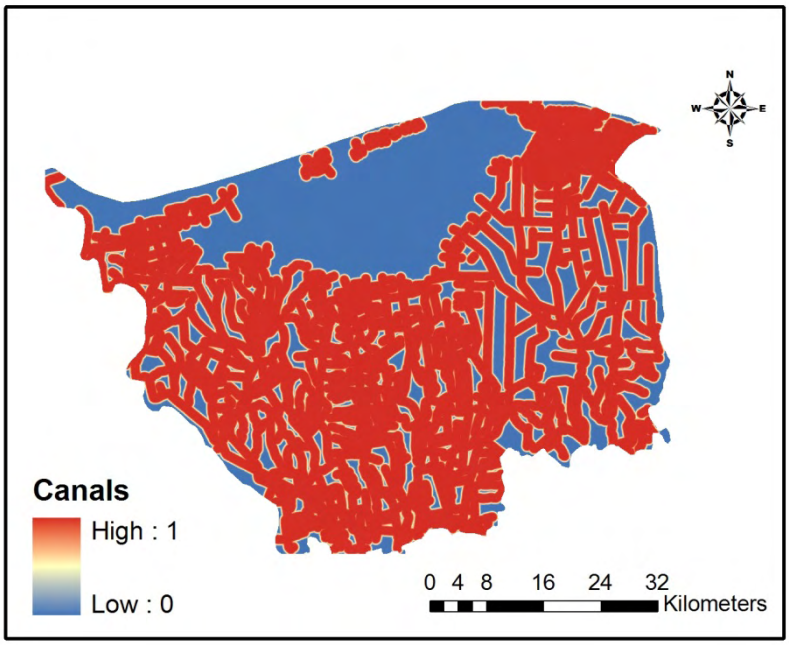

Figure 5.35: Distance from Canals network suitability map for Kafr El Sheikh Governorate.

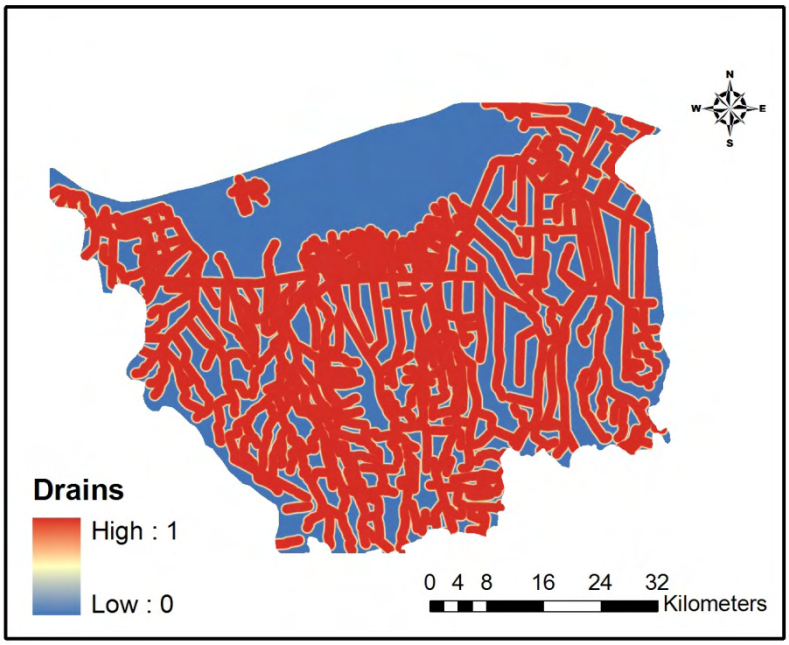

Figure 5.36: Distance from Drainage network suitability map for Kafr El Sheikh Governorate.

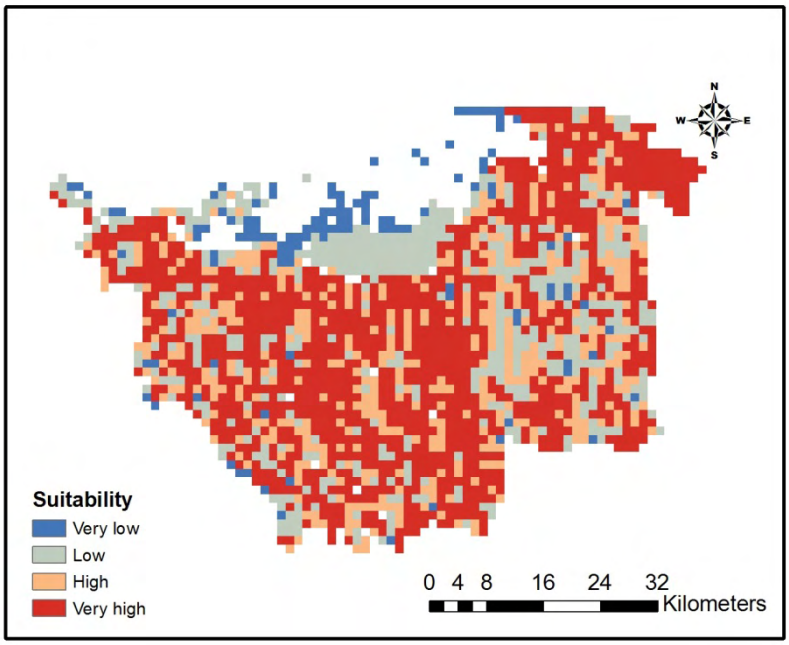

Figure 5.37: Overlaid suitability map for rice cultivation in Kafr El Sheikh Governorate.

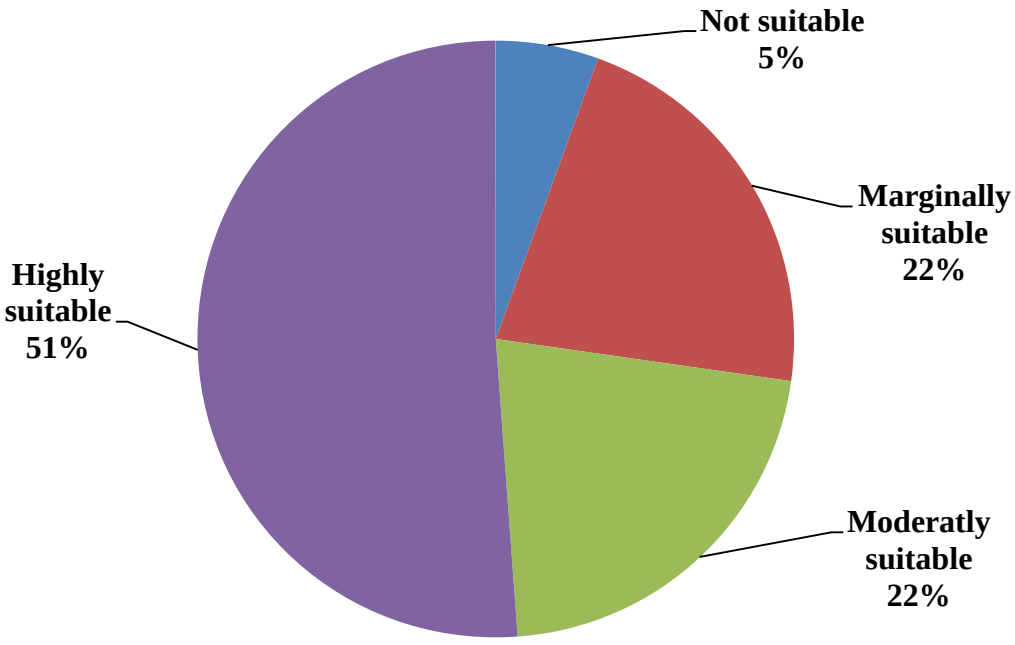

Figure 5.38: Rice cultivation land suitability percentages in Kafr El Sheikh.

6. Research Conclusions

6.1. Daily evapotranspiration

The objective of this research was to present a simplified method for the ET estimates based on the land surface energy balance theory over the Nile Delta region. With the collected ground measurements and satellite remote sensing data during the summer of 2008, the land surface albedo, vegetation coverage fraction were derived from MERIS data, and the surface temperature was retrieved by using the "split-window" algorithm with the AATSR data. The instantaneous latent heat fluxes estimated from satellite remote sensing data were converted to daily ET by using an algorithm, and the results were validated by using the ground measurements.

In this simple algorithm for daily ET estimate, the required variables are land surface albedo, vegetation fraction, land surface temperature and relevant ground meteorological data. The estimated daily ET values were ranged from 1.2 mm to 7.1 mm in the study area. The average square relative error (ASRE) was about 15.0%, and it was smaller in the area with high vegetation coverage. This implied that energy balance modeling is a feasible algorithm for irrigation management and monitoring crop water requirement in the arid regions.

Simulated evapotranspiration through the SEBS model and satellite imagery demonstrated very high correlation with the ground truth data. Larger areas may be reliably assessed using space-borne data instead of in situ measurements. The application of the SEBS model over the entire Nile Delta region mapped the daily evapotranspiration and evaporative fraction to be at maximum values of specific areas, within but mainly surrounding the Delta region. This fact may draw the attention of the decision makers towards adjustment of the agriculture practices in those areas, and may propose proper water resources management based on the land use changes.

6.2. Change detection

Post classification comparison technique is used in this study based on five different supervised classification algorithms. Five LULC classes were produced and only two main classes (urban area, fish farms) have increased rapidly in the study area. The urban class has been increased almost 6% during the period 1984–2005. Meanwhile, the agricultural lands class has also increased by almost the same percentage (6.5%), regardless the proportional area of each class and regardless reclamation and drying projects at the southern eastern part of Burullus Lake. The desert class has decreased due to reclamation processes and human intervention. Not all of the desert reclamation processes agrees with water saving practices running in Delta, due to the facts that the potential evapotranspiration in these areas is as high as double in comparing to the central area of the Nile Delta and due to the loss of irrigational water through the water delivery systems required for irrigation of those areas.

The use of remote sensing data in term multi-spectral and multi-temporal imageries provides a cost-effective tool to obtain valuable information for better understanding and monitoring land development patterns and processes. Knowledge of GIS delivers a flexible environment for storing, analyzing, and visualizing digital data necessary for change detection and database development.

It is also of great interest to investigate, in further research, the sub-classes of the agricultural land e.g. cotton, soya beans, corn, wheat, maize and rice. This could provide the status analysis for the agricultural land, determine the exact water demand for each crop and set the foundations for the implementation of sustainable water resources management.

Finally, the findings of the study strongly propose new policies to take into consideration the surrounding regions that may directly or indirectly affect the development of the study area. For instance the urban expansion should be strongly prohibited over the fertile agricultural

land and the expansion of the agricultural land towards the desert areas should be wisely selected to peruse a water saving plan.

6.3. Time series analysis

Estimation of daily evapotranspiration values over the Nile Delta region using Remote Sensing data proved to be applicable with appreciated accuracy (Elhag et al., 2011). Application of ARIMA model, without refereeing to the seasonality of the processed data, may lead to unreliably results regardless iterations of the ARIMA input parameters and resulted in inadequate model of forecasting. The accuracy of prediction is low and unstable along with time over the area of concern, while the refinement of ARIMA using 6 lags of seasonality [(2,1,2) (1,1,2)6], showed a robust forecasting model with a steady accuracy extended up to 30 months of prediction based on both Akaike's 'A' Information Criterion and Schwarz's Bayesian Criterion which also agreed with inverse R^2 (Pfaff, 2008) and -2LogLH values despite the value of the mean absolute percentage error .

Combining the use of Remote Sensing data, to estimate the daily evapotranspiration, and the use of Seasonal ARIMA model provides the keystone of advance and rational water resources management in arid ecosystems, to be agreed with similar results conducted by Landeras et al., (2010). The possible impacts of climate change on the water budget in Egypt are governed by rainfall patterns in the Nile Basin countries, rainfall patterns on the coastal area of Egypt, evaporation rates from open water bodies and wetlands, and evaporative demand of crops. It is possible that water quality may be affected as well. It may deteriorate due to excessive evaporation from free water surfaces and seawater intrusion into shallow groundwater aquifers and drainage canals in the coastal area. Loss of fertile arable land might also take place, due to inundation and waterlogging.

The impacts of higher temperatures and higher evapotranspiration values, lead to increased demands of agricultural water uses in Egypt and is an additional factor for the changes in the Nile water supply. Irrigation water losses are likely to increase from the Nile and the extensive system of irrigation canals, in addition to increases in crop water use and other water demands, so it is a complex task to estimatie the possible amounts of these losses. In terms of climate change impacts, the increase of the daily evapotranspiration is an important issue that should be considered and then regulated to mitigate the direct effects of higher temperatures on water resources. Higher temperatures shortened the grain-filling period resulting in crop yield reductions. Daily evapotranspiration increased in the warmer climate although it was partially offset by improvements in crop water use efficiency. The results shown that to cope with 1.3 mm/day increment, an additional 23.43 BCM will be demanded.

6.4. Rice cultivation

The **Pairwise Comparison Matrix** was constructed with the seven important factors mentioned previously and the relative importance of each one was measured through the calculation of weights. The computed weight of different parameters/factors with composite layers is shown in Table 5.9. Once the factor maps and the weight of composite layers were obtained, and then the physical suitability map at four suitability classes (highly suitable, moderately suitable, marginally suitable and not suitable) was evaluated for the rice cultivation by weighted overlay.

In this study, application of Remote Sensing (RS) and GIS techniques to identify suitable areas for rice crop was successful. The results obtained from this study indicate that the integration of RS-GIS and application of Multi-Criteria Evaluation using **Pairwise Comparison Matrix** could provide a superior database and guide map for decision makers considering crop substitution in order to achieve better agricultural production (Wu et al.,

2004). This approach has been used in some studies in other countries. However, in Egypt this approach is a new and original application in agriculture, because it has not been used to identify suitable areas for rice crop intensively. The study clearly brought out the spatial distribution of rice crop derived from Remote Sensing data in conjunction with evaluation of biophysical variables of soil and topographic information in GIS context is helpful in crop management options for intensification or diversification.

This investigation is a biophysical evaluation that provides information at a local level that could be used by farmers to select their cropping pattern. Additionally, the results of this study could be useful for other investigators who could use these results for diverse studies. This study has been done considering current land use/cover, topography and soil properties that affected the suitability classification of land use types. Therefore, it gives primary results. For further study, we propose to select more number of factors like soil, climate, irrigation facilities and socio-economic factors which influence the sustainable use of the land.

The common thread in rice cultivation water requirements is an attempt to achieve greater accuracy from remotely sensed data. In order to accomplish this, researchers have looked into various alternatives. Most of these alternatives have to do with the type of sensor (i.e., optical or microwave), number of images (i.e., single-date or multi-date), timing of the imagery, or processing technique. Although these characteristics certainly make a difference in the results attained, the trait that seemed to be most relevant was an appropriate use of the spatial data in combination with process understanding. Appropriate ground validation data and accuracy assessment is also critical for testing and reporting results.

The fundamental concept of rational water resources management in arid environment is to estimate and continuously monitor daily evapotranspiration. Figure 6.1 demonstrates the quest of daily evapotranspiration estimation over the Nile Delta region for last three decades.

The amount of water transpired by the agricultural lands in Nile Delta region is widely observed from a temporal date to a successive one. In the year 1984 the total amount of transpired water was 7.34 BCM and the total agricultural land was about three million feddan (15000 km^2). For that corresponding time, equilibrium between irrigational water demand and supply was maintained (Allam and Allam, 2007). Regardless the agricultural practices and water saving strategies implemented by either the government or the farmers that took place till the year 2012, those practices and strategies are obviously failed to maintain the demand and supply balance. In the year 2012, the total transpired water is about 2.21 times more than the transpired water in the year 1984 even though the total agricultural area is increased only by 1.6 times than the total area of the year 1984. Such a conclusion is a robust evidence of a defective water resources management planes used by either the government or the farmers and all of these management planes need to reformed, estimation and forecasting of daily evapotranspiration values must be concentric.

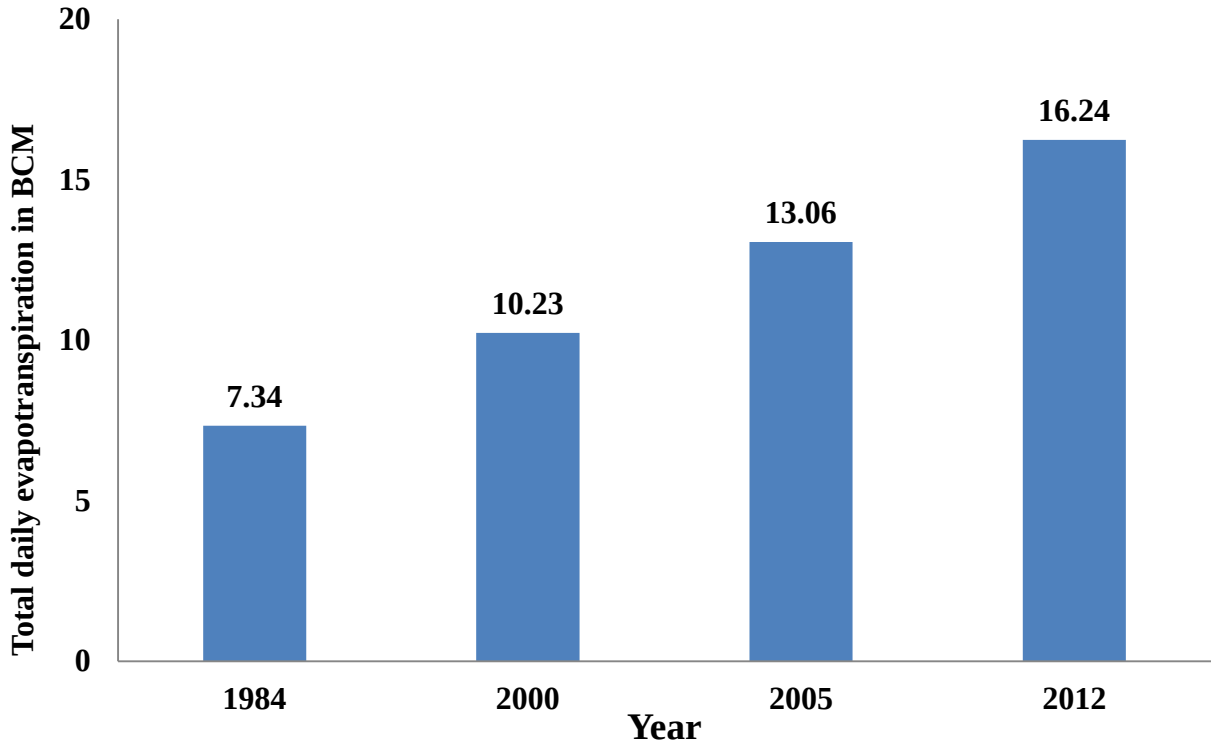

Figure 6.1: Total daily evapotranspiration in Billion Cubic Meter

7. Recommendation and outlook

The expansion of any new agricultural lands should always concern the daily evapotranspiration values in order to maintain roughly the same water requirements for irrigation in the Nile Delta. The use or Remote Sensing data could ease the effort needed to estimate daily evapotranspiration over vast agricultural land. The monitoring of daily evapotranspiration values over the Nile Delta region requires an equipped Remote Sensing and Geographical Information System laboratory based closer to the main weather station in the study area. The role of the weather station is very important because of the Surface Energy Balance System model input requirements. The estimation of the daily evapotranspiration values will be available on a weekly basis considering the temporal resolution of AATSR and MERIS images is three days.

Urban encroachment process should be immediately and forcefully stopped over the agricultural land in Nile Delta. The loss of the fertile land in Nile Delta for urbanization purposes is irreversible and causes a great damage to the quality of the soils. The imbalance of the water delivery systems because of the urbanization, makes the water available where it's not needed and short where it's needed. The urban area within the Nile Delta doesn't requires billions of cubic meter of irrigational water, while the new agricultural land at the peripherals of the old land not only requires a larger amount of irrigational water but also have higher daily evapotranspiration values. Fish farms industry within the old land of the Nile Delta should be always included in any master plan of the area due to its water requirements.

Nile Delta region is highly susceptible by any slight change in climate. Rising of the sea level creates the second drastic hazard on the Nile Delta lands after the increase of the temperature. The costal part of the Nile Delta suffers from soils saltation because of the rise of the sea

level leaving behind a very low soil quality. Estimation of daily evapotranspiration values in the Nile Delta is strongly correlated to the temperature fluctuations thus forecasting of daily evapotranspiration is essential in the study area. The use of S-ARIMA model provides a powerful tool of accurate prediction. Decision makers could trustfully base their own decisions regarding to water resources management plans on the results of the forecasting model to ensure the rational use of water.

Spatial distribution of water consuming crops, like rice, should be carefully selected. Rice field requires specific criteria if the optimum use of water is taking into consideration. Vegetation indices are with great importance to maintain the balance of water demand and supply especially for rice fields. Advance Remote Sensing techniques are now well implemented to provide a variety of reliable vegetation indices which could be useful for the decision makers. Spatial Decision Support System is the quest for the specialists to use different input parameter which all seeks the balance between demands and supply to unsure the rational use of water. Proper and knower based thresholds of the vegetation indices are highly appreciated to simulate the actual water demand of the crops.

Figure 7.1 illustrates the total cultivated area and each of total water consumed and water required for both of summer and winter crops with respect to its consumption vales according to table 5.2. it quite noticeably that the required amount of water is almost doubled from the year 1984 till the year 2005 taking into consideration that the mean value of water requirements according to the cultivations crop coefficient is constant and also the huge difference between the total demand and the total supply is explained by the high water use efficiency that reaches almost 1.9 fold of the supplied water (Table 5.2; MPWWR, 1998). It's crucial to mitigate the difference between the demand and the supply especially when the water reuse efficiency is not reliable because of the raw reuse of the water with no treatment.

The raw reuse of the water creates water quality problems to be added to the water quantity problem that we are dealing with.

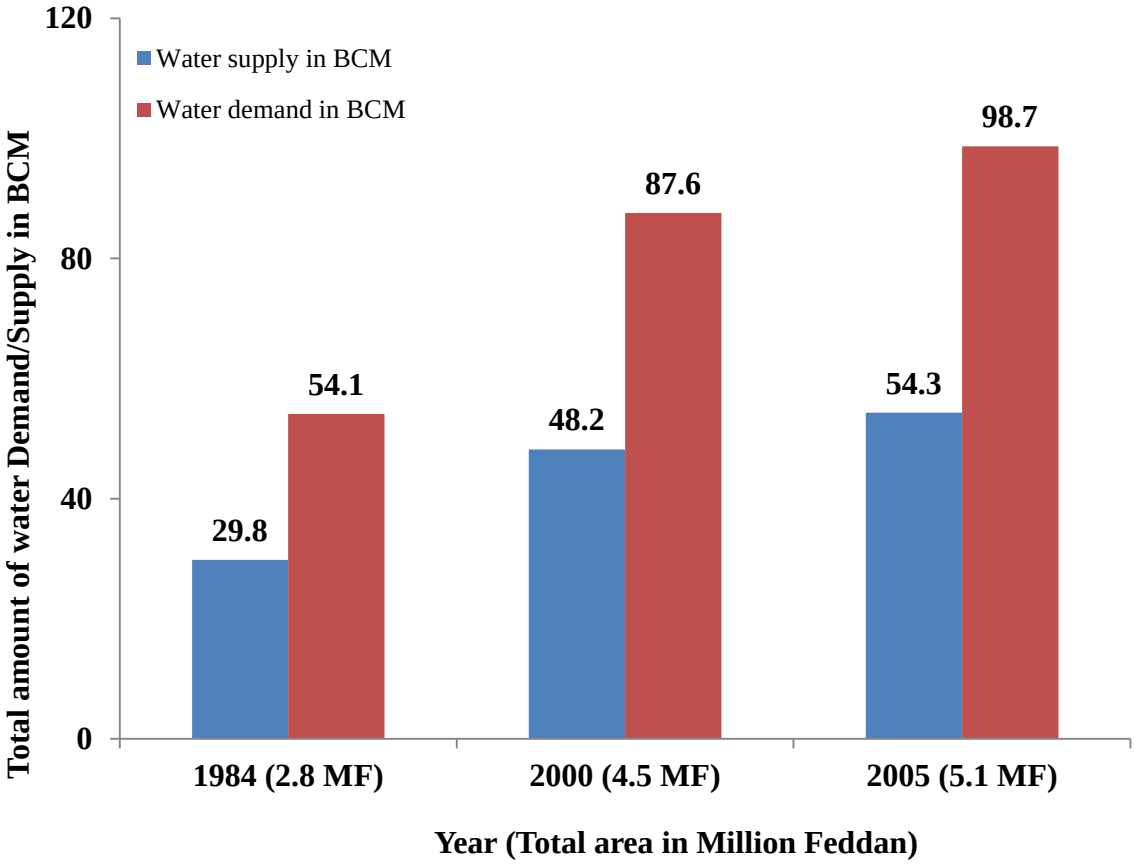

Figure 7.1: Difference between water demans and water supply in Nile Delta

Summarizing previsouly mentioned water requirement figures in a simple chart is essential to understand the trend of water requirements in Nile Delta region. Figure 7.2 illustrates the essential water requirements of successive three decades. The numerous increases in water needs in the year 2012 exceed 2.5 folds of the water need in the year 1984. This is easily to be explained by the huge land reclamation projects that added about 1.5 million feddan (5000 km^2) keeping in mind that the water resources in term of quantity and barely quality remains the same may lead to nothing but to imbalance the demand and the supply equilibrium. The above chart is basically indicates that the sustainable water requirements of agricultural sector in Egypt cannot be maintained. The total water requirement in the year 2000 is barley

sustained according to demand and supply needs (demand is about 48.2 BCM, supply is 55.5 BCM). Continuation of urban expansion over the agricultural lands and the massive land reclamation projects over the desert requires additional and unconventional water resources management. Adequate water resources management may utilize all of the above findings to ensure water sustainability in the near future.

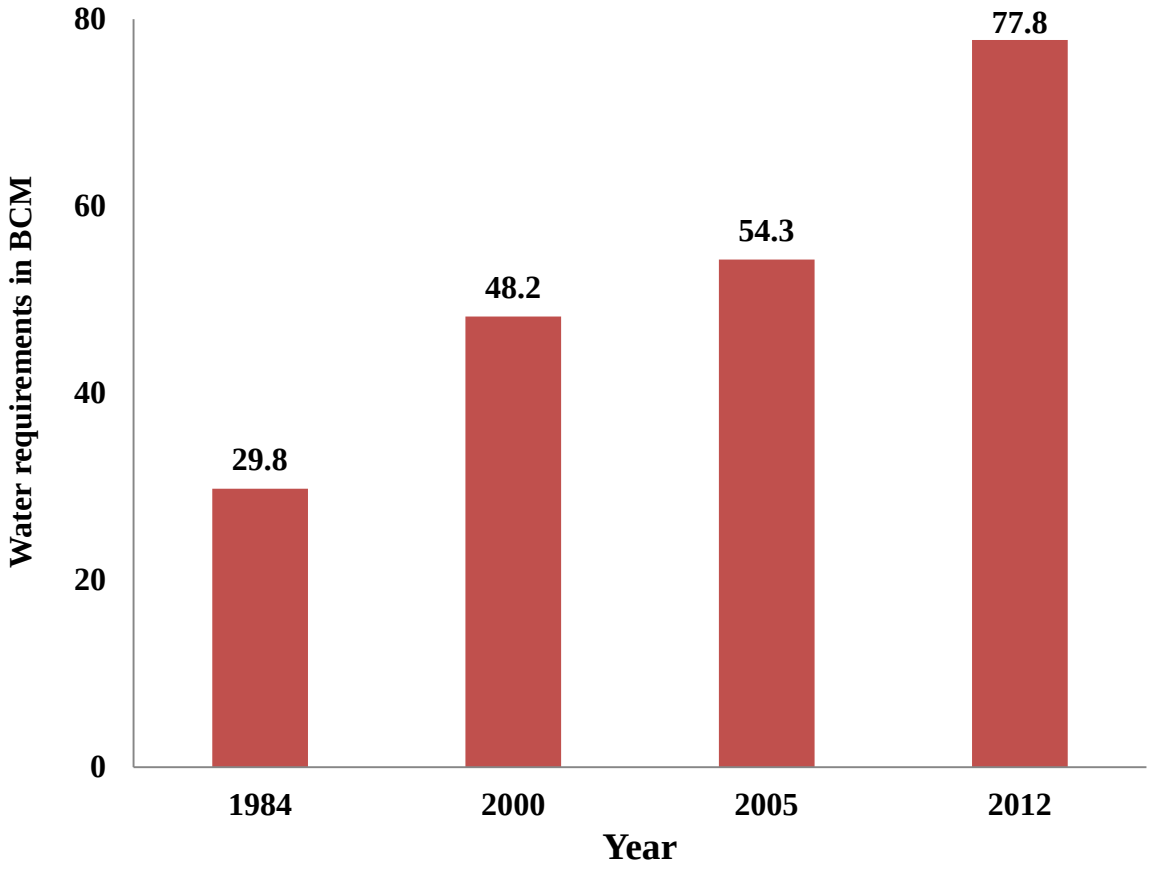

Figure 7.2: Total water supply in Billion Cubic Meter

All of the above findings are the keystone of modernized water saving techniques need to be adopted by related governmental institutions that have either direct or indirect impacts on the water resources in the country.

7.1. The Challenge for water demand management

It is to be feared that the share of water available for agriculture in the Old Lands will proportionally decrease with the increase of water consumption and water pollution for what

are considered will be more profitable and socially more urgent purposes. As a result of increased awareness for the need to conserve natural resources, it has become quite obvious to many observers that Egypt's water resources are not going to be sufficient for attaining all of the ambitious development objectives unless a sound water demand management system is established. It is imperative to shift the emphasis from the former paradigm of solving water problems by mobilizing additional fresh water resources (which are nearly fully mobilized) to an active water demand management system, especially with regard to the irrigation sector.

7.2. Creating the technical and agronomic preconditions

The Government of Egypt has taken a first step in the direction of introducing a system of Water Demand Management in the agricultural irrigation: For the irrigation of newly reclaimed desert areas the use of “modern” (and supposedly water saving) irrigation techniques like drip and sprinkler irrigation has been made compulsory. Even if the use of modern equipment alone does not guarantee an efficient water use, it is a first step in the right direction, and at least this equipment does permit easy water metering.

In the Old Lands, a national Irrigation Improvement Project (IIP) has been created in order to modernize the traditional irrigation system and to put an end to the problems which have arisen with the recent replacement of the “saqias” by mobile diesel-driven pumps. IIP aims to replace these again by fewer and larger stationary pumping units at the head of each tertiary canal, and to replace the current rotational system of water distribution with its inherent tail-end problems to a continuous flow system. Therefore, at secondary (branch) canal level, new hydraulic structures (downstream level operated gates combined with modular discharge control gates, see photos) are being built to introduce a continuous water delivery to branch canals and to control and limit the discharge into these canals. Branch canal based "Water

Boards" are being created and they shall be given responsibilities in the fields of operation and maintenance within their command area.

In addition to the technical innovations, the agricultural research system in Egypt is working on identifying a bundle of agronomic innovations, which it is hoped will contribute to improving the water use by farmers. The newly created project "Water Management in the Egyptian Irrigated Agriculture" through improving the service provision of extension staff and irrigation advisors is looking at how best to introduce such innovations into the irrigated farming system[1].

7.3. Creating the necessary institutions and laws

As outlined above, the replacement of fixed “saqias” by mobile pumping units resulted in an anarchic water abstraction from the secondary and tertiary canals. The planned introduction of continuous flow in the branch canals and the delegation of the competence for water distribution to the (secondary) branch canal based Water Boards is expected to solve this problem[2]. However, if this mechanism is to work in the sense of a sustainable Water Demand Management system, the corresponding legislation urgently needs to be effected. The main point of discussion is the need to grant a certain degree of financial autonomy to Water Boards and Districts. This autonomy is feared to lead to an uncontrollable rise of decentralized decision making, which may go beyond the narrow mandate of the water issue.

Nonetheless, an Institutional Reform Unit in the Ministry of Water Resources and Irrigation has been established and is working on the institutional and legal preconditions for this necessary decentralization process.

[1] This project is supported by the German Government through assistance provided by the German Agency for Technical Cooperation, GTZ

7.4. Using pricing of irrigation water

In Egypt, water in general, and the water of the Nile River in particular, is not considered an economic commodity which can be given a price and sold. With arguments often reinforced by reference to religious or Islamic principles, water is considered a gift from God - like life itself and the air we breathe. The only water charges ever likely to be tolerated in Egypt would be for water delivery services, which would still need to be introduced gradually. However, as is the case in most of the countries in the region, these charges will most probably be far below the elastic part of the demand curve, where no significant impact on the water demand can be expected. This means that water pricing, as a tool for limiting the agricultural water demand in Egypt, is virtually outside any political and cultural feasibility. The only rational use of irrigational water is applied in the new lands where the cost of the water delivery and the water distribution is high.

7.5. Using direct intervention

Egypt has a long tradition in the field of using direct interventions to attain the targets for national agricultural production. Since the middle of the 19th century, cotton growing, for example, has been promoted not only through many sorts of incentives, but also by using direct interventions in the form of compulsory dedication of certain areas for that crop. With the more complex problem of introducing a resource saving water management system any direct intervention, like the limitation of the rice area for example, can only be part of the solution. After the start of the successful and on-going liberalization process, direct interventions no longer related to the general policy of the government. Especially in Egypt, trying to impose centrally decided regulations without the political willingness to apply sanctions too, would bear the risk of lacking enforcement by local authorities and disrespect by the water users.

7.6. Imposing the cropping pattern

Until the year 1997, Egypt practiced a central cropping planning. The enforcement all over the Old Lands was done through a huge number of agricultural extension workers. With the liberalization process of the late nineties, the choice of the individual cropping pattern was given to the farmers, who based their decisions on subsistence needs, economic criteria and the anticipated water supply situation. There are a few regulations remaining, which concern limitations of the area for rice and sugar cane growing, and prohibiting the expansion of tree crops in the Old Lands. This liberalization process resulted in an increased imbalance between the supply and demand for water delivery. Because of very attractive farm-gate prices for rice, farmers on head reaches of canals have shifted to rice growing on an area of around 1.5 million feddan, which is much greater than the regulated 900,000 feddan. Against all rules and regulations, this was also done in areas far away from the northern Delta. Only near the northern coast is rice growing appropriate and permitted in order to leach the soils and to recharge the shallow aquifer. This is necessary to prevent sea-water intrusion into this aquifer. The unauthorized rice cultivation in other regions was undertaken despite the efforts of the government to promote the cultivation of cotton instead. This example shows that strong economic incentives cannot be counteracted by non-market measures like persuasion and advice. Given the impossibility of using economic tools like water pricing in Egypt, and given the lack of regulation enforcement, the cropping pattern and the corresponding agricultural water demand are exclusively dependent on farm-gate prices and the market mechanism.

7.7 Imposing water quotas

The only effective tool for introducing a better water management system in irrigation and for solving the rising problem of competition between different water users is seen by the author in a volumetric limitation of supply. This limitation could be realized through the

introduction of yearly or seasonal quotas of water delivered to each water district, to each individual branch canal and to other non-agricultural demand centers. The quotas allocated would not only permit consideration to be given to the aspect of a changing pattern of water demand within the country, but also to the varying availability of water resources over the years.

This feasible, but drastic, measure can only be established if the Government of Egypt takes such a decision on the basis of a broad political and popular consensus, and it can only be gradually introduced. This process could be greatly facilitated by substituting the practice of monitoring water levels with direct volumetric readings which would then be accessible to water users themselves. The increase in transparency of water allocation and water distribution would greatly enhance the possible participation of water users and facilitate the acceptance of quotas. In parallel, more farmers' organizations like Water Boards and Water Users' Associations need to be created and empowered. These institutions will have to be entitled, and legally obliged, to decide on the priorities of the water use, especially on the cropping pattern within their respective command area (and/or on the water use within their communal water demand center). It is clear that agricultural water users must be informed of the amount of water that they can expect before each cropping season. In doing this, the practice of centrally decided, but not enforced, limitations of an area for certain crops such as rice in the Delta, as well as the largely futile attempts to influence farmers' behavior through advice and exhortation, will become obsolete. Also, the agricultural extension services will be in a better position to dispense effective advice on the best use of the then limited water supply. Farmers may then be more inclined to substitute the cultivation of water-inefficient crops with water-efficient and high value and, potentially, exportable crops[2]. Thus, the

[2] Growing crops for export in the Old Lands and especially in the Delta might first need major investments into the water quality (hygiene), since water quality considerations significantly restrict the range of high-value exportable crops.

introduction of a water demand management system could contribute to both an increase of Egypt's GDP through the irrigation sector, and quite possibly to the country's export earnings.

It could also help in achieving a reasonable level of self-sufficiency in essential agricultural products. The price to be paid for such a development would be the importation of low value or highly water consuming agricultural products and meat (with the corresponding amount of virtual water[2] which these products represent) to meet the populations' needs.

7.8 Water saving scenarios

Recognizing that in the future, even more than the present, the primary constraints in Egyptian agriculture will be water and land. The current research presents herewith a number of alternative scenarios extracted from Intergovernmental Panel on Climate Change (IPCC) working group in 2001a. Scenariors are hypothetical cases regarding the availability, quality, and use of water, and regarding soil fertility, salinity and drainage. The assumptions of the scenarios are listed in Table 7.1.

The alternative scenarios are based on the present cropping systems in Egypt and used for 50 years projections, methods for projecting crop yields under climate change conditions, and offer definitions of some concepts critical to projecting the future of Egyptian agriculture. According to Allam and Allam (2007), there are two different types of scenarios, static scenarios and dynamic scenarios. Static scenario assumes that no change will happen and the future is exactly projected from the present. In fact, most of the existing water policies are impressive and sensitive to the need to overcome a number of water problems (Luzi, 2010).

Unfortunately, these water policies include several questionable issues. These issues are not only compromising the results of these policies, but also their effectiveness.

Three scenarios for the future water status in year 2050 are presented. The first scenario assumes the continuity of the current water practices without major changes. The second scenario assumes a relative development of the water policies, and the third scenario is ambitious and reflects a radical development in water management practice in Egypt.

Table 7. 1: Main Assumptions of the Proposed Scenarios

Assumption	Scenario		
	No change	Pessimistic	Optimistic
Total Population (Million)	84	100	91
Surface Irrigation Improvement (million km^2)	0.50	0.40	0.80
Irrigation Network Rehabilitation	Current practice	More Attention	More Attention
Municipal and Industrial Water Use Rationalization	No serious steps	More attention	Privatization + Tariffs
Drinking Water Supply Network Rehabilitation	None	Main parts	Privatization
Drinking Water Supply Network Losses (%)	40 – 50	30	20
Wastewater Treatment Compared to Population Growth	Much lower	Lower	Privatized and improved
Water User Association, Water Boards and Water Councils	As Current	Established	Empowered & Granted Legal Liabilities
Restriction of High Water Requirement Crops	Breeds with less water requirements	Decrease in areas of Rice and Banana	Reach the optimal areas of Rice and Banana
Government Control over Pollution	No Actions	Efforts decrease	Law and regulation empowerments
Illegal Practices of Drainage Reuse	Continue	Less	Prohibited
Modern Irrigation for Orchard and Fruit Farms	No funds	No funds	Yes
Completion of Horizontal Expansion Projects (million km^2)	0.20	0.60	1.00
Public Awareness	Current	Increasing	High

7.8.1. Scenario 1, No changes to the current agricultural practice or water resources

A continuation of current trends in Egypt will lead to an intensifying loss of agricultural land to waterlogging and salinization, as well as to urbanization. Field water application efficiency values (defined as the fraction of the water applied that is actually used, or transpired, by the crop) in Egypt are typically well below 50 %, and in many cases are below 30 %. Such low values imply that more than half (and often two thirds) of the water applied in the field exceeds the irrigation requirement of the crop (Yates and Strzepek, 1998).

Excess irrigation will lead to reduced crop yields below potential insofar as it impedes aeration, leaches nutrients, and induces water-table rise, salinization, and the need for expensive drainage. Concurrently, irrigation water quality will deteriorate, altogether resulting in a decrease in agricultural productivity. Average crop yields will diminish, notwithstanding the expectable improvements of varieties, fertilization, and pest control. Especially vulnerable to the progressive degradation of land and water resources are the ill-drained areas of the lower Nile Delta that are already subject to land subsidence, water-table rise, and saline-water intrusion. Combatting these processes will require large investments in expensive drainage, and greater government intervention and regulation; if investments, interventions, and regulations are lacking or are haphazardly implemented, these lands will certainly become unusable for agriculture. The strains to the coastal and delta system may also lead to clashes among competing interests, e.g., among agricultural, urban, and industrial sectors as it described in Table 7.2.

7.8.2. Scenario 2, Pessimistic scenario: No adaptation to climate change

The expectable impact of climate change on the supply of water (i.e., on the flow of the Nile) is greatly uncertain. On the other hand, the warmer climate is certain and will impose a greater evaporational demand and hence will increase irrigation water requirements. This

effect may be mitigated in part by the higher water use efficiency of some crops in a CO_2 enriched atmosphere. Higher evaporation rates will have the secondary effect of worsening the tendency toward soil salinization, by speeding the transport of damaging salts to the soil surface.

Table 7. 2: Water uses and available resources for scenario (1)

Water Uses (BCM/year)		Water Resources (BCM/year)	
Sector	Amount	Resource	Amount
Municipalities and Industry	15.20	Nile River	55.50
		Groundwater (Delta and Valley)	7.50
River Transport	0.30	Deep Groundwater	2.25
Fisheries	0.00	Drainage Water Reuse	
Hydropower	0.00	- Canals in the Delta Region	6.50
Agriculture	63.60	- Nile river and Bahr Youssef	5.00
		- Illegal Uses	3.00
		Waste Water Reuse	1.00
		Rainfall and Flash Floods	0.50
		Desalination	0.00
		Evaporation Losses	2.50
Total	79.10	Total	78.75

* Source: Allam and Allam, (2007)

In the traditional regime of infrequent irrigation common in Egypt, sensitive crops are therefore likely to suffer from increased moisture stress and salt stress. Yields may suffer additionally from the hastened maturation in a warmer climate and greater infestations of

pests. Heat sensitive crops that are already near the limit of their heat tolerance will be especially vulnerable.

Equally serious is the potential effect of sea-level rise resulting from the thermal expansion of seawater and the melting of land-based glaciers. Even a slight rise of sea-level will exacerbate the already active process of coastal erosion along the shores of the Delta (currently 50 cm per year at the head of the Rosetta branch of the Nile at Rashid), a process that accelerated after the building of the Aswan High Dam. For a 1 meter sea-level rise, 12 to 15 % of the existing agricultural land in the Delta may be lost. Sea-level rise will also accelerate the intrusion of saline water into surface bodies of water (the lagoons and lakes of the northern Delta) as well as into the underlying coastal aquifer. The rise in the base level of drainage will further increase the tendency toward waterlogging and salinization of low-lying lands, with the consequence that significant areas will become unsuitable for agriculture. At the very least, the costs of drainage will increase.

Coupled with the deleterious effects described in the pessimistic case without climate change, global warming is likely to reduce agricultural productivity in Egypt yet further. Crop modeling simulations with GCM climate change scenarios at the high end of the IPCC (2001a) range (4^{o}C) found that maize and wheat yields declined in the Delta by as much as 30 % and in Middle Egypt by more than 50%. In view of the continuing increase of population, Egypt may suffer a worsening shortage of food and an eventual crisis. This is indeed a worst case scenario (Table 7.3).

7.8.3. Scenario 3, Optimistic scenario: Improved resource management and effective adaptation to climate change

Much can be done to mitigate the potential dire consequences of climate change and the earlier the task is recognized and undertaken the more likely it is to succeed. The first

imperative is to improve both the technical water application efficiency and the agronomic water use efficiency. This involves nothing less than revamping the entire system of water delivery and control. Ideally, water should be made available on demand (rather than on a fixed schedule), and be delivered in measured quantities in closed conduits subject to effective monitoring and regulation while avoiding seepage losses.

Table 7. 3: Water Uses and Available Resources for Scenario (2)

Water Uses (BCM/year)		Water Resources (BCM/year)	
Sector	Amount	Resource	Amount
Municipalities and Industry	12.75	Nile River	55.50
		Groundwater (Delta and Valley)	5.50
River Transport	0.00	Deep Groundwater	2.00
Fisheries	0.00	Drainage Water Reuse	
Hydropower	0.00	- Canals in the Delta Region	8.50
Agriculture	69.75	- Nile river and Bahr Youssef	5.00
		- Illegal Uses	2.00
		Waste Water Reuse	2.00
		Rainfall and Flash Floods	1.25
		Desalination	0.25
		Evaporation Losses	2.00
Total	82.50	Total	80.00

* Source: Allam and Allam, (2007)

While this will be difficult to achieve in the Old Lands, where traditional systems exist and traditional concepts die hard, it is certainly achievable from the outset in the New Lands. To facilitate adoption of water conservation, the authorities should provide farmers with explicit

guidance regarding optimal crop selection, irrigation, and fertilization, and should institute strong incentives to avoid excessive water use (including of the suggested but seldom implemented pricing of water in increasing proportion to the amount used). Modern methods of irrigation based on the high-frequency, low-volume application of water and fertilizers directly to the plants need to be adapted to the scale of operation and local practicalities of Egyptian farming.

Fortunately, such systems are flexible and lend themselves readily to downsizing so as to accommodate the small-scale nature of most Egyptian farming units. Moreover, such systems can be applied successfully to sandy and even to gravelly desert soils (potential New Lands) that are not considered irrigable by the traditional surface-irrigation methods.

An additional set of measures involves the careful selection and/or breeding of heat tolerant, salinity tolerant, water conserving crops; as well as controlled-environment production methods that minimize water use while maximizing the production of high-value crops (e.g., all-season vegetables and fruits, spices, medicinal).

A further set of mitigation measures involves the management of the low-lying lands on the northern fringe of the Delta, where the consequences of sea-level rise (submergence and salinization) are certain to wreak their greatest damage. Some of those lands must be retired from agriculture, and the amount of water made available consequently should be diverted to the irrigation of New Lands outside the Nile Valley and the Delta.

The overall effect of the measures listed herewith, in light of the future either with or without climate change, will be to raise the potential and actual productivity of Egyptian agriculture. Thus, climate change may not thwart progress toward the goal of providing sufficiently for the Egyptian people. A final caveat, however, is that much depends on whether the rate of population growth in Egypt, which has already begun to decline, continues to do so fast

enough to allow agricultural productivity to keep pace with the country's growing needs. Indeed, Scenario 3 is considered to be the best case scenario according to Table 7.4.

Table 7. 4: Water Uses and Available Resources for Scenario (3)

Water Uses (BCM/year)		Water Resources (BCM/year)	
Sector	Amount	Resource	Amount
Municipalities and Industry	11.50	Nile River	58.50
		Groundwater (Delta and Valley)	8.50
River Transport	0.00	Deep Groundwater	3.20
Fisheries	0.00	Drainage Water Reuse	
Hydropower	0.00	- Canals in the Delta Region	9.50
Agriculture	73.70	- Nile river and Bahr Youssef	6.50
		- Illegal Uses	0.00
		Waste Water Reuse	2.50
		Rainfall and Flash Floods	1.70
		Desalination	0.90
		Evaporation Losses	2.00
Total	85.20	Total	89.30

* Source: Allam and Allam, (2007)

7.8.4. Mini scenarios

Mini-scenarios are numerous and they are either time and/or space specific and requires certain sanctions to be taken in order to empower these mini-scenarios. For a country like Egypt the top ten mini-scenarios are categorized into pivot driving forces and non-pivot driving forces, both are used for 10 years projections. The mini-scenarios are summarized as below:

7.8.4.1. Pivot driving forces mini-scenarios

1. International Treaties:

• The revision of international treaties and water rights in the near future without resulting in a change in the Egyptian quota of the River Nile.

• The signing of more recent and agreed-upon treaties by all concerned parties (Nile Basin countries) to establish stronger mutual relations.

• Growing demand for Nile Waters by riparian countries and the failure of Nile basin countries discussions and disbanding of Nile countries forums. This might be a result of or may result in unilateral actions from upstream countries to control Nile water that would reduce the water flow to Egypt.

• The success of the Nile Basin Initiative and the re-visitation and reshaping of Nile agreements on the basis of trust and respect of the benefit and interests of all countries. Joint water-saving projects and hydropower projects will also be carried out.

• Eruption of war inside the Sudan between the North and the South or between other Nile basin countries.

• Shortage of funds needed for water and energy projects.

2. Science and Technology:

• The achievement of higher water re-use in Egypt (currently water is being reused two times on average) to reach a value of 5 times or more using the proper technologies.

• The use of saline water for the irrigation of some crops where the cost of brackish or sweater desalination will have reached agriculturally economically feasible levels.

• The technical and economic separation in the treatment of different wastewaters to make the process of water treatment more feasible economically and health-wise.

• Support of national and regional programs to enhance the application of advances in technology to reduce desalination costs, improve the management of water, and reduce the environmental impacts of desalinization.

• The enforcement of embargos on technological transfer might mean no advances in desalination.

• Environmental impacts of desalination can be detrimental and irrecoverable.

• Application of modern techniques of irrigation to newly reformed lands (the new techniques will be taken up by farmers faster than the government if they are given enough freedom), while the Delta and the lands along the Nile will deteriorate rapidly.

3. Water Pollution:

• A fall in the level of water pollution due to enforcement of environmental laws which will lead to minimization of water pollution, the implementation of "polluters pay" principles, the availability of degradable substances, better awareness campaigns and/or a drastic change in the prevailing culture.

• Minimizing water pollution from the source rather than focusing on the treatment of secondary sources of pollution.

• Applying appropriate technologies to different cases of water pollution accordingly.

• Absence of law enforcement leading to an increase in water-borne diseases associated with negative impacts on investment, tourism, etc. and the increase in pollution levels despite international warnings. This will lead to the imposition of external amendments to the situation by other countries or of internal amendments by the government on the citizens. These new amendments are not likely to be applied by small peasants and farmers due to ignorance.

• State investment and implementation of low cost techniques for wastewater treatment.

• A continuation of the current situation where sanitary sewage coverage is less than 100%, industry is not treating its wastewater, and agriculture is using excessive quantities of chemicals. Water pollution will continue to increase as human activities increase.

4. Water Management:

• The direction of efforts to discover new water resources which will lead to the increase of the supply of groundwater and will make up for the gap in the water balance.

• Unsustainable trends of groundwater and surface water resources development leading to high investment costs that do not match the amount of water returns or savings, and further fragmentation of landholdings.

• Introduction of Integrated Water Resources Management, Integrated Irrigation Improvement Projects and Private Public Partnerships leading to an increase in national water use efficiency and higher economic return per drop of water.

• The government will take steps towards the formation of associations and organizations to improve water management although response of citizens is expected to be very feeble since the government usually ignores the public opinion concerning its projects. This will lead to a continuous wasting of resources (i.e. part of national income to establish water management systems).

5. Water Pricing Policies:

• The application of an indirect way for water pricing (e.g. cost recovery of water projects, application of incentives and penalties) rather than a direct one because of water scarcity and the increased awareness of the significance of minimizing water consumption in all aspects of life.

• Military intervention in the Middle East to seek water security.

• The partial transfer of some of the agricultural activities (the most water consuming) to Sudan for example.

• An increase in water subsidies which will further burden the national economy, and the continuance of irrational water uses and significant wastes leading to further deterioration of water supply and sanitation services. Moreover, the state will be unable to provide services to those deprived or to extend them to new areas.

• Application of water pricing (possibly due to pressure from riparian countries or from social and political international movements) which will lead to social unrest. This scenario might be applied through the privatization of the water supply and sanitation systems to ensure better services.

• Implementation of a cost recovery system for providing water supply and sanitation systems while ensuring the basic needs of water for survival are satisfied for those who cannot afford it.

• Application of water pricing to a specific category of users (e.g large investors)

• Private public partnership (PPP)

1 Multilateral Agreement and Treaties	2 Water Pollution	3 Science and Technology	4 Water Management	5 Water Pricing
1.1 Enforcement of bilateral agreements with the NB countries	2.1 "Business as usual": continuation of the current trends of water pollution	3.1 Application of modern irrigation techniques and systems to newly reclaimed lands, leading to improve efficient use of water.	4.1 Narrowing the deficit gap between supply and demand of water.	5.1 Water is a private good which leads to applying water pricing
1.2 Negotiation with the NB countries to revise the present Nile quotas.	2.2 Enhancement the role of government and civil society in preventing water pollution to avoid contamination of vital natural resources	3.2 Introduction of suitable technology for developing non-conventional water	4.2 Sustainable development of natural resources is a must for the coming generations.	5.2 Water is a public good which leads to not applying water pricing
1.3 Trans-boundaries water issues to be considered a catalyst for co-operation among the NB countries (the Nile Initiative)		3.3 Introduction / breeding crop varieties tolerant to salt and heat resistance.	4.3 Enhancement of public private partnerships to play role in improving water management	5.3 Applying Cost recovery / cost sharing to the major water management projects.
			4.4 Reluctance of civil society and NGO's to play their role to preserve and maintain water resources and ecosystems.	5.4 Introduction of water pricing in irrigation water will leads to instability
			4.5 Insure equity of water distribution among competences (drinking water, agriculture, and industry) respectively	

* Source: Allam & Allam, (2007).

Figure 7. 3: mini scenarios for pivot driving forces

7.8.4.2. Non-pivot driving forces mini-scenarios

1. Development and Economic Growth:

• The economic growth of Egypt will be based on industry -which requires less water than agriculture i.e. it will be an industrially based economy, and there will be a partial transfer of some agricultural activities abroad. Hence, competition between economic sectors on water will not be in favor of agricultural production.

• The hindrance of future co-operation between Arab countries (including Egypt and Sudan) due to instability in the region.

• The establishment of multinational companies to reflect the interests of the concerned people in the region. This will strengthen cooperation with riparian countries on the rational and organized use of Nile water.

• Uncontrolled expansion in agricultural and economic development in riparian countries leading to a reduction in quality and quantity of Nile flow to Egypt.

This will also lead to an increase in the gap between food consumption and production in Egypt. Development programs will not be able to meet the increase in population and some basic crops (such as rice) will disappear.

• Establishing a balance in Egypt between production of cash crops for export and traditional crops for national consumption.

• Major starvation problems due to the failure of the agricultural sector to reconsider its water use policies, and the cessation of development projects in the newly reclaimed lands due to lack of water availability.

2. Environmental Phenomenon:

• Rainfall in the region will be affected by the increase in temperature (a warmer climate) which will reflect on the share of water used in agriculture.

• Re-organization of the crop pattern to achieve maximum benefit from climate changes.

• Climate changes leading to a flooding of some parts of the delta or possible sea water intrusion due to increased sea water level.

• The natural transformation of some lands into desert and the loss of others to construction of facilities and homes.

• Repetition of the dark cloud phenomena and conflicts in the region due to such phenomena.

• Application of General Circulation Models (GCM's) and Local Area Models (LAM's) which can be used to predict environmental changes

3. Availability of Safe Energy:

• More widespread use of renewable and clean energy sources (such as wind and solar energies) in many areas in Egypt as it is more economic, accompanied by a decrease of dependence on fossil fuels (as the price of oil may continue to increase reaching $100/barrel).

• Continual use of finite energy sources (such as petrol) which might lead to opposition movements internally.

4. Sustainable Development:

• Establishing a democratic society in Egypt which acts as a measure for achieving sustainable development.

• The continuance of the current trend of water resource development dependent on engineering dimension while neglecting the social and economic dimensions, due to the deep rooted red tape policies.

• The government will reconsider its current plans due to the dryness of lakes and small surface waters.

5. Social Values:

• The achievement of higher standards of living which means better life quality and health indicators which means high production and greater GNP.

• No state guarantee for access to water supply and sanitation for all citizens.

• Carrying out national water awareness campaigns on the cost of water supply and sanitation.

• Improvement in social values leading to changes in water use.

• Globalization of social, cultural and ethical values accompanied by education, human development and capacity building to raise social values and to formulate water ethics programs.

• Cut-side terrorism.

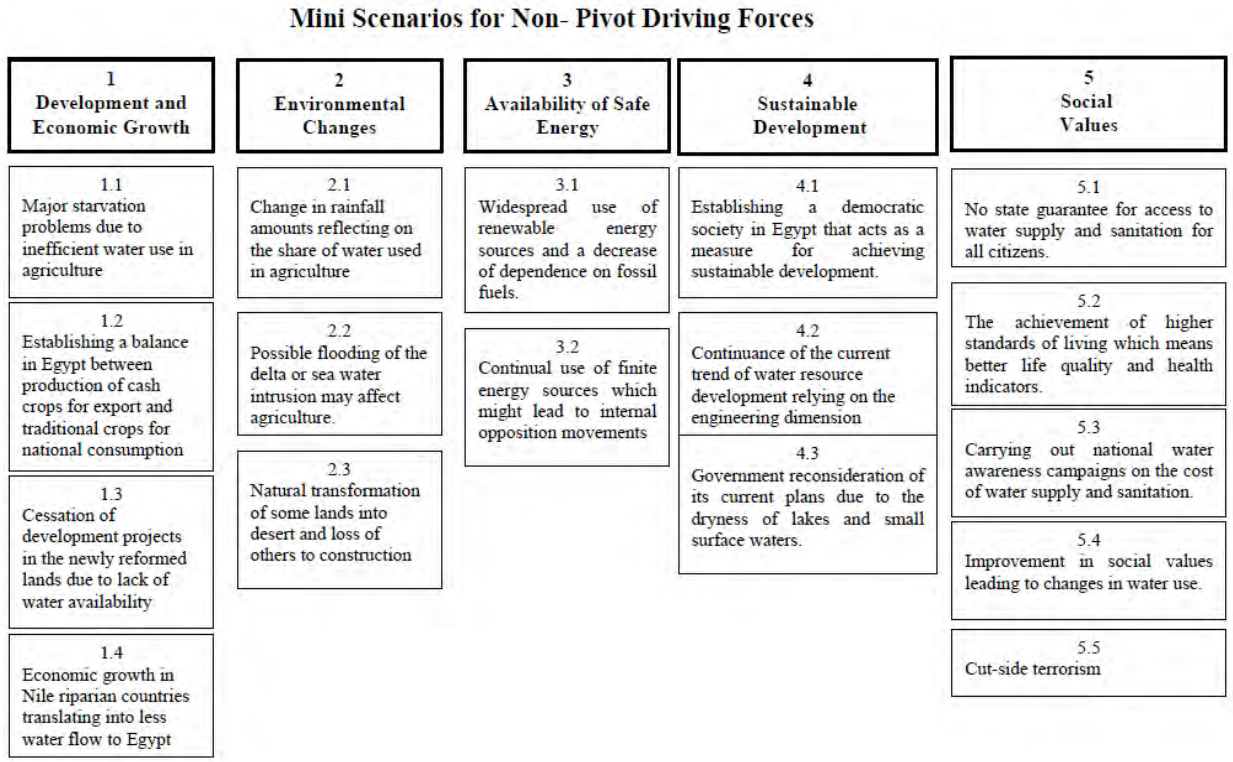

* Source: Allam & Allam, (2007).

Figure 7. 4: Mini sceanrios for non—pivot driving forces

8. Research summaries

8.1. English summary

Estimation of evapotranspiration is always a major component in water resources management. The reliable estimation of daily evapotranspiration supports decision makers to review the current land use practices in terms of water management, while enabling them to propose proper land use changes. Traditional techniques of calculating daily evapotranspiration based on field measurements are valid only for local scales. Earth observation satellite sensors are used in conjunction with Surface Energy Balance (SEB) models to overcome difficulties in obtaining daily evapotranspiration measurements on a regional scale. In this study the SEB System (SEBS) is used to estimate daily evapotranspiration and evaporative fraction over the Nile Delta along with data acquired by the Advance Along Track Scanning Radiometer (AATSR) and the Medium Spectral Resolution Imaging Spectrometer (MERIS), and six in situ meteorological stations. The simulated daily evapotranspiration values are compared against actual ground-truth data taken from 92 points uniformly distributed all over the study area. The derived maps and the following correlation analysis show strong agreement, demonstrating SEBS' applicability and accuracy in the estimation of daily evapotranspiration over agricultural areas.

Sustainable water resources management plans depend on reliable monitoring of Land Use – Land Cover (LULC) changes. The use of the remote sensing techniques in LULC changes detection brings consistency and reliability to the decision maker at regional scale. Three temporal data sets of images were used to obtain the land cover changes in this study: Landsat-5 Thematic Mapper (TM) acquired in 1984, and Landsat-7 Enhanced Thematic Mapper (ETM+), acquired in 2000 and 2005 consequently (Dewan and Yamaguchi, 2009). Each temporal data set consists of four Landsat scenes, which were mosaicked to cover the whole Nile Delta. Two different supervised classification algorithms were implemented to

produce classification maps in thematic form. Support Vector Machine showed higher classification accuracies in comparison to Maximum Likelihood classification. The results indicated that the rapid imbalance changes occurred among three land cover classes (urban, desert, and agricultural land). These changes powered the land degradation and land fragmentation processes over the agricultural land exclusively due to urban encroachment. Slight land cover changes were detected between fish farms, and surface water land cover classes.

Daily evapotranspiration is a major component in rational water resources management plans, consequently the accurate estimation and the forecasting of daily evapotranspiration over the Nile Delta region is the keystone for any effective management plans in the area. The estimation of daily evapotranspiration was carried out using Surface Energy Balance System (SEBS), while the monitoring and the forecasting of the daily evapotranspiration were carried out using Auto Regressive Integrated Moving Average (ARIMA) and Seasonal ARIMA. Remote sensing data were downloaded from European Space Agency (ESA) website and used to estimate daily evapotranspiration values. Data were collected from August 2005 till December 2009 on a monthly basis. The application of the most adequate ARIMA (2,1,2) to the evapotranspiration data set failed to sustain the forecasting accuracy over a long period of time. Although, time series analysis of daily evapotranspiration data set showed a seasonality behavior and thus, using seasonal ARIMA [(2,1,2) (1,1,2)6] was the finest to forecast the daily evapotranspiration over the study area and sustain the forecasting accuracy. The forecasting model projects an increase of the average daily evapotranspiration over the Nile Delta region with about 1.3 mm per day.

Monitoring the locations and distributions of rice cultivation in Kafr El Sheikh Governorate in Nile Delta region is important for establishing linkages between policy decisions, regulatory actions and subsequent irrigational water requirements. Given the importance to

the rice cultivation water requirements in water conservation plans, adequate scenarios and efficient multi-disciplinary remote sensing indices related to water availability and water consumption were obtained. In principle, Normalized Difference Vegetation Index (NDVI) was obtained from EgySat-1 satellite sensor acquired in June 2008 to drive four different water related indices calculated as NDVI derivatives. Seven factors and two constrains were implemented in Spatial Decision Support System (SDSS) to obtain final rice cultivation suitability map. Reciprocal matrix for the seven factors was established with accepted consistency ratio of 0.08. Final suitability map indicated that only half of Kafr El Sheikh Governorate is area highly suitable for rice cultivation, but in reality the whole agricultural land of the governorate is occupied by rice cultivation as symbol of mismanagement of water resources in Nile Delta region.

8.2. Greek summary

Ο πλανήτης γη, βιώνει μία εξαιρετικά αυξανόμενη ζήτηση του νερού και των τροφίμων, σε σημείο που στο εγγύς μέλλον θα οδηγηθεί σε ανεπάρκεια των υδατικών πόρων. Οι πιέσεις είναι μεγαλύτερες στα μεσογειακά και υποτροπικά κλίματα, όπου επιδεινώνονται με τα φαινόμενα της παρατεταμένης ανομβρίας και λειψυδρίας.

Στην περίπτωση της Αιγύπτου, το 90% των υδατικών της πόρων, προσφέρεται μέσω του ποταμού Νείλου. Ο μεγαλύτερος καταναλωτής του νερού στην Αίγυπτο είναι ο γεωργικός τομέας. Οι αγρότες στο δέλτα του Νείλου εξακολουθούν να καλλιεργούν τα χωράφια με τη χρήση παραδοσιακών μεθόδων με τις οποίες σπαταλούνται τεράστιες ποσότητες νερού. Κατά συνέπεια, ο προσδιορισμός της καταλληλότητας των αρδευόμενων εκτάσεων για συγκεκριμένες καλλιέργειες, με βάση συγκεκριμένα κριτήρια, δείκτες, παράγοντες και περιορισμούς και η δημιουργία ενός εργαλείου άμεσης λήψης αποφάσεων (**Decision Support System – DSS**) είναι κυρίαρχης σημασίας στην παρούσα διατριβή.

Τα Γεωγραφικά Συστήματα Πληροφοριών (**GIS**) σε συνδυασμό με μεθόδους τηλεπισκόπισης (**Remote Sensing – RS**) και χρήση καταλλήλων προγραμμάτων – μοντέλων λογισμικού για τον υπολογισμό της εξατμισοδιαπνοής και του υδατικού ισοζυγίου, όπως το Surface Energy Balance System – SEBS, θα αποτελέσουν τα εργαλεία πάνω στα οποία θα στηριχθεί η έρευνα αυτή.

Η εκτίμηση της εξατμισοδιαπνοής αποτέλεσε πάντα μια ιδιαίτερα σημαντική παράμετρο στον προσδιορισμό του Υδατικού Ισοζυγίου μιας λεκάνης απορροής και στη Διαχείριση των Υδατικών Πόρων. Η αξιόπιστη εκτίμηση της ημερήσιας εξατμισοδιαπνοής, μπορεί να υποστηρίξει ένα εργαλείο λήψης αποφάσεων έτσι ώστε να επανεξεταστούν και να επικαιροποιηθούν οι τρέχουσες πρακτικές των χρήσεων γης, σε ότι αφορά τη Διαχείριση των Υδατικών πόρων για γεωργική χρήση. Δίνεται παράλληλα η δυνατότητα να προταθούν και κατάλληλες αλλαγές στις χρήσεις γης, όπως για παράδειγμα αναδιάρθρωση καλλιεργειών, κάτι το οποίο είναι αρκετά φλέγον και επιτακτικό στα πλαίσια της λειψυδρίας και κλιματικής αλλαγής.

Παραδοσιακές τεχνικές υπολογισμού της ημερήσιας εξατμισοδιαπνοής, που βασίζονται σε μετρήσεις πεδίου, είναι αξιόπιστες μόνο σε τοπική κλίμακα. Σε ότι αφορά εκτιμήσεις με χρήση δορυφόρων και μεθόδων τηλεπισκόπησης, σε συνδυασμό με μαθηματικά μοντέλα όπως το **Surface Energy Balance System – SEBS** που χρησιμοποιήθηκε στην παρούσα διατριβή, συμβάλουν στην απόκτηση αξιόπιστων μετρήσεων και εκτιμήσεων εξατμισοδιαπνοής σε περιφερειακή κλίμακα.

Η διδακτορική διατριβή, χωρίζεται σε τέσσερις βασικούς άξονες – βήματα:

1. *Εκτίμηση της ημερήσιας πραγματικής εξατμισοδιαπνοής και σύγκριση του μοντέλου SEBS με επίγειες μετρήσεις.*

Στην παρούσα μελέτη το μοντέλο SEBS χρησιμοποιείται για την εκτίμηση της ημερήσιας εξατμισοδιαπνοής και του λόγου της πραγματικής μετρημένης ημερήσιας προς την υπολογισμένη με το μοντέλο SEBS, στην περιοχή του Δέλτα του Νείλου. Τα απαραίτητα δεδομένα για την εφαρμογή του μοντέλου αποκτήθηκαν από τους δορυφόρους **Advance Across Track Scanner Radiometer – AATSR**, **Moderate Resolution Image Spectrometer – MERIS** και έξι μετεωρολογικούς σταθμούς. Οι προσομοιωμένες τιμές της εξατμισοδιαπνοής (**μοντέλο SEBS**) συγκρίθηκαν με τα πραγματικά δεδομένα των μετρήσεων που λήφθηκαν από 92 ομοιόμορφα κατανεμημένα σημεία στο Δέλτα του Νείλου (**Ground Control Points – GCP**) με τη βοήθεια φορητών λυσιμέτρων που μας χορηγήθηκαν από την **Εθνική Υπηρεσία Τηλεπισκόπησης και Διαστημικών επιστημών της Αιγύπτου (National Authority of Remote Sensing and Space Sciences – NARSS)**. Τα αποτελέσματα που προέκυψαν από την ανάλυση συσχέτισης των μετρημένων τιμών στο ύπαιθρο με τις προσομοιωμένες από το μοντέλο SEBS, έδειξαν ότι προέκυψε συντελεστής συσχέτισης ίσος με 84,12% αποδεικνύοντας ότι το μοντέλο SEBS είναι μια πολύ αξιόπιστη λύση στην εκτίμηση της ημερήσιας πραγματικής εξατμισοδιαπνοής σε αγροτικές περιοχές (Elhag et al., 2011).

2. *Προσδιορισμός των αλλαγών στις χρήσεις γης (LULC)*

Η Αειφορική Διαχείριση των Υδατικών Πόρων εξαρτάται από την αξιόπιστη παρακολούθηση των χρήσεων και της κάλυψης γης (**Land Use Land Cover – LULC)**. Η χρήση των τεχνικών Τηλεπισκόπισης και Γεωγραφικών Συστημάτων Πληροφοριών στην ανίχνευση των LULC, οδηγεί σε λήψη αξιόπιστων αποφάσεων σε περιφερειακό επίπεδο. Χρησιμοποιήθηκαν τρεις (3) χρονοσειρές δεδομένων για τον προσδιορισμό των αλλαγών κάλυψης γης στην παρούσα μελέτη: α) το έτος 1984 με τη βοήθεια του δορυφόρου LANDSAT-5, THEMATIC MAPPER (TM), β) το έτος 2000 με τη βοήθεια του δορυφόρου

LANDSAT-7, ENCHANCED THEMATIC MAPPER και γ) το έτος 2005 επίσης με ότι χρησιμοποιήθηκε το έτος 2000.

Κάθε χρονικό σύνολο δεδομένων αποτελείται από τέσσερις χάρτες Landsat, οι οποίοι μετά από γεωαναφορά, καλύπτουν ως «μωσαϊκό» όλο το Δέλτα του Νείλου. Στη συνέχεια εφαρμόζονται δύο διαφορετικοί αλγόριθμοι για τη διερεύνηση της ακρίβειας ταξινόμησης στην κατασκευή των θεματικών χαρτών. Βρέθηκε ότι η μέθοδος Support Vector Machine – SVM έδειξε υψηλότερη ακρίβεια ταξινόμησης (84,19%, 91,38% και 93,91% για τα έτη 1984, 2000 και 2005 αντίστοιχα) σε σχέση με τη Maximum Likelihood – ML (81,64%, 88,60% και 89,89% για τα έτη 1984, 2000 και 2005 αντίστοιχα) σε ότι αφορά το συντελεστή "kappa". Τα αποτελέσματα έδειξαν ότι υπάρχουν σημαντικές αλλαγές μεταξύ των τριών κατηγοριών κάλυψης γης (αστική, έρημος και γεωργικές εκτάσεις) και μικρότερες σε ότι αφορά τα επιφανειακά υδάτινα σώματα και τις ιχθυοκαλλιεργητικές δραστηριότητες. Έτσι μεταξύ των ετών 1984 και 2005, παρατηρήθηκε αύξηση 2,61% στις εκτάσεις των υδατοκαλλιεργειών, 5,94% των αστικών περιοχών, 6,52% των αγροτικών περιοχών και μείωση 14,05% της ερήμου και 1,02% των επιφανειακών νερών. Σε ότι αφορά την ποιοτική πληροφορία, η αύξηση της αστικοποίησης έγινε σε βάρος των εύφορων γεωργικών εκτάσεων του Δέλτα του Νείλου οι οποίες με τη σειρά του επεκτάθηκαν σε βάρος εκτάσεων της ερήμου με αποτέλεσμα πολύ μεγαλύτερο κόστος νερού, ακριβή μεταφορά και μεγάλες απώλειες λόγω έντονης εξατμισοδιαπνοής.

3. *Εφαρμογή στοχαστικών μοντέλων για τον προσδιορισμό της εξατμισοδιαπνής*

Η ακρίβεια στον προσδιορισμό της ημερήσιας εξατμισοδιαπνοής είναι θεμελιώδους σημασίας για την εφαρμογή των μέτρων διαχείρισης των υδατικών πόρων στο Δέλτα του Νείλου. Επιπλέον, η ακριβής εκτίμηση και πρόβλεψη στο μέλλον, αποτελεί τον ακρογωνιαίο λίθο για τη αποτελεσματική εφαρμογή των σχεδίων διαχείρισης. Έτσι μετά την εκτίμηση της

ημερήσιας εξατμισοδιαπνοής με το μοντέλο SEBS, έγιναν και τα βήματα της χρονικής προσομοίωσης και πρόβλεψης με τη χρήση μοντέλων ARIMA και SARIMA. Συγκεκριμένα, χρησιμοποιήθηκαν μηνιαία δεδομένα τηλεπισκόπισης από την Ευρωπαϊκή Επιτροπή Διαστήματος (ESA) τα οποία αφορούσαν τη χρονική περίοδο από Αύγουστο του 2005 έως τον Αύγουστο του 2009. Αρχικά, μετά από δοκιμές πολλών δυνατών εναλλακτικών μοντέλων ARIMA, εφαρμόστηκε το βέλτιστο από ένα σύνολο δεκατεσσάρων μοντέλων (14) και ήταν ένα ARIMA (2,1,2) (R^2 = 85,1%). Το μοντέλο αυτό, απέτυχε να διατηρήσει την ακρίβεια της πρόβλεψης σε μεγάλο χρονικό διάστημα, αφού μέχρι τον Αύγουστο του 2010, η ακρίβεια πρόβλεψης ήταν στο 62%, ενώ μέχρι τον Αύγουστο του 2011, η ακρίβεια μειώθηκε στο 38%. Στη συνέχεια, εφαρμόστηκε ένα εποχιακό μοντέλο SARIMA [(2,1,2)(1,1,2)6] (R^2 = 0,2%), ως το βέλτιστο από ένα σύνολο επίσης δεκατεσσάρων (1) εποχιακών SARIMA μοντέλων. Το μοντέλο αυτό, πέτυχε να διατηρήσει την ακρίβεια της πρόβλεψης σε μεγάλο χρονικό διάστημα, αφού μέχρι τον Αύγουστο του 2010, η ακρίβεια πρόβλεψης ήταν στο 87% και 85% μέχρι τον Αύγουστο του 2011. Το μοντέλο αυτό παρέχει την καλύτερη πρόβλεψη της ημερήσιας εξατμισοδιαπνοής για την περιοχή μελέτης απ' όσα δοκιμάστηκαν και προβλέπει αύξηση κατά 1,3mm/d, η οποία σημαίνει μία επίσης αύξηση των ετήσιων υδατικών αναγκών ίση με 23,43 * 10^9 m^3 (BCM).

4. *Εφαρμογή ενός εργαλείου άμεσης λήψης αποφάσεων (Decision Support System – DSS) για την κατανάλωση νερού στο Δέλτα του Νείλου. Παράδειγμα σε καλλιέργεια ρυζιού.*

Πολύ σημαντική είναι η εφαρμογή ενός εργαλείου DSS για την κατανάλωση νερού στο Δέλτα του Νείλου και η διερεύνηση του εάν ενδείκνυται η συγκεκριμένη καλλιέργεια στη συγκεκριμένη περιοχή. Ως περιοχή μελέτης, επιλέγεται το Κυβερνείο του Kafr el Seikh. Είναι ιδιαίτερης σημασίας η παρακολούθηση των ορυζώνων, σημαντικότατης καλλιέργειας για α) την αγροτική παραγωγή στο Δέλτα του Νείλου, β) την εφαρμογή αποφάσεων

αγροτικής πολιτικής, γ) την εφαρμογή κανονιστικών διατάξεων και τέλος δ) τον προσδιορισμό των απαιτήσεων σε νερό άρδευσης. Δεδομένης της σημασίας των υδατικών αναγκών για την άρδευση των περιοχών αυτών και ταυτόχρονα των σχεδίων διαχείρισης και εξοικονόμησης νερού, αναπτύχθηκαν σενάρια διαχείρισης. Αυτά είχαν ως σκοπό, με τη χρήση κατάλληλων δεικτών τηλεπισκόπισης οι οποίοι σχετίζονται με τη διαθεσιμότητα του προσφερόμενου νερού, να αποφανθούμε για περιοχές που ενδείκνυνται ή αντενδείκνυνται για την καλλιέργεια ρυζιού. Κατ ’αρχήν υπολογίστηκε ο δείκτης Κανονικοποιημένης Βλάστησης (**Normalized Difference Vegetation Index – NDVI**) από το δορυφόρο EgySat-1 για την περίοδο Ιουνίου 2008 και με τη σειρά τους τέσσερις (4) δείκτες σχετικοί με την κατανάλωση νερού ως παράγωγοι του δείκτη NDVI: α) **Leaf Area Index (LAI)**, β) **Water Supply Vegetation Index (WSVI)**, γ) **Crop Water Shortage Index (CWSI)** και δ) **Drought Severity Index (DSI)**. **Επτά (7) παράγοντες** (όλοι οι παραπάνω και επιπλέον οι **αποστάσεις από αρδευτικές διώρυγες – CANALS**, **στραγγιστικές τάφρους – DRAINS** και η **πραγματική εξατμισοδιαπνοή – ET**) και **δύο (2) περιορισμοί** (**αποστάσεις από αρδευτικές διώρυγες – CANALS, στραγγιστικές τάφρους – DRAINS**) λήφθηκαν υπόψη για τη δημιουργία των χαρτών καταλληλότητας για την άρδευση της περιοχής για τη συγκεκριμένη καλλιέργεια. Το χωρικό σύστημα υποστήριξης απόφασης που προέκυψε (Spatial Decision Support System – SDSS) βασίστηκε στην εφαρμογή του «reciprocal» μητρώου και υποδεικνύει ότι από τη συνολική έκταση του Κυβερνείου του Kafr El Sheikh, μόνο η μισή έκταση εμφανίζει υψηλή καταλληλότητα για καλλιέργεια ρυζιού, ενώ στην πράξη ολόκληρη σχεδόν η έκτασή του χρησιμοποιείται για καλλιέργεια, οδηγώντας έτσι σε φαινόμενα μη ορθολογικής διαχείρισης του νερού για γεωργική χρήση.

Με βάση τα παραπάνω και για να έχει πραγματική εφαρμογή ένα χωρικό σύστημα λήψης αποφάσεων, πρέπει να δοθεί έμφαση στα εξής:

1. Διαχείριση της ζήτησης του νερού

2. Δημιουργία των καταλλήλων τεχνικών και αγρονομικών προϋποθέσεων
3. Θεσμοθέτηση Φορέων και Νομοθεσίας
4. Τιμολόγηση του νερού για γεωργική χρήση
5. Άμεση παρέμβαση του κράτους για στοχευμένες καλλιέργειες
6. Επιβολή συγκεκριμένων καλλιεργητικών πρακτικών
7. Χρήση καταλλήλων ποσοστώσεων για την τιμολόγηση νερού (π.χ. ογκομέτρηση)
8. Σενάρια εξοικονόμησης νερού και ειδικότερα
    a. Σενάριο 1 Χωρίς αλλαγές στις υπάρχουσες πρακτικές για τους υδατικούς πόρους.
    b. Σενάριο 2 Απαισιόδοξο σενάριο: Μη προσαρμογή στην κλιματική αλλαγή
    c. Σενάριο 3 Αισιόδοξο σενάριο: Βέλτιστη διαχείριση των υδατικών πόρων και αποτελεσματική προσαρμογή στην κλιματική αλλαγή
    d. Διάφορα μικρο – σενάρια

8.3. Arabic summary

تقدير التبخر هو دائما عنصرا رئيسيا في إدارة الموارد المائية. تقدير موثوق بها من التبخر اليومي تدعم صانعي القرار لإعادة النظر في استخدام الأراضي الممارسات الحالية في مجال إدارة المياه، في حين تمكينهم من اقتراح المناسب التغيرات في استخدام الأراضي. التقنيات التقليدية لحساب التبخر يوميا على أساس القياسات الميدانية صالحة فقط للجداول المحلية. وتستخدم أجهزة استشعار الأقمار الصناعية لمراقبة الأرض جنبا إلى جنب مع نماذج طاقة السطح (SEB) الرصيد للتغلب على الصعوبات في الحصول على قياسات التبخر اليومي على النطاق الاقليمي. في هذه الدراسة على نظام SEB (SEBS) وتستخدم لتقدير التبخر اليومية وجزء التبخر فوق دلتا النيل جنبا إلى جنب مع البيانات التي يحصل عليها في التقدم على المسار المسح الاشعاعي (AATSR) ومتوسطة الطيفي القرار التصوير الطيفي (ميريس)، وستة في محطات الرصد الموقعي. تتم مقارنة محاكاة قيم التبخر اليومي على البيانات الأرضية الحقيقة الفعلية التي أخذت من 92 نقطة وزعت بشكل موحد في جميع أنحاء منطقة الدراسة. الخرائط المشتقة وتحليل الارتباط التالية تظهر اتفاق قوي، مما يدل على تطبيق SEBS 'والدقة في تقدير التبخر يوميا على المناطق الزراعية.

خطط الإدارة المستدامة للموارد المائية تعتمد على رصد موثوق بها من استخدام الأراضي - الغطاء الأرضي (ينبغي زيادة التأكيد) التغيرات. استخدام تقنيات الاستشعار عن بعد في الكشف عن التغييرات ينبغي زيادة التأكيد يجلب الاتساق والموثوقية لصانع القرار في نطاق إقليمي. واستخدمت ثلاثة مجموعة بيانات مؤقتة من الصور للحصول على تغيرات الغطاء النباتي في هذه الدراسة: لاندسات-5 رسم الخرائط الموضوعية (TM) حصلت في عام 1984، ولاندسات-7 رسم الخرائط الموضوعية المعزز (ETM +)، حصلت في 2000 و 2005 وبناء على ذلك. كل مجموعة البيانات الزمانية وتتألف من أربعة مشاهد لاندسات، والتي كانت mosaicked لتغطية كامل دلتا النيل. تم تنفيذ اثنين من مختلف خوارزميات تصنيف تشرف على انتاج خرائط تصنيف في شكل الموضوعية. وأظهرت دعما آلة المتجهات دقة أعلى تصنيف مقارنة تصنيف الإمكان الأعظم. أشارت النتائج إلى أن التغييرات السريعة الخلل وقعت بين ثلاث فئات الغطاء الأرضي (في المناطق الحضرية، الصحراوية، والأراضي الزراعية). هذه التغييرات مدعوم من تدهور الأراضي وعمليات تجزئة الأراضي على الأراضي الزراعية بسبب الزحف العمراني على وجه الحصر ل. تم الكشف عن طفيف تغيرات الغطاء النباتي بين المزارع السمكية، والطبقات السطحية غطاء المياه والأرض.

التبخر اليومي يشكل عنصرا رئيسيا في خطط إدارة موارد المياه عقلانية، وبالتالي تقدير دقيق والتنبؤ التبخر يوميا على منطقة دلتا النيل هو حجر الزاوية في أي خطط للإدارة الفعالة في المنطقة. وأجري تقدير التبخر يوميا خارج باستخدام نظام السطح ميزان الطاقة (SEBS)، في حين نفذت عملية الرصد والتنبؤ والتبخر يوميا خارج باستخدام سيارات تراجعية المتكاملة المتوسط المتحرك (اريما)، وأريما الموسمية. تم تحميل بيانات الاستشعار عن بعد من الفضاء الأوروبي الموقع (ESA) وكالة والمستخدمة لتقدير قيم التبخر يوميا. وقد تم جمع البيانات من أغسطس 2005 حتى ديسمبر 2009 على أساس شهري. تعيين فشل تطبيق ARIMA معظم الكافي (2،1،2) لبيانات التبخر للحفاظ على دقة التنبؤ على مدى فترة طويلة من الزمن. على الرغم من أن أظهر تحليل السلاسل الزمنية لمجموعة البيانات اليومية التبخر سلوك الموسمية، وبالتالي، وذلك باستخدام ARIMA الموسمية [(2،1،2) (1،1،2) 6] وكان أفضل للتنبؤ التبخر يوميا فوق منطقة الدراسة و الحفاظ على دقة التنبؤ. نموذج التنبؤ تتوقع زيادة التبخر اليومي متوسط فوق منطقة دلتا النيل مع ما يقرب من 1.3 ملم في اليوم الواحد.

رصد مواقع وتوزيعات من زراعة الأرز في بمحافظة كفر الشيخ في منطقة دلتا النيل من المهم لإقامة الروابط بين القرارات المتعلقة بالسياسات، والإجراءات التنظيمية والاحتياجات من المياه المستعملة في الري الزراعي لاحق. نظرا لأهمية لمتطلبات زراعة الأرز المياه في خطط المحافظة على المياه، والسيناريوهات كافية ومتعددة التخصصات عن بعد

مؤشرات كفاءة الاستشعار عن بعد المتعلقة توافر المياه واستهلاك المياه التي تم الحصول عليها. من حيث المبدأ، تم الحصول على الرقم القياسي النباتي الفرق (NDVI) من أجهزة الاستشعار EgySat-1 الأقمار الصناعية حصلت في حزيران 2008 لطرد أربعة مؤشرات المياه المختلفة ذات الصلة محسوبة على المشتقات NDVI. ونفذت سبع العوامل والقيود المكانية اثنين في نظام دعم القرار (التي يجريها التكتل أو) للحصول على نهائي ملاءمة زراعة الأرز خريطة. تأسست مصفوفة متبادل للعوامل سبعة مع نسبة مقبولة من الاتساق 0.08. وأشارت الخريطة النهائية ملاءمة ذلك سوى نصف بمحافظة كفر الشيخ هي منطقة مناسبة جدا لزراعة الأرز، ولكن في الواقع تحتل كل الأرض الزراعية في المحافظة من زراعة الأرز كرمز من سوء إدارة موارد المياه في منطقة دلتا النيل

10. References

Abd El-Kawy, O. R., Rod, J. K., Ismail, H. A., Suliman, A. S. (2011). Land Use and Land Cover Change Detection In The Western Nile Delta Of Egypt Using Remote Sensing Data. Applied Geography, 31: 483-494.

Abdel Elmontalbe, A. (2006). Precision Farming In The Small Farmland In The Eastern Nile Delta Egypt Using Remote Sensing And GIS. Inaugural-Dissertation Zur Erlangung Der Doktorwürde Der Fakultät Für Forst- Und Umweltwissenschaften Der Albert-Ludwigs Universität Freiburg Im Breisgau, Pp: 89 – 125.

Abebe, A., Forech, G. (2008). Stochastic Simulation of The Severity Of Hydrological Drought. Water And Environment Journal, 22(1): 2-10.

Aboul Enien, R., Abdel Shafi, A., Abdel Monem, M., Kamel, A., Solh, M., Bedier, M., Khalifa. H., (2000). A New Research Paradigm For Sustainability Research In Egypt. Experimental Agriculture, 36(2): 265-271.

Abu Zeid, M. (1991). Water Resources Assessment for Egypt. Ministry Of Water Resources And Irrigation. Egypt.

Abu Zeid, M. (1998). Water And Sustainable Development: The Vision for World Water, Life and Environment. Water Policy. 1:9-19

Ackerman, A. S., Toon, O. B., Stevens, D. E., Heymsfield, A. J., Ramanathan, V., Welton, E. J. (2000). Reduction of Tropical Cloudiness By Soot. Science, 288: 1042-1047.

Adamo, S. B., Crews-Meyer, K. A. (2006). Aridity and Desertification: Exploring Environmental Hazards in Jáchal, Argentina. Applied Geography, 26(1): 61-85.

Afify, A. A., Arafat, S. M., Aboel Ghar, M. N. (2011). Delineating Rice Belt Cultivation In The Nile Pro-Delta Of Vertisols Using Remote Sensing Data Of Egypt Sat-1. Journal Of Agricultural Research, 35 (6): 2263–2279

Ahmad, M. (2002). Water Pricing and Markets In Near East: Policy Issues And Options. Water Policy. 2: 229-242.

Ahmed, M., El Leithy, B., Thompson J., Flower R., Ramdani, M., Ayache, F., Hassan, S. (2009). Applications of Remote Sensing to Site Characterization and Environmental Change Analysis of North African Coastal Lagoons. Hydrobiologia, 622: 147–171.

Allam, M. N., Allam, G. I. (2007). Water Resources In Egypt: Future Challenges and Opportunities. Water International, 32(2): 20 5- 218.

Allen, R. G., Pereira, L. S., Raes, D., Smith, M. (1998). Crop Evapotranspiration. Guidelines for Computing Crop Water Requirements. FAO Irrigation and Drainage Paper 56, Food and Agriculture Organization Of The United Nations, Rome.

Allen, R. G., Tasumi, M., Morse, A. (2005). Satellite-Based Evapotranspiration by METRIC and Landsat For Western States Water Management. US Bureau of Reclamation Evapotranspiration Workshop, Feb 8–10, 2005, Ft. Collins.

Allen, R. G., Tasumi, M., Trezza, R. (2002). METRIC TM: Mapping Evapotranspiration at High Resolution—Application Manual for Landsat Satellite Imagery. University of Idaho, Kimberly.

Allen, R., Tasumi, M., Trezza, R., (2007). Satellite-Based Energy Balance for Mapping Evapotranspiration with Internalized Calibration (METRIC): Model ASCE. Journal of Irrigation and Drainage Engineering, 133(4): 380-394.

Asrar, G., Myneni, R. B., And Choudhury, B. J. (1992). Spatial Heterogeneity in Vegetation Canopies and Remote Sensing of Absorbed Photosynthetically Active Radiation: A Modeling Study. Remote Sensing of Environment, 41: 85–103.

Ball, J. R. (1952). Geology and Mineral Resources of The Carlinville Quadrangle: Illinois State Geologcal Survey Bulletin 77, 110 P.

Barnes, E. M., Clarke, T. R., Richards, S. E., Colaizzi, P. D., Haberland, J., Kostrzewski, M., Waller, P., Choi, C., Riley, E., Thompson, T., Lascano, R. J., Li, H., Moran, M. S. (2001). Coincident Detection of Crop Water Stress, Nitrogen Status and Canopy Density Using Ground-Based Multispectral Data. CD ROM, Unpaginated. In 5th International Conference on Precision Agriculture Abstracts and Proceedings, Bloomington, Minnesota, July 16-19, 2000.

Barnes, E. M., Moran, M. S., Pinter, P. J., Clarke, T. R. (1996). Multispectral Remote Sensing and Site-Specific Agriculture: Examples of Current Technology and Future Possibilities. Published In "Proceedings Of The 3rd International Conference on Precision Agriculture". June 23-26, 1996, Minneapolis, Minnesota. ASA, 677 S. Segoe Rd., Madison, WI 53771, USA. Pp. 843-854.

Bartholic, J. F., Namken, L. N., Wiegand, C. L. (1972). Aerial Thermal Scanner to Determine Temperatures of Soils and of Crop Canopies Differing in Water Stress. Agronomy Journal, 64: 603–608.

Bastiaanssen, W. G. M., Menenti, M., Feddes, R. A., Holtslang, A. A. (1998). A Remote Sensing Surface Energy Balance Algorithm for Land (SEBAL): 1. Formulation. Journal of Hydrology, 212–213:198–212

Batisani, N., Yarnal, B. (2009). Urban Expansion in Centre County, Pennsylvania: Spatial Dynamics and Landscape Transformations. Applied Geography, 29(2): 235-249.

Bau, J. (1994). Research on Water Conservation in Portugal. . Chapter 6. in “Efficient Water Use”. (H. Gaduno and F. Arreguin-Cortes, Eds.). Programa Hidrologico International De La UNESCO Para America Latina Y El Caribe, Montevideo. Uruguay

Bazza, M., Ahmad, M. (2003). A Comparative Assessment of Links between Irrigation Water Pricing and Irrigation Performance in the Near East. Food and Agriculture Organization of The United Nations, Pp. 254-298.

Beljaars, A. C. M., Holtslag, A. A. M. (1991). Flux Parameterization Over Land Surfaces For Atmospheric Models, J. Appl. Meteorol., 30, 327–341.

Berry, J. K. (1998). Site-Specific Farming Comes Of Age: Managing Field Variability. California Farm Tech Conference – Santa Barbara, California, USA.

Berry, J. K., Delgado, J. A., Khosla, R., Pierce, F. J. (2005). Applying Spatial Analysis for Precision Conservation across the Landscape. Journal of Soil and Water Conservation, 60(6): 22-29.

Berry, K. J. (1999). The Precision Farming Primer. Berry and Associates // Spatial Information Systems, Inc. (BASIS).

Berry, K. J. (2005): Map Analysis (Procedures and Applications in GIS Modelling). Berry and Associates // Spatial Information Systems, Inc.

Boegh, E., Soegaard, H., Thomsen, A., (2002). Evaluating Evapotranspiration Rates and Surface Conditions Using Landsat TM to Estimate Atmospheric Resistance and Surface Resistance. Remote Sensing of Environment, 79: 329–343.

Bosveld, F. C. (1999). Exchange Processes between a Coniferous Forest and The Atmosphere. Ph.D. Dissertation, Wageningen University, 181pp.

Bouman. B. A., Tuong,. T. P. (2001). Field Water Management to Save Water and Increase Its Productivity in Irrigated Lowland Rice. Agricultural Water Management, (49): 11-30.

Box, G. E. P., Jenkins, G. M. (1976). Time Series Analysis: Forecasting and Control, Holden-Day, San Fransisco.

Box, G. E. P., Jenkins, G. M., Reinsel, G. C. (1994). Time Series Analysis, Forecasting and Control, Prentice-Hall, Englewood Cliffs.

Box, G. E. P., Jenkis, G. M., Reinsel, G. C. (2008). Time Series Analysis, Forecasting and Control. 4th Edn., John Wiley And Sons, Inc., New Jersey, ISBN-10: 0470272848, Pp: 484.

Bregt, K. A. (1997): GIS Support for Precision Agriculture: Problems and Possibilities. Symposium on Precision Agriculture: Spatial and Temporal Variability of Environmental Quality, Held in Collaboration with The European Environmental Research Organization, Wageningen, The Netherlands On 21–23 January.

Brest, C. L., Goward, S. N. (1987). Driving Surface Albedo Measurements from Narrow Band Satellite Data. International Journal of Remote Sensing, 8: 351–367.

Brockwell, P. J., Davis, R. A. (2001). Introduction to Time Series and Forecasting. Springer – Verlag, New York.

Bronson, K. F., Booker, J. D., Keeling, T. W., Boman, R. K., Wheeler, T. A., Lascano, R. J., Nichols, R. L. (2005). Cotton Canopy Reflectance at Landscape Scale As Affected by Nitrogen Fertilization. Agronomic Journal, 97: 654-660.

Brown, K. W. (1974). Calculations of Evapotranspiration from Crop Surface Temperature. Department Of Soil and Crop Science, College Station

Brown, K. W., Rosenberg, N. J. (1973). A Resistance Model to Predict Evapotranspiration and Its Application to A Sugar Beet field. Agronomy Journal, 68: 635–641.

Brunsell, N. A., Gillies, R. (2002). Incorporating Surface Emissivity into a Thermal Atmospheric Correction. Photogrammetric Engineering of Remote Sensing Journal, 68(12): 1263–1269.

Brutsaert W. Sugita M (1992) Application of Self-Preservation in the Diurnal Evolution of the Surface Energy Budget to Determine Daily Evaporation. Journal of Geophysics Research, 97: 18377–18382

Brutsaert, W. (1975). On A Derivable Formula for Long-Wave Radiation from Clear Skies. Water Resources Research Journal, 11: 742–744.

Brutsaert, W. (1982). Evaporation into The Atmosphere. D. Reidel, 299pp.

Brutsaert, W. (1999). Aspect of Bulk Atmospheric Boundary Layer Similarity under Free-Convective Conditions. Reviews of Geophysics Journal, 37: 439–451.

Buick, R. D. (1997). Precision Agriculture: An Integration of Information Technologies with Farming. 50th Conference Proceeding of The New Zealand Plant Protection Society Incorporated.

Byrne, G., Crapper, P., Mayo, K. (1980). Monitoring Land Cover Change by Principal Component Analysis of Multi-Temporal Landsat Data, Remote Sensing of Environment, 10: 175- 184.

Carruthers, J., Rosegrant, M. W., Seckler. D. (1997). Irrigation and Food Security. Irrigation and Drainage Systems, 11: 83-101.

Casady, W. W., Palm, H. L. (2002): Precision Agriculture: Remote Sensing and Ground Truthing. Published by Mu Extension, University of Missouri-Columbia EQ453 (Www. Muextension.Missouri.Edu/Xplor/).

Chavez, J. L., Neale, C. M. U. (2003). Validating Airborne Multispectral Remotely Sensed Heat fluxes with Ground Energy Balance Tower and Heat flux Source Area (Footprint) Functions. ASAE Paper No. 033128. St. Joseph, Michigan

Chavez, J. L., Neale, C. M. U., Hipps, L. E., Prueger, J. H., Kustas, W. P. (2005). Comparing Aircraft-Based Remotely Sensed Energy Balance fluxes with Eddy Covariance Tower Data Using Heat flux Source Area Functions. Journal of Hydrometeorology, AMS 6(6): 923–940.

Chavez, P. S., Sides, S.C., Anderson, J. A. (1991). Comparison of Three Different Methods to Merge Multi-Resolution and Multi- Spectral Data: Landsat TM and SPOT Panchromatic, Photogram- Metric Engineering of Remote Sensing, 57(3): 295-303.

Chehbouni, A., Lo-Seen, D., Njoku, E. G., Monteny, B. (1996). Examination of the Difference between Radiative and Aerodynamic Surface Temperatures over Sparsely Vegetated Surfaces. Remote Sensing of Environment, 58: 177–186.

Chehbouni, A., Nouvellon, Y., Lhomme, J. P., Watts, C., Boulet, G., Kerr, Y. H., Moran, M. S., Goodrich, D. C. (2001). Estimation of Surface Sensible Heat flux Using Dual Angle Observations of Radiative Surface Temperature. Journal of Agriculture Forest Meteorology, 108: 55–65.

Chen, C. F., Chang, Y. H., Chang, Y. W. (2009). Seasonal ARIMA Forecasting of Inbound Air Travel Arrivals to Taiwan. Transportmetrica, 5: 125-140. DOI: 10. 1080/ 18128600802591210.

Chen, X., Vierling, L., Deering, D. (2005). A Simple And Effective Radiometric Correction Method to Improve Landscape Change Detection Across Sensors and Across Time. Remote Sensing of Environment, 98(1): 63-79.

Choudhury, B. J., Monteith, J. L. (1988). A Four Layer Model for the Heat Budget of Homogeneous Land Surfaces. Quarterly Journal of the Royal Meteorological Society, 114: 373–398.

Choudhury, F. J., Idso, S. B., Reginato, R. J. (1987). Analysis of an Empirical Model for Soil Heat Flux under a Growing Wheat Crop for Estimating Evaporation by an Infrared-

Temperature Based Energy Balance Equation. Journal of Agriculture Forest Meteorology, 39: 283–297.

Choudhury, J., Karumuri, S. R., Sarkar, N. K., Bhattacharjee, R. (2008). Algebraic Approach to Analyze the Vibrational Spectra of Tetrahedral Molecules. Indian Journal of Physics, 82: 561 - 573.

Chowdary, V. M., Srivastava, Y. K., Chandran, V., Jeyaram, A. (2009). Integrated Water Resource Development Plan for Sustainable Management of Mayurakshi Watershed, India Using Remote Sensing and GIS. Water Resource Management, 23: 1581 – 1602.

Cohen, J. (1960). A Coefficient of Agreement for Nominal Scales. Educational and Psychological Measurement 20: 37-46.

Conca, K., Fengshi, W., Ciqi, M. (2006). Global Regime Formation or Complex Institution Building? The Principled Content of International River Agreements. International Studies Quarterly, 50 (2): 263–285.

Congalton , R., Mead, R. (1983). A Quantitative Method to Test for Consistency and Correctness in Photointerpretation. Photogrammetric Engineering and Remote Sensing, 49(1) :69-74.

Congalton, R. (1991). A Review of Assessing the Accuracy of Classification of Remote Sensed Data. Remote Sensing of Environment, 37: 35-46.

Coppin, P., Jonckheere, I., Nackaerts, K., Muys, B., Lambin, E. (2004). Digital Change Detection Methods in Ecosystem Monitoring: A Review. International Journal of Remote Sensing, 25(9): 1565-1596.

Corwin, D. L. (2005): Delineating Site-Specific Crop Management Units: Precision Agriculture Application in GIS. ESRI International User Conference Proceedings.

Crago, R. D. (2000.) Conservation and Variability of the Evaporative Fraction during the Daytime. Journal of Hydrology, 180(1–4): 173–194.

Crago, R., Friedl, M., Kustas, W., Wang, Y. (2004). Investigation of Aerodynamic and Radiometric Land Surface Temperatures. NASA Scientific and Technical Aerospace Reports (STAR) 42(1).

Dalsted, K., Clay, D. E., Clay, S.A., Reese, C., Chang, J. (2003). Selecting the Appropriate Remote Sensing Product for Precision Farming. Site-Specific Management Guideline # 40. Potash and Phosphate Institute. Online At: Www.Ppi-Far.Org/SSMG.

Delwart, S., Preusker, R., Bourg, L., Santer, R., Ramon, D., Fischer, J., (2007). MERIS In-Flight Spectral Calibration. International Journal of Remote Sensing, MERIS Special Issue, (28): 3- 4.

Dewan, A. M., Yamaguchi, Y. (2009). Using Remote Sensing and GIS to Detect and Monitor Land Use and Land Cover Change in Dhaka Metropolitan of Bangladesh during 1960–2005. Environmental Monitoring and Assessment, 150: 237 – 249.

Dewidar, M. (2002). Landfill Detection in Hurghada, North Red Sea, Egypt, Using Thematic Mapper Images. International Journal of Remote Sensing, 23: 939–948.

Dewidar, M. (2004). Detection of Land Use/ Land Cover Changes for the Northern Part Of The Nile Delta (Burullus Region), Egypt. International Journal of Remote Sensing, 25: 4079–4089.

Diaz, R. A., Matthias, A. D., Hanks, R. J. (1983). Evapotranspiration and Yield Estimation of Spring Wheat from Canopy Temperature. Agronomy Journal, 75: 805 – 810.

Diker, K., Unlu, M. (1999). Remote Sensing for Precision Agriculture. Journal of Agriculture, 14(1): 7-14.

Dragan, M., Feoli, E., Fernetti, M., Zerihun, W. (2003). Application of Spatial Decision Support System (SDSS) to Reduce Soil Erosion in Northern Ethiopia. Environmental Modeling and Software, 18(10): 861 – 686.

DWIP, (1997). Final Report on Drainage Water Irrigation Project. The Drainage Research Institute, Louis Berger International, Inc., Pacer Consultants with the Technical Participation of the United States Department of Agriculture, Egypt.

EAAE, (2000). Pattern of Changes in the Economic Value of Irrigation Water during the Era of Agricultural Policies Reform 1986-1996. Egyptian Association of Agricultural Economics Report, 37-38.

Eastman, J. R. (2003). 'IDRISI Kilimanjaro: Guide to GIS and Image Processing' Clark Laboratories, Clark University, Worcester, USA.

Edward, P. G., Alfredo R. H., Pamela L. N., Stephen G. N. (2008). Relationship between Remotely-Sensed Vegetation Indices, Canopy Attributes and Plant Physiological Processes: What Vegetation Indices Can and Cannot Tell Us About The Landscape. Sensors, 8: 2136-2160.

El Banna, M., Frihy, O. (2009). Human-Induced Changes in the Geomorphology of the Northeastern Coast of the Nile Delta, Egypt. Geomorphology, 107: 72–78.

El Filaly, M., Samy H., Enas, M., Saleh, A. (2004). Egypt's Experience with Regard to Water Demand Management in Agriculture. In: Eights International Water Technology Conference, 2004, Alexandria

Elhag, M. (2010). Land Suitability for Afforestation and Nature Conservation Practices Using Remote Sensing and GIS Techniques. CATRINA, 6 (1): 11-17.

Elhag, M., Psilovikos, A. Manakos, I., Perakis, K. (2011). Application of SEBS Model in Estimating Daily Evapotranspiration and Evaporative Fraction from Remote Sensing Data over Nile Delta. Water Resources Management, 25(11): 2731-2742.

ENVI, (2009). ENVI Version 4.7 User Tutorials August Edition. ITT Visual Information Solutions, 20REF47DOC.

ESRI, (2008). Arcmap. Version 9.3 User Manual. Redlands, CA, USA, 135-137

Faivre, R., Leenhardt, D., Voltz, M., Benoît, M., Papy, F., Dedieu, G. And Wallach, D. (2004): Spatialising Crop Models. Agronomy, 24: 205-217.

FAO, (1976). Framework for Land Evaluation. Soils Bulletin No 32. Rome.

FAO, (1978). "Report on the Agroecological Zone Project." Methodology and Results for Africa, World Soil Resource Report, FAO, 1(48).

FAO, (1983). Guidelines: Land Evaluation for Rainfed Agriculture. Soils Bulletin No. 52 Rome.

FAO, (1984). Guidelines: Land Evaluation for Forestry. Soils Bulletin No 48. Rome.

FAO, (1985). Guidelines: Land Evaluation for Irrigated Agriculture. Soils Bulletin No 42. Rome.

FAO, (1995). Irrigation and Drainage Paper 56, Food and Agriculture Organization of the United Nations, Rome.

FAO, (1998). World Reference Base for Soil Resources. Rep.84. Rome.

FAO, (2003). The Strategy of Agriculture Development in Egypt until the Year 2017, 68-72.

FAO, (2005). Environment and Natural Resources Service Series, No. 8, Rome, Italy.

Fernandez-Jauregui, C. (1994). Why A Multidimensional Approach. Chapter 1. In "Efficient Water Use" (H. Gaduno and F. Arreguin-Cortes, Eds.). Programa Hidrologico International De La UNESCO Para America Latina Y El Caribe, Montevideo. Uruguay

Frey, C., Parlow, E., Vogt, R., Harhash, M., Abel Wahab., M. (2010). Flux Measurements in Cairo. Part 1: In Situ Measurements and Their Applicability for Comparison with Satellite Data. International Journal of Climatology, Online Early View.

Frey, C., Rigo, G., Parlow, E., (2007). Urban Radiation Balance of Two Coastal Cities in a Hot and Dry Environment. International Journal of Remote Sensing, 28 (12): 2695 – 2712.

Frihy, O., Dewidar, M., Nasr, S., El Raey, M. (1998). Change Detection of the Northeastern Nile Delta of Egypt: Shoreline Changes, Spit Evolution, Margin Changes of Manzala Lagoon and Its Islands. International Journal of Remote Sensing, 19: 1901–1912.

Gage, S. H., Helly, J., Colunga, M. (2000): A Framework to Integrate Analytical and Visual Applications to Regional Models: Development of an Application for Simulation of Daily Crop Productivity in the Corn Belt. 4th International Conference on Integrating

GIS and Environmental Modelling (GIS/EM4): Problems, Prospects and Research Needs. Banff, Alberta, Canada, September 2– 8.

Gang, L., Jishuang, K., Maohua, W. (1999): Research on Soil Sampling Strategy for Precision Agriculture. Proceedings of 99 International Conferences on Agricultural Engineering Beijing, China.

Gao, J., Liu, Y. (2010). Determination of Land Degradation Causes in Tongyu County, Northeast China via Land Cover Change Detection. International Journal of Applied Earth Observation And Geoinformation, 12: 9–16.

Geymen, A., Baz, I. (2008). The Potential of Remote Sensing for Monitoring Land Cover Changes and Effects on Physical Geography in the Area of Kayisdagi Mountain and Its Surroundings (Istanbul). Environmental Monitoring and Assessment, 140: 33 - 42.

Gillies, R. R., Carlson, T. N., Cui, J., Kustas, W. P., Humes, K. S. (1997). A Verification of the 'Triangle' Method for Obtaining Surface Soil Water Content and Energy Fluxes from the Remote Measurements of the Normalized Difference Vegetation Index (NDVI) and Surface Radiant Temperature. International Journal of Remote Sensing, 18: 3145-3166.

Gleick, P. H. (2001). "Global Water: Threats and Challenges Facing the United States. Issues for the New U.S. Administration." Environment, 43(2): 18-26.

Go´Mez, M., Olioso, A., Sobrino, J. A., Jacob, F. (2005). Retrieval of Evapotranspiration over the Alpille/Reseda Experimental Site Using Airborne POLDER Sensor and a Thermal Camera. Remote Sensing of Environment, 96: 399–408.

Gouveia, N., Fletcher, T. (2000). Time Series Analysis for Air Pollution and Mortality: Effects by Cause, Age and Socioeconomic Status. Journal of Epidemiology and Community Health, 54: 750 – 755.

Gower, S., Kucharik, C., Norman, J., (1999). Direct and Indirect Estimation of Leaf Area Index, fAPAR and Net Primary Production of Terrestrial Ecosystems. Remote Sensing of Environment, 70: 29 –51.

Hamdy, A., Ragab, R., Scarascia-Mugnozza, E. (2003). Coping With Water Scarcity: Water Saving and Increasing Water Productivity. Irrigation and Drainage. 52: 3-20.

Hanna, F. (2000). Pedological studies development in Egypt during the last 50 years (1950-2000). Egyptian Soil Science Society (ESSS) – Golden Jubilee Congress 1950- 2000 , Oct. 23-25 -2000 Cairo.

Hanson, R., (1991). Evapotranspiration and Droughts. In: Paulson RW, Chase EB, Roberts RS, Moody DW, Compilers, National Water Summary 1988-89-Hydrologic Events and Floods and Droughts: U.S. Geological Survey Water-Supply Paper 2375, 99–104.

Hatfield, J. L., Perrier, A., Jackson, R. D. (1983). Estimation of Evapotranspiration at on Time-of-Day Using Remotely Sensed Surface Temperatures. Agriculture Water Management, 7: 341–350

Hayes, M., Svoboda, M., Wilhite, D., Vanyarkho, O., (1999). Monitoring the Drought Using the Standardized Precipitation Index. Bulletin of the American Meteorological Society, 80 (3): 429–438.

Heilman, J. L., Kanemasu, E. T., Rosenberg, N. J., Blad, B. L. (1976). Thermal Scanner Measurements of Canopy Temperatures to Estimate Evapotranspiration. Remote Sensing of Environment, 5: 137–145.

Helman, K. (2011). SARIMA Models for Temperature and Precipitation Time Series in the Czech Republic for The Period 1961 – 2008. Journal of Applied Mathematics, 4: 281-290.

Hereher, M. (2010). Sand Movement Patterns in the Western Desert of Egypt: An Environmental Concern. Environmental Earth Science, 59: 1119–1127.

Hillel, D. (2000). Salinity Management for Sustainable Irrigation. Integrating Science, Environment and Economics. The World Bank: Environmentally and Socially Sustainable Development, Rural Development. Washington DC., USA

Hipps, L. E. (1989). The Infrared Emissivities of Soil and Artemisia Tridentate and Subsequent Temperature Corrections in a Shrubsteppe Ecosystem. Remote Sensing of Environment, 27: 337–342.

Holmen, H. (1991). Building Organizations for Rural Development. State and Cooperatives in Egypt. Lund University Press. Sweden

Hsu, C. W., Chang, C. C., Lin, C. J. (2007). A Practical Guide to Support Vector Classification. National Taiwan University.

Huang, W., Liu, H., Luan, Q., Jiang, Q., Liu, J., Liu, H. (2008). Detection And Prediction of Land Use Change in Beijing Based on Remote Sensing and GIS. The International Archives of The Photogrammetry, Remote Sensing and Spatial Information Sciences. Vol. XXXVII. Part B6b, Beijing.

Huete, A. (1988). A Soil Adjusted Vegetation Index (SAVI). Remote Sensing of Environment, 25: 295–309.

Huete, A., Didan, K., Van Leeuwen, W., Miura, T.; Glenn, E. (2008). MODIS Vegetation Indices. In Land Remote Sensing and Global Environmental Change: NASA's Earth Observing System and the Science of ASTER And MODIS 2008, 125 - 146.

Huot, P., Tait, H., Rast, M., Delwart, S., Bézy, L., Levrini, G., (2001). The Optical Imaging Instruments and Their Applications: AATSR and MERIS. European Space Agency Bulletin, 106: 55 – 66.

Idso, S. B., Schmugge, T. J., Jackson, R. D., Raginato, R. J. (1975). The Utility of Surface Temperature Measurements for the Remote Sensing of the Soil Water Status. Journal of Geophysics Research, 80: 3044–3049.

IPCC. (2001a). Climate Change 2001: The Scientific Basis, Contribution of Working Group I to the IPCC Third Assessment Report 2001 .Cambridge, UK, Cambridge University Press, 2001.

Jackson, R. D. (1984). Remote Sensing of Vegetation Characteristics for Farm Management. SPIE 475: 81–96.

Jackson, R. D., Idso, S. B., Reginato, R. J., Pinter, P. J. (1981). Canopy Temperature as a Crop Water Stress Indicator. Water Resources Research 17: 1133-1138.

Jackson, R. D., Moran, M. S., Gay, L. W., Raymond, L. H. (1987). Evaluating Evaporation from field Crops Using Airborne Radiometry and Ground-Based Meteorological Data. Irrigation Science, 8: 81–90.

Jackson, R. D., Pinter, P. J, Reginato, R. J. (1985). Net Radiation Calculated from Remote and Multispectral and Ground Station Meteorological Data. Agriculture Forest Meteorology, 35: 153–164,

Jackson, R. D., Reginato, R. J., Idso, S. B. (1977). Wheat Canopy Temperature: A Practical Tool for Evaluating Water Requirements. Water Resources Research, 13: 651–656.

Jacob, F., Olioso, A., Gu, X., Su, Z., Seguin, B., (2002). Mapping Surface fluxes Using Airborne Visible, Near Infrared, Thermal Infrared Remote Sensing Data and a Spatialized Surface Energy Balance Model. Agronomy, 22: 669–680.

Jennifer, L. F., Varco, J. J. (2004): Dependency of Cotton Leaf Nitrogen, Chlorophyll, and Reflectance on Nitrogen And Potassium Availability. Agronomy, 96: 63-69.

Jensen, J., (1996). Introductory Digital Image Processing: A Remote Sensing Perspective, Second Edition, Prentice Hall, Upper Saddle River, N.J., 305 P.

Jensen, J., Rutchey, K., Koch, M., Narumalani, S. (1995). Inland Wetland Change Detection in the Everglades Water Conservation Area 2A Using a Time Series of Normalized Remotely Sensed Data. Photogrammetric Engineering and Remote Sensing. 51: 199–209.

Jin, X., Wan, L., Su, Z., (2005). Research on Evaporation of Taiyuan Basin Area by Using Remote Sensing. Hydrology and Earth System Sciences Discussion, 2: 209 – 227.

Johansson, R., Tsur, Y., Roe, T.L., Doukkali, R., Dinar, A. (2002). Pricing Irrigation Water: a Review of Theory and Practice. Water Policy. 4: 173–199.

Jürgens, C. (2000). Overview of Remote Sensing Systems Related to Precision Farming. 2nd International Symposium on New Technologies for Environmental Monitoring and Agro-Applications, 18-20 October 2000, Tekirdag, Turkey.

Kalma, J., Jupp, D., (1990). Estimating Evaporation from Pasture Using Infrared Thermometry: Evaluation of a One-Layer Resistance Model. Agricultural and Forest Meteorology, 51: 223–246.

Kanemasu, E. T., Stone, L. R., Powers, W. L. (1977). Evapotranspiration Model Tested for Soybeans and Sorghum. Agronomy, 68: 569–572.

Katul, G. G., Parlange, M.B. (1992). A Penman-Brutsaert Model for Wet Surface Evaporation. Water Resources Research, 28: 121–126.

Keller, J. (1992). Implications of Improving Agricultural Water Use Efficiency on Egypt's Water and Salinity Balances. Paper for The Roundtable on Egyptian Water Policy 1992. Alexandria, Egypt.

Kerr, J., Ostrovsky, M. (2003). From Space to Species: Ecological Applications for Remote Sensing. Trends in Ecology and Evolution, 18: 299-305.

Kijne, J. W. (2001). Lessons Learned from the Change from Supply to Demand Water Management in Irrigated Agriculture: A Case Study from Pakistan. Water Policy. 3: 109-123.

King, M. D., Kaufman, Y. J., Menzel, W. P., Tanré, D. (1992). Remote Sensing of Cloud, Aerosol, and Water Vapor Properties from the Moderate Resolution Imaging Spectrometer (MODIS). IEEE Transactions on Geoscience and Remote Sensing, 30, 1-27.

Kloer, B. (1994). Hybrid Parametric/Non-Parametric Image Classification. Technical Papers, ACSM-ASPRS Annual Convention, 307-316.

Kocak, K., Saylan, L., Sen, O. (2000). Nonlinear Time Series Prediction of O^3 Concentration in Istanbul. Atmospheric Environment, 34: 1267 – 1271.

Kumar, V. (1998). An Early Warning System for Agricultural Drought in an Arid Region Using Limited Data. Journal of Arid Environments, 40(2): 109 – 209.

Kumar, V. And Panu, U. (1997). Predictive Assessment of Severity of Agricultural Droughts Based on Agro-Climatic Factors. Journal of American Water Resources Association, 33(6): 1255 – 1264.

Kustas, W. P., Daughtry, C. S. T. (1990). Estimation of the Soil Heat flux/Net Radiation Ratio from Multispectral Data. Agriculture Forest Meteorology, 49: 205–223.

Kustas, W., Norman, J., (1996). Use of Remote Sensing for Evapotranspiration Monitoring over Land Surfaces. Hydrological Sciences Journal, 41 (4): 495–516.

Kyriakidis, P. C., Journal, A. G. (2001). Stochastic Modeling of Atmospheric Pollution: A Special Time Series Framework. Part II: Application to Monitoring Monthly Sulfate Deposition over Europe. Atmospheric Environment, 35: 2339 – 2348.

Lagouarde, J., Jacob, F., Gu, X., Olioso, A., Bonnefond, J., Kerr, Y., Mcaneney, K., Irvine, M., (2002). Spatialization of Sensible Heat flux over a Heterogeneous Landscape. Agronomy, 22: 627–633.

Landeras, G., Ortiz-Barredo, A., López, J. (2010). Discussion of "Forecasting Weekly Evapotranspiration with ARIMA and Artificial Neural Network Models". Journal of Irrigation and Drainage Engineering, 136(6): 435 – 439.

Li, F., Kustas, W., Preuger, J., Neale, C., Jackson, T. (2005). Utility of Remote Sensing-Based Two-Source Balance Model under Low- and High-Vegetation Cover Conditions. Journal of Hydrometeorology, 6: 878-891.

Li, Z., Tang, R., Wan, Z., Bi, Y., Zhou, C., Tang, B., Yan, G., Zhang, X., (2009). A Review of Current Methodologies for Regional Evapotranspiration Estimation from Remotely Sensed Data. Sensors, 3801 – 3853.

Liu, C., Wang, H., (1999). The Interface Processes of Water Movement in the Soil-Crop-Atmosphere System and Water-Saving Regulation. Beijing Science Press, 24-101.

Loheide, S. P., Gorelick, S. M. (2005). A Local-Scale, High Resolution Evapotranspiration Mapping Algorithm (ETMA) with Hydroecological Applications at Riparian Meadow Restoration Sites. Remote Sensing of Environment, 98: 182–200.

Lowi, M. R. (1999). Water And Conflict In The Middle East and South Asia: are Environmental Issues and Security Issues Linked. Journal of Environment and Development, 8(4): 376- 392.

Lu, D., Mausel, P., Brondizio, E., Moran, E. (2004). Change Detection Techniques. International Journal of Remote Sensing, 25(12), 2365-2407.

Luzi, S. (2010_. Driving forces and patterns of water policy making in Egypt. Water Policy 12 (2010): 92 – 113.

Malczewski, J. (1999). GIS and Multicriteria Decision Analysis. USA and Canda, John Wiley and Sons. 392 P.

Manakos I., Liebler, J., Schneider, T. (2000). Parcel Based Calibration of Remote Sensing Data for Precision Farming Purposes (Eichung Von Fernerkundungsdaten Anhand Von Testparzellen Für Precision Farminganwendungen). Proceedings: Angewandte Geographische Informationsverarbeitung XII, Salzburg, Austria, Wichmann Verlag, Pp.333-344.

Martinez, P. (1994). Efficiency Use of Irrigation Water. Chapter 4. In "Efficient Water Use". (H. Gaduno And F. Arreguin-Cortes, Eds.). Programa Hidrologico International De La UNESCO Para America Latina Y El Caribe, Montevideo. Uruguay

Mas, J. F. (1999). Monitoring Land-Cover Changes: A Comparison of Change Detection Techniques. International Journal of Remote Sensing, 20(1): 139-152.

Mason, S. (2004). From Conflict to Cooperation in the Nile Basin. Ph. D. Thesis, Swiss Federal Institute of Technology, ETH. Switzerland. Online Available at www.Css.Ethz.Ch/Publications

Massman, W. J. (1997). An Analytical One-Dimensional Model of Momentum Transfer by Vegetation of Arbitrary Structure. Boundlay. Meteorology, 83: 407–421.

Massman, W. J. (1999). Molecular Diffusivities of Hg Vapor in Air, O_2 and N_2 near STP and the Kinematic Viscosity and the Thermal Diffusivity of Air near STP. Atmosphere of Environment: 33, 453– 457.

Matsushima, D. (2000). An Estimation Method for Regional Sensible Heat flux on Vegetation Using Satellite Infrared Temperature. In: Proceedings of The 15th Conference of Hydrology/80th AMS Annual Meeting, P1.29. Long Beach

Matzafleri N., Psilovikos, A., Mplanta A. (2009). Water Quality Monitoring and Modeling in Lake Kastoria, using GIS. Assessment and Management of Pollution Sources. Water Resources Management, 23(15): 3221 – 3254.

Mccabe, M. F., Wood, E. F. (2006). "Scale Influences on the Remote Estimation of Evapotranspiration Using Multiple Satellite Sensors." Remote Sensing of Environment, 105(4): 271-285.

Menenti, M., (1984). Physical Aspects and Determination of Evaporation in Deserts Applying Remote Sensing Techniques Report 10 (Special Issue). Institute for Land and Water Management Research (ICW). The Netherlands, 202-203.

Menenti, M., Choudhury, B. J. (1993). Parameterization of Land Surface Evapotranspiration Using a Location Dependent Potential Evapotranspiration and Surface Temperature Range. In: Bolle HJ Et Al (Eds) Proceedings of Exchange Processes at the Land Surface for a Range of Space and Time Scales. IAHS Publ 212, Pp 561–568.

Menenti, M., Jia, L., Su, Z. (2003). On SEBI-SEBS Validation in France, Italy, Spain, USA and China. In: Co-Chair Allen, R. G., Bastiaanssen, W. (Eds) Proceedings of the Workshop on Use of Remote Sensing of Crop Evapotranspiration for Large Regions. International Commission on Irrigation and Drainage (ICID), Montpellier

Mohamed, A. S. Savenije, H. G. (2000). Water Demand Management: Positive Incentives, Negative Incentives or Quota Regulation. Physics and Chemistry of the Earth, Part B. 23: 251-258.

Monteith, J. L. (1965) Evaporation and Environment. Symposia of the Society for Experimental Biology, 19: 205–234.

Monteith, J. L. (1981) Evaporation and Surface Temperature. Quarterly Journal of The Royal Meteorological Society, 107: 1–27.

Monteith, J. L. (1973). Principles of Environmental Physics. Elsevier, New York.

Moran, M. S., Jackson, R. D., Raymond, L. H., Gay, L. W., Slater, P. N. (1989). Mapping Surface Energy Balance Components by Combining Landsat Thematic Mapper and Ground-Based Meteorological Data. Remote Sensing of Environment, 30: 77–87.

Moran, M. S., Rahman, A. F., Washburne, J. C., Goodrich, D. C., Weltz, M. A. And Kustas, W. P. (1996). Combining the Penman-Monteith Equation with Measurements of Surface Temperature and Reflectance to Estimate Evaporation Rates of Semiarid Grassland. Agricultural and Forest Meteorology, 80: 87-109.

Moran, M., Clarke, T., Inoue, Y., Vidal, A., (1994). Estimating Crop Water Deficit Using the Relation between Surface-Air Temperature and Spectral Vegetation Index. Remote Sensing of Environment, 49: 246–263.

Morgan, M. T., Ess, D. R. (1997). The Precision Farming Guide for Agriculturalists. John Deere Publishing, Moline, IL. First Edition Pp. 153 – 184.

MPWWR, (1998). Assessment of Egypt's Rice Policy and Strategies for Water Management, Report no. 6, PCE-I-00-96-00002-00. Ministry of Public Work and Water Resources, Agricultural Policy Reform Program, 1-46.

Muthuwatta, L. P., Ahmad, M. D., Bos, M. G., Rientjes, T. H. M. (2010). Assessment of Water Availability and Consumption in the Karkheh River Basin, Iran- Using Remote Sensing and Geo-Statistics. Water Resource Management, 24: 459 – 484.

MWRI, (2002). Adopted Measures to Trace Major Challenges in the Egyptian Water Sector. A Report Submitted at the Request of World Water Council for 3rd World Water Forum by Ministry of Water Resources and Irrigation, Egypt.

MWRI, (2005). National Water Resources Plan for Egypt – 2017, Cairo, Egypt. Ministry of Water Resources and Irrigation.

Myers, N., Kent, J. (1998). Perverse Subsidies: Tax $S Undercutting our Economics and Environments alike. International Institute for Sustainable Development, Winnipeg, Canada.

NBI, (2001). Nile Basin Initiative, Transboundary Environmental Analysis, Shared Vision Program, GEF, UNDP, World Bank, Washington.

Nehme, C.C., Simões, M. (1999). Spatial Decision Support System for Land Assessment. ACMGIS Press New York, USA, ACM 1-58113-2352/99/0011.

Norman, J. M., Kustas, W. P., Humes, K. S. (1995). A Two-Source Approach for Estimating Soil and Vegetation Energy fluxes from Observations of Directional Radiometric Surface Temperature. Agriculture for Meteorology, 77: 263–293.

NWRP, (2001). National Water Resource Plan For Egypt. Interim Report No. 1. Ministry of Water Resources and Irrigation-Planning Sector, Cairo- May 2001, 205 Pp.

NWRP, (2005). National Water Resources Plan for Egypt: Facing the Challenge, NWRP Final Report, Ministry or Water Resources and Irrigation, Cairo, Egypt.

Olioso, A., Chauki, H., Courault, D., Wigneron, J., (1999). Estimation of Evapotranspiration and Photosynthesis by Assimilation of Remote Sensing Data into SVAT Models. Remote Sensing of Environment, 68: 341–356.

Oppelt, N., Mauser, W. (2003). Hyperspectral Remote Sensing - A Tool for The Derivation of Plant Nitrogen and Its Spatial Variability Within Maize and Wheat Canopies. In: Stafford, J.; Werner, A. (Eds.): Precision Agriculture. Wageningen Academic Publishers.

Ormsby, J., Choudry, B., Owe, M. (1987). Vegetation Spatial Variability and Its Effect on Vegetation Indexes. International Journal of Remote Sensing, 8: 1301-1306.

Ortigosa, R. G., De Leo, G. A., Gatto., M. (2000). VVF: Integrating Modeling and GIS in a Software Tool for Habitat Suitability Assessment. Environmental Modeling and Software, 15: 1-12.

Park, A. B., Colwell, R. N., Meyers, V. F. (1968). Resource Survey by Satellite; Science Fiction Coming True. Yearbook of Agriculture, 13–19.

Perry, C. J. (1999). The IWMI Water Resources Paradigm Definitions. Agriculture Water Management, 40: 45-50.

Perry, C. J. (2001). Water at Any Price? Issues and Options in Charging for Irrigation Water. Irrigation and Drainage, 50: 1-7.

Pettorelli, N., Vik, J., Mysterud, A., Gaillard, J., Tucker, C., Stenseth, N. (2005). Using the Satellite-Derived NDVI to Assess Ecological Responses to Environmental Change. Trends in Ecology and Evolution, 20: 503-510.

Pfaff, B. (2008). Analysis of Integrated and Cointegrated Time Series with R. 2nd ed., 2008, XX, 190 p. ISBN 978-0-387-75966-1, Springer

Postel, S. (1997). Last Oasis. Facing Water Scarcity. W.W. Norton and Company. New York, London.

Press, W. H., Teukolsky, S. A., Vetterling, W. T., Flannery, B. P. (1997). Numerical Recipes in C: The Art of Scientific Computing. Cambridge Univ. Press. 994 Pp.

Price, J. C. (1982). Estimation of Regional Scale Evapotranspiration through Analysis of Satellite Thermal-Infrared Data. IEEE Trans Geoscience of Remote Sensing, 20: 286–292.

Priya, S., Ryosuke S., Shiro, O. (1998). Modelling Spatial Crop Production: A GIS Approach. The 19th Asian Conference on Remote Sensing was Held on November 16-20, 1998 In Manila (www.gisdevelopment.net).

Psilovikos, A., Pennos, P., Margoni, S., Spyridis A., (2004). The (non) rational quantitative and qualitative management of water resources in the large scale irrigation works in Serrer plain. Proceedings of the 1st Environmental Conference titled: «Modern Environmental Issues», pp. 498 – 508, N. Orestiada, May 2004.

Psilovikos, A., Sentas, A., Sahanidis, C., Laopoulos T. (2011). Simulation and Trend Analysis of R.E.MO.S. Water Quality and Quantity Data in Lignite Mines of Western Macedonia–Greece, for the Years 2007 – 2009. Desalination and Water Treatment, 33: 44 – 52.

Rahman, H., Dedieu, G. (1994). SMAC: A Simplified Method for the Atmospheric Correction of Satellite Measurements in The Solar Spectrum. International Journal of Remote Sensing, 15(1): 123-143.

Randazzo, D., Stanley, D., Geronimo, I., Amore, C. (1998). Humaninduced Sedimentological Changes in Manzala Lagoon, Nile Delta, Egypt. Environmental Geology, 36: 235–258.

Reetz, J. H. F., Westervelt, J. D. (2004). Geographic Information Systems (GIS) in Site-Specific Systems. Site-Specific Management Guidelines Series is Published by the Potash and Phosphate Institute (PPI). SSMG-29.

Reginato, R. J., Jackson, R. D., Pinter, P. J. (1985). Evapotranspiration Calculated from Remote Multi-Spectral and Ground Station Meteorological Data. Remote Sensing of Environment, 18: 75–89.

Richard, L. (2003). Irrigation Scheduling 0f Surface-Irrigated Crops during a Drought. University of California Drought Tip, 92-51 Pp. Roberts, S. (2003). Combining Data from Multiple Monitors in Air Pollution Mortality Time Series Studies. Atmospheric Environment, 37: 3317 – 3322.

Richards J. (1999). Remote Sensing Digital Image Analysis, Springer-Verlag, Berlin, P. 240-280.

Rivera, V. O. (2005). Hyperspectral Change Detection Using Temporal Principal Component Analysis. Spain: University Of Puerto Rico.

Roberts, S. (2003).Combining Data from Multiple Monitors in Air Pollution Mortality Time Series Studies. Atmosphere of Environment, 37: 3317-3322.

Roerink, G. J., Su, B., Menenti, M. (2000). S-SEBI A Simple Remote Sensing Algorithm to Estimate the Surface Energy Balance. Physics of Climate Earth (B), 25(2): 147–157.

Rogers, P. De-Silva, R., Bhatia, R. (2002). Water is Economic Good: How to Use Price to Promote Sustainability. Water Policy. 4:1-17

Rosegrant, M. W., Cai, X., Cline, S. A. (2002). Global Water Outlook to 2025: Averting an Impending Crisis. Food Policy Report 2020 Vision. Washington, DC, IFPRI.

Rosenberg, N. J., Blad, B. L., Verma, S. B. (1983). Microclimate, the Biological Environment, 2nd Edn. Wiley, New York, 495 Pp.

Rouse, J. W., Haas, R. H. Jr., Schell, J. A., Deering, D. W. (1974). Monitoring Vegetation Systems in the Great Plains with ERTS. In: Proceedings of the ERTS-1 3rd Symposium, Vol 1. NASA SP-351. NASA, Washington, 309–317 Pp.

Saaty, T. L. (1977). "A scaling method for priorities in hierarchical structures." Journal of mathematical psychology, 15(3): 234 - 281.

Saaty, T. L. (1980). The Analytic Hierarchy Process. McGraw Hill, New York.

Sadler, E. J., Camp, C. P., Evans, D. E., Millen, J. A. (2002). Analysis of Corn Response to Irrigation. ASA-CSSA-SSSA, 677 South Segoe Road, Madison, WI 53711, USA. Six International Conference on Precision Agriculture.

Said, M. (1980). The Geological Evolution of the River Nile. Springer, Heidelberg, Ney York, 151 Pp.

Sall, J., Lehman, A. (1996). JMP Start Statistics: A Guide to Statistical and Data Analysis Using JMP Software. SAS Institute Inc., Duxbury Press, New York.

Saunders, R. W., Kriebel, R. T. (1988). An Improved Method for Detecting Clear Sky and Cloudy Radiances from AVHRR Data. International Journal of Remote Sensing, 9: 123 – 150.

Seckler, D. (1992). Irrigation Policy, Management and Monitoring In Developing Countries. Paper for the Roundtable on Egyptian Water Policy 1992. Alexandria, Egypt.

Seckler, D. (1999). Revisiting the "IWMI Paradigm:" Increasing the Efficiency and Productivity of Water Use. IWMI Water Brief 2. Colombo, Sri Lanka: International Water Management Institute.

Seguin, B., Itier, B. (1983). Using Midday Surface Temperature to Estimate Daily Evapotranspiration from Satellite Thermal Data IR. International Journal of Remote Sensing, 4(2): 371–383.

Sellers, P., Randall, D., Collatz, J., Berry, J., Field, C., Dazlich, D., Zhang, C., Collelo, G., Bounous, A., (1996). A Revised Land Surface Parameterization (Sib_2) for Atmospheric Gcms: Model Formulation. Journal of Climate, 9: 676–705.

Sentas, A., Psilovikos Ar. (2010). Comparison of ARIMA and Transfer Function (TF) Models in Water Temperature Simulation in Dam–Lake Thesaurus, Eastern Macedonia, Greece». Environmental Hydraulics, Christodoulou and Stamou (Eds), Vol 2, 929 – 934 Pp., CRC Press – Taylor and Francis Group, 2010.

Shalaby, A., Gad, A. (2010). Urban Sprawl Impact Assessment on the Fertile Agricultural Land of Egypt Using Remote Sensing and Digital Soil Database, Case Study: Qalubiya Governorate. US Egypt Workshop on Space Technology and Geoinformation for Sustainable Development, Cairo, Egypt 14-17 June, 2010.

Shalaby, A., Tateishi, R. (2007). Remote Sensing and GIS for Mapping and Monitoring Land Cover and Land-Use Changes in The Northwestern Coastal Zone Of Egypt. Applied Geography, 27(1): 28-41.

Singh, A. (1989). Digital Change Detection Techniques Using Remotely-Sensed Data. International Journal of Remote Sensing, 10(6): 989-1003.

Smith, A. M., Nadeau, C., Freemantle, J., Wehn, H., Teillet, P. M., Kehler, I., Daub, N., Bourgeois, G., De Jong, R. (2005). Leaf Area Index from CHRIS Satellite Data and Applications in Plant Yield Estimation. Presented at the 26th Canadian Symposium on Remote Sensing in Wolfville, Nova Scotia. June 14-16.

Smith, R. L. (1998). Extreme Value Analysis of Environmental Time Series: An Application to Trend Detection in Ground Level Ozone. Statistical Science, 4: 367 – 383.

Sonka, S. T., Marvin, E. B., Edward, T. C., John, W. C., Ralph, E. H., Deborah, A. J., John, B. L., Erik, L., David, A. M., Searcy, S. W., Susan L. U., Stephen J. V. (1997). Precision Agriculture in the 21st Century: Geospatial and Information Technologies in Crop Management. National Academy Press Washington.

Springborg, R., (1979). Patrimonialism and Policy Making in Egypt: Nasser and Sadat and the Tenure Policy for Reclaimed Lands. Middle Eastern Studies, 15(1): 49-69.

Stone, L. R., Horton, M. L. (1974) Estimating Evapotranspiration Using Canopy Temperatures: field Evaluation. Agronomy, 66: 450–454.

Strzepek, K., Yates, D., El Qusy, D. (1996). Vulnerability Assessment of Water Resources in Egypt to Climatic Change in the Nile Basin. Climate Research, 6: 89-95.

Stull, R.B. (1988). An Introduction to Boundary Layer Meteorology. Kluwer Academic Publication 670 Pp.

Su, H., Mccabe, M., Wood, E., Su, Z., Prueger. J., (2005). Modeling Evapotranspiration During SMACEX: Comparing Two Approaches for Local and Regional-Scale Prediction. Journal of Hydrometerology, 6(6): 910-922.

Su, Z., (2001). A Surface Energy Balance System (SEBS) For Estimation of Turbulent Heat fluxes From Point to Continental Scale. In: Su, Z., Jacobs, C. (Eds.), Advanced Earth Observation Land Surface Climate. Publications of the National Remote Sensing Board (BCRS), USP-2, 01-02, 184-185.

Su, Z., (2002). The Surface Energy Balance System SEBS for Estimation of Turbulent Heat fluxes. Hydrology and Earth System Sciences, 6 (1): 85–99.

Su, Z., Pelgrum, M., Menenti, M., (1999). Aggregation Effects of Surface Heterogeneity in Land Surface Processes. Hydrology and Earth System Sciences, 3 (4): 549–563.

Su, Z., Schmugge, T., Kustas, W. P., Massman, W. J. (2001). An Evaluation of Two Models for Estimation of the Roughness Height for Heat Transfer between the Land Surface and the Atmosphere. Journal of Applied Meteorology, 40: 1933–1951.

Su, Z., Yacob, A., Wen, J., Roerink, G., He, Y., Gao, B., Boogaard, H., Diepen, C., (2003). Assessing Relative Soil Moisture with Remote Sensing Data: Theory, Experimental Validation, and Application to Drought Monitoring Over the North China Plain. Physics and Chemistry Of The Earth, 28: 89–101.

Suhartono, (2011). Time Series Forecasting by Using Seasonal Autoregressive Integrated Moving Average: Subset, Multiplicative or Additive Model. Journal of Mathematics and Statistics, 7(1): 20-27.

Sur, M., Umali-Deininger, D., A. Dinar. (2002). Water Related Subsidies in Agriculture: Environmental and Equity Consequences. OECD Workshop of Environmentally Harmful Subsidies. World Bank.

Taconet, O., Bernard, R., Vidal-Madjar, D. (1986). Evapotranspiration over an Agricultural Region Using a Surface flux/Temperature Model Based On NOAA-AVHRR Data. Journal of Climate And Applied Meteorology, 25: 284–307.

Tate, D. M. (1994). Principles Of Water Use Efficiency. Chapter 2. In “Efficient Water Use”. (H. Gaduno and F. Arreguin-Cortes, Eds.). Programa Hidrologico International De La UNESCO Para America Latina Y El Caribe, Montevideo. Uruguay

Taylor, A. (1981). A Method for Surface Irrigation Design Based on Infiltration Using the Border Strip As An Infiltrometer. Phd Thesis, University of Canterbury, Lincoln College, New Zealand. 228 Pp.

Tiwari, D., Dinar, A. (2002). Role and Use of Economic Incentives in Irrigated Agriculture. World Bank. Washington DC.

Ultman, R., (1983). “Redefining Security”. International Security 8(1): 129 – 153.

Umali, D. (1993). Irrigation Induced Salinity. A Growing Problem for Development and the Environment. The World Bank Technical Paper No 215, Washington DC, USA

UNCCA, (2001). United Nation’s Common Country Assessment-Egypt. Cairo, Egypt.

UNDSD, (2003). Guidance for Preparing National Sustainable Development Strategies. United Nations Division for Sustainable Development.. Guidance for Preparing National Sustainable Development Strategies.

Van Den Hurk, B. J. J., Holtslag, A. A. M. (1995). On The Bulk Parameterization of Surface Fluxes for Various Conditions and Parameter Ranges. Bound-Lay. Meteorology, 82: 199–234.

Vandaele, W. (1983). Applied Time Series and Box-Jenkins Models, Academic Press Inc, New York.

Varco, J. J., Salin, M. L., Bridges, S. M. (2000): Remote Sensing Applications in the Optimization of Cotton Nitrogen Fertilization 1999-2000 RSTC Funded Final Research Report.

Vaughan, P. J., Suarez, D. L. (1998): Spatial Prediction of Irrigation Efficiency with the Unsatchemgeo Model. ESRI User Conference Proceedings, ESRI, San Diego (USA).

Verma, S. B., Rosenberg, N. J., Blad, B. L., Baradas, M. W. (1976.) Resistance Energy Balance Method for Predicting Evapotranspiration: Determination of Boundary Layer Resistance and Evaluation of Error Effects. Agronomy 68: 776–782.

Walter, C., Mcbratney, A. B., Douaoui, A., Minasny, B. (2001): Spatial Prediction of Topsoil Salinity in The Chelif Valley, Algeria, Using Local Kriging with Local Variograms Versus Local Kriging with Whole-Area Variogram. Australian Journal of Soil Research, 39: 259-272.

Wang, F., Xu, Y. J. (2010). Comparison of Remote Sensing Change Detection Techniques for Assessing Hurricane Damage to Forests. Environmental Monitoring and Assessment, 162: 311 – 326.

Warner, T. A., Campagna, D. J. (2009). Remote sensing with IDRISI Taiga: A beginner's guide. Hong Kong: Geocarto International Centre.

Water Management in Fayoum Governarate, (2002). Eurocosult, Central Department of Water Resources and Irrigation in Co-Operation with Darwish Consulting Engineers. Egypt.

Welch, R., Ehlers, W. (1987). Merging Multiresolution SPOT HRV and Landsat TM Data. Photogrommetric Engineering and Remote Sensing, 53(3): 301-303.

Whelan, B. M., Macbratney, A. B., Minasny, B. (2001). VESPER-Spatial Prediction Software for Precision Agriculture. 139–144 Pp. In G. Grenier and S. Blackmore (Ed.). ECPA 2001, Proc. 3rd European Conference on Precision Agriculture, Montpellier, France.18–20 June. Ecol. Nationale Supérieure Agronomique, Montpellier, France.

Wieringa, J. (1986). Roughness-Dependent Geographical Interpolation of Surface Wind Speed Averages. Quarterly Journal of The Royal Meteorological Society, 112: 867–889.

Wieringa, J. (1993). Representative Roughness Parameters for Homogeneous Terrain. Bound-Lay. Meteorology, 63:3 23–363.

World Meteorological Organization, (1966). Measurement and estimation of evaporation and evapotranspiration. Technical note No.83. WMO - No. 201 TP 105.

Wu, C. D., Lo, H. C., Cheng, C. C., Chen, Y. K. (2010). Application of SEBAL and Markov Models for Future Stream Flow Simulation through Remote Sensing. Water Resource Management, 24: 3773 – 3797.

Wu, T. F., Lin, C. J., Weng, R. C. (2004). Probability Estimates for Multi-Class Classification by Pairwise Coupling. Journal of Machine Learning Research, 5: 975-1005.

Yager, R. R. (1988). On Oredered Weighted Averaging Aggergation Operwtors in Multi-Criteria Decision Making. "IEEE Transaction on Systems, Man and Cybernetics, 18: 183 - 190.

Yang, H., Zhang, X., Zehnder, A. (2003). Water Scarcity, Pricing Mechanism and Institutional Reform in Northern China Irrigated Agriculture. Agricultural Water Management. 61: 143–161.

Yang, X. (1997). Georeferencing CAMS Data: Polynomial Rectification and Beyond, Dissertation, University of South Carolina, Columbia.

Yang, X., Zhou, Q., Melville, M. (1997). Estimating Local Sugarcane Evapotranspiration Using LANDSAT TM Image and A VITT Concept. International Journal of Remote Sensing 18, 453-459.

Yates, D. N., Strzepek, K. M. (1998). An Assessment of Integrated Climate Change Impacts on the Agricultural Economy of Egypt. Climatic Change, 38(3): 261287.

Yuan, D., Elvidge, C. D., Lunetta, R. S. (1998). Survey of Multispectral Methods for Land Cover Change Analysis. In R. S. Lunetta, And C. D. Elvidge (Eds.), Remote Sensing Change Detection: Environmental Monitoring Methods and Applications, 21-39 Pp. Chelsea, MI: Ann Arbor Press.

Yuan, F., Sawaya, K. E., Loeffelholz, B., Bauer, M. E. (2005). Land Cover Classification and Change Analysis of the Twin Cities (Minnesota) Metropolitan Area by Multitemporal Landsat Remote Sensing. Remote Sensing of Environment, 98 (2-3): 317-328.

Zhang, L., Lemeur, R. (1995). Evaluation of Daily ET Estimates from Instantaneous Measurements. Agriculture Forest Meteorology, 74: 139–154.

Zhou, W., Troy, A., Grove, M. (2008). Object-Based Land Cover Classification and Change Analysis in the Baltimore Metropolitan Area Using Multitemporal High Resolution Remote Sensing Data. Sensors, 8(3): 1613-1636.

11. Appendices

11.1. Appendix Tables

Appendix Table 1: Characteristics of ETM+ data

Band No.	Wavelength Interval (μm)	Spectral Response	Resolution (m)
1	0.45 – 0.52	Blue-Green	30
2	0.52 – 0.60	Green	30
3	0.63 – 0.69	Red	30
4	0.76 – 0.90	Near IR	30
5	1.55 – 1.75	Mid-IR	30
6	10.40 – 12.50	Thermal IR	60
7	2.08 – 2.35	Mid-IR	30
8	0.52 – 0.90	Pan	15

Appendix Table 2: Characteristics of TM data

Band No.	Wavelength Interval (μm)	Spectral Response	Resolution (m)
1	0.45 – 0.52	Blue-Green	30
2	0.52 – 0.60	Green	30
3	0.63 – 0.69	Red	30
4	0.76 – 0.90	Near IR	30
5	1.55 – 1.75	Mid-IR	30
6	10.40 – 12.50	Thermal IR	120
7	2.08 – 2.35	Mid-IR	30

Appendix Table 3: Characteristics of Egypt-Sat_1 data

Band No.	Wavelength Interval (μm)	Spectral Response	Resolution (m)
1	**0.45 – 0.52**	**Blue-Green**	**7.8**
2	**0.52 – 0.60**	**Green**	**7.8**
3	**0.63 – 0.69**	**Red**	**7.8**
4	**0.76 – 0.90**	**Near IR**	**7.8**

Appendix Table 4: Characteristics of ASTER data

Instrument	VNIR	SWIR	TIR
Bands	**1-3**	**4-9**	**10-14**
Spatial resolution	**15m**	**30m**	**90m**
Swath width	**60km**	**60km**	**60km**
Cross track pointing	**± 318km (24 deg)**	**±116km (8.55 deg)**	**±116km (8.55 deg)**
Quantization (bits)	**8**	**8**	**12**
Spectral Range	**Band 1: 0.52 - 0.60 «m (visible green) Nadir looking**	**Band 4: 1.600 - 1.700 «m**	**Band 10: 8.125 - 8.475 «m**
	Band 2: 0.63 - 0.69 «m (visible red) Nadir looking	**Band 5: 2.145 - 2.185 «m**	**Band 11: 8.475 - 8.825 «m**
	Band 3: 0.76 - 0.86 «m (near infra-red) Nadir looking	**Band 6: 2.185 - 2.225 «m**	**Band 12: 8.925 - 9.275 «m**
	Band 3: 0.76 - 0.86 «m (near infra-red) Backward looking	**Band 7: 2.235 - 2.285 «m**	**Band 13: 10.25 - 10.95 «m**
	-	**Band 8: 2.295 - 2.365 «m**	**Band 14: 10.95 - 11.65 «m**
	-	**Band 9: 2.360 - 2.430 «m**	**-**

Note: Band 3 has nadir and backward telescopes for stereo pairs from a single orbit.

Appendix Table 5: Characteristics of ENVISAT ATS_TOA_1P data, AATSR Gridded brightness temperature and reflectance

a. Tie-Point Grids of ENVISAT

Index	Identifier	Type	Description	Units
0	"latitude"	Float	Latitudes	deg
1	"longitude"	Float	Longitudes	deg
2	"lat_corr_nadir"	Float	Latitude corrections, nadir view	deg
3	"lon_corr_nadir"	Float	Longitude corrections, nadir view	deg
4	"lat_corr_fward"	Float	Latitude corrections, forward view	deg
5	"lon_corr_fward"	Float	Longitude corrections, forward view	deg
6	"altitude"	Float	Topographic altitude	m
7	"sun_elev_nadir"	Float	Solar elevation, nadir view	deg
8	"view_elev_nadir"	Float	Satellite elevation, nadir view	deg
9	"sun_azimuth_nadir"	Float	Solar azimuth, nadir view	deg
10	"view_azimuth_nadir"	Float	Satellite azimuth, nadir view	deg
11	"sun_elev_fward"	Float	Solar elevation, forward view	deg
12	"view_elev_fward"	Float	Satellite elevation, forward view	deg
13	"sun_azimuth_fward"	Float	Solar azimuth, forward view	deg
14	"view_azimuth_fward"	Float	Satellite azimuth, forward view	deg

b. Bands of ENVISAT

Index	Identifier	Type	Description	Units
15	"btemp_nadir_1200"	Float	Brightness temperature, nadir (11500-12500 nm)	K
16	"btemp_nadir_1100"	Float	Brightness temperature, nadir (10400-11300 nm)	K
17	"btemp_nadir_0370"	Float	Brightness temperature, nadir (3505-3895 nm)	K
18	"reflec_nadir_1600"	Float	Reflectance, nadir view (1580-1640 nm)	%
19	"reflec_nadir_0870"	Float	Reflectance, nadir view (855-875 nm)	%
20	"reflec_nadir_0670"	Float	Reflectance, nadir view (649-669 nm)	%
21	"reflec_nadir_0550"	Float	Reflectance, nadir view (545-565 nm)	%
22	"btemp_fward_1200"	Float	Brightness temperature, forward (11500-12500 nm)	K
23	"btemp_fward_1100"	Float	Brightness temperature, forward (10400-11300 nm)	K
24	"btemp_fward_0370"	Float	Brightness temperature, forward (3505-3895 nm)	K
25	"reflec_fward_1600"	Float	Reflectance, forward view (1580-1640 nm)	%
26	"reflec_fward_0870"	Float	Reflectance, forward view (855-875 nm)	%
27	"reflec_fward_0670"	Float	Reflectance, forward view (649-669 nm)	%
28	"reflec_fward_0550"	Float	Reflectance, forward view (545-565 nm)	%
29	"confid_flags_nadir"	UShort	Confidence flags, nadir view	*n/a*
30	"confid_flags_fward"	UShort	Confidence flags, forward view	*n/a*
31	"cloud_flags_nadir"	UShort	Cloud flags, nadir view	*n/a*
32	"cloud_flags_fward"	UShort	Cloud flags, forward view	*n/a*

Appendix Table 6: Characteristics of ENVISAT MER_RR__1P data, MERIS Level 1b Reduced Resolution Geophysical Product

a. Tie-Point Grids of ENVISAT

Index	Identifier	Type	Description	Units
0	"latitude"	Float	Latitude of the tie points (WGS-84), positive N	deg
1	"longitude"	Float	Longitude of the tie points (WGS-84), positive E	deg
2	"dem_alt"	Float	Digital elevation model altitude	m
3	"dem_rough"	Float	Digital elevation model roughness	m
4	"lat_corr"	Float	Digital elevation model latitude corrections	deg
5	"lon_corr"	Float	Digital elevation model longitude corrections	deg
6	"sun_zenith"	Float	Sun zenith angle	deg
7	"sun_azimuth"	Float	Sun azimuth angles	deg
8	"view_zenith"	Float	Viewing zenith angles	deg
9	"view_azimuth"	Float	Viewing azimuth angles	deg
10	"zonal_wind"	Float	Zonal wind	m/s
11	"merid_wind"	Float	Meridional wind	m/s
12	"atm_press"	Float	Mean sea level pressure	hPa
13	"ozone"	Float	Total ozone	DU
14	"rel_hum"	Float	Relative humidity	%

b. Bands of ENVISAT

Index	Identifier	Type	Description	Units
15	**"radiance_1"**	**Float**	**TOA radiance band 1**	**mW/(m^2*sr*nm)**
16	**"radiance_2"**	**Float**	**TOA radiance band 2**	**mW/(m^2*sr*nm)**
17	**"radiance_3"**	**Float**	**TOA radiance band 3**	**mW/(m^2*sr*nm)**
18	**"radiance_4"**	**Float**	**TOA radiance band 4**	**mW/(m^2*sr*nm)**
19	**"radiance_5"**	**Float**	**TOA radiance band 5**	**mW/(m^2*sr*nm)**
20	**"radiance_6"**	**Float**	**TOA radiance band 6**	**mW/(m^2*sr*nm)**
21	**"radiance_7"**	**Float**	**TOA radiance band 7**	**mW/(m^2*sr*nm)**
22	**"radiance_8"**	**Float**	**TOA radiance band 8**	**mW/(m^2*sr*nm)**
23	**"radiance_9"**	**Float**	**TOA radiance band 9**	**mW/(m^2*sr*nm)**
24	**"radiance_10"**	**Float**	**TOA radiance band 10**	**mW/(m^2*sr*nm)**
25	**"radiance_11"**	**Float**	**TOA radiance band 11**	**mW/(m^2*sr*nm)**
26	**"radiance_12"**	**Float**	**TOA radiance band 12**	**mW/(m^2*sr*nm)**
27	**"radiance_13"**	**Float**	**TOA radiance band 13**	**mW/(m^2*sr*nm)**
28	**"radiance_14"**	**Float**	**TOA radiance band 14**	**mW/(m^2*sr*nm)**
29	**"radiance_15"**	**Float**	**TOA radiance band 15**	**mW/(m^2*sr*nm)**
30	**"l1_flags"**	**UChar**	**Level 1b classification and quality flags**	***n/a***
31	**"detector_index"**	**SShort**	**Detector index**	***n/a***

Appendix Table 7: Standard configuration of the smile correction (equal to the current setting in Level 2 processor).

		Land			Water			
band (lam_0)	activation switch	lower band (lam_1)	upper band (lam_2)	activation switch	lower band (lam_1)	lower band (lam_1)	reference wavength (lam_ref)	F0_ref
1	1	1	2	1	1	2	412.5	1713.641724
2	1	1	3	1	1	3	442.5	1877.435669
3	1	2	4	1	2	4	490	1929.325562
4	0	3	5	1	3	5	510	1926.839233
5	0	4	6	1	4	6	560	1800.486328
6	0	5	7	1	5	7	620	1649.709839
7	0	6	9	1	6	9	665	1530.904175
8	0	7	9	0	7	9	681.25	1470.22644
9	0	8	9	1	8	9	708.75	1405.468872
10	0	10	12	1	10	12	753.75	1266.198853
11	0	10	12	0	10	12	761.875	1249.881592
12	0	10	12	1	10	12	778.75	1175.723267
13	0	13	14	1	13	14	865	958.885498
14	0	13	14	0	13	14	885	929.7631836
15	0	13	14	0	13	14	900	895.4086304

Appendix Table 8: Confusion Matrix Classification method: Mahalanobis Distance

Image acquisition date and sensor type: 1984, Landsat TM

Number of classes: five classes

Overall Accuracy = (370170/476698) 77.6529%

Kappa Coefficient = 0.7144

Ground Truth (Pixels)

Class	Lake	Fish Farm	Desert	Urban	Agri_land	Total
Lake	158260	3473	0	1600	180	163513
Fish Farm	415	39634	0	79	2514	42642
Desert	0	6	31983	4	1	31994
Urban	0	6400	75104	63290	9742	154536
Agri_land	0	220	5211	1579	77003	84013
Total	158675	49733	112298	66552	89440	476698

Ground Truth (Percent)

Class	Lake	Fish Farm	Desert	Urban	Agri_land	Total
Lake	99.74	6.98	0.00	2.40	0.20	34.30
Fish Farm	0.26	79.69	0.00	0.12	2.81	8.95
Desert	0.00	0.01	28.48	0.01	0.00	6.71
Urban	0.00	12.87	66.88	95.10	10.89	32.42
Agri_land	0.00	0.44	4.64	2.37	86.09	17.62
Total	100.00	100.00	100.00	100.00	100.00	100.00

Accuracies

a)

Class	Commission (Percent)	Omission (Percent)	Commission (Pixels)	Omission (Pixels)
Lake	3.21	0.26	5253/163513	415/158675
Fish Farm	7.05	20.31	3008/42642	10099/49733
Desert	0.03	71.52	11/31994	80315/112298
Urban	59.05	4.90	91246/154536	3262/66552
Agri_land	8.34	13.91	7010/84013	12437/89440

b)

Class	Prod. Acc. (Percent)	User Acc. (Percent)	Prod. Acc. (Pixels)	User Acc. (Pixels)
Lake	99.74	96.79	158260/158675	158260/163513
Fish Farm	79.69	92.65	39634/49733	39634/42642
Desert	28.48	99.97	31983/112298	31983/31994
Urban	95.10	40.95	63290/66552	63290/154536
Agri_land	86.09	91.66	77003/89440	77003/84013

Appendix Table 9: Confusion Matrix Classification method: Minimum Distance

Image acquisition date and sensor type: 1984, Landsat TM

Number of classes: five classes

Overall Accuracy = (372050/476698) 78.0473%

Kappa Coefficient = 0.7212

Ground Truth (Pixels)

Class	Lake	Fish Farm	Desert	Urban	Agri_land	Total
Lake	109682	10324	0	15	221	120242
Fish Farm	48993	31686	0	18	762	81459
Desert	0	21	98727	158	0	98906
Urban	0	4929	13571	49433	5935	73868
Agri_land	0	2773	0	16928	82522	102223
Total	158675	49733	112298	66552	89440	476698

Ground Truth (Percent)

Class	Lake	Fish Farm	Desert	Urban	Agri_land	Total
Lake	69.12	20.76	0.00	0.02	0.25	25.22
Fish Farm	30.88	63.71	0.00	0.03	0.85	17.09
Desert	0.00	0.04	87.92	0.24	0.00	20.75
Urban	0.00	9.91	12.08	74.28	6.64	15.50
Agri_land	0.00	5.58	0.00	25.44	92.27	21.44
Total	100.00	100.00	100.00	100.00	100.00	100.00

Accuracies
a)

Class	Commission (Percent)	Omission (Percent)	Commission (Pixels)	Omission (Pixels)
Lake	8.78	30.88	10560/120242	48993/158675
Fish Farm	61.10	36.29	49773/81459	18047/49733
Desert	0.18	12.08	179/98906	13571/112298
Urban	33.08	25.72	24435/73868	17119/66552
Agri_land	19.27	7.73	19701/102223	6918/89440

b)

Class	Prod. Acc. (Percent)	User Acc. (Percent)	Prod. Acc. (Pixels)	User Acc. (Pixels)
Lake	69.12	91.22	109682/158675	109682/120242
Fish Farm	63.71	38.90	31686/49733	31686/81459
Desert	87.92	99.82	98727/112298	98727/98906
Urban	74.28	66.92	49433/66552	49433/73868
Agri_land	92.27	80.73	82522/89440	82522/102223

Appendix Table 10: Confusion Matrix Classification method: Maximum Likelihood

Image acquisition date and sensor type: 1984, Landsat TM

Number of classes: five classes

Overall Accuracy = (383801/476698) 80.5124%

Kappa Coefficient = 0.7501

Ground Truth (Pixels)

Class	Lake	Fish Farm	Desert	Urban	Agri_land	Total
Lake	157333	23	0	0	0	157356
Fish Farm	1341	44070	5	32	212	45660
Desert	0	0	33598	0	0	33598
Urban	1	5381	32480	64928	5356	108146
Agri_land	0	259	46215	1592	83872	131938
Total	158675	49733	112298	66552	89440	476698

Ground Truth (Percent)

Class	Lake	Fish Farm	Desert	Urban	Agri_land	Total
Lake	99.15	0.05	0.00	0.00	0.00	33.01
Fish Farm	0.85	88.61	0.00	0.05	0.24	9.58
Desert	0.00	0.00	29.92	0.00	0.00	7.05
Urban	0.00	10.82	28.92	97.56	5.99	22.69
Agri_land	0.00	0.52	41.15	2.39	93.77	27.68
Total	100.00	100.00	100.00	100.00	100.00	100.00

Accuracies
a)

Class	Commission (Percent)	Omission (Percent)	Commission (Pixels)	Omission (Pixels)
Lake	0.01	0.85	23/157356	1342/158675
Fish Farm	3.048	11.39	1590/45660	5663/49733
Desert	0.00	70.08	0/33598	78700/112298
Urban	39.96	2.44	43218/108146	1624/66552
Agri_land	36.43	6.23	48066/131938	5568/89440

b)

Class	Prod. Acc. (Percent)	User Acc. (Percent)	Prod. Acc. (Pixels)	User Acc. (Pixels)
Lake	99.15	99.99	157333/158675	157333/157356
Fish Farm	88.61	96.52	44070/49733	44070/45660
Desert	29.92	100.00	33598/112298	33598/33598
Urban	97.56	60.04	64928/66552	64928/108146
Agri_land	93.77	63.57	83872/89440	83872/131938

Appendix Table 11: Confusion Matrix Classification method: Neural Network

Image acquisition date and sensor type: 1984, Landsat TM

Number of classes: five classes

Overall Accuracy = (61704/164480) 37.5146%

Kappa Coefficient = 0.1854

Ground Truth (Pixels)

Class	Lake	Fish Farm	Desert	Urban	Agri_land	Total
Lake	0	0	0	0	0	0
Fish Farm	36338	37384	1308	305	138	75473
Desert	155	7789	23326	17948	920	50138
Urban	7	151	17927	994	19790	38869
Agri_land	0	0	0	0	0	0
Total	36500	45324	42561	19247	20848	164480

Ground Truth (Percent)

Class	Lake	Fish Farm	Desert	Urban	Agri_land	Total
Lake	0.00	0.00	0.00	0.00	0.00	0.00
Fish Farm	99.56	82.48	3.07	1.58	0.66	45.89
Desert	0.42	17.19	54.81	93.25	4.41	30.48
Urban	0.02	0.33	42.12	5.16	94.93	23.63
Agri_land	0.00	0.00	0.00	0.00	0.00	0.00
Total	100.00	100.00	100.00	100.00	100.00	100.00

Accuracies
a)

Class	Commission (Percent)	Omission (Percent)	Commission (Pixels)	Omission (Pixels)
Lake	0.00	100.00	0/0	36500/36500
Fish Farm	50.47	17.52	38089/75473	7940/45324
Desert	53.48	45.19	26812/50138	19235/42561
Urban	97.44	94.84	37875/38869	18253/19247
Agri_land	0.00	100.00	0/0	20848/20848

b)

Class	Prod. Acc. (Percent)	User Acc. (Percent)	Prod. Acc. (Pixels)	User Acc. (Pixels)
Lake	0.00	0.00	0/36500	0/0
Fish Farm	82.48	49.53	37384/45324	37384/75473
Desert	54.81	46.52	23326/42561	23326/50138
Urban	5.16	2.56	994/19247	994/38869
Agri_land	0.00	0.00	0/20848	0/0

Appendix Table 12: Confusion Matrix Classification method: Parallelepiped

Image acquisition date and sensor type: 1984, Landsat TM

Number of classes: five classes

Overall Accuracy = (310294/476698) 65.0924%

Kappa Coefficient = 0.5743

Ground Truth (Pixels)

Class	Lake	Fish Farm	Desert	Urban	Agri_land	Total
Lake	152261	446	0	0	0	152707
Fish Farm	6414	43101	0	8895	11895	70305
Desert	0	0	23291	1	0	23292
Urban	0	5874	5997	57090	42660	111621
Agri_land	0	167	2	71	34551	34791
Total	158675	49733	112298	66552	89440	476698

Ground Truth (Percent)

Class	Lake	Fish Farm	Desert	Urban	Agri_land	Total
Lake	95.96	0.90	0.00	0.00	0.00	32.03
Fish Farm	4.04	86.66	0.00	13.37	13.30	14.75
Desert	0.00	0.00	20.74	0.00	0.00	4.89
Urban	0.00	11.81	5.34	85.78	47.70	23.42
Agri_land	0.00	0.34	0.00	0.11	38.63	7.30
Total	100.00	100.00	100.00	100.00	100.00	100.00

Accuracies
a)

Class	Commission (Percent)	Omission (Percent)	Commission (Pixels)	Omission (Pixels)
Lake	0.29	4.04	446/152707	6414/158675
Fish Farm	38.69	13.34	27204/70305	6632/49733
Desert	0.00	79.26	1/23292	89007/112298
Urban	48.85	14.22	54531/111621	9462/66552
Agri_land	0.69	61.37	240/34791	54889/89440

b)

Class	Prod. Acc. (Percent)	User Acc. (Percent)	Prod. Acc. (Pixels)	User Acc. (Pixels)
Lake	95.96	99.71	152261/158675	152261/152707
Fish Farm	86.66	61.31	43101/49733	43101/70305
Desert	20.74	100.00	23291/112298	23291/23292
Urban	85.78	51.15	57090/66552	57090/111621
Agri_land	38.63	99.31	34551/89440	34551/34791

Appendix Table 13: Confusion Matrix Classification method: Mahalanobis Distance

Image acquisition date and sensor type: 2000, Landsat ETM

Number of classes: five classes

Overall Accuracy = (128020/164480) 77.8332%

Kappa Coefficient = 0.7174

Ground Truth (Pixels)

Class	Lake	Fish Farm	Desert	Urban	Agri_land	Total
Lake	26449	13615	0	773	212	41049
Fish Farm	9851	25570	0	268	256	35945
Desert	0	1	42243	43	236	42526
Urban	200	4445	318	17349	3735	26047
Agri_land	0	1693	0	811	16409	18913
Total	36500	45324	42561	19247	20848	164480

Ground Truth (Percent)

Class	Lake	Fish Farm	Desert	Urban	Agri_land	Total
Lake	72.46	30.04	0.00	4.02	1.02	24.96
Fish Farm	26.99	65.42	0.00	1.39	1.23	21.85
Desert	0.00	0.00	99.25	0.24	1.13	25.85
Urban	0.55	9.81	0.75	90.14	17.92	15.84
Agri_land	0.00	3.47	0.00	4.21	78.71	11.50
Total	100.00	100.00	100.00	100.00	100.00	100.00

Accuracies
a)

Class	Commission (Percent)	Omission (Percent)	Commission (Pixels)	Omission (Pixels)
Lake	35.57	27.54	14600/41049	10051/36500
Fish Farm	28.86	43.58	10375/35945	19754/45324
Desert	0.67	0.75	283/42526	318/42561
Urban	33.39	9.86	8698/26047	1898/19247
Agri_land	13.24	21.29	2504/18913	4439/20848

b)

Class	Prod. Acc. (Percent)	User Acc. (Percent)	Prod. Acc. (Pixels)	User Acc. (Pixels)
Lake	72.46	64.43	26449/36500	26449/41049
Fish Farm	56.42	71.14	25570/45324	25570/35945
Desert	99.25	99.33	42243/42561	42243/42526
Urban	90.14	66.61	17349/19247	17349/26047
Agri_land	78.71	86.76	16409/20848	16409/18913

Appendix Table 14: Confusion Matrix Classification method: Minimum Distance

Image acquisition date and sensor type: 2000, Landsat ETM

Number of classes: five classes

Overall Accuracy = (113249/164480) 68.8527%

Kappa Coefficient = 0.5990

Ground Truth (Pixels)

Class	Lake	Fish Farm	Desert	Urban	Agri_land	Total
Lake	22849	20097	0	157	149	43252
Fish Farm	13651	19921	0	3066	3931	40569
Desert	0	13	42650	2057	156	44786
Urban	0	3330	1	13148	1841	18320
Agri_land	0	1963	0	819	14771	17553
Total	36500	45324	42651	19247	20848	164480

Ground Truth (Percent)

Class	Lake	Fish Farm	Desert	Urban	Agri_land	Total
Lake	62.60	44.34	0.00	0.82	0.71	26.30
Fish Farm	37.40	43.95	0.00	15.93	18.86	24.67
Desert	0.00	0.03	100.00	10.69	0.75	27.23
Urban	0.00	7.35	0.00	68.31	8.83	11.14
Agri_land	0.00	4.33	0.00	4.26	70.85	10.67
Total	100.00	100.00	100.00	100.00	100.00	100.00

Accuracies

a)

Class	Commission (Percent)	Omission (Percent)	Commission (Pixels)	Omission (Pixels)
Lake	47.17	37.40	20403/43252	13651/36500
Fish Farm	50.90	56.05	20648/40569	25403/45324
Desert	4.97	0.00	2226/44786	1/42561
Urban	28.23	31.69	5172/18320	6099/19247
Agri_land	15.85	29.15	2782/17553	6077/20848

b)

Class	Prod. Acc. (Percent)	User Acc. (Percent)	Prod. Acc. (Pixels)	User Acc. (Pixels)
Lake	62.60	52.83	22849/36500	22849/43252
Fish Farm	43.95	49.10	19921/45324	19921/40569
Desert	100.00	95.03	42560/42561	42560/44786
Urban	68.31	71.77	13148/19247	13148/18320
Agri_land	70.85	84.15	14771/20848	14771/17553

Appendix Table 15: Confusion Matrix Classification method: Maximum Likelihood

Image acquisition date and sensor type: 2000, Landsat ETM

Number of classes: five classes

Overall Accuracy = (153865/164480) 93.5463%

Kappa Coefficient = 0.9173

Ground Truth (Pixels)

Class	Lake	Fish Farm	Desert	Urban	Agri_land	Total
Lake	35447	925	0	1	0	36373
Fish Farm	1045	40306	0	920	652	42923
Desert	0	0	42505	1	30	42536
Urban	1	2273	55	17042	1601	20972
Agri_land	7	1820	1	1283	18565	21676
Total	36500	45324	42651	19247	20848	164480

Ground Truth (Percent)

Class	Lake	Fish Farm	Desert	Urban	Agri_land	Total
Lake	97.12	2.04	0.00	0.01	0.00	22.11
Fish Farm	2.86	88.93	0.00	4.78	3.13	26.10
Desert	0.00	0.00	99.87	0.01	0.14	25.86
Urban	0.00	5.02	0.13	88.54	7.68	12.75
Agri_land	0.02	4.02	0.00	6.67	89.05	13.18
Total	100.00	100.00	100.00	100.00	100.00	100.00

Accuracies

a)

Class	Commission (Percent)	Omission (Percent)	Commission (Pixels)	Omission (Pixels)
Lake	2.55	2.88	926/36373	1053/36500
Fish Farm	6.10	11.07	2617/42923	5018/45324
Desert	0.07	0.13	31/42536	56/42561
Urban	18.74	11.46	3930/20972	2205/19247
Agri_land	14.35	10.95	3111/21676	2283/20848

b)

Class	Prod. Acc. (Percent)	User Acc. (Percent)	Prod. Acc. (Pixels)	User Acc. (Pixels)
Lake	97.12	97.45	35447/36500	35447/36373
Fish Farm	88.93	93.90	40306/45324	40306/42923
Desert	99.87	99.93	42505/42561	42505/42536
Urban	88.54	81.26	17042/19247	17042/20972
Agri_land	89.05	85.65	18565/20848	18565/21676

Appendix Table 16: Confusion Matrix Classification method: Neural Network

Image acquisition date and sensor type: 2000, Landsat ETM

Number of classes: five classes

Overall Accuracy = (35901/164480) 21.8270%

Kappa Coefficient = -0.0530

Ground Truth (Pixels)

Class	Lake	Fish Farm	Desert	Urban	Agri_land	Total
Lake	32425	825	0	107	88	33445
Fish Farm	3278	3447	42556	16714	764	66759
Desert	797	40843	5	2404	19711	63760
Urban	0	208	0	22	283	513
Agri_land	0	1	0	0	2	3
Total	36500	45324	42561	19247	20848	164480

Ground Truth (Percent)

Class	Lake	Fish Farm	Desert	Urban	Agri_land	Total
Lake	88.84	1.82	0.00	0.56	0.42	20.33
Fish Farm	8.98	7.61	99.99	88.84	3.66	40.59
Desert	2.18	90.11	0.01	12.49	94.55	38.76
Urban	0.00	0.46	0.00	0.11	1.36	0.31
Agri_land	0.00	0.00	0.00	0.00	0.01	0.00
Total	100.00	100.00	100.00	100.00	100.00	100.00

Accuracies

a)

Class	Commission (Percent)	Omission (Percent)	Commission (Pixels)	Omission (Pixels)
Lake	3.05	11.16	1020/33445	4075/36500
Fish Farm	94.84	92.39	63312/66759	41877/45324
Desert	99.99	99.99	63755/63760	42556/42561
Urban	95.71	99.89	491/513	19225/19247
Agri_land	33.33	99.99	1/3	20846/20848

b)

Class	Prod. Acc. (Percent)	User Acc. (Percent)	Prod. Acc. (Pixels)	User Acc. (Pixels)
Lake	88.84	96.95	32425/36500	32425/33445
Fish Farm	7.61	5.16	3447/45324	3447/66759
Desert	0.01	0.01	5/42561	5/63760
Urban	0.11	4.29	22/19247	22/513
Agri_land	0.01	66.67	2/20848	2/3

Appendix Table 17: Confusion Matrix Classification method: Parallelepiped

Image acquisition date and sensor type: 2000, Landsat ETM

Number of classes: five classes

Overall Accuracy = (117934/164480) 71.7011%

Kappa Coefficient = 0.6292

Ground Truth (Pixels)

Class	Lake	Fish Farm	Desert	Urban	Agri_land	Total
Lake	35234	8480	0	1	1	43716
Fish Farm	1129	34973	0	13302	10679	60083
Desert	0	0	41882	3	6	41891
Urban	137	967	14	5242	8814	15174
Agri_land	0	36	0	39	603	678
Total	36500	45324	42561	19247	20848	164480

Ground Truth (Percent)

Class	Lake	Fish Farm	Desert	Urban	Agri_land	Total
Lake	96.53	18.71	0.00	0.01	0.00	26.58
Fish Farm	3.09	77.16	0.00	69.11	51.22	36.53
Desert	0.00	0.00	98.40	0.02	0.03	25.47
Urban	0.38	2.13	0.03	27.24	42.28	9.23
Agri_land	0.00	0.08	0.00	0.20	2.89	0.41
Total	100.00	100.00	100.00	100.00	100.00	100.00

Accuracies
a)

Class	Commission (Percent)	Omission (Percent)	Commission (Pixels)	Omission (Pixels)
Lake	19.40	3.47	8482/43716	1266/36500
Fish Farm	41.79	22.84	25110/60083	10351/45324
Desert	0.02	1.60	9/41891	679/42561
Urban	65.45	72.76	9932/15174	14005/19247
Agri_land	11.06	97.11	75/678	20245/20848

b)

Class	Prod. Acc. (Percent)	User Acc. (Percent)	Prod. Acc. (Pixels)	User Acc. (Pixels)
Lake	96.53	80.60	35234/36500	35234/43716
Fish Farm	77.16	58.21	34973/45324	34973/60083
Desert	98.40	99.98	41882/42561	41882/41891
Urban	27.24	34.55	5242/19247	5242/15174
Agri_land	2.89	88.94	603/20848	603/678

Appendix Table 18: Confusion Matrix Classification method: Mahalanobis Distance

Image acquisition date and sensor type: 2005, Landsat ETM

Number of classes: five classes

Overall Accuracy = (129841/143793) 90.2972%

Kappa Coefficient = 0.8778

Ground Truth (Pixels)

Class	Lake	Fish Farm	Desert	Urban	Agri_land	Total
Lake	20207	6769	0	32	0	27008
Fish Farm	2253	22482	0	671	641	26047
Desert	0	0	38177	23	789	38989
Urban	6	2431	6	22306	79	24828
Agri_land	94	88	2	68	26669	26921
Total	22560	31770	38185	23100	28178	143793

Ground Truth (Percent)

Class	Lake	Fish Farm	Desert	Urban	Agri_land	Total
Lake	89.57	21.31	0.00	0.14	0.00	18.78
Fish Farm	9.99	70.76	0.00	2.90	2.27	18.11
Desert	0.00	0.00	99.98	0.10	2.80	27.11
Urban	0.03	7.65	0.01	96.56	0.28	17.27
Agri_land	0.42	0.28	0.01	0.29	94.64	18.72
Total	100.00	100.00	100.00	100.00	100.00	100.00

Accuracies

a)

Class	Commission (Percent)	Omission (Percent)	Commission (Pixels)	Omission (Pixels)
Lake	25.18	10.43	6801/27008	2353/22560
Fish Farm	13.69	29.24	3565/26047	9288/31770
Desert	2.08	0.02	812/38989	8/38185
Urban	10.16	3.44	2522/24828	794/23100
Agri_land	0.94	5.36	252/26921	1509/28178

b)

Class	Prod. Acc. (Percent)	User Acc. (Percent)	Prod. Acc. (Pixels)	User Acc. (Pixels)
Lake	89.57	74.82	20207/22560	20207/27008
Fish Farm	70.76	86.31	22482/31770	22482/26047
Desert	99.98	97.92	38177/38185	38177/38989
Urban	96.56	89.84	22306/23100	22306/24828
Agri_land	94.64	99.06	26669/28178	26669/26921

Appendix Table 19: Confusion Matrix Classification method: Minimum Distance

Image acquisition date and sensor type: 2005, Landsat ETM

Number of classes: five classes

Overall Accuracy = (121571/143793) 84.5458%

Kappa Coefficient = 0.8056

Ground Truth (Pixels)

Class	Lake	Fish Farm	Desert	Urban	Agri_land	Total
Lake	20480	11863	0	0	0	32343
Fish Farm	2080	17471	0	159	295	20005
Desert	0	25	38161	2379	423	40988
Urban	0	1762	24	19485	1486	22757
Agri_land	0	649	0	1077	25974	27700
Total	22560	31770	38185	23100	28178	143793

Ground Truth (Percent)

Class	Lake	Fish Farm	Desert	Urban	Agri_land	Total
Lake	90.78	37.34	0.00	0.00	0.00	22.49
Fish Farm	9.22	54.99	0.00	0.69	1.05	13.91
Desert	0.00	0.08	99.94	10.30	1.50	28.50
Urban	0.00	5.55	0.06	84.35	5.27	15.83
Agri_land	0.00	2.04	0.00	4.66	92.18	19.26
Total	100.00	100.00	100.00	100.00	100.00	100.00

Accuracies
a)

Class	Commission (Percent)	Omission (Percent)	Commission (Pixels)	Omission (Pixels)
Lake	36.68	9.22	11863/32343	2080/22560
Fish Farm	12.67	45.01	2534/20005	14299/31770
Desert	6.90	0.06	2827/40988	24/38185
Urban	14.38	15.65	3272/22757	3615/23100
Agri_land	6.23	7.82	1726/27700	2204/28178

b)

Class	Prod. Acc. (Percent)	User Acc. (Percent)	Prod. Acc. (Pixels)	User Acc. (Pixels)
Lake	90.78	63.32	20480/22560	20480/32343
Fish Farm	54.99	87.33	17471/31770	17471/20005
Desert	99.94	93.10	38161/38185	38161/40988
Urban	84.35	85.62	19485/23100	19485/22757
Agri_land	92.18	93.77	25974/28178	25974/27700

Appendix Table 20: Confusion Matrix Classification method: Maximum Likelihood

Image acquisition date and sensor type: 2005, Landsat ETM

Number of classes: five classes

Overall Accuracy = (140684/143793) 97.8379%

Kappa Coefficient = 0.9727

Ground Truth (Pixels)

Class	Lake	Fish Farm	Desert	Urban	Agri_land	Total
Lake	22241	36	0	0	0	22277
Fish Farm	319	29897	0	182	0	30398
Desert	0	0	38117	4	0	38121
Urban	0	1658	1	22290	39	23988
Agri_land	0	179	67	624	28139	29009
Total	22560	31770	38185	23100	28178	143793

Ground Truth (Percent)

Class	Lake	Fish Farm	Desert	Urban	Agri_land	Total
Lake	98.59	0.11	0.00	0.00	0.00	15.49
Fish Farm	1.41	94.10	0.00	0.79	0.00	21.41
Desert	0.00	0.00	99.82	0.02	0.00	26.15
Urban	0.00	5.22	0.00	96.49	0.14	16.68
Agri_land	0.00	0.56	0.18	2.70	99.86	20.17
Total	100.00	100.00	100.00	100.00	100.00	100.00

Accuracies

a)

Class	Commission (Percent)	Omission (Percent)	Commission (Pixels)	Omission (Pixels)
Lake	0.16	1.41	36/22277	319/22560
Fish Farm	1.65	5.90	501/30398	1873/31770
Desert	0.01	0.18	4/38121	68/38185
Urban	7.08	3.51	1698/23988	810/23100
Agri_land	3.00	0.14	870/29009	39/28178

b)

Class	Prod. Acc. (Percent)	User Acc. (Percent)	Prod. Acc. (Pixels)	User Acc. (Pixels)
Lake	98.59	99.84	22241/22560	22241/22277
Fish Farm	94.10	98.35	29897/31770	29897/30398
Desert	99.82	99.99	38117/38185	38117/38121
Urban	96.49	92.92	22290/23100	22290/23988
Agri_land	99.86	97.00	28139/28178	28139/29009

Appendix Table 21: Confusion Matrix Classification method: Neural Network

Image acquisition date and sensor type: 2005, Landsat ETM

Number of classes: five classes

Overall Accuracy = (38504/143793) 26.7774%

Kappa Coefficient = 0.0406

Ground Truth (Pixels)

Class	Lake	Fish Farm	Desert	Urban	Agri_land	Total
Lake	0	0	0	0	0	0
Fish Farm	20094	219	1	23	7	20344
Desert	6	31459	38177	22978	90	92710
Urban	2460	92	7	99	28072	30730
Agri_land	0	0	0	0	9	9
Total	22650	31770	38185	23100	28178	143793

Ground Truth (Percent)

Class	Lake	Fish Farm	Desert	Urban	Agri_land	Total
Lake	0.00	0.00	0.00	0.00	0.00	0.00
Fish Farm	89.07	0.69	0.00	0.10	0.02	14.15
Desert	0.03	99.02	99.98	99.47	0.32	64.47
Urban	10.90	0.29	0.02	0.43	99.62	21.37
Agri_land	0.00	0.00	0.00	0.00	0.03	0.01
Total	100.00	100.00	100.00	100.00	100.00	100.00

Accuracies

a)

Class	Commission (Percent)	Omission (Percent)	Commission (Pixels)	Omission (Pixels)
Lake	0.00	100.00	0/0	22560/22560
Fish Farm	98.92	99.31	20125/20344	31551/31770
Desert	58.82	0.02	54533/92710	8/38185
Urban	99.68	99.57	30631/30730	23001/23100
Agri_land	0.00	99.97	0/9	28169/28178

b)

Class	Prod. Acc. (Percent)	User Acc. (Percent)	Prod. Acc. (Pixels)	User Acc. (Pixels)
Lake	0.00	0.00	0/22560	0/0
Fish Farm	0.69	1.08	219/31770	219/20344
Desert	99.98	41.18	38177/38185	38177/92710
Urban	0.43	0.32	99/23100	99/30730
Agri_land	0.03	100.00	9/28178	9/9

Appendix Table 22: Confusion Matrix Classification method: Parallelepiped

Image acquisition date and sensor type: 2005, Landsat ETM

Number of classes: five classes

Overall Accuracy = (113015/143793) 78.5956%

Kappa Coefficient = 0.7321

Ground Truth (Pixels)

Class	Lake	Fish Farm	Desert	Urban	Agri_land	Total
Lake	19480	9666	0	0	0	29146
Fish Farm	3080	19991	0	5859	216	29149
Desert	0	0	37602	1	0	37603
Urban	0	1168	0	16297	7654	25119
Agri_land	0	6	1	15	19645	19667
Total	22650	31770	38185	23100	28178	143793

Ground Truth (Percent)

Class	Lake	Fish Farm	Desert	Urban	Agri_land	Total
Lake	86.35	30.42	0.00	0.00	0.00	20.27
Fish Farm	13.65	62.92	0.00	25.36	0.77	20.27
Desert	0.00	0.00	98.47	0.00	0.00	26.15
Urban	0.00	3.68	0.00	70.55	27.16	17.47
Agri_land	0.00	0.02	0.00	0.06	69.72	13.68
Total	100.00	100.00	100.00	100.00	100.00	100.00

Accuracies
a)

Class	Commission (Percent)	Omission (Percent)	Commission (Pixels)	Omission (Pixels)
Lake	33.16	13.65	9666/29146	3080/22560
Fish Farm	31.41	37.08	9155/29146	11779/31770
Desert	0.00	1.53	1/37603	583/38185
Urban	35.12	29.45	8822/25119	6803/23100
Agri_land	0.11	30.28	22/19667	8533/28178

b)

Class	Prod. Acc. (Percent)	User Acc. (Percent)	Prod. Acc. (Pixels)	User Acc. (Pixels)
Lake	86.35	66.84	19480/22560	19480/29146
Fish Farm	62.92	68.59	19991/31770	19991/29146
Desert	98.47	100.00	37602/38185	37602/37603
Urban	70.55	64.88	16297/23100	16297/25119
Agri_land	69.72	99.89	19645/28178	19645/19667

11.2. Appendix Figures

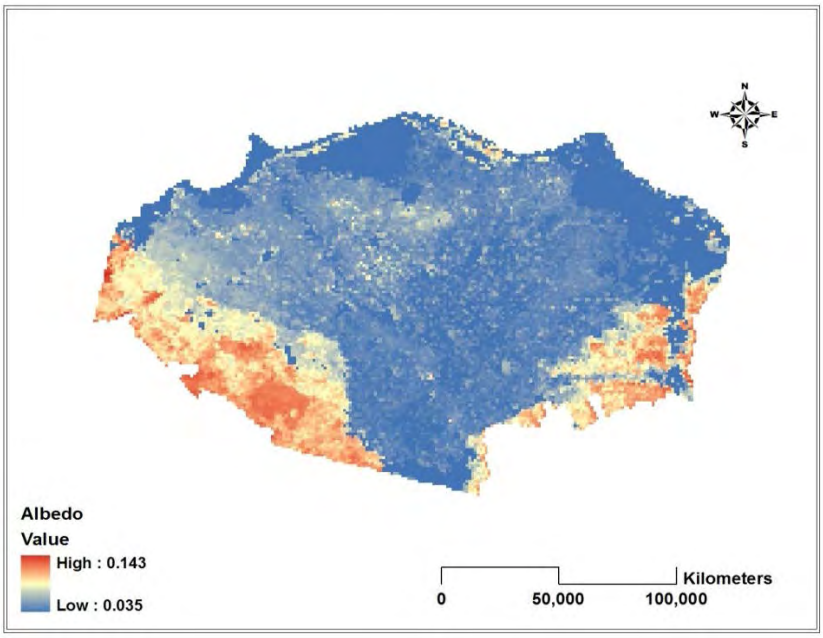

Appendix Figure 1: Surface Albedo Map Acquired in August 2008 over Nile Delta Region

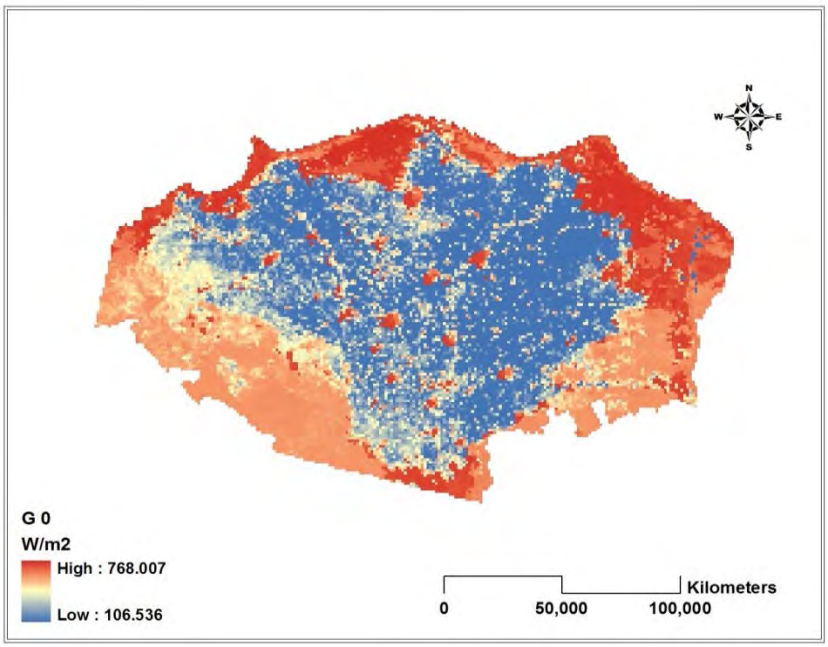

Appendix Figure 2: Net Radiation Map Acquired in August 2008 over Nile Delta Region

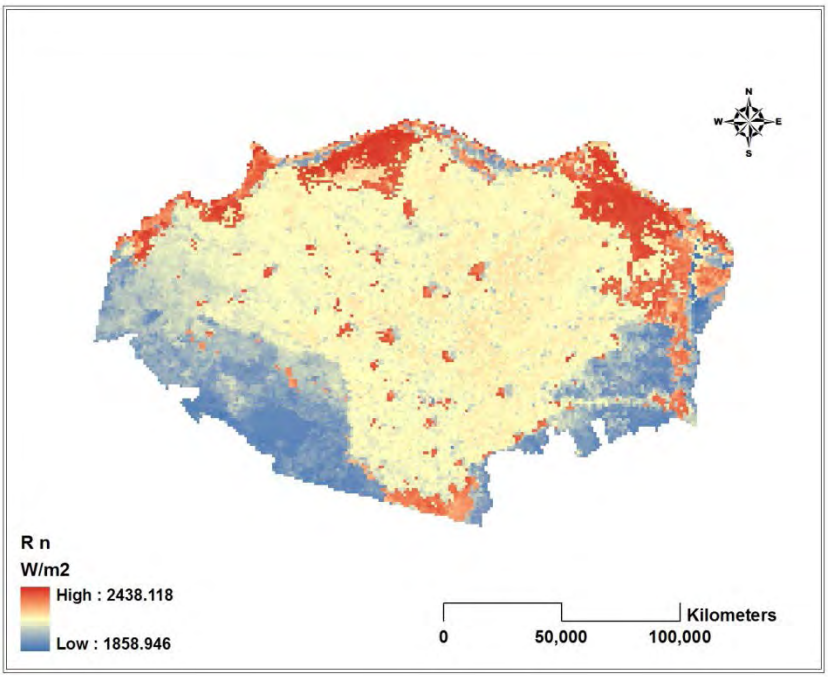

Appendix Figure 3: Soil Radiation Map Acquired in August 2008 over Nile Delta Region

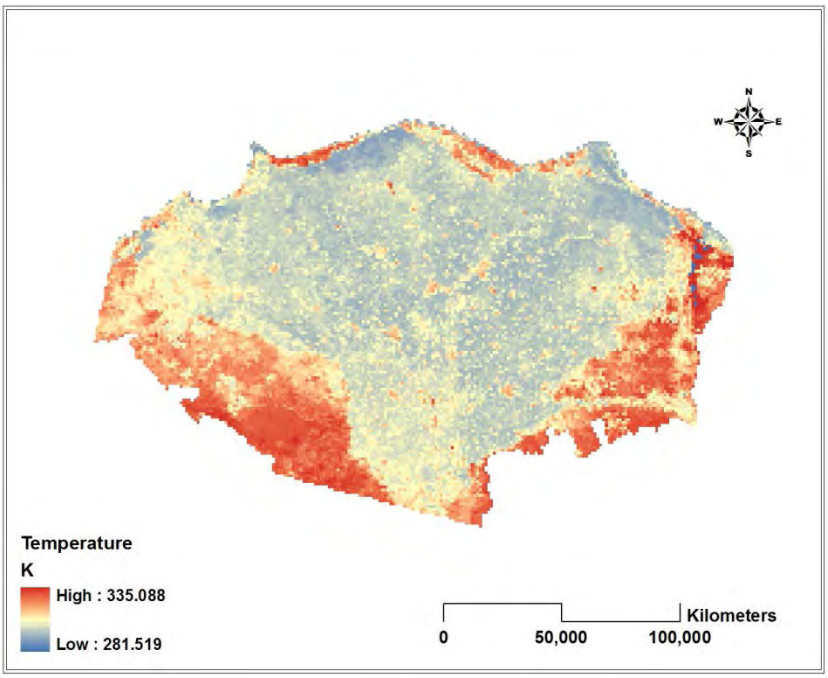

Appendix Figure 4: Surface Temperature Map Acquired in August 2008 over Nile Delta Region

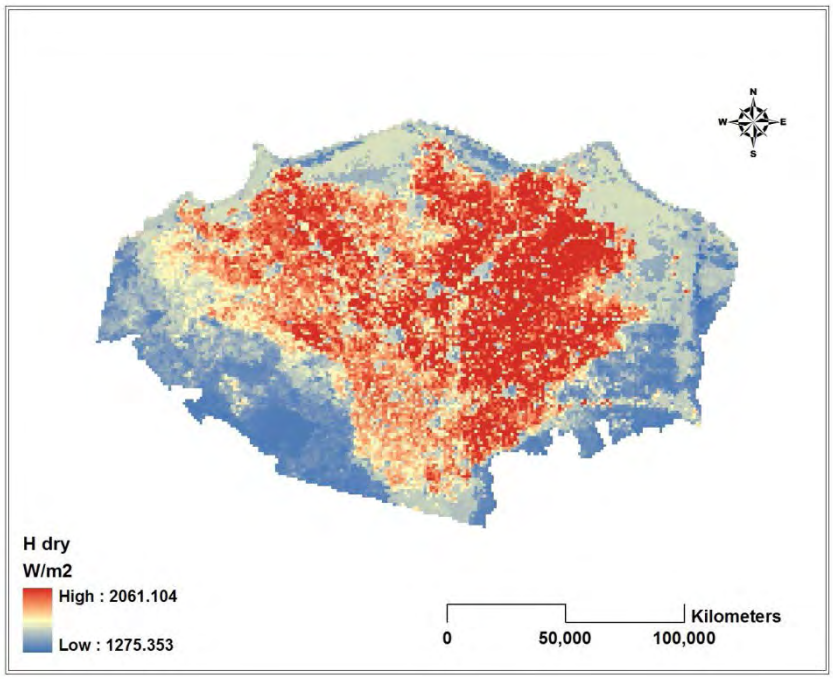

Appendix Figure 5: Dry Pixel Map Acquired in August 2008 over Nile Delta Region

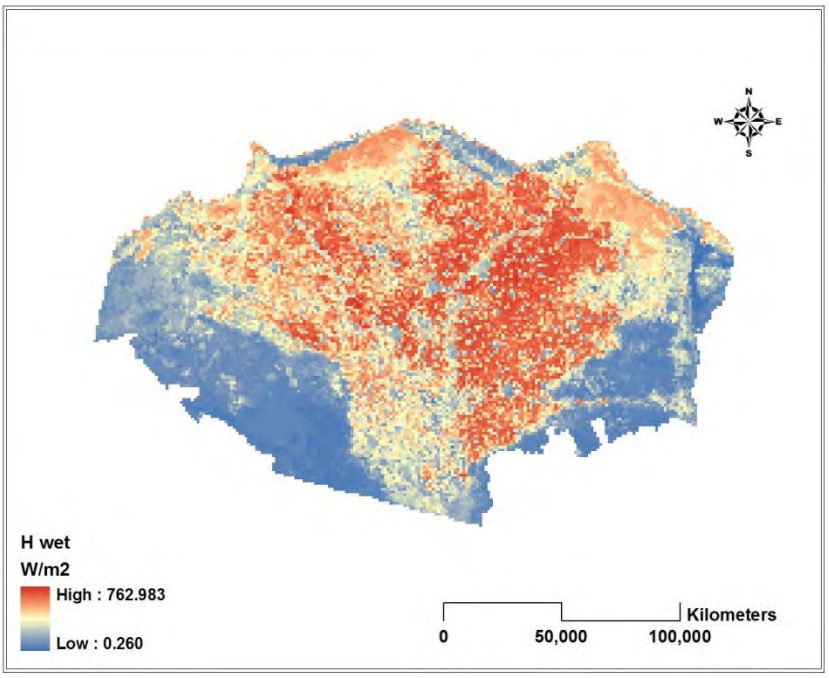

Appendix Figure 6: Wet Pixel Map Acquired in August 2008 over Nile Delta Region

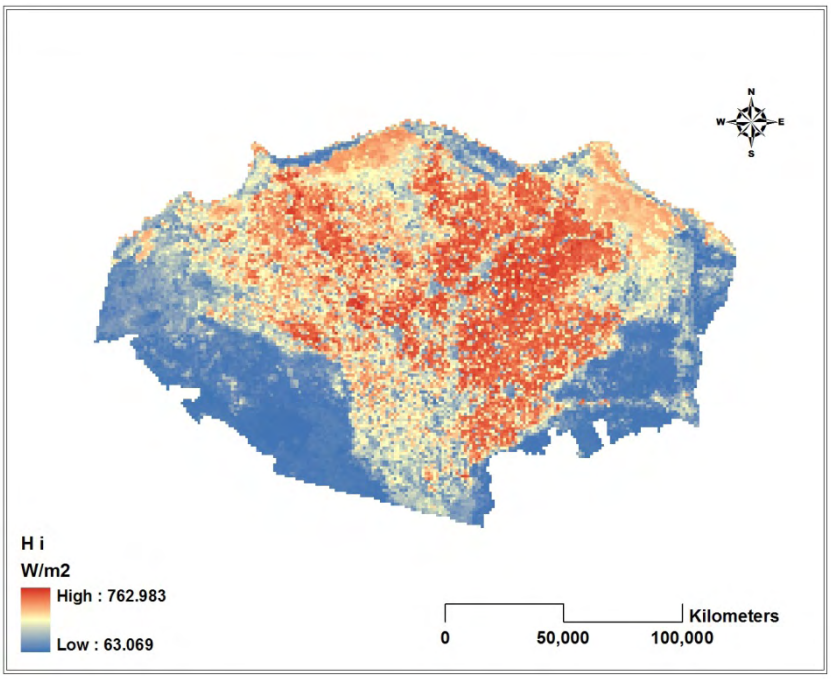

Appendix Figure 7: Latent Heat Map Acquired in August 2008 over Nile Delta Region

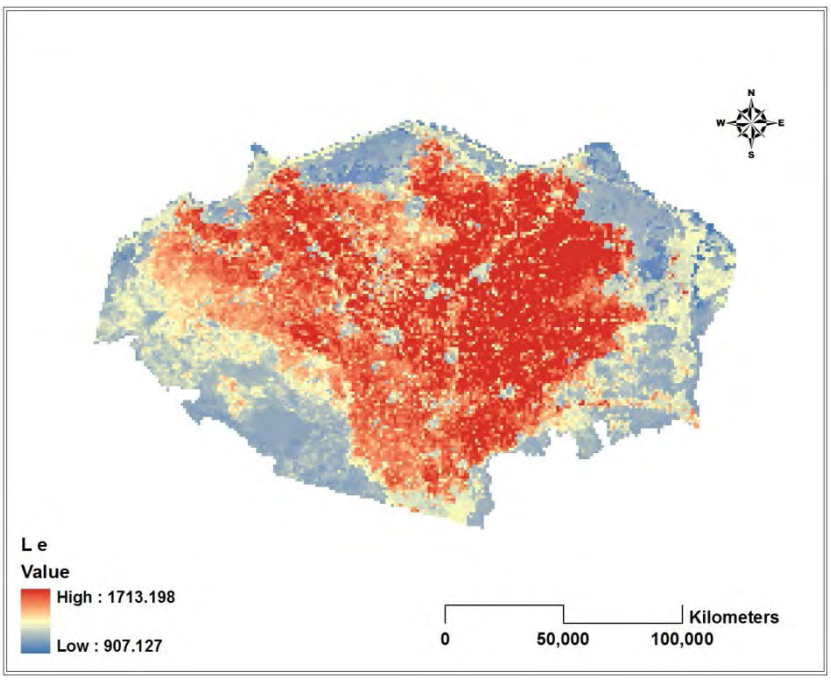

Appendix Figure 8: Turbulent Heat Map over Nile Delta Region

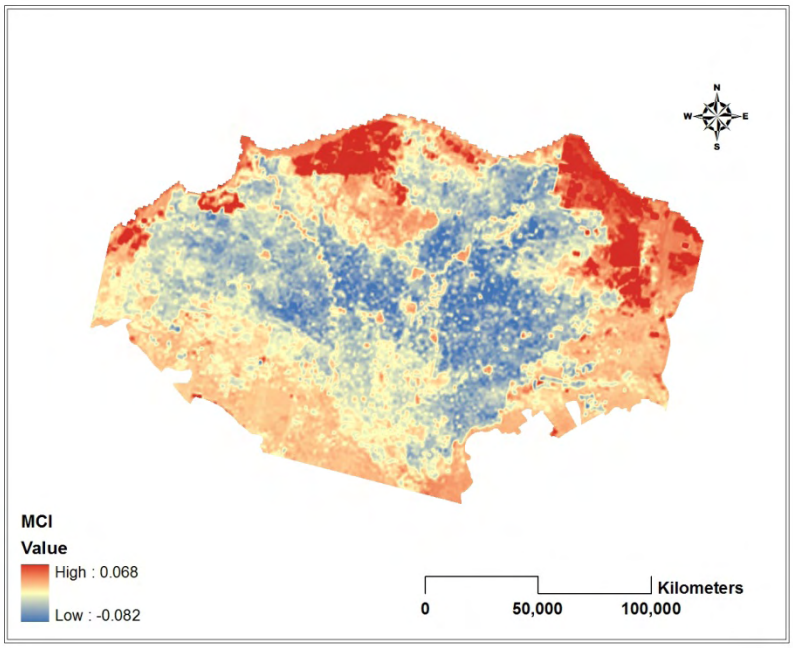

Appendix Figure 9: Maximum Chlorophyll Content Map over Nile Delta Region

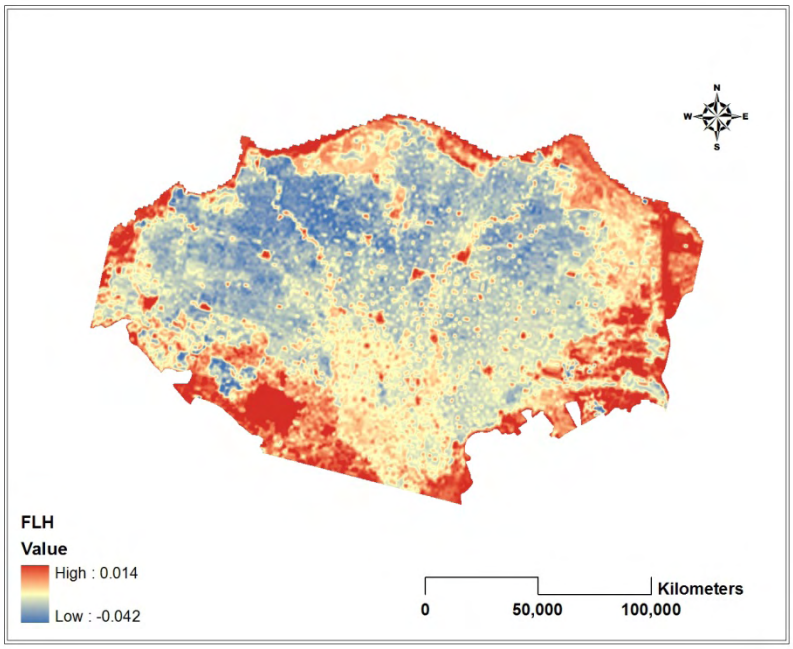

Appendix Figure 10: Florescent Height Map over Nile Delta Region

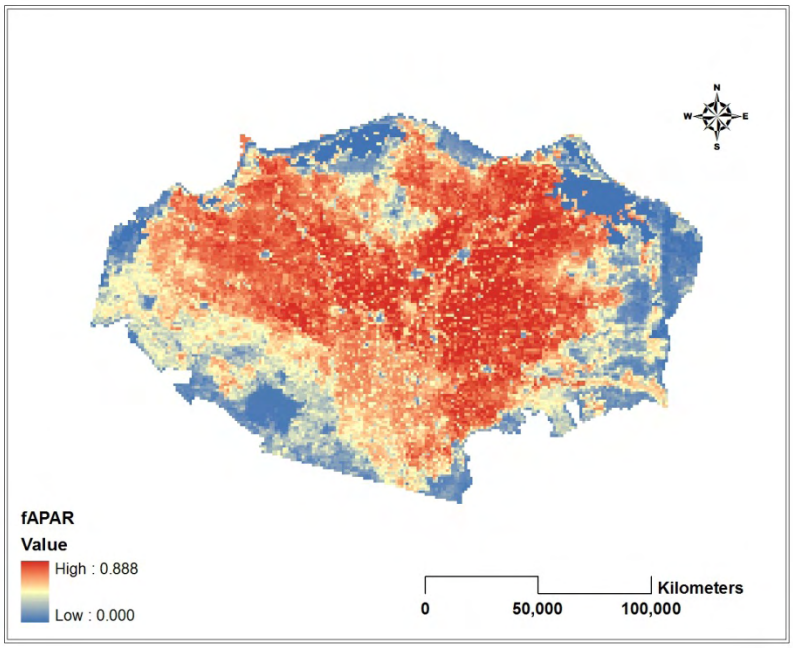

Appendix Figure 11: Fraction of Photosynthetically Active Radiation Map over Nile Delta Region

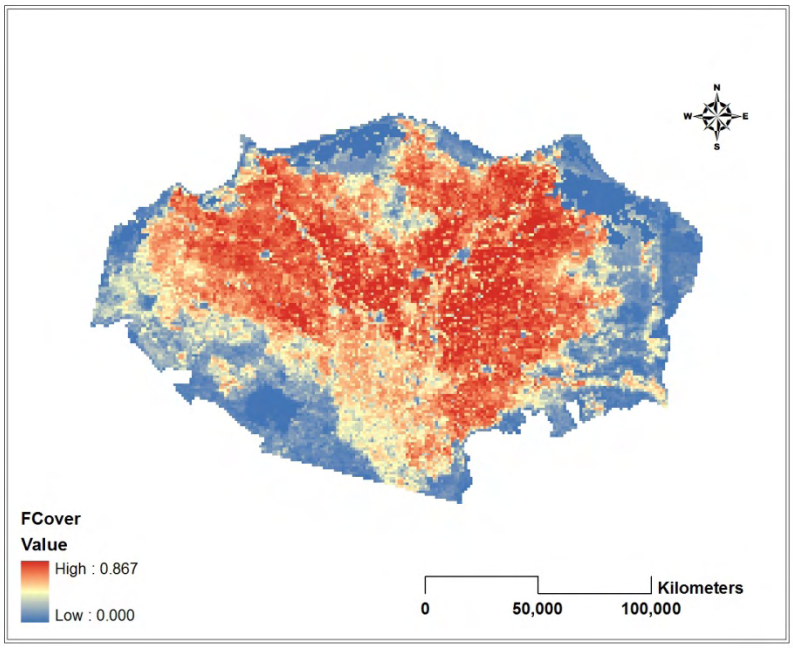

Appendix Figure 12: Gap Fraction for Nadir Direction Map over Nile Delta Region

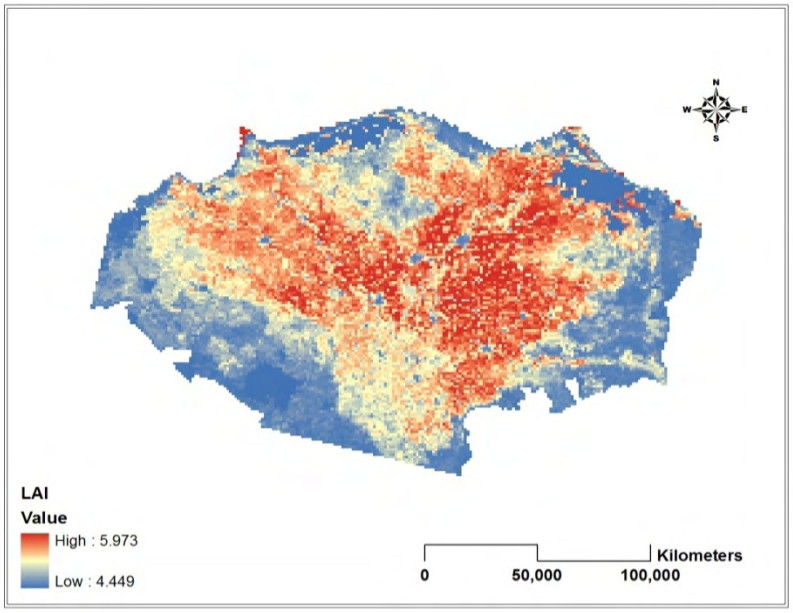

Appendix Figure 13: Leaf Area Index Map over Nile Delta Region

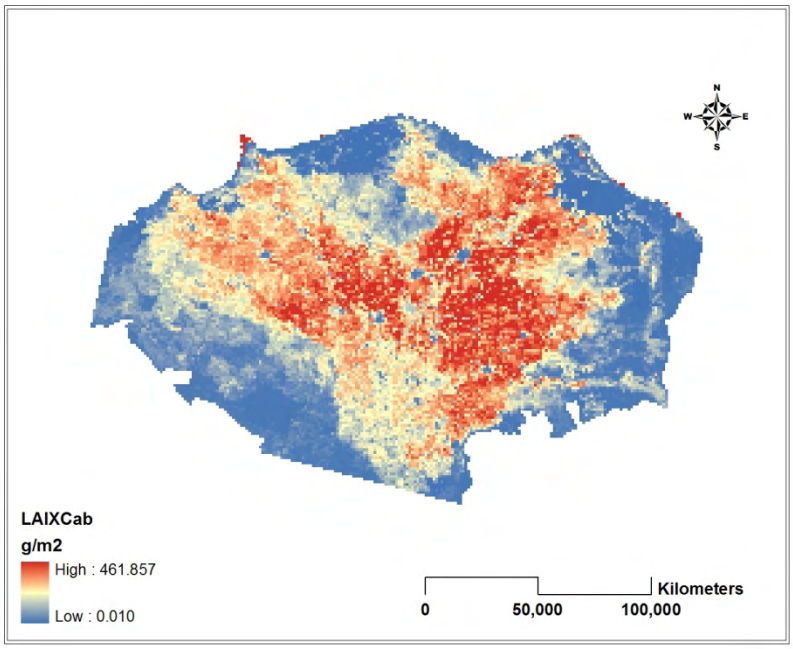

Appendix Figure 14: Calculated Chlorophyll Content Map over Nile Delta Region

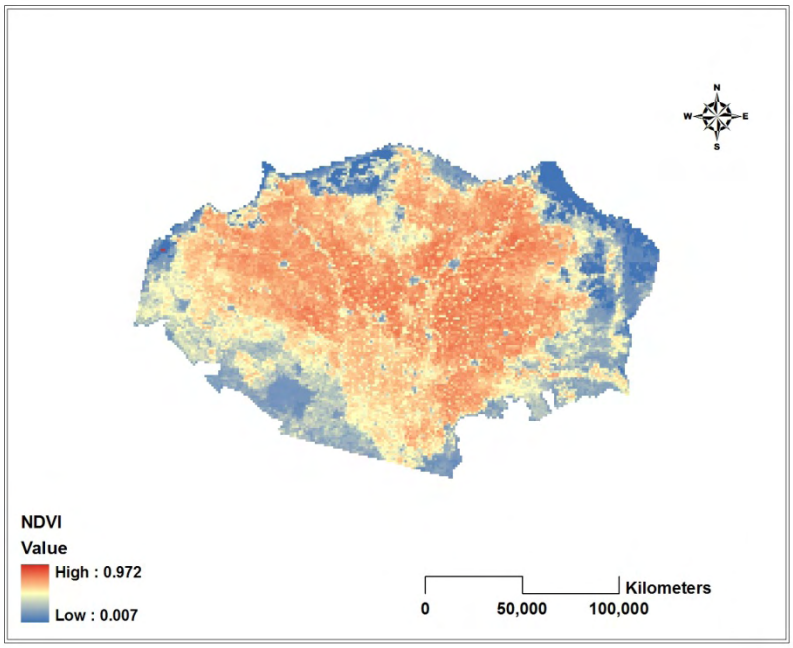

Appendix Figure 15: Normalized Difference Vegetation Index Map over Nile Delta Region

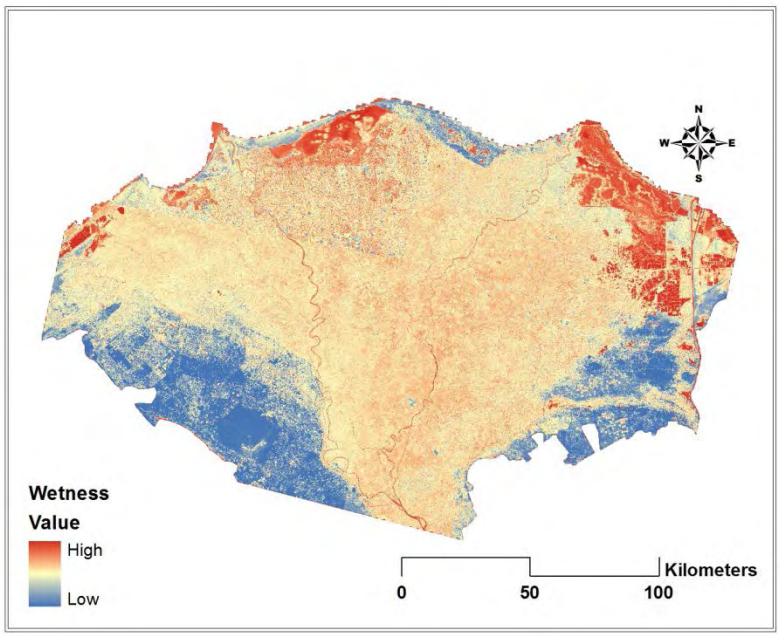

Appendix Figure 16: Soil Wetness Map over Nile Delta Region

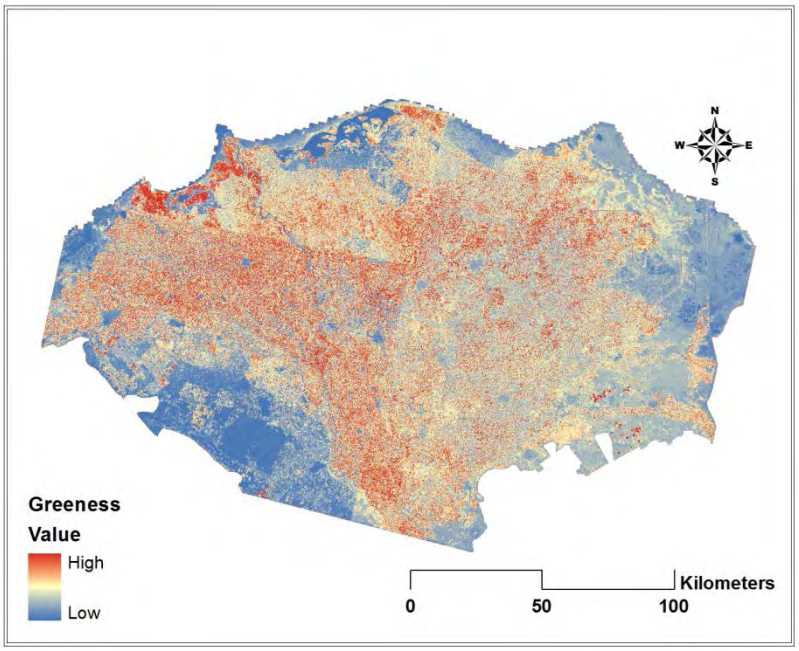

Appendix Figure 17: Vegetation Greeness Map over Nile Delta Region

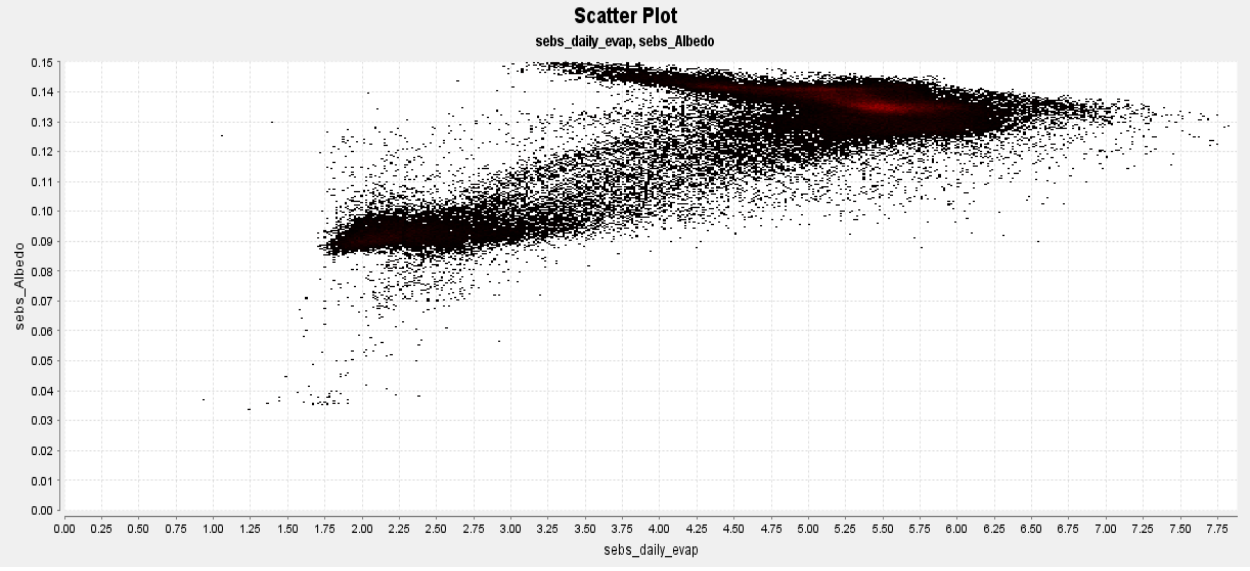

Appendix Figure 18: Relationship between Daily Evapotranspiration and Albedo

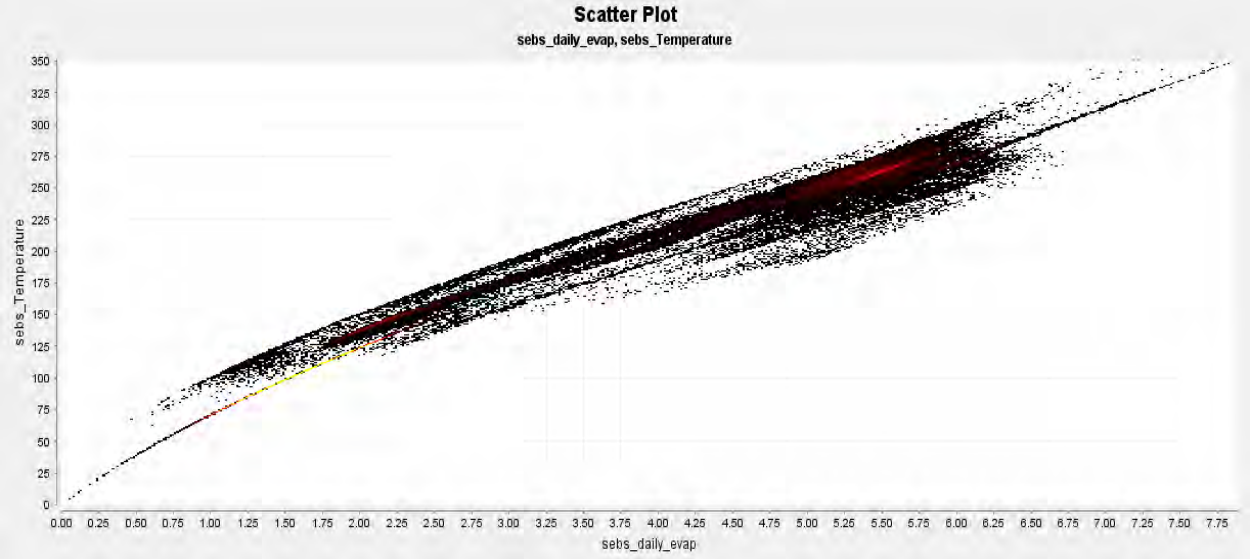

Appendix Figure 19: Relationship between Daily Evapotranspiration and Temperature